POLITECNICO DI MILANO
Aerospace Science and Technology Department
Space Engineering Master Degree

Characterization of Relative 6DOF Natural and Controlled Dynamics in Cislunar Space

Supervisor: Prof. Michèle Lavagna
Co-supervisor: Dr. Andrea Colagrossi

Candidate:
Francesco Colombi
863800

Academic Year 2017-2018

Contents

List of Figures

List of Tables

ABSTRACT

At the 50th anniversary of Apollo 11, the Moon is back to the scene of scientific and commercial space exploration interests. During the next decade, the establishment of a Gateway in cislunar non-Keplerian orbits will open the space frontiers to sustainable manned and robotic missions on and around the Moon. This asset will be exploited to advance technologies, capabilities and best practices to tackle challenges for the next journey to Mars and beyond, while mitigating possible risks. Such infrastructure will require several logistic operations for its assembly and maintenance, which lean on rendezvous and docking/undocking capabilities. Even if few missions have flown on non-Keplerian orbits, thank to the recent progresses in multi-body trajectory design, rendezvous and docking (RV&D) operations have not been performed but in LEO.

Investigations about 6DOF relative dynamics in non-Keplerian environment are now mandatory to highlight criticalities in the design of the cislunar gateway and to translate RV&D protocols, consolidated in LEO for the ISS, to the new non-Keplerian environment.

In this direction, the paper first analyses the orbit-attitude dynamics within the CR3BP framework. A novel perspective of the dynamical structures constituting 6DOF manifolds allows to better characterize the natural relative dynamics in proximity of non-Keplerian orbits. The importance of orbit-attitude manifolds exploitation is underlined for designing reliable and efficient rendezvous trajectories and formation flying applications.

Then, an ephemeris cislunar model is exploited to address cislunar RV&D operations. The control capability is included in the dynamics of the chaser vehicle, which is employed to solve the 6DOF rendezvous problem. The results obtained with the controlled dynamics are compared to those available thanks to natural motion, discussing the energetic and time costs to complete the maneuvers. Operational challenges are discussed about the identified favourable locations along the orbit to perform RV&D operations, highlighting possible relations between RV&D time and non-Keplerian orbit's period.

Chapter 1

INTRODUCTION

Space agencies belonging to the International Space Exploration Coordination Group (ISECG), the partners collaborating at the International Space Station (ISS), have endorsed plans to establish a new space asset orbiting in the vicinity of the Moon. The Cislunar Gateway, also known as Lunar Orbital Platform-Gateway (LOPG) or Deep Space Gateway (DSG), represents a fundamental step in the sustainable, reusable, long-term architecture to support the next generation of human and robotic space exploration and commercial mission on and around the Moon. Moreover, it is serving as technologies and operations testbed in preparation for deep space exploration which will ultimately brings human to Mars [1]. Recent studies has selected Earth-Moon Near-Rectilinear Halo Orbit (NRHO) as the most attractive staging orbit candidate for the cislunar gateway [2].

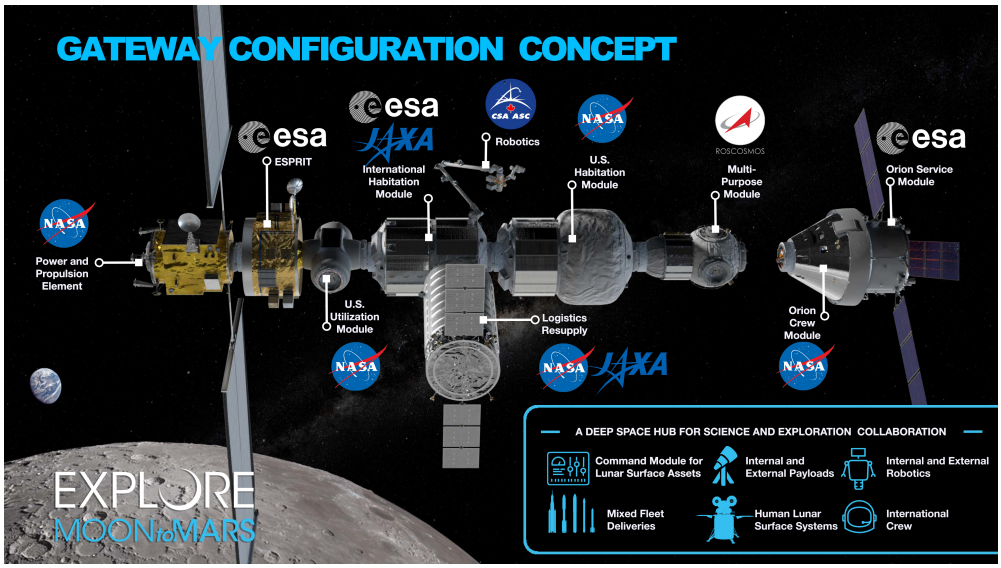

Figure 1.1: Lunar Orbital Platform-Gateway (LOPG): Cislunar Gateway concept unveiled by NASA

Thank to the progress in multi-body trajectory design, few missions have already flown near collinear libration point of Earth-Moon and Sun-Earth systems [3, 4, 5]. Space agencies are proposing several new ambitious mission which are based on the understanding of the dynamical environment described by the Circular Restricted Three-Body Problem (CR3BP). Among them there are new generation astronomical observatories [6, 7, 8], refuelling station and communication relays across the Solar system, repositioning of small asteroid within the Earth-Moon system.

It is important to have a better understanding of the natural attitude dynamics in a complex environment such as the non-Keplerian orbits about the libration points. The discovery of bounded periodic or quasi-periodic orbit-attitude behaviours may aid in the design of the mission operational

modes and support the Attitude Control System (ACS). For example, their implementation could drastically reduce the orbit-attitude maintenance cost for the cislunar gateway.
The assembly and the maintenance of an in-orbit infrastructure such as the cislunar gateway will lean on periodic and continuous visiting vehicles, which have to perform rendezvous and docking/undocking procedures in a reliable and efficient manner. The ability to predict and control the relative motion of both orbital and attitude dynamics is fundamental in the design of proximity operations.
Therefore, the interest in a better understanding of absolute and relative coupled orbit-attitude behaviours in proximity of periodic solution existing in the CR3BP dynamical regime is justified.

1.1 Problem Definition and Research Objectives

From a general perspective, this preliminary investigation aims to increase the understanding of absolute and relative 6DOF motions characterizing periodic non-Keplerian orbits about the libration points existing in the orbit-attitude CR3BP dynamical environment. Particular attention has been dedicated to the analysis of Halo orbits and NRHOs, being of particular interest for the design of the cislunar gateway. Moreover, the outcomes of these three-dimensional symmetric orbits can be easily extended to the other families of orbits about the collinear libration points.
The definition of a general procedure to explore the dynamical structures surrounding periodic orbit-attitude solutions constitutes an important piece of the characterization of the solution space for a complex dynamical system such as the orbit-attitude CR3BP. The natural extension deriving from this formulation is the inclusion of the rotational motion into the orbital manifolds. Note that the attitude dynamics coupling could affect the orbital motion in the case of large space infrastructure, leading to possible differences with their classical structure known in the only orbital CR3BP. The identification of new manifold surfaces could supply natural corridors for reorientation maneuvers.
The study of these peculiar surfaces in the orbital-attitude domain could improve the understanding of the relative 6DOF dynamics of spacecraft moving in proximity of a non-Keplerian orbit. Particular manifolds surfaces could be implemented in actual design of low-energy rendezvous and docking (RV&D) operations and formation flying applications.
Moreover, the motion characterizing these surfaces is strictly related to the stability properties of the corresponding periodic orbit-attitude solution. For example, quasi-periodic behaviours could be exploited for coarse-pointing or contingency configurations in the design of deep-space stations, as well as enabling passive stable configurations on a long-term horizon for redirected asteroids in the vicinity of the Moon for scientific and commercial missions.

The preliminary results coming from the analysis of the natural orbit-attitude dynamics will aid at the definition of operational requirements and constraints driving the design of the Guidance, Navigation and Control (GNC) system to perform RV&D operations in cislunar environment. Then, a preliminary investigation is presented to assess the feasibility and the cost to perform RV&D operations controlling continuously the 6DOF relative dynamics of a chaser spacecraft placed in proximity of a target moving on a NRHO in the Earth-Moon system. Only the final stage of the rendezvous mission, denoted as “close-range rendezvous and docking phase”, is considered in this analysis because it constitutes the most important phase where the actual relative 6DOF dynamics of the spacecrafts has to be evaluated.

1.2 State of the Art

1.2.1 Orbit-Attitude Dynamics and Periodic Solutions in the CR3BP

The earliest studies concerning the attitude stability of a satellite within the CR3BP have been conducted by Kane, Marsh and Robinson. They have assumed the satellite artificially maintained at the exact location of the libration points and they studied the attitude stability for different spacecraft configurations (symmetric [9], dumbbell and asymmetric rigid bodies [10]). Abad et al. introduced the use of Euler parameters, namely quaternions, into the attitude dynamics of a rigid body fixed at the libration point [11]. More recently, Brucker et al. explored the attitude dynamics and stability of a spacecraft fixed at the equilibrium point location in the Sun-Earth system by exploiting Poincaré maps [12]. Wong et al. extended the analysis of attitude motion of a single rigid body orbiting on linearized of Lyapunov and Halo orbits in the Sun-Earth system [13]. However, since these orbit represent a linear approximation, the simulation is valid only for relatively small orbits about the equilibrium points. Later, Guzzetti explored the non-linear orbit-attitude dynamics in the CR3BP exploiting as reference orbits those belonging to the Lyapunov family. However, this analysis concern the solely rotational motion limited to the orbital plane [14]. The full three-dimensional rotational motion has been explored by Knutson and Howell, considering a multi-body spacecraft moving along non-linear Lyapunov and Halo orbits [15, 16]. In their analysis, attitude maps have been proven useful to recognize orbital characteristics and body inertia properties which enable the spacecraft to keep its initial attitude configuration. Guzzetti has exploited Floquet's theory and Poincaré maps to identify bounded orbit-attitude solutions in the rotating frame of the CR3BP [17]. The rotational motion in the orbital plane of a spacecraft moving on Distant Retrograde Orbit (DRO) in the Earth-Moon system has been investigated by Bucci. This analysis has considered also the perturbation introduced by the Solar Radiation Pressure (SRP) and possible interferences considering a simple model of a flexible large space structure [18]. Colagrossi and Lavagna explored the natural bounded orbit-attitude dynamics of a large space infrastructures moving along Near-Rectilinear Halo Orbit (NRHO) in the Earth-Moon system, and possible effects on the flexible structure of the spacecraft are investigated [19].

1.2.2 Rendezvous and Docking

From a space mission point of view, the rendezvous involves a spacecraft moving on its operational orbit, which is denoted as "target", and a controlled spacecraft that is approching the target, which is denoted as "chaser". Rendezvous operations between two spacecraft in Low Earth Orbit (LEO) have been extensively studied and tested in the past years [20], especially thanks to the International Space Station (ISS) programme. The different phases of a rendezvous mission are constitude by several orbital maneuvers which progressively drive the chaser to approach the target. For example, the rendezvous of the Soyuz service module to the ISS starts with a bi-elliptic transfer, which is followed by an homing maneuver, a closing maneuver, and a final translation towards the docking port [21].

Many arguments of the orbital CR3BP in the Earth-Moon system are covered by a wide literature: from detailed orbital catalogues [22] to studies of the corresponding invariant manifolds, from low-energy transfer applications to station-keeping strategies for different families of orbits [23]. More recently, many authors have proposed new studies concerning rendezvous strategies design with a target moving along an reference non-Keplerian orbit existing in the Earth-Moon CR3BP framework. In these analysis, an automated transfer vehicles (the chaser) has to reach a cislunar gateway (the target) from different locations, such as the Earth, the Moon or a different non-Keplerian orbit, within reasonable time and cost which can limit actual mission design. Lizy-

Destrez and Murakami et al. have analysed the transfer and the rendezvous phases of a chaser spacecraft departing from the Earth and approaching a target spacecraft on a Earth-Moon L_2 Halo orbit [24, 25]. Colagrossi et al. have investigated a low-energy transfer solution to lead a chaser vehicle to the non-Keplerian orbit of the target spacecraft, departing the transfer from a different non-Keplerian orbit in the Earth-Moon system (namely Halo orbits, DRO and NRHO) [26, 27]. More recently, Bucci et al. have investigated possible mission requirements and constraints of the phasing phase, as well as of the rendezvous phase considering the target as a large space structure orbiting on a Earth-Moon NRHO [28, 29]. However, these studies have investigated almost solely the orbital part of the CR3BP dynamics, while the attitude part, which is fundamental for the close-range rendezvous and docking phase, is not considered.

1.3 Current Work

The current investigation concerns two main topics. First, the characterization of natural relative 6DOF motion in proximity of non-Keplerian orbits in the CR3BP framework is analysed. Then, a preliminary analysis for the relative 6DOF guidance of RV&D operations in cislunar environment is presented taking in consideration the outcomes from the first part.

The organization of this study is briefly introduced as follows.

Chapter 2

In this chapter, the dynamics and kinematics relations governing the classical orbital CR3BP and the rotational motion of a rigid body are introduced. The attitude dynamics is included into the CR3BP formulation to obtain the coupled orbit-attitude CR3BP. Then, relative kinematics relations are defined for the orbit-attitude motion between a chaser and a target spacecrafts moving in the CR3BP dynamical regime. Finally, the absolute and relative 6DOF dynamics are included in a cislunar ephemeris four-body model to support high-level design stages for space mission located in this particular environment.

Chapter 3

Differential corrector algorithms are extensively employed in the CR3BP. Leaning on the work of Guzzetti in [17], a multiple-shooting differential corrector is developed for a general problem in the orbit-attitude CR3BP dynamical system. The differential corrector has been applied to discover periodic orbit-attitude solutions, especially for Halo and NRHOs in the Earth-Moon system, and continuation scheme are used for the generation of the corresponding families. The formulation of a targeting scheme to aim a desired final orbit-attitude state is presented and possible applications are discussed.

Chapter 4

In this chapter, the Floquet's theory is discussed and applied to the orbit-attitude CR3BP problem. Particular effort has been dedicated to validate possible simplification at the orbit-attitude CR3BP model describing the motion of nowadays and near-future spacecrafts within the Earth-Moon system. The orbital and the attitude modes constituting the local approximation of the global invariant manifolds are presented in a novel perspective to characterize the relative 6DOF dynamics in proximity of non-Keplerian orbits existing in the CR3BP environment. Favourable and challenging dynamical behaviours are discussed taking in consideration the possible implementation

of Floquet modes for the design of RV&D operations, orbit-attitude maintenance (namely station-keeping and attitude stabilization), and formation flying applications.

Chapter 5

The relative orbit-attitude dynamics of a chaser spacecraft having an initial offset position from a target spacecraft is investigated within the CR3BP in order to have further insights about the natural drift behaviours in proximity of periodic orbit-attitude solution, such as Halo orbits and NRHOs.

Chapter 6

In this investigation, the chaser spacecraft constitutes the active commanded vehicle, while the target cislunar gateway is a passive cooperative vehicle. A direct transcription of the 6DOF rendezvous problem is implemented considering the cislunar ephemeris model. The continuous control action is directly included in the dynamics of the chaser vehicle. The performance and the costs of the optimal energy rendezvous guidance are explored in function of the initial relative orbit-attitude state of the chaser and of the time allocated for the maneuver. Then, the optimal energy 6DOF guidance is applied to a close-range rendezvous and docking example to demonstrate the feasibility of executing proximity operations.

Chapter 7

A final summary of the most relevant results and outcomes of this preliminary investigation research are summarized in this final chapter. Then, some consideration and recommendation for future work are included.

Chapter 2

BACKGROUNG

The CR3BP orbital dynamics and the attitude dynamics of the spacecraft are the basis to constitute the orbit-attitude model which will be employed in the investigation proposed in this paper. The understanding, the prediction and the control of these dynamics are fundamental for the design of rendezvous and docking operations in the new challenging scenario of non-Keplerian orbit in cislunar environment.

2.1 Notation Convention

Before starting going deep in the formulation of the problem, the notation convention exploited through this paper is shown as a common baseline.

- Vectors are expressed as bold symbols, e.g. the vector "v" is $\boldsymbol{v}$. While their corresponding modulus is referred with the same symbol but in normal font, so that $\|\boldsymbol{v}\| = v$. Vectors may be expressed in different reference frames. The basis may be specified as $\underset{\hat{a}}{\boldsymbol{v}}$ or as $\boldsymbol{v}^{\hat{a}}$, where $\{\hat{a}\}$ is a generic reference frame.
- Unit vectors are expressed through the hat formalism $\hat{\cdot}$.
- Matrices are denoted as capitol letters, eventually within square brackets, e.g. the matrix A correspond to the symbol $[A]$.
- A vectrix is defined as a matrix of vectors. They are typically employed to represent in compact form the base of reference frames. The curly bracket notation is used referring to the generic $\{\hat{a}\}$-frame.
$$\{\hat{a}\} = \begin{bmatrix} \hat{\boldsymbol{a}}_1 \\ \hat{\boldsymbol{a}}_2 \\ \hat{\boldsymbol{a}}_3 \end{bmatrix}$$
- To describe frame transformations from an initial $\{\hat{a}\}$-frame to a final $\{\hat{b}\}$-frame, the corresponding Direction Cosine Matrix (DCM) is written as $C_{\hat{b}/\hat{a}}$ or as $[C_{\hat{b}/\hat{a}}]$. Quaternion and other quantities which describe the attitude of the $\{\hat{b}\}$-frame respect to the $\{\hat{a}\}$-frame are written as ${}^{\hat{a}}\boldsymbol{q}^{\hat{b}}$.
- Time derivatives exploit the Newton's convention such as $\dfrac{d\boldsymbol{v}}{dt} = \dot{\boldsymbol{v}}$.
- Partial derivatives of the vector $\boldsymbol{v}$ with respect to the vector $\boldsymbol{x}$ are written as $\dfrac{\partial \boldsymbol{v}}{\partial \boldsymbol{x}} = \boldsymbol{v}_{/\boldsymbol{x}}$. The same notation applies to scalar quantities.

2.2 Circular Restricted Three-Body Problem

This section breafly introduce at the Circular Restricted Three-Body Problem (CR3BP) fundamentals to provide the background necessary to understand the formulation and the work presented in this investigation.

There exist regions of space where the traditional Keplerian model no longer provide a nice interpretation of the dynamical environment, because the spacecraft motion becomes strongly influenced by multiple gravitational bodies. The restricted three-body problem is the first step towards a multiple-body dynamical regime. It offers an effective interpretation of binary systems, such as the Earth-Moon system, opening new unique possibilities for trajectories design in novel space missions.

The CR3BP rules the dynamics of a small body, namely the spacecraft, assumed as a point mass m moving in the gravitational field of two massive attractors, the primaries P_1 and P_2.

There are two basic assumptions which characterize the CR3BP:

- The mass of the particle, m, is negligible compared to the masses of the primaries, m_1 and m_2 respectively. This means the motion of the main attractors is not affected by the spacecraft. Thus, the motion of the primaries is Keplerian, orbiting around their common barycenter.
- The primaries move on circular orbits, with constant angular velocity Ω.

The motion of spacecrafts within cislunar environment of the Earth-Moon system will be the main focus of this investigation. The Earth corresponds to the largest primary of the system, while the smaller one will be the Moon. The particularly large mass ratio between the two attractors makes the motion of a spacecraft easily influenced simultaneously by both the primaries. Even if neglecting the eccentricity characterizing the orbit of the Moon around the Earth (average lunar orbit eccentricity $\bar{e}_M = 0.055$) could result in a strong approximation, the CR3BP constitutes a powerful model of the particular gravitational cislunar environment, offering useful insights about the actual dynamics of the system.

The mathematical expression of the dynamics in CR3BP exploits the definition of two reference frames, which are shown in figure 2.1. The inertial $\{\hat{i}\}$-frame is defined by the triad $\hat{\boldsymbol{X}}, \hat{\boldsymbol{Y}}, \hat{\boldsymbol{Z}}$. The $\hat{\boldsymbol{Z}}$-axis is aligned with the direction of the angular velocity of the primaries. The synodic $\{\hat{r}\}$-frame is rotating fixed to the primaries, and is composed by the basis $\hat{\boldsymbol{x}}, \hat{\boldsymbol{y}}, \hat{\boldsymbol{z}}$. Both frames are located at the barycenter of the system, O. At time $t = 0$ the rotating frame is assumed to be aligned with the inertial frame. The rotating frame $\hat{\boldsymbol{x}}$-axis is always aligned with the position vector from P_1 to P_2. The $\hat{\boldsymbol{z}}$-axis is aligned with the direction of the angular velocity of the synodic frame, $\boldsymbol{\omega} = \Omega\hat{\boldsymbol{z}}$. The $\hat{\boldsymbol{y}}$-axis completes the right-handed triad.

The system is uniquely described by the mass parameter μ.

$$\mu = \frac{m_2}{m_1 + m_2} \tag{2.1}$$

Furthermore, the mass parameter μ determines the position in non-dimensional units for the primaries within the rotating frame: P_1 is located at $-\mu$ along $\hat{\boldsymbol{x}}$, while P_2 is located at $1 - \mu$.

The angular velocity Ω of the synodic frame is constant and corresponds to the angular motion of the primaries orbiting on circular orbits.

$$\Omega = \sqrt{\frac{G(m_1 + m_2)}{{R_{12}}^3}} \tag{2.2}$$

Where R_{12} is the distance between the two primaries, and G is the universal gravitational constant.

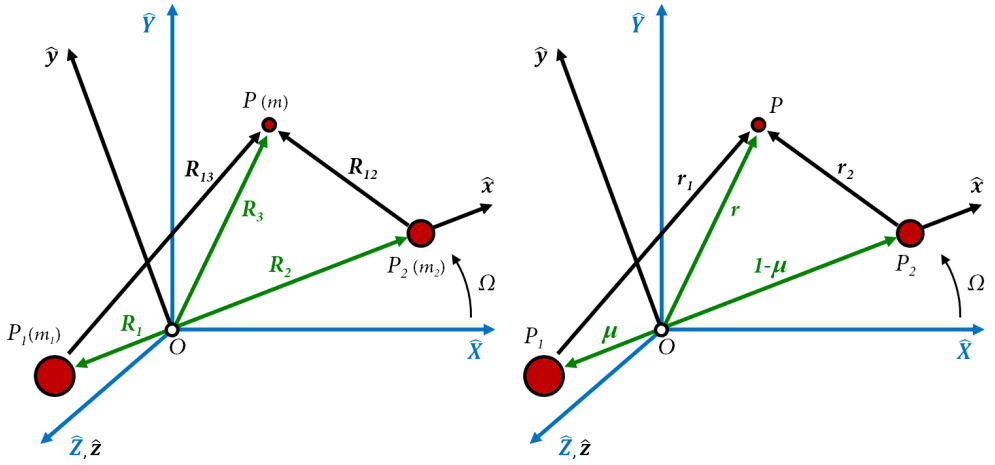

(a) Dimensional CR3BP (b) Non-dimensional CR3BP

Figure 2.1: Graphical representation of the CR3BP model

The orbital period of the system corresponds to the orbital period of the primaries circular orbit which is defined by Keplerian dynamics.

$$T = \frac{2\pi}{\Omega} = 2\pi\sqrt{\frac{{R_{12}}^3}{G(m_1 + m_2)}} \tag{2.3}$$

The equation of motion are typically normalized to simplify and generalize the problem, such that the total mass of the system, the distance between the two attractors, the universal gravitational constant and the angular motion Ω are unitary in non-dimensional units. The main characteristic quantities of the system are length, mass and time. All the other normalization quantities can be derived as a combination of these three characteristic quantities.
The characteristic length corresponds to the distance of the two primaries. The characteristic mass is defined as the total mass of the system, that is the sum of the mass of the two primaries. The characteristic time is selected such that the universal gravitational constant is equal to unity in non-dimensional formulation. As a consequence the non-dimensional orbital period of the primaries results $T = 2\pi$, and the non-dimensional time represents also to the angle θ covered by the rotating frame. Equation (2.3) allows to derive the characteristic time of the system.

$$T^\star = \frac{1}{\Omega} = \sqrt{\frac{{L^\star}^3}{G\,M^\star}} \tag{2.4}$$

The main characteristic quantities of the Earth-Moon (EM) and of the Sun-Earth (SE) systems are summarized in tables 2.1 and 2.2. This work will employ these values in its dynamical model.

Considering only gravitational force, the Newton's law gives the following dimensional equation of motion.

$$\ddot{\boldsymbol{R}}_{\boldsymbol{3}} = \left(\frac{d^2\boldsymbol{R_3}}{dt^2}\right)_i = -\frac{Gm_1}{{R_{13}}^3}\boldsymbol{R_{13}} - \frac{Gm_2}{{R_{23}}^3}\boldsymbol{R_{23}} \tag{2.5}$$

Here, the symbol in bold font $\boldsymbol{R_{13}}$ correspond to the position vector of the body P_3 from P_1, while the same symbol in normal font corresponds to the distance. The same representation is exploited for $\boldsymbol{R_{23}}$, which is the position of the body from P_2.
Thanks to the relation of the derivatives of a vector between an inertial and a rotating frames, the

Parameter	Value	Unit
$L^\star$	384400000	m
$M^\star$	$6.045638 \cdot 10^{24}$	kg
$T^\star$	$3.751578 \cdot 10^{5}$	s
μ	0.01215059	$ndim$
μ_E	$3.986694 \cdot 10^{14}$	m^3/s^2
μ_M	$4.903650 \cdot 10^{12}$	m^3/s^2
R_E	6371000	m
R_M	1738000	m
G	$6.675443 \cdot 10^{-11}$	$m^3/kg \cdot s^2$

Table 2.1: Main characteristic constants of the Earth-Moon system

Parameter	Value	Unit
$L^\star$	149597870700	m
$M^\star$	$1.989006 \cdot 10^{30}$	kg
$T^\star$	$5.021460 \cdot 10^{6}$	s
μ	$3.002595 \cdot 10^{-6}$	$ndim$
μ_S	$1.327745 \cdot 10^{20}$	m^3/s^2
μ_E	$3.986694 \cdot 10^{14}$	m^3/s^2
R_S	695508000	m
R_E	6371000	m
G	$6.675443 \cdot 10^{-11}$	$m^3/kg \cdot s^2$

Table 2.2: Main characteristic constants of the Sun-Earth system

first order time derivatives of the body P_3 is obtained directly in the rotating frame.

$$\left(\frac{d\boldsymbol{R_3}}{dt}\right)_i = \left(\frac{d\boldsymbol{R_3}}{dt}\right)_r + {}^{\hat{i}}\boldsymbol{\omega}^{\hat{r}} \times \boldsymbol{R_3} \tag{2.6}$$

The subscript "i" and "r" represent the differentiation in the inertial and rotating frame, respectively. The term ${}^{\hat{i}}\boldsymbol{\omega}^{\hat{r}}$ is the angular velocity of the rotating frame relative to the inertial.
Deriving a second time, the following relation is obtained.

$$\left(\frac{d^2\boldsymbol{R_3}}{dt^2}\right)_i = \left(\frac{d^2\boldsymbol{R_3}}{dt^2}\right)_r + 2\,{}^{\hat{i}}\boldsymbol{\omega}^{\hat{r}} \times \left(\frac{d\boldsymbol{R_3}}{dt}\right)_r + \left(\frac{d^{\hat{i}}\boldsymbol{\omega}^{\hat{r}}}{dt}\right)_r \times \boldsymbol{R_3} + {}^{\hat{i}}\boldsymbol{\omega}^{\hat{r}} \times \left({}^{\hat{i}}\boldsymbol{\omega}^{\hat{r}} \times \boldsymbol{R_3}\right) \tag{2.7}$$

Now, the relation obtained from equation (2.7) is substituted into the dynamics in (2.5) in order to obtain the dynamical equation of the system expressed in the rotating frame. Then, it can be normalized thanks to the characteristic quantities describing the system.

$$\ddot{\boldsymbol{r}} = \left(\frac{d^2\boldsymbol{r}}{dt^2}\right)_r + 2\,\boldsymbol{\Omega} \times \left(\frac{d\boldsymbol{r}}{dt}\right)_r + \boldsymbol{\Omega} \times (\boldsymbol{\Omega} \times \boldsymbol{r}) = -\frac{1-\mu}{{r_1}^3}\boldsymbol{r_1} - \frac{\mu}{{r_2}^3}\boldsymbol{r_2} \tag{2.8}$$

The left term side of equation (2.8) is expanded in the rotating frame obtaining the following kinematics relation.

$$\ddot{\boldsymbol{r}} = \left(\ddot{x} - 2\,\Omega\dot{y} - \Omega^2 x\right)\hat{\boldsymbol{x}} + \left(\ddot{y} + 2\Omega\dot{x} - \Omega^2 y\right)\hat{\boldsymbol{y}} + \ddot{z}\hat{\boldsymbol{z}} \tag{2.9}$$

Note that the angular velocity Ω is unitary in non-dimensional units, and it has been included here only for completeness.
The right term side of equation (2.8) represents the non-dimensional gravity forces on the spacecraft exerted by the primaries, where the relative position vectors of the spacecraft respect the two primaries, $\boldsymbol{r_1}$ and $\boldsymbol{r_2}$, are written in rotating non-dimensional coordinates.

$$\boldsymbol{r_1} = (x+\mu)\,\hat{\boldsymbol{x}} + y\hat{\boldsymbol{y}} + z\hat{\boldsymbol{z}} \tag{2.10}$$

$$\boldsymbol{r_2} = (x-1+\mu)\,\hat{\boldsymbol{x}} + y\hat{\boldsymbol{y}} + z\hat{\boldsymbol{z}} \tag{2.11}$$

By substituting the equations (2.9), (2.10), and (2.11) into equation (2.8), the second order differential equation of motion for the CR3BP is obtained. Considering the spacecraft orbital states $\boldsymbol{x_{orb}} = [x; y; z; v_x; v_y; v_z]$, expressed in non-dimensional rotating frame, the dynamics equations can be reduced to a system of Ordinary Differential Equations (ODE).

$$\boldsymbol{f}_{\text{CR3BP}} = \begin{cases} \dot{x} = & v_x \\ \dot{y} = & v_y \\ \dot{x} = & v_x \\ \dot{v}_x = & x + 2v_y - \dfrac{(1-\mu)(x+\mu)}{{r_1}^3} - \dfrac{\mu(x-1+\mu)}{{r_2}^3} \\ \dot{v}_y = & y - 2v_x - \dfrac{(1-\mu)y}{{r_1}^3} - \dfrac{\mu y}{{r_2}^3} \\ \dot{v}_z = & -\dfrac{(1-\mu)z}{{r_1}^3} - \dfrac{\mu z}{{r_2}^3} \end{cases} \tag{2.12}$$

Where r_1 and r_2 are the spacecraft relative distance from the first and the second primaries.

$$r_1 = \sqrt{(x+\mu)^2 + y^2 + z^2} \tag{2.13}$$

$$r_2 = \sqrt{(x-1+\mu)^2 + y^2 + z^2} \tag{2.14}$$

The numerical integration of the ODE system (2.12) allows to predict the motion of the spacecraft expressed directly in the rotating frame.
A modified expression of the gravitational potential, also known as pseudo-potential, is introduced.

$$U^*(x,y,z) = \frac{1}{2}\left(x^2+y^2\right) + \frac{1-\mu}{r_1} + \frac{\mu}{r_2} \tag{2.15}$$

The first term represents the centrifugal contribution, while the others terms corresponds to the gravitational potential of the two primaries respectively.
Finally, in the CR3BP there exists an integral of motion, also known as Jacobi constant, which describes the mechanical energy associated to the motion of a spacecraft from the perspective of a rotating observer.

$$JC = 2U^* - \left(\dot{x}^2 + \dot{y}^2 + \dot{z}^2\right) = -2E \tag{2.16}$$

2.2.1 Libration Points

The Libration or Lagrangian Points are the equilibrium points of the CR3BP, locations where the gravitational force of the primaries and the apparent centrifugal force of the rotating frame are balanced. A spacecraft at rest in these locations ideally remains still in the synodic frame, if

nothing perturbs its states.
The location of these equilibria points corresponds to the critical points of the pseudo-potential function $U^*(x, y, z)$.

$$\nabla U^*(x_{eq}, y_{eq}, z_{eq}) = 0 \tag{2.17}$$

The Libration points are typically divided in two groups:

- Three equilibrium solution lie on the x-axis, and are known as Collinear Points. L_1 is located between the two primaries. L_2 is placed beyond the smaller primary. L_3 is the antithesis of the smaller primary P_2. Euler has been the first to notice these Collinear Points in 1765 [30].
- Two equilibrium solution form equilateral triangles with the primaries. For this reason, they are also known as Equilateral Point L_4 and L_5. Lagrange has been the first to identify these Equilateral Points in 1772 [30].

2.2.2 Libration Point Orbits

Periodic orbits seen in the rotating frame constitute an important library to understand and study the complex non-Keplerian dynamical environment.
In the chaotic system described by the CR3BP, numerical scheme are exploited to find periodic solutions Γ which are characterized by seven variable: the initial states $\boldsymbol{x_0} = \{x_0, y_0, z_0, v_{x0}, v_{y0}, v_{z0}\}$ and the orbital period T. A periodic orbit in the dynamical flow $\phi(\boldsymbol{x}, t)$ is defined such that any state along it will recur after an orbital period.

$$\forall \boldsymbol{x} \in \Gamma(\boldsymbol{x_0}, T) \ : \ \boldsymbol{x} = \phi(\boldsymbol{x}, T) \tag{2.18}$$

A generic point along the periodic orbit may be identified by the time of flight, $t_0 \in (0, T)$, the spacecraft has to cover to reach that specific location along the orbit departing from the initial condition. In the CR3BP, the initial reference point is typically chosen as the furthest locus from the primaries.
It is useful define an orbital mean anomaly, or phase angle, to uniquely identify a location of the body m along its LPO.

$$\theta_M = \frac{t_0}{T} \tag{2.19}$$

The orbital mean anomaly over one period is between $\theta_M \in [0, 1]$, where $\theta_M = 0$ means the spacecraft is at its initial location, while after a full orbital period $\theta_M = 1$.
Poincaré showed that an infinite number of periodic solution exists, and many of them are still unknown. Periodic orbits are typically classified in different families, which members share similar motion features. They may be simple and smooth trajectories, but also have very complex and fancy geometry. Some of them may not present a particular attractor like in the Keplerian model, orbiting around one of the Libration Point. Here the definition of Libration Point Orbit (LPO).
There are four main families of LPO of particular interest for mission application in the Eath-Moon system:

- DRO: Distant Retrograde Orbit are planar symmetric orbits orbiting around the Moon (see figure 2.2(a)) which are characterized by high stability properties.
- LYAP: Lyapunov Orbit are planar symmetric orbit, orbiting around L_1 or L_2 (see figure 2.2(b)).
- HALO: Halo Orbit are three-dimensional symmetric orbits, orbiting around L_1 or L_2 (see figure 2.3(a)).

- NRHO: Near Rectilinear Halo Orbit are a subset of the highest Halo orbit (see figure 2.3(b)) which are characterized by an higher stability respect the rest of Halo family. They can be seen as particular lunar-polar orbit with natural precession synchronized with the synodic frame.

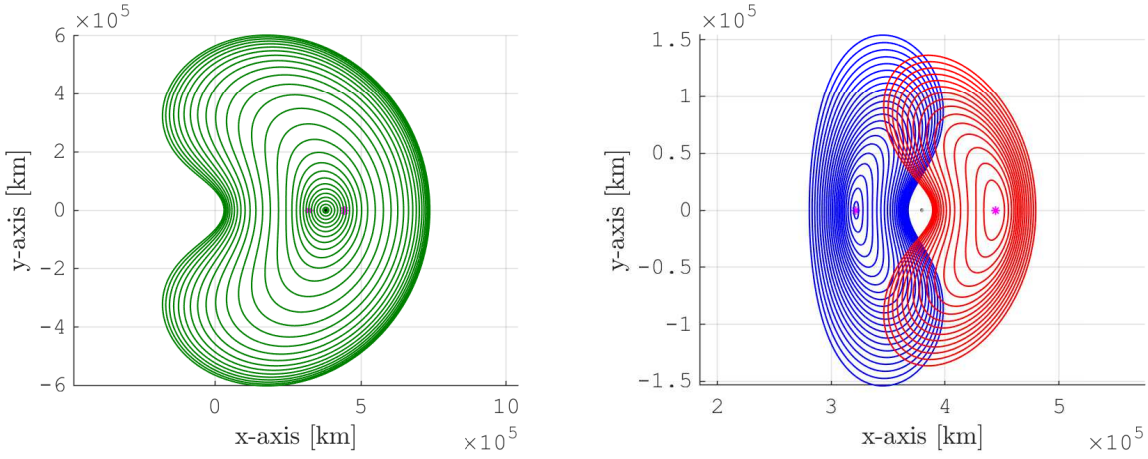

(a) EM DRO orbits (b) EM L1/L2 Lyapunov orbits

Figure 2.2: Families of planar-symmetric non-Keplerian orbits in Earth-Moon system

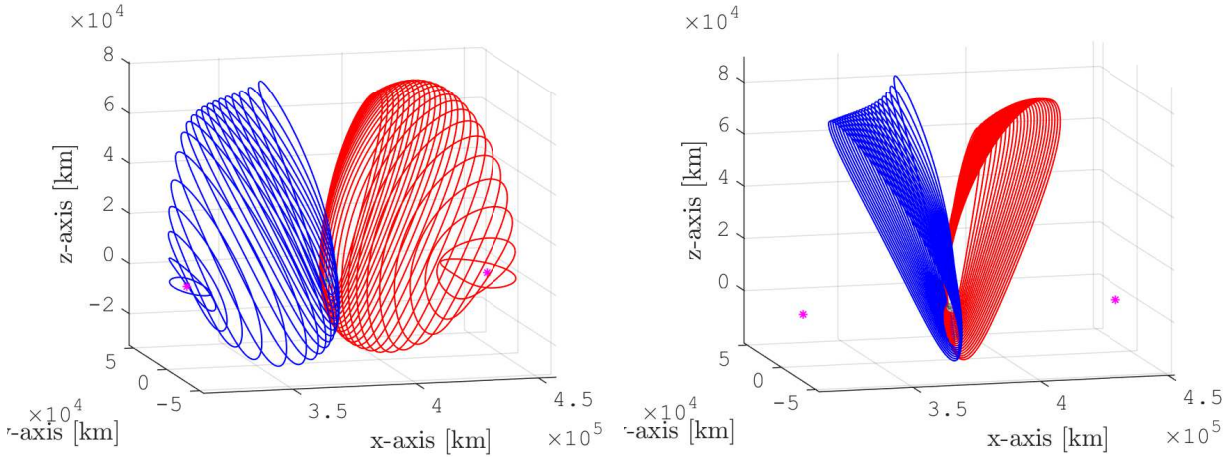

(a) EM L1/L2 Halo orbits (b) EM L1/L2 NRHO orbits

Figure 2.3: Families of three-dimensional symmetric non-Keplerian orbits in Earth-Moon system

Detailed analysis in the Earth-Moon system for DRO, Lyapunov, Halo and NRHO orbits, but also about other important LPO families, has been widely carried out in literature [31, 32].
In this paper, after a general investigation of the phase space of the main families, NRHO will be the focus for the rendezvous and docking (RV&D) scenario application.

2.3 Attitude Dynamics

This discipline rules the orientation of the spacecraft in the three dimensional space and its evolution in time. Basic concept of Attitude Dynamics and Control (ADC) are essential for the development of the orbit-attitude model. Attitude representations, frame transformations, attitude kinematics and dynamics are briefly discussed in the following from a space engineering point of view.

2.3.1 Direction Cosine Matrix

The Direction Cosine Matrix (DCM) is the mother of all the orientation parametrization. By definition, a DCM leads the frame transformation from an initial $\{\hat{a}\}$-frame to a final $\{\hat{b}\}$-frame, which are represented respectively by the vectrices $\{\hat{a}\}$ and $\{\hat{b}\}$.

$$\{\hat{b}\} = [C_{\hat{b}/\hat{a}}]\{\hat{a}\} \tag{2.20}$$

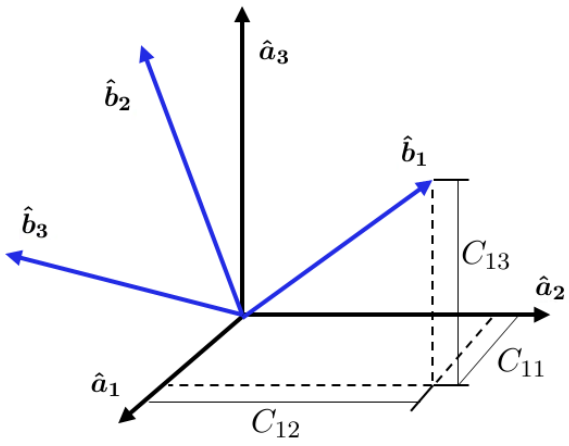

Figure 2.4: Definition of Direction Cosine Matrix

The elements of the DCM $[C_{\hat{b}/\hat{a}}]$ constitute the nine direction cosines of the unit vectors composing the $\{\hat{b}\}$-frame respect to the unit vectors composing the $\{\hat{a}\}$-frame, as it is shown in figure 2.4.

$$C_{ij} \triangleq \cos\left(\angle\hat{\boldsymbol{b}}_{\boldsymbol{i}}, \hat{\boldsymbol{a}}_{\boldsymbol{j}}\right) = \hat{\boldsymbol{b}}_{\boldsymbol{i}} \cdot \hat{\boldsymbol{a}}_{\boldsymbol{j}} \tag{2.21}$$

Therefore, the frame unit vectors are related through the following relation.

$$\begin{aligned}
\hat{\boldsymbol{b}}_{\boldsymbol{1}} &= C_{11}\hat{\boldsymbol{a}}_{\boldsymbol{1}} + C_{12}\hat{\boldsymbol{a}}_{\boldsymbol{2}} + C_{13}\hat{\boldsymbol{a}}_{\boldsymbol{3}} \\
\hat{\boldsymbol{b}}_{\boldsymbol{2}} &= C_{21}\hat{\boldsymbol{a}}_{\boldsymbol{1}} + C_{22}\hat{\boldsymbol{a}}_{\boldsymbol{2}} + C_{23}\hat{\boldsymbol{a}}_{\boldsymbol{3}} \\
\hat{\boldsymbol{b}}_{\boldsymbol{3}} &= C_{31}\hat{\boldsymbol{a}}_{\boldsymbol{1}} + C_{32}\hat{\boldsymbol{a}}_{\boldsymbol{2}} + C_{33}\hat{\boldsymbol{a}}_{\boldsymbol{3}}
\end{aligned} \tag{2.22}$$

By definition, the DCM $[C_{\hat{b}/\hat{a}}]$ is the rotation matrix that transforms a vector $\boldsymbol{v}$ initially expressed in the $\{\hat{a}\}$-frame, into the same vector projected into the final $\{\hat{b}\}$-frame.

$$\underset{\hat{b}}{\boldsymbol{v}} = [C_{\hat{b}/\hat{a}}]\underset{\hat{a}}{\boldsymbol{v}} \tag{2.23}$$

Moreover, according to DCM properties, the inverse transformation corresponds to the transpose.

$$\underset{\hat{a}}{\boldsymbol{v}} = [C_{\hat{a}/\hat{b}}]\underset{\hat{b}}{\boldsymbol{v}} = [C_{\hat{b}/\hat{a}}]^T\underset{\hat{b}}{\boldsymbol{v}} \tag{2.24}$$

2.3.2 Quaternion

Quaternion, also known as Euler parameters, are commonly exploited in space field for numerical simulation of the attitude dynamics. They express the orientation of a $\{\hat{b}\}$-frame respect to

an $\{\hat{a}\}$-frame via a four-dimensional vector, defined as follow.

$$ {}^{\hat{a}}\boldsymbol{q}^{\hat{b}} = \begin{bmatrix} q_1 \\ q_2 \\ q_3 \\ q_4 \end{bmatrix} = \begin{bmatrix} \boldsymbol{q}_{1:3} \\ q_4 \end{bmatrix} = \begin{bmatrix} \hat{\boldsymbol{e}} \sin(\theta/2) \\ \cos(\theta/2) \end{bmatrix} \tag{2.25} $$

Where $\hat{\boldsymbol{e}}$ is the eigenvector of the corresponding DCM, also known as Euler axis of rotation.

$$ \hat{\boldsymbol{e}} = [C_{\hat{b}/\hat{a}}]\hat{\boldsymbol{e}} \tag{2.26} $$

While θ is the rotation angle, also known as Euler angle.

$$ \cos\theta = \frac{1}{2}\left(tr\left([C_{\hat{b}/\hat{a}}]\right) - 1\right) \tag{2.27} $$

A graphical interpretation of a quaternion represents the orientation of an object as a rotation around the axis $\hat{\boldsymbol{e}}$ by an angle θ.
The corresponding DCM of a quaternion describing the orientation of a $\{\hat{b}\}$-frame respect to a $\{\hat{a}\}$-frame is expressed by the following relation.

$$ [C_{\hat{b}/\hat{a}}] = \begin{bmatrix} q_1^2 - q_2^2 - q_3^2 + q_4^2 & 2(q_1q_2 + q_3q_4) & 2(q_1q_3 - q_2q_4) \\ 2(q_1q_2 - q_3q_4) & -q_1^2 + q_2^2 - q_3^2 + q_4^2 & 2(q_2q_3 + q_1q_4) \\ 2(q_1q_3 + q_2q_4) & 2(q_2q_3 - q_1q_4) & -q_1^2 - q_2^2 + q_3^2 + q_4^2 \end{bmatrix} \tag{2.28} $$

The quaternion formulation avoids the gimbal lock singularity, which is present in Euler angles representation, and have to satisfy only one constraint.

$$ q_1^2 + q_2^2 + q_3^2 + q_4^2 = 1 \tag{2.29} $$

It means that one of the quaternion components can be derived knowing the other three, and as a consequence it can be expressed as a function of the remaining three quaternion elements.

2.3.3 Spacecraft Attitude Relative to Inertial and Rotating Frame

The spacecraft attitude is described by the body-fixed frame, labelled $\{\hat{b}\}$-frame, with respect to a given observer, e.g. the reference inertial $\{\hat{i}\}$-frame or the CR3BP rotating $\{\hat{r}\}$-frame.
The direction cosine matrix $[C_{\hat{r}/\hat{i}}]$ of the rotating frame with respect to the reference inertial frame is described through the following matrix.

$$ [C_{\hat{r}/\hat{i}}] = \begin{bmatrix} \cos(t) & \sin(t) & 0 \\ -\sin(t) & \cos(t) & 0 \\ 0 & 0 & 1 \end{bmatrix} \tag{2.30} $$

Knowing the DCM $[C_{\hat{r}/\hat{i}}]$, the corresponding quaternion ${}^{\hat{i}}\boldsymbol{q}^{\hat{r}}$ is directly obtained.

$$ {}^{\hat{i}}\boldsymbol{q}^{\hat{r}} = \begin{bmatrix} 0 \\ 0 \\ \sin(t/2) \\ \cos(t/2) \end{bmatrix} \tag{2.31} $$

Given the quaternion ${}^{\hat{i}}\boldsymbol{q}^{\hat{b}} = [q_1; q_2; q_3; q_4]$ describing the attitude of the spacecraft body-fixed $\{\hat{b}\}$-frame in the inertial reference frame, the corresponding direction cosine matrix $[C_{\hat{b}/\hat{i}}]$ is obtained using equation (2.28). The attitude of the body with respect the rotating frame can be obtained via the product of the DCM.

$$[C_{\hat{b}/\hat{r}}] = [C_{\hat{b}/\hat{i}}]\,[C_{\hat{i}/\hat{r}}] = [C_{\hat{b}/\hat{i}}]\,[C_{\hat{r}/\hat{i}}]^T \tag{2.32}$$

The same result can be obtained using quaternion formalism by applying the rule of successive rotation. Note that the quaternion multiplication has inverse order respect to the direction cosine matrix product.

$${}^{\hat{r}}\boldsymbol{q}^{\hat{b}} = {}^{\hat{r}}\boldsymbol{q}^{\hat{i}} \odot {}^{\hat{i}}\boldsymbol{q}^{\hat{b}} = \left({}^{\hat{i}}\boldsymbol{q}^{\hat{r}}\right)^{-1} \odot {}^{\hat{i}}\boldsymbol{q}^{\hat{b}} = \left[\left({}^{\hat{i}}\boldsymbol{q}^{\hat{r}}\right)^{-1} \odot\right] {}^{\hat{i}}\boldsymbol{q}^{\hat{b}} \tag{2.33}$$

The operator $[\boldsymbol{q}\odot]$ is the quaternion left product operator, as it is defined in [33], and corresponds to the MATLAB function "quatmultiply.m".

$$[\boldsymbol{q}\odot] \triangleq \begin{bmatrix} q_4\, I_3 + [\boldsymbol{q}_{1:3}\times] & \boldsymbol{q}_{1:3} \\ -\boldsymbol{q}_{1:3}{}^T & q_4 \end{bmatrix} = \begin{bmatrix} \Psi(\boldsymbol{q}) & \boldsymbol{q} \end{bmatrix} \tag{2.34}$$

Where I_3 is the 3-by-3 identity matrix, while $[\boldsymbol{u}\times]$ is the cross-product matrix operator.

$$[\boldsymbol{u}\times] \triangleq \begin{bmatrix} 0 & -u_3 & u_2 \\ u_3 & 0 & -u_1 \\ -u_2 & u_1 & 0 \end{bmatrix} \tag{2.35}$$

Therefore, the matrix form of equation (2.33) is obtained.

$${}^{\hat{r}}\boldsymbol{q}^{\hat{b}} = \begin{bmatrix} \cos(t/2) & \sin(t/2) & 0 & 0 \\ -\sin(t/2) & \cos(t/2) & 0 & 0 \\ 0 & 0 & \cos(t/2) & -\sin(t/2) \\ 0 & 0 & \sin(t/2) & \cos(t/2) \end{bmatrix} \begin{bmatrix} q_1 \\ q_2 \\ q_3 \\ q_4 \end{bmatrix} \tag{2.36}$$

2.3.4 Quaternion Kinematics

Let be $\{\hat{a}\}$ and $\{\hat{b}\}$ two frames which are moving relative to each other. The angular velocity of the $\{\hat{b}\}$-frame respect to the $\{\hat{a}\}$-frame can be expressed via the following expression.

$${}^{\hat{a}}_{\hat{b}}\boldsymbol{\omega}^{\hat{b}} = \omega_1 \hat{\boldsymbol{b}}_{\boldsymbol{1}} + \omega_2 \hat{\boldsymbol{b}}_{\boldsymbol{2}} + \omega_3 \hat{\boldsymbol{b}}_{\boldsymbol{3}} \tag{2.37}$$

Where the components $\omega_1(t)$, $\omega_2(t)$ and $\omega_3(t)$ may be in general a function of time t. The relative angular velocity leads to a time evolution of the relative attitude. Given the relative quaternion ${}^{\hat{a}}\boldsymbol{q}^{\hat{b}} = [q_1; q_2; q_3; q_4]$, the following kinematics equation holds.

$$\begin{bmatrix} \dot{q}_1 \\ \dot{q}_2 \\ \dot{q}_3 \\ \dot{q}_4 \end{bmatrix} = \frac{1}{2} \begin{bmatrix} 0 & \omega_3 & -\omega_2 & \omega_1 \\ -\omega_3 & 0 & \omega_1 & \omega_2 \\ \omega_2 & -\omega_1 & 0 & \omega_3 \\ -\omega_1 & -\omega_2 & -\omega_3 & 0 \end{bmatrix} \begin{bmatrix} q_1 \\ q_2 \\ q_3 \\ q_4 \end{bmatrix} = \frac{1}{2} \left[\boldsymbol{\Omega}({}^{\hat{a}}\boldsymbol{\omega}^{\hat{b}})\right] {}^{\hat{a}}\boldsymbol{q}^{\hat{b}} \tag{2.38}$$

Where the matrix operator $[\boldsymbol{\Omega}(\boldsymbol{\omega})]$ is a 4-by-4 skew-symmetric matrix.

$$\Omega(\boldsymbol{\omega}) \triangleq \begin{bmatrix} -[\boldsymbol{\omega}\times] & \boldsymbol{\omega} \\ -\boldsymbol{\omega}^T & 0 \end{bmatrix} \tag{2.39}$$

The numerical integration of equation (2.38) allows to determine the attitude profile in function of time t. The propagation process applies at each integration step the quaternion normalization to satisfy the quaternion constraint.

2.3.5 Dynamics Equations

The dynamics equation describing the rotational motion for a rigid body are directly derived from the angular momentum conservation law. This vectorial differential equations is known in literature as Euler equation.
Let be $\{\hat{b}\}$ the body-fixed frame anchored at the center of mass of the body and aligned to its principal axis of inertia. Let be ${}^{\hat{i}}\boldsymbol{\omega}^{\hat{b}} = \omega_1\hat{\boldsymbol{b}}_{\mathbf{1}} + \omega_2\hat{\boldsymbol{b}}_{\mathbf{2}} + \omega_3\hat{\boldsymbol{b}}_{\mathbf{3}}$ the angular velocity of the spacecraft respect the inertial $\{\hat{i}\}$, and expressed in the body-fixed frame coordinates. If the body-fixed frame $\{\hat{b}\}$ is aligned to the principal axis of inertia, the angular momentum conservation law is simplified to the following set of scalar differential equation.

$$\begin{cases} \dot{\omega}_1 = \dfrac{I_2 - I_3}{I_1}\omega_2\omega_3 + \dfrac{M_1}{I_1} \\ \dot{\omega}_2 = \dfrac{I_3 - I_1}{I_2}\omega_1\omega_3 + \dfrac{M_2}{I_2} \\ \dot{\omega}_3 = \dfrac{I_1 - I_2}{I_3}\omega_1\omega_2 + \dfrac{M_3}{I_3} \end{cases} \tag{2.40}$$

Here, $\boldsymbol{M} = M_1\hat{\boldsymbol{b}}_1 + M_2\hat{\boldsymbol{b}}_2 + M_3\hat{\boldsymbol{b}}_3$ represents the general external torques applied to the body center of mass. An analytical solution of the system may exist for particular system configuration, e.g. torque-free motion. For a generic time-varying torque function, the differential equations in (2.40) are numerically integrated to obtain the solution of the angular velocity evolution.

2.4 CR3BP Orbit-Attitude Model

A generic extended, three-dimensional, and rigid body (e.g. a spacecraft) has six degrees of freedom: the position of its center of mass and the orientation of its body-fixed frame. It follows that it requires six dynamics equations, plus those required to determine the kinematics relations which allow to obtain a system of ordinary differential equations.

In this investigation the orbit-attitude dynamical model is developed within the non-dimensional Circular Restricted Three-Body Problem framework. The orbital states $\boldsymbol{x_{orb}} = [x; y; z; v_x; v_y; v_z]$ are expressed in the rotating frame $\{\hat{r}\}$. The body-fixed frame $\{\hat{b}\}$ is located at the center of mass of the spacecraft and aligned with the principal axis of inertia directions $\hat{\boldsymbol{b}}_{\mathbf{1}}, \hat{\boldsymbol{b}}_{\mathbf{2}}, \hat{\boldsymbol{b}}_{\mathbf{3}}$. The four-dimensional quaternion vector ${}^{\hat{i}}\boldsymbol{q}^{\hat{b}} = [q_1; q_2; q_3; q_4]$ is selected as attitude parameter. It relates the orientation of the $\{\hat{b}\}$-frame to the reference $\{\hat{i}\}$-frame. The angular velocity of the spacecraft ${}^{\hat{i}}\boldsymbol{\omega}^{\hat{b}} = [\omega_1; \omega_2; \omega_3]$ is defined as the relative angular velocity of the body respect to the $\{\hat{i}\}$-frame and is expressed in the $\{\hat{b}\}$-frame. A simple grafical representation of the coupled orbit-attitude model is sketched in figure 2.5. In this illustration the spacecraft is represented as a solid cube. The blue vectors represent the inertial $\{\hat{i}\}$-frame, the black vectors indicate the synodic $\{\hat{r}\}$-frame, and the red vectors describe the body-fixed $\{\hat{b}\}$-frame of the spacecraft.

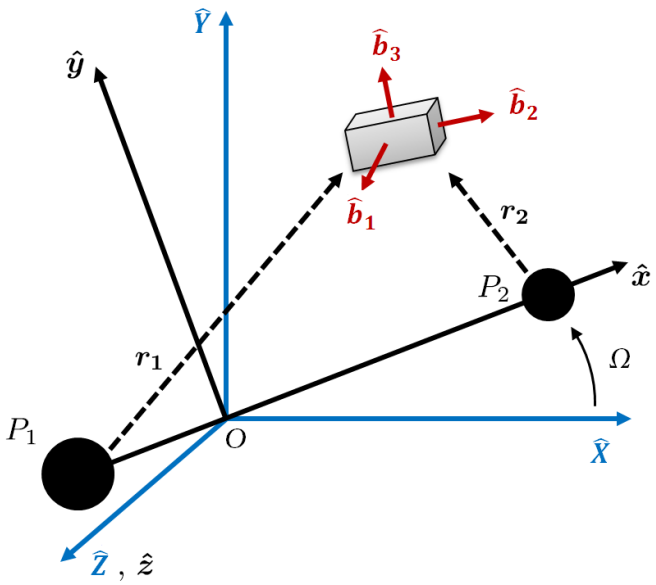

Figure 2.5: Sketch of the coupled orbit-attitude CR3BP model. Not in scale.

The coupled orbit-attitude system can be formulated in the following set of vectorial differential equations.

$$\begin{cases} \dot{\boldsymbol{x}}_{\boldsymbol{orb}} &= \boldsymbol{f}_{\boldsymbol{orb}}\left(\boldsymbol{x}_{\boldsymbol{orb}}, {}^{\hat{i}}\boldsymbol{q}^{\hat{b}}, {}^{\hat{i}}\boldsymbol{\omega}^{\hat{b}}, t\right) \\ {}^{\hat{i}}\dot{\boldsymbol{q}}^{\hat{b}} &= \boldsymbol{f}_{\boldsymbol{q}}\left(\boldsymbol{x}_{\boldsymbol{orb}}, {}^{\hat{i}}\boldsymbol{q}^{\hat{b}}, {}^{\hat{i}}\boldsymbol{\omega}^{\hat{b}}, t\right) \\ {}^{\hat{i}}\dot{\boldsymbol{\omega}}^{\hat{b}} &= \boldsymbol{f}_{\boldsymbol{\omega}}\left(\boldsymbol{x}_{\boldsymbol{orb}}, {}^{\hat{i}}\boldsymbol{q}^{\hat{b}}, {}^{\hat{i}}\boldsymbol{\omega}^{\hat{b}}, t\right) \end{cases} \tag{2.41}$$

The generic functions at the right hand side of this system are characterized in the following sections considering the gravity effects exerted by the two primaries (e.g. the Earth and the Moon) on a rigid body of finite dimensions, the Solar Radiation Pressure (SRP) and the gravitational pull exerted by a fourth body (e.g. the Sun for the Earth-Moon system).

2.4.1 Gravity Force Exerted by a Particle on an Extended Body

Within the framework of the CR3BP, the two primaries are lumped at their barycenter as point-masses. A simple illustration of an extended (not necessarily rigid) body floating within the gravity field of an attractor is sketched in figure 2.6. The total net force $\boldsymbol{F_i}$ exerted on a small extended body of mass m by the i-th primary P_i of mass m_i can be expressed as the integral of all gravity forces over the entire body $\mathfrak{B}$.

$$\boldsymbol{F_i} = \int_{\mathfrak{B}} d\boldsymbol{F_g} = -Gm_i \int_{\mathfrak{B}} \frac{\boldsymbol{R_i}}{{R_i}^3} dm \tag{2.42}$$

Where $d\boldsymbol{F_g} = -\frac{Gm_i\, dm}{{R_i}^2}\frac{\boldsymbol{R_i}}{R_i}$ is the gravity force acting on the infinitesimal mass dm. The vector $\boldsymbol{R_i} = (\boldsymbol{R_{G,i}} + \boldsymbol{\rho})$ is the position of dm respect the primary P_i, the position of the center of mass of the body respect to the i-th primary is $\boldsymbol{R_{G,i}}$ and $\boldsymbol{\rho}$ is the position of dm from the barycenter G of the body.
This body integral can be approximated via the following series expansion, as shown in [34].

$$\boldsymbol{F_i} = -\frac{Gmm_i}{{R_i}^2}\left(\hat{\boldsymbol{R}}_{\boldsymbol{Bi}} + \sum_{j=2}^{\infty} \boldsymbol{f}^{(j)}\right) \tag{2.43}$$

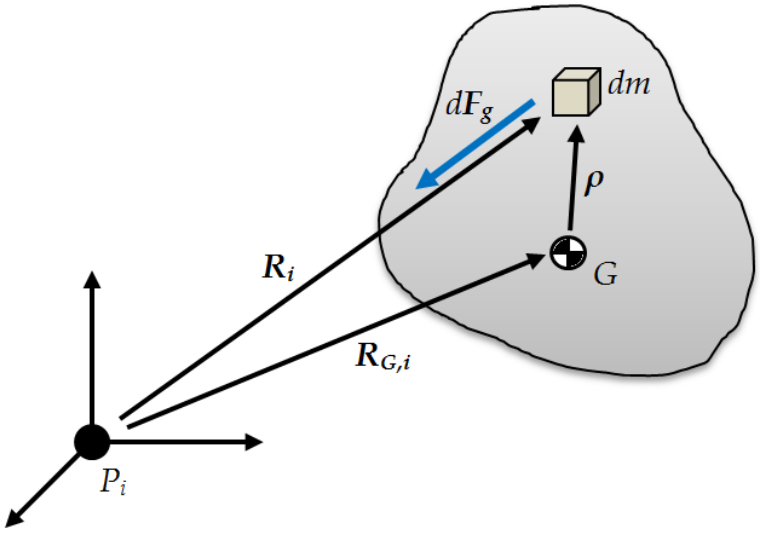

Figure 2.6: Sketch of an extended body under the influence of the gravity field of an attractor.

The elements $\boldsymbol{f}^{(j)}$ are a collection of terms proportional to the j-th power of $\|\boldsymbol{\rho}\|/R_i$, where ρ is the distance of a generic point of the body with respect to its center of mass. This expansion is valid when $\|\boldsymbol{\rho}\| \ll R_i$, which is a reasonable assumption considering a spacecraft orbiting in the Earth-Moon system. Note that the first element in the bracket corresponds to the usual gravity force due to attraction of two point masses, which is already considered in the traditional CR3BP. The summation term represents the variation of gravitational attraction due to the extended body. Approximating the net force in (2.43) up to the second order expansion, the only survival term of the series is $\boldsymbol{f}^{(2)}$. This term is given by the following expression.

$$\boldsymbol{f}^{(2)} = \frac{1}{m\,{R_i}^2}\left\{\frac{3}{2}[tr([\mathbb{I}]) - 5\hat{\boldsymbol{a}}_{\mathbf{1}} \cdot [\mathbb{I}] \cdot \hat{\boldsymbol{a}}_{\mathbf{1}}]\,\hat{\boldsymbol{a}}_{\mathbf{1}} + 3[\mathbb{I}] \cdot \hat{\boldsymbol{a}}_{\mathbf{1}}\right\} \tag{2.44}$$

The tensor $[\mathbb{I}]$ is the central inertia dyadic tensor of the body about its center of mass. The attitude is needed to find the direction cosines of the body with respect to the frame $\{A_i\}$, defined by the axis $\{\hat{\boldsymbol{a}}_{\mathbf{1}}, \hat{\boldsymbol{a}}_{\mathbf{2}}, \hat{\boldsymbol{a}}_{\mathbf{3}}\}$. The first axis is aligned with the radial from the i-th primary, while the other two form a right-handed orthogonal triad. They are chosen to be mutually perpendicular to $\hat{\boldsymbol{r}}_{\boldsymbol{i}}$ and $\hat{\boldsymbol{z}}$. This definition can't be exploited if the body passes through the vertical $\hat{\boldsymbol{z}}$ of one of the primaries and, if the case, an alternative definition has to be found. However, the classical Halo and NRHO orbits are expected to not have passages through the $\hat{\boldsymbol{z}}$-axis, therefore the former definition is employed without encountering singularities.
A compact formulation of $\boldsymbol{f}^{(2)}$ is obtained employing variable moments and products of inertia, which are defined as $I_{jk} \triangleq \hat{\boldsymbol{a}}_{\boldsymbol{j}} \cdot [\mathbb{I}] \cdot \hat{\boldsymbol{a}}_{\boldsymbol{k}}$.

$$\boldsymbol{f}^{(2)} = \frac{3}{m\,{R_i}^2}\left[\frac{1}{2}(I_{22} + I_{33} - 2I_{11})\,\hat{\boldsymbol{a}}_{\mathbf{1}} + I_{21}\hat{\boldsymbol{a}}_{\mathbf{2}} + I_{31}\hat{\boldsymbol{a}}_{\mathbf{3}}\right] \tag{2.45}$$

Employing the principal moments of inertial defined as $I_j \triangleq \hat{\boldsymbol{b}}_{\boldsymbol{j}} \cdot [\mathbb{I}] \cdot \hat{\boldsymbol{b}}_{\boldsymbol{j}}$, the effect of the body orientation become explicit through the direction cosines $C_{ij} \triangleq \hat{\boldsymbol{a}}_{\boldsymbol{i}} \cdot \hat{\boldsymbol{b}}_{\boldsymbol{j}}$.

$$\begin{aligned} \boldsymbol{f}^{(2)} = \frac{3}{m\,{R_i}^2}\Bigg\{ & \frac{1}{2}\left[I_1(1-3{C_{11}}^2)+I_2(1-3{C_{12}}^2)+I_3(1-3{C_{13}}^2)\right]\hat{\boldsymbol{a}}_{\boldsymbol{1}} \\ & +(I_1C_{21}C_{11}+I_2C_{22}C_{12}+I_3C_{23}C_{13})\hat{\boldsymbol{a}}_{\boldsymbol{2}} \\ & +(I_1C_{31}C_{11}+I_2C_{32}C_{12}+I_3C_{33}C_{13})\hat{\boldsymbol{a}}_{\boldsymbol{3}}\Bigg\} \end{aligned} \tag{2.46}$$

It follows that the order of magnitude of the second order term of the net force exerted on a finite dimension body by a primary attractor compared to the classical point-mass approximation is

$$\|\boldsymbol{f}^{(2)}\| \sim \left(\frac{l^{\star}_{SC}}{R_i}\right)^2 \tag{2.47}$$

Where $l^{\star}_{SC}$ represents a characteristic length of the spacecraft, intrinsically linked to the ratio between its inertial moments and its mass. For a rough computation to understand what could be the magnitude of this term, let consider as a reference the International Space Station (ISS) and let suppose its characteristic length could be in the order of $l^{\star} = 100$ meters. If the ISS would orbiting on an NRHO in the Earth-Moon system, the order magnitude of the perturbation due to the second-order term of the net force exerted by the attraction of the Moon at the perilune passage (about 3000 km) will be an infinitesimal $o(10^{-9})$ compared to the point-mass approximation term. Moreover, this infinitesimal becomes $o(10^{-12})$ at the apolune zone of the NRHO. For smaller spacecraft, these infinitesimal becomes even smaller due to the quadratic relation shown above. Instead, an asteroid mission scenario may have distances from the primaries R_i much closer to the values of $l^{\star}_{SC}$. Thus, it is expected to have significant contribution due to this coupling effect.
From equations (2.43) and (2.46), the acceleration term due to variation considering a finite extended body is obtained.

$$\begin{aligned} \hat{\boldsymbol{a}}_{\boldsymbol{i}}{}^{(2)} = -\frac{3\,\mu_i}{m\,{R_i}^4}\Bigg\{ & \frac{1}{2}\left[I_1(1-3{C_{11}}^2)+I_2(1-3{C_{12}}^2)+I_3(1-3{C_{13}}^2)\right]\hat{\boldsymbol{a}}_{\boldsymbol{1}} \\ & +(I_1C_{21}C_{11}+I_2C_{22}C_{12}+I_3C_{23}C_{13})\hat{\boldsymbol{a}}_{\boldsymbol{2}} \\ & +(I_1C_{31}C_{11}+I_2C_{32}C_{12}+I_3C_{33}C_{13})\hat{\boldsymbol{a}}_{\boldsymbol{3}}\Bigg\} \end{aligned} \tag{2.48}$$

The perturbing acceleration exerted by the two primaries on the body due to its finite extension has to be included coherently in the coupled orbit-attitude system. Therefore, $\hat{\boldsymbol{a}}_{\boldsymbol{i}}{}^{(2)}$ has to be transformed from body $\{\hat{b}\}$-frame to synodic $\{\hat{r}\}$-frame coordinates, and has to be non-dimensionalized respect the CR3BP formulation.

2.4.2 Gravity Torque Exerted by a Particle on an Extended Body

Let consider again the model sketched in figure 2.6. The system of gravitational forces exerted on a (not necessarily rigid) body $\mathfrak{B}$ of mass m by a particle P_i of mass m_i may produce a moment $\boldsymbol{M_i}$ about the center of mass of the body.

$$\boldsymbol{M_i} = \int_{\mathfrak{B}} \boldsymbol{\rho} \times d\boldsymbol{F_g} = -\int_{\mathfrak{B}} \boldsymbol{\rho} \times \frac{Gm_i}{{R_i}^3}(\boldsymbol{R_{G,i}} + \boldsymbol{\rho})dm \tag{2.49}$$

As before, considering a spacecraft orbiting in the Earth-Moon system, the condition $\|\boldsymbol{\rho}\| \ll R_i$ is a reasonable assumption. Therefore, it is possible to approximate the body integral as a series expansion [34].

$$\boldsymbol{M_i} = \frac{3Gm_i}{{R_i}^3}\hat{\boldsymbol{a}}_\mathbf{1} \times [\mathbb{I}] \cdot \hat{\boldsymbol{a}}_\mathbf{1} + \frac{Gmm_i}{R_i}\sum_{j=3}^{\infty}\boldsymbol{m}^{(j)} \tag{2.50}$$

The first term at the right hand side is the classical gravity gradient torque. The terms of the summation, $\boldsymbol{m}^{(j)}$ are proportional to the j-th power of $\|\boldsymbol{\rho}\|/R_i$. They are infinitesimal with order higher than the second, hence they can be neglected. This means that the approximation up to the second order for the torque exerted by the gravity attraction of the i-th primary on an extended body corresponds to the classical gravity gradient torque.

$$\boldsymbol{M_i} \approx \frac{3Gm_i}{{R_i}^3}\Big[(I_3 - I_2)C_{12}C_{13}\hat{\boldsymbol{b}}_\mathbf{1} + (I_1 - I_3)C_{11}C_{13}\hat{\boldsymbol{b}}_\mathbf{2} + (I_2 - I_1)C_{11}C_{12}\hat{\boldsymbol{b}}_\mathbf{3}\Big] \tag{2.51}$$

There are particular shapes of body that can make the gravity gradient torque equal to zero. This happens when all the principal moments of inertia are equal, e.g. for a sphere or for a cube. Moreover, there are particular attitude configuration so that the gravity gradient torque goes to zero for any shape of the body. This happens when one of the principal axis of inertia is aligned with the orbital radial axis respect the i-th primary.
The gravity gradient torque defined in equation (2.51) is expressed in body-fixed frame coordinates. Therefore, it can be directly added to the attitude dynamics after non-dimensionalization respect the CR3BP formulation.

2.4.3 Fourth Body Effects

Considering the Earth-Moon system, the gravitational presence of the Sun is one of the most important perturbation effects that should be considered in higher-fidelity model, especially when the body is at significant distance from the two primaries.
The position of Sun is determined exploiting the numerical integration of ephemeris models in the SPICE Toolkit by NASA/JPL. The ephemerides returns the position of the Sun respect the Earth-Moon barycenter expressed in inertial Ecliptic J2000 coordinates, at a given date-time. It should be noticed that in general, the reference inertial $\{\hat{\imath}\}$-frame is not aligned with the inertial Ecliptic J2000 $\{\hat{I}\}$-frame, therefore the Sun position is projected on the instantaneous synodic $\{\hat{r}\}$-frame, which is built exploiting the ephemerides of Earth and Moon (the detailed procedure can be found in section 2.6.1). This modelling assumption allows to obtain an enhanced version of the Bi-Circular Fourth-Body Problem.
The fourth-body gravitational force has been formulated following the standards of the well-known N-body formulation.

$$\boldsymbol{F_{4th}} = -Gmm_S\left(\frac{\hat{\boldsymbol{R}}_{\boldsymbol{BS}}}{{R_{BS}}^2} - \frac{\hat{\boldsymbol{R}}_{\boldsymbol{OS}}}{{R_{OS}}^2}\right) \tag{2.52}$$

The mass of the Sun is denoted as m_S, $\hat{\boldsymbol{R}}_{\boldsymbol{BS}}$ and R_{BS} are the direction and the magnitude of the position vector from the Sun to the center of mass of the body m, while $\hat{\boldsymbol{R}}_{\boldsymbol{OS}}$ and R_{OS} are the direction and the magnitude of the position vector from the Sun to the barycenter of the Earth-Moon system O. The perturbing acceleration on the spacecraft due to the fourth-body gravitational attraction is obtained directly from equation (2.52). Finally, the normalization for the CR3BP formalization is required to include the acceleration term in the orbital dynamics

equations.

$$\boldsymbol{a_{4th}} = -\mu_S \left(\frac{\hat{\boldsymbol{r}}_{\boldsymbol{BS}}}{{r_{BS}}^2} - \frac{\hat{\boldsymbol{r}}_{\boldsymbol{OS}}}{{r_{OS}}^2} \right) \tag{2.53}$$

A spacecraft experiences the gravitational field of the Sun is subjected to a gravity gradient torque, exactly like it happens for the Earth and the Moon.

$$\boldsymbol{M_{4th}} = \frac{3Gm_S}{{R_{BS}}^3} \left[(I_3 - I_2)c_2c_3\hat{\boldsymbol{b}}_{\boldsymbol{1}} + (I_1 - I_3)c_1c_3\hat{\boldsymbol{b}}_{\boldsymbol{2}} + (I_2 - I_1)c_1c_2\hat{\boldsymbol{b}}_{\boldsymbol{3}} \right] \tag{2.54}$$

Now the terms c_j are the direction cosines of the spacecraft position relative to the Sun expressed in principal axis of inertia of the body, $\{\hat{b}\}$-frame. Once normalized respect the CR3BP formulation, the gravity gradient torque due to the Sun is included in the rotational dynamics of the spacecraft.

2.4.4 Solar Radiation Pressure Effects

Radiation pressure is the pressure exerted upon any surface due to the exchange of momentum coming from the interaction of an electromagnetic field investing a non-transparent object.
Any body with temperature above absolute zero $0°K$ emits radiation. Within the context of the Earth-Moon system, the most important radiation pressure effect is coming from the Sun. Therefore, only the Solar Radiation Pressure (SRP) has been modelled in this investigation. However, the same procedure can be followed to consider radiation pressure effect due to other sources, such as the infrared radiation of the Earth or of the Moon.

The total SRP effect is obtained as the summation of forces and torques acting on the illuminated surface of the spacecraft. For sake of simplicity, the actual external surface of the spacecraft is discretized in N planar surfaces.
The force generated due to the solar radiation pressure interaction with a body is approximated considering the radiation pressure effect on flat surfaces and modelling the real body of the spacecraft as an ensemble of N flat surfaces with proper optical properties. The self-shadowing effect can be also taken into account with simple geometrical considerations knowing the Sun direction and the spacecraft orientation.
The force acting on a flat surface illuminated by a radiation can be characterized as

$$\boldsymbol{F}_i = -PA_i \left(\rho_a(\hat{\boldsymbol{s}}_b \cdot \hat{\boldsymbol{n}}_i)\hat{\boldsymbol{s}}_b + 2\rho_r(\hat{\boldsymbol{s}}_b \cdot \hat{\boldsymbol{n}}_i)^2\hat{\boldsymbol{n}}_i + \rho_d(\hat{\boldsymbol{s}}_b \cdot \hat{\boldsymbol{n}}_i) \left(\hat{\boldsymbol{s}}_b + \frac{2}{3}\hat{\boldsymbol{n}}_i \right) \right) \tag{2.55}$$

Where $\hat{\boldsymbol{s}}_b$ is the versor (expressed in body-fixed frame) representing the Sun direction from the spacecraft, and $\hat{\boldsymbol{n}}_i$ is the normal outward to the i-th surface (in body-fixed frame). The area of the i-th surface of the spacecraft is A_i, while the coefficients ρ_a, ρ_r, ρ_d are respectively the absorption coefficient, the specular reflection coefficient and the diffusive reflection coefficient characterizing the optical properties of the i-th surface.
The radiation pressure P is modelled as typically done in astrodynamics literature. The irradiance of the Sun at a distance of an astronomical unit (AU) is equal to $\varphi_0 \simeq 1361$ W/m^2. This is also referred as solar constant, representing the mean flux density of the solar electromagnetic radiation per unit area measured at the mean distance of the Earth from the Sun. The irradiance is related to the distance of the source via an inverse square law. Therefore the radiation pressure of the Sun at a generic distance can be formulated.

$$P = \frac{\varphi}{c} = \frac{\varphi_0}{R^2}\frac{1}{c} \tag{2.56}$$

Where R is the distance from the Sun expressed in AU, and c is the speed of light in vacuum. The relation linking the optical coefficients allows to write equation (2.55) in a more compact way.

$$\boldsymbol{F}_i = -PA_i(\hat{\boldsymbol{s}}_b \cdot \hat{\boldsymbol{n}}_i)\left((1-\rho_r)\hat{\boldsymbol{s}}_b + \left(2\rho_r(\hat{\boldsymbol{s}}_b \cdot \hat{\boldsymbol{n}}_i) + \frac{2}{3}\rho_d\right)\hat{\boldsymbol{n}}_i\right) \tag{2.57}$$

If the spacecraft is not in eclipse, the illumination condition for the i-th surface is $\hat{\boldsymbol{s}}_b \cdot \hat{\boldsymbol{n}}_i > 0$.

$$\boldsymbol{F}_i = \begin{cases} \boldsymbol{F}_i & \text{if} \quad \hat{\boldsymbol{s}}_b \cdot \hat{\boldsymbol{n}}_i > 0 \\ 0 & \text{if} \quad \hat{\boldsymbol{s}}_b \cdot \hat{\boldsymbol{n}}_i \leq 0 \end{cases} \tag{2.58}$$

Finally, the net force due to SRP acting on the center of mass (CoM) of the spacecraft is obtained as vectorial summation of all the $\boldsymbol{F}_i$ and considering the corresponding illumination condition for each surface.

$$\boldsymbol{F}_{SRP} = \sum_{i=1}^{N} \boldsymbol{F}_i \tag{2.59}$$

The term $\boldsymbol{F}_{SRP}$ is expressed in the body-fixed frame. Therefore, it has to be transformed to the synodic frame to be added coherently into the equation of motion of the orbital states.
The solar radiation torque can be obtained knowing the position of center of pressure with respect to the body CoM for each face of the spacecraft model.

$$\boldsymbol{M}_{SRP} = \sum_{i=1}^{N} \boldsymbol{M}_i = \sum_{i=1}^{N} \boldsymbol{c}_{\boldsymbol{p}_i} \times \boldsymbol{F}_i \tag{2.60}$$

The acceleration perturbation is obtained knowing the mass of the spacecraft. Then, it has to be non-dimensionalize and to be expressed in synodic frame coordinates to be added at the orbital dynamics. Analogously, the torque has to be non-dimensionalized and expressed in body-fixed frame coordinates. Thus it can be added into the attitude dynamics.

2.4.5 Orbit-Attitude Simplified-Coupled Dynamics

A simplified version of the coupled orbit-attitude dynamical model is proposed to consider the solely one-way inertial coupling of the orbital motion on the attitude dynamics, which is manifested though the gravity gradient torque. All the other perturbations, such as the solar radiation effect, have been neglected in this first approximation.
In this model assumption, the gravitational pull of the primaries is neglecting the variational term due to the finite extension of the spacecraft. Therefore, the orbital dynamics are modelled via the classical CR3BP dynamical model valid for the point-mass approximation of the spacecraft, which has been presented as the system of equations $\boldsymbol{f}_{\text{CR3BP}}$ in (2.12).
The rotational dynamics is expressed through the Euler equation of motion including the gravity gradient torque acting on the spacecraft due to the two primaries and no other external torques.

$$\boldsymbol{f}_{\boldsymbol{\omega}} = \begin{cases} \dot{\omega}_1 = & \dfrac{I_3 - I_2}{I_1}\left(\dfrac{3(1-\mu)}{{r_1}^5}g_2 g_3 + \dfrac{3\mu}{{r_2}^5}h_2 h_3 - \omega_2\omega_3\right) \\ \dot{\omega}_2 = & \dfrac{I_1 - I_3}{I_2}\left(\dfrac{3(1-\mu)}{{r_1}^5}g_1 g_3 + \dfrac{3\mu}{{r_2}^5}h_1 h_3 - \omega_1\omega_3\right) \\ \dot{\omega}_3 = & \dfrac{I_2 - I_1}{I_3}\left(\dfrac{3(1-\mu)}{{r_1}^5}g_1 g_2 + \dfrac{3\mu}{{r_2}^5}h_1 h_2 - \omega_1\omega_2\right) \end{cases} \tag{2.61}$$

In this formulation the attitude of the spacecraft enters in the terms g_i and h_i, which represents the direction cosines of the radial vector going from one of the two primaries to the spacecraft respect the body-fixed frame of the vehicle.

$$\boldsymbol{g} = [A_{\hat{b}/\hat{i}}][A_{\hat{i}/\hat{r}}]\,\boldsymbol{r_1} \tag{2.62}$$

$$\boldsymbol{h} = [A_{\hat{b}/\hat{i}}][A_{\hat{i}/\hat{r}}]\,\boldsymbol{r_2} \tag{2.63}$$

Note that the set of equation describing the Simplified-Coupled Model are applicable to a spacecraft moving within a gravitational environment influenced by two primary attractors and whose characteristic dimension is infinitesimal respect to the distance of the vehicle from the primaries. Being considered the solely inertial coupling due to the gravity gradient torque, the orbital dynamics is not dependent from the attitude states and the resulting set of equation can be resumed as follow.

$$\begin{cases} \dot{\boldsymbol{x}}_{\boldsymbol{orb}} &= \boldsymbol{f}_{\text{CR3BP}}\left(\boldsymbol{x}_{\boldsymbol{orb}}\right) \\ {}^{\hat{i}}\dot{\boldsymbol{q}}^{\hat{b}} &= \boldsymbol{f}_{\boldsymbol{q}}\left({}^{\hat{i}}\boldsymbol{q}^{\hat{b}}, {}^{\hat{i}}\boldsymbol{\omega}^{\hat{b}}\right) \\ {}^{\hat{i}}\dot{\boldsymbol{\omega}}^{\hat{b}} &= \boldsymbol{f}_{\boldsymbol{\omega}}\left(\boldsymbol{x}_{\boldsymbol{orb}}, {}^{\hat{i}}\boldsymbol{q}^{\hat{b}}, {}^{\hat{i}}\boldsymbol{\omega}^{\hat{b}}\right) \end{cases} \tag{2.64}$$

The model can be easily augmented with the variational force term due to the finite extension of the spacecraft. These models will be employed to better understand the impact of the inertially fully-coupled model respect to the simplified one-way coupling approximation, on both the absolute and the relative 6DOF dynamics.

2.4.6 Orbit-Attitude Fully-Coupled Dynamics

A more detailed version of the orbit-attitude dynamical model for a spacecraft moving in the Earth-Moon system is developed starting from the basic Simplified-Coupled Model. Next, the more relevant perturbations integrate the dynamics to refine its fidelity.
One of the most important perturbation effect in the cislunar environment is represented by the Sun, which can contribute as source of solar radiation pressure effects and as fourth-body gravitational presence.
The variational effect in the gravity pull of a primary due to the finite dimension of the spacecraft may be considered as additional contribution in the equations of motion. It follows that, the model can be applied to any kind of body assumed to be rigid, and no more limited only to small objects. The resulting system is modelled via the following 13 differential equations.

$$\begin{bmatrix} \boldsymbol{f_x} \\ \boldsymbol{f_v} \end{bmatrix} = \begin{cases} \dot{x} = & v_x \\ \dot{y} = & v_y \\ \dot{x} = & v_x \\ \dot{v}_x = & x + 2v_y - \dfrac{(1-\mu)(x+\mu)}{{r_1}^3} - \dfrac{\mu(x-1+\mu)}{{r_2}^3} + a_{1,x} + a_{2,x} + a_{4th,x} + a_{SRP,x} \\ \dot{v}_y = & y - 2v_x - \dfrac{(1-\mu)y}{{r_1}^3} - \dfrac{\mu y}{{r_2}^3} + a_{1,y} + a_{2,y} + a_{4th,y} + a_{SRP,y} \\ \dot{v}_z = & -\dfrac{(1-\mu)z}{{r_1}^3} - \dfrac{\mu z}{{r_2}^3} + a_{1,z} + a_{2,z} + a_{4th,z} + a_{SRP,z} \end{cases} \tag{2.65}$$

$$\boldsymbol{f_q} = \begin{cases} \dot{q}_1 = & \frac{1}{2}(\omega_3 q_2 - \omega_2 q_3 + \omega_1 q_4) \\ \dot{q}_2 = & \frac{1}{2}(-\omega_3 q_1 + \omega_1 q_3 + \omega_2 q_4) \\ \dot{q}_3 = & \frac{1}{2}(\omega_2 q_1 - \omega_1 q_2 + \omega_3 q_4) \\ \dot{q}_4 = & -\frac{1}{2}(\omega_1 q_1 + \omega_2 q_2 + \omega_3 q_3) \end{cases} \tag{2.66}$$

$$\boldsymbol{f_\omega} = \begin{cases} \dot{\omega}_1 = & \frac{I_3 - I_2}{I_1}\left(\frac{3(1-\mu)}{{r_1}^5} g_2 g_3 + \frac{3\mu}{{r_2}^5} h_2 h_3 - \omega_2\omega_3\right) + a_{4th,1} + a_{SRP,1} \\ \dot{\omega}_2 = & \frac{I_1 - I_3}{I_2}\left(\frac{3(1-\mu)}{{r_1}^5} g_1 g_3 + \frac{3\mu}{{r_2}^5} h_1 h_3 - \omega_1\omega_3\right) + a_{4th,2} + a_{SRP,2} \\ \dot{\omega}_3 = & \frac{I_2 - I_1}{I_3}\left(\frac{3(1-\mu)}{{r_1}^5} g_1 g_2 + \frac{3\mu}{{r_2}^5} h_1 h_2 - \omega_1\omega_2\right) + a_{4th,3} + a_{SRP,3} \end{cases} \tag{2.67}$$

The orbital inertial coupling on the attitude dynamics is expressed via the gravity gradient torque contribution due to the two primaries. The attitude inertial coupling effect on the orbital dynamics appears through the perturbation terms $a_{1,i}$ and $a_{2,i}$ (with $i = x, y, z$), which represent the acceleration perturbation due to the second order term of gravity attraction of the two primaries considering the finite extension of the spacecraft.
The terms $a_{4th,i}$ represent the contribution due to the presence of the Sun as fourth gravitational attractor, while the terms $a_{SRP,i}$ are the contribution due to solar radiation pressure. The acceleration perturbation terms are identified by the subscripts $i = x, y, z$, while the angular acceleration perturbation are associated to the subscripts $i = 1, 2, 3$.
Note that the external perturbations may be an addition source of coupling between the orbit and attitude dynamics. For example, the SRP force depends directly by the orientation of the spacecraft because it determines the illuminated surface of the body and the angle of incidence of the radiation on its surface.

It is important to notice that the gravity gradient terms do not depends on the magnitudes of the moments of inertia, but it is function of the only inertial ratio K_1, K_2 and K_3.

$$K_1 = \frac{I_3 - I_2}{I_1}, \quad K_2 = \frac{I_1 - I_3}{I_2}, \quad K_3 = \frac{I_2 - I_1}{I_3} \tag{2.68}$$

It is also important to highlight that the same perturbation magnitude will have a larger impact on the orbit-attitude dynamics when the spacecraft is farther from the primaries. In fact, the natural dynamics terms due to the gravity attraction of the primaries is proportional to the inverse cubic law of the distance from the primary for the orbital dynamics, and is proportional to the inverse of the fifth power law of the distance from the primary for the attitude dynamics.

The complete set of non-linear differential equation describing the orbit-attitude model will be denoted in this paper as $\boldsymbol{f}_{\text{OrbAtt}} = [\boldsymbol{f_x}; \boldsymbol{f_v}; \boldsymbol{f_q}; \boldsymbol{f_\omega}]$.
The model can be easily integrated with additional contribution terms to consider other effects which will increase the fidelity of the model, or to include control force and control torque of the Attitude and Orbital Control System (AOCS) of the spacecraft. The system can be also employed in a multi-body tool environment by adding kinematics constraints in order to simulate the motion of complex space structures.

2.5 Linear Variational Equations

Even in a non-linear system, the linearised dynamics near a reference solution offers very useful information. In fact, it allows to define a linear mapping relating a variation on the final state $\delta \boldsymbol{X} = \delta \boldsymbol{X}(t)$ due to a variation on the initial state $\delta \boldsymbol{X_0} = \delta \boldsymbol{X}(t_0)$.
A first order Taylor series approximation of the non-linear equations of motion leads to the first-order variational equation of the system about a reference solution.

$$\delta \dot{\boldsymbol{X}}(t) = A(t)\, \delta \boldsymbol{X}(t) \tag{2.69}$$

In this notation $\delta \boldsymbol{X}(t) = \boldsymbol{X}(t) - \boldsymbol{X_{ref}}(t)$ denotes the state error vector relative to the reference solution. The matrix $A(t)$ is the Jacobian of the system, which is obtained as the partial derivatives of the dynamics equations with respect to the independent variable of the system and evaluated at on the base of the reference solution. In general, $A(t)$ is a time dependant matrix. However, if the reference solution is periodic, also the Jacobian will be periodic.
As a solution of the first-order variational equation (2.69), the impact of a variation in the initial state, $\delta \boldsymbol{X_0}$, on a variation in the final state, $\delta \boldsymbol{X}$, can be expressed in a linear sense via the following relation.

$$\delta \boldsymbol{X}(t) = \left(\frac{\partial \boldsymbol{X}}{\partial \boldsymbol{X_0}} \right) \delta \boldsymbol{X}(t_0) = \Phi(t + t_0, t_0)\, \delta \boldsymbol{X_0} \tag{2.70}$$

This linear differential relationship maps the sensitivity of the variational state and is also known as State Transition Matrix (STM), which is typically denoted as $\Phi(t + t_0, t_0) = \left(\frac{\partial \boldsymbol{X}}{\partial \boldsymbol{X_0}} \right)$.
Substituting the solution expressed in (2.70) in equation (2.69), the first-order variational equation governing the STM is obtained.

$$\dot{\Phi}(t, t_0) = A(t)\, \Phi(t + t_0, t_0) \tag{2.71}$$

This equation has to be integrated together the dynamics equation of the system in order to obtain the STM at any time along the propagated trajectory.
Obviously, a variation on the initial state can affect itself only at time $t = t_0$. Thus, the initial condition for the STM in equation (2.71) is the identity matrix.

$$\Phi(t_0, t_0) = I \tag{2.72}$$

2.5.1 State Transition Matrix in the Orbit-Attitude System

The orbit-attitude system $\boldsymbol{f}_{\text{OrbAtt}}$ is composed by 13 differential equations, but only 12 independent variable are needed to completely describe the orbit-attitude state of the spacecraft. The existence of the quaternion constraint equation (2.29) makes redundant one of the quaternion kinematics equations. Let define the independent state vector $\boldsymbol{X}$, which contains all the independent variable of the system.

$$\boldsymbol{X} = [x; y; z; v_x; v_y; v_z; q_1; q_2; q_3; \omega_1; \omega_2; \omega_3] = [\boldsymbol{x_{orb}}; \boldsymbol{x_{att}}] \tag{2.73}$$

The orbital states and the attitude states are respectively denoted as $\boldsymbol{x_{orb}} = [\boldsymbol{x}; \boldsymbol{v}]$ and $\boldsymbol{x_{att}} = [\boldsymbol{q}_{1:3}; \boldsymbol{\omega}]$. The dynamics of the system is kept described by the 13 differential equation for practical purposes, but the Jacobian and the STM are reduced to 12-by-12 matrices relating only the independent variables of the system.
The variational relation among the quaternion elements can be obtained from the quaternion

constraint (2.29).

$$q_1\delta q_1 + q_2\delta q_2 + q_3\delta q_3 + q_4\delta q_4 = 0 \tag{2.74}$$

This allows to obtain the relation to describe the partials of the Jacobian relative to the solely independent quaternion elements.

$$\frac{df_i}{dq_j}(q_1, q_2, q_3, q_4(q_1, q_2, q_3)) = \frac{\partial f_i}{\partial q_j} - \frac{q_j}{q_4}\frac{\partial f_i}{\partial q_4} \tag{2.75}$$

In this formulation, f_i represents the i-th differential function composing the orbit-attitude system. The Jacobian contains the partials derivatives of the system $\boldsymbol{f}_{\text{OrbAtt}}$ respect to the independent state vector $\boldsymbol{X}$, resulting in the following matrix block structure.

$$A(t) = \begin{bmatrix} \boldsymbol{f_{x/x}} & \boldsymbol{f_{x/v}} & \boldsymbol{f_{x/q}} & \boldsymbol{f_{x/\omega}} \\ \boldsymbol{f_{v/x}} & \boldsymbol{f_{v/v}} & \boldsymbol{f_{v/q}} & \boldsymbol{f_{v/\omega}} \\ \boldsymbol{f_{q/x}} & \boldsymbol{f_{q/v}} & \boldsymbol{f_{q/q}} & \boldsymbol{f_{q/\omega}} \\ \boldsymbol{f_{\omega/x}} & \boldsymbol{f_{\omega/v}} & \boldsymbol{f_{\omega/q}} & \boldsymbol{f_{\omega/\omega}} \end{bmatrix} \tag{2.76}$$

The Jacobian has been derived analytically for the coupled orbit-attitude dynamics, including the variation in gravitational attraction due to the finite dimension of the spacecraft. All the details about the derivation of the expression of each component constituting the Jacobian $A(t)$ can be found in [17].
Instead, the terms due to the Solar Radiation Pressure and the Sun gravitational influence has to be computed numerically since the model exploits the ephemeris position of the Sun. A completely analytical Jacobian and State Transition Matrix could be derived reducing the fidelity of the model for the Sun position, for example employing the original Bi-Circular Four-Body system.
Finally, the fundamental linear differential equation governing the STM evolution for the orbit-attitude CR3BP model is obtained.

$$\begin{cases} \dot{\Phi}(t + t_0, t_0) = A(t)\,\Phi(t + t_0, t_0) \\ \Phi(t_0) = I_{12\times 12} \end{cases} \tag{2.77}$$

It has to be integrated together the dynamics equations, resulting in a system of 13+144 equations. Its integration allows to propagate the system response and simultaneously access the linear differential relationship between initial and final orbit-attitude states along the whole trajectory.

2.6 Orbit-Attitude Ephemeris Model

Cislunar space is a particular dynamical environment and its idealization through the CR3BP is a very powerful toll capable to catch some peculiar behaviours present in its actual dynamics. However, the level of accuracy required to support the later stages in designing actual space missions can be provided only by higher-fidelity models.

The first step in the refinement of the model is represented by the development of an N-body ephemeris gravitational model governing the orbit-attitude dynamics of a small (rigid) body for a spacecraft-Earth-Moon-Sun system. The model is denoted “ephemeris” because the positions of the massive bodies (namely the Earth, the Moon and the Sun) are gathered via the NASA’s NAIF (Navigation and Ancillary Information Facility) SPICE toolkit ephemeris data.
The orbital motion of the spacecraft is computed conveniently relative to an inertial frame centered at the main central attractor. Being the cislunar space the main focus of this investigation, the

Moon has been chosen as main central body, while the inertial J2000 $\{\hat{I}\}$-frame has been selected as reference inertial frame. For sake of simplicity, the $\{\hat{I}\}$-frame has been chosen also as reference frame for the rotational motion.

This enhanced version of restricted fourth-body problem includes intrinsically the most relevant effects which has been neglected in the CR3BP approximation of the cislunar environment: the gravitational pull of the Sun and the orbital eccentricity of the lunar orbit around the Earth.
The solar radiation pressure effect can be included additionally to further increase the accuracy of the higher-fidelity model. However, the SRP is expected to have a relevant effect only in the case of particularly extensive spacecraft.
Instead, the variation in acceleration due to the gravitational attraction of the primaries on a finite extended body has been not considered due to its negligible influence respect the other perturbations.

No major differences are present in the formulation of the rotational motion of the spacecraft: the dynamical equations remains the same as in (2.67), but now they are expressed respect a different inertial frame, the inertial J2000 $\{\hat{I}\}$-frame. Instead, the characteristic centrifugal terms entering the classical CR3BP dynamics disappears because now the orbital motion is referred to an inertial reference.
As representative example, the "absolute" orbital dynamics of a spacecraft, or of a generic body "i", relative to the Moon in cislunar space is presented via the following higher-fidelity ephemeris model dynamical equation.

$$\ddot{\boldsymbol{r}}_{\boldsymbol{qi}} = -\frac{\mu_q}{{r_{qi}}^3}\boldsymbol{r}_{\boldsymbol{qi}} - \sum_{j=1}^{N}\mu_j\left(\frac{\boldsymbol{r}_{\boldsymbol{ji}}}{{r_{ji}}^3} + \frac{\boldsymbol{r}_{\boldsymbol{qj}}}{{r_{qj}}^3}\right) + \boldsymbol{a}_{\boldsymbol{SRP}} \tag{2.78}$$

The main central attractor is labelled as "q", and in the cislunar space it identifies the Moon. The Earth and the Sun, the other two massive perturbing attractors of the four-body model, are labelled as "j". Let assume the Earth is associated to $j = 1$, while the Sun is $j = 2$. The gravitational planetary constant of each attractor is denoted as $\mu_{(\cdot)}$. The syntax used for the subscript of the generic position vector $\boldsymbol{r}_{\boldsymbol{ab}}$ identifies the position of the body "b" respect to "a" in the inertial J2000 $\{\hat{I}\}$-frame. The same symbol in normal font is associated to the corresponding modulus, representing the distance between the two bodies. Therefore, $\boldsymbol{r}_{\boldsymbol{qi}}$ is the position of the spacecraft relative to the Moon, $\boldsymbol{r}_{\boldsymbol{ji}}$ is the position of the spacecraft relavite to the j-th perturbing attractor, while $\boldsymbol{r}_{\boldsymbol{qj}}$ is the position of the j-th attractor respect to the Moon. It should be noticed that the gravitational attraction of Earth and Sun are modelled like a third-body perturbation. The perturbing acceleration due to the solar radiation pressure is computed exploiting the same procedure proposed before for the CR3BP model, and is coherently included as $\boldsymbol{a}_{\boldsymbol{SRP}}$.
It should be highlighted that, if necessary, the formulation of the orbital motion expressed in equation (2.78) can be easily extended to include other perturbing bodies, for example starting from the largest planet of the solar system, Jupiter.

2.6.1 Transition from CR3BP to Ephemeris Model

The CR3BP model describes the orbital dynamics in the rotating $\{\hat{r}\}$-frame, a particular non-inertial frame fixed in the system of its two primaries (e.g. Earth-Moon system). For a space mission, which is designed exploiting such particular dynamical environment, the capability to transform the trajectories obtained in the $\{\hat{r}\}$-frame to a desired inertial frame is fundamental.
This frame transformation not only allows to view the same trajectories from different point of view, but it is also a fundamental tool to transit the solution between dynamical models with

different levels of fidelity. For example, a transformation of this kind is required to transit the solution obtained from the CR3BP model to an higher-fidelity multi-body ephemeris model to compute the whole trajectories during the high-level stages of mission design.

The method to transit the orbital states from the CR3BP to the ephemeris four-body problem has been inspired to the work of Pavlak in [35] and [36]. Considering the ephemeris four-body model developed in this investigation, the orbital states coming from the coupled 6DOF CR3BP model has to be transitioned to the inertial J2000 $\{\hat{I}\}$-frame and centered at the Moon location. Since in an ephemeris model the barycenter of the system is not fixed relative to either of the primary attractors, the transformation has been implemented directly relative to one of the main attractor of the system. In particular, the Moon will be the central body since it constitutes the main attractor for EM NRHOs, the non-Keplerian orbital family of greatest interest in this work. Once the orbital states has been shifted to the Rotating Moon-Centered representation (RMC), they are dimensionalized by using the "instantaneous" characteristic quantities of the system computed using the ephemeris data. In particular, the "instantaneous" characteristic unit length corresponds to the distance between the Earth and the Moon at the epoch of interest, while the "instantaneous" characteristic unit time is obtained as the inverse of the "instantaneous" angular motion of the Moon respect to the Earth.
Next, the ephemeris data are used to build the "instantaneous" rotating $\{\hat{\tilde{R}}\}$-frame of the Earth-Moon system in the inertial J2000 $\{\hat{I}\}$-frame.

$$\hat{\tilde{\boldsymbol{x}}} = \frac{\tilde{\boldsymbol{R}}}{\tilde{R}} \tag{2.79}$$

$$\hat{\tilde{\boldsymbol{z}}} = \frac{\tilde{\boldsymbol{h}}}{\tilde{h}} = \frac{\tilde{\boldsymbol{R}} \times \tilde{\boldsymbol{V}}}{\|\tilde{\boldsymbol{R}} \times \tilde{\boldsymbol{V}}\|} \tag{2.80}$$

$$\hat{\tilde{\boldsymbol{y}}} = \hat{\tilde{\boldsymbol{z}}} \times \hat{\tilde{\boldsymbol{x}}} \tag{2.81}$$

The vectors $\tilde{\boldsymbol{R}}$ and $\tilde{\boldsymbol{V}}$ are the "instantaneous" position and velocity of the Moon respect to the Earth at the epoch of interest and are obtained in $\{\hat{I}\}$-frame directly via the SPICE toolkit, while the vector $\tilde{\boldsymbol{h}}$ is the angular momentum of the Moon. The axis of the "instantaneous" rotating $\{\hat{\tilde{R}}\}$-frame constitute the columns of the DCM $[C_{I/\tilde{R}}]$.

$$[C_{I/\tilde{R}}] = \left[\hat{\tilde{\boldsymbol{x}}},\, \hat{\tilde{\boldsymbol{y}}},\, \hat{\tilde{\boldsymbol{z}}}\right] = \begin{bmatrix} C_{11} & C_{12} & C_{13} \\ C_{21} & C_{22} & C_{23} \\ C_{31} & C_{32} & C_{33} \end{bmatrix} \tag{2.82}$$

This rotation matrix is used to transform the dimensional position vector from being expressed in the RMC frame to the Inertial J2000 Moon-Centered (IMC) frame.

$$\begin{bmatrix} x_{IMC} \\ y_{IMC} \\ z_{IMC} \end{bmatrix} = \begin{bmatrix} C_{11} & C_{12} & C_{13} \\ C_{21} & C_{22} & C_{23} \\ C_{31} & C_{32} & C_{33} \end{bmatrix} \begin{bmatrix} x_{RMC} \\ y_{RMC} \\ z_{RMC} \end{bmatrix} \tag{2.83}$$

The inertial velocity of the spacecraft is obtained thanks to the kinematic relation (2.6).

$$\boldsymbol{v_{IMC}} = \left(\dot{x}_{RMC} - \dot{\tilde{\theta}}\, y_{RMC}\right) \hat{\tilde{\boldsymbol{x}}} + \left(\dot{y}_{RMC} + \dot{\tilde{\theta}}\, x_{RMC}\right) \hat{\tilde{\boldsymbol{y}}} + \dot{z}_{RMC} \hat{\tilde{\boldsymbol{z}}} \tag{2.84}$$

Note that, in the dimensional case, the angular velocity enters directly in the kinematic relation being not unitary. Therefore, the "instantaneous" angular rate of the Moon respect the Earth is

computed exploiting the definition of angular momentum $\tilde{\boldsymbol{h}}$ in the Keplerian model.

$$\dot{\tilde{\theta}} = \frac{\tilde{h}}{\tilde{R}^2} \tag{2.85}$$

Combining the relations (2.83) and (2.84), the transition of the orbital states from dimensional-rotating to dimensional-inertial J2000 representation can be accomplished in one step using the following transition matrix.

$$\begin{bmatrix} x_{IMC} \\ y_{IMC} \\ z_{IMC} \\ \dot{x}_{IMC} \\ \dot{y}_{IMC} \\ \dot{z}_{IMC} \end{bmatrix} = \begin{bmatrix} C_{11} & C_{12} & C_{13} & 0 & 0 & 0 \\ C_{21} & C_{22} & C_{23} & 0 & 0 & 0 \\ C_{31} & C_{32} & C_{33} & 0 & 0 & 0 \\ \dot{\tilde{\theta}}C_{12} & -\dot{\tilde{\theta}}C_{11} & 0 & C_{11} & C_{12} & C_{13} \\ \dot{\tilde{\theta}}C_{22} & -\dot{\tilde{\theta}}C_{21} & 0 & C_{21} & C_{22} & C_{23} \\ \dot{\tilde{\theta}}C_{32} & -\dot{\tilde{\theta}}C_{31} & 0 & C_{31} & C_{32} & C_{33} \end{bmatrix} \begin{bmatrix} x_{RMC} \\ y_{RMC} \\ z_{RMC} \\ \dot{x}_{RMC} \\ \dot{y}_{RMC} \\ \dot{z}_{RMC} \end{bmatrix} \tag{2.86}$$

Note that, the transformation of the orbital states from the inertial J2000 frame to the rotating frame representation can be achieved directly through the inverse of the transition matrix just presented.
Finally, the transitioned IMC orbital states can be non-dimensionalized via the standard characteristic quantities of the system if necessary for computation (e.g. for the propagation of the dynamics in higher-fidelity model).

For what concerning the transition of the attitude states, the procedure is quite simpler. Knowing the attitude of the body-fixed frame of the spacecraft respect to the rotating frame, the kinematic relation of successive rotation is exploited to find the attitude states of the body-fixed frame of the spacecraft respect the inertial J2000 reference frame.
For example, the quaternion representing the configuration of the "instantaneous" rotating $\{\hat{\tilde{R}}\}$-frame respect to the inertial J2000 $\{\hat{I}\}$-frame can be obtained by the DCM $[C_{I/\tilde{R}}]$, which is computed using ephemeris data. Then the successive rotation rule for quaternion is applied to obtain the quaternion of the body-fixed frame of the spacecraft relative to the inertial J2000 frame.
The angular velocity of the spacecraft obtained from the 6DOF coupled CR3BP is already relative to an inertial frame and is expressed in the body-fixed frame of the spacecraft. Therefore, it does not require any transformation except the dimensionalization through the "instantaneous" characteristic angular rate $\dot{\tilde{\theta}}$.

2.7 Relative Orbit-Attitude Model

This investigation aims to obtain useful insights about the relative orbit-attitude motion of a chaser spacecraft in proximity of a target space station orbiting on a non-Keplerian orbit in cislunar environment.

The preliminary analysis on the natural orbit-attitude motion will be carried out within the framework of the circular restricted three-body problem.
The natural dynamical model will be based on the absolute natural coupled orbit-attitude dynamics for both the chaser and the target spacecrafts. Therefore, the orbital dynamics is described in the rotating $\{\hat{r}\}$-frame, while the rotational dynamics is obtained in inertial frame for the corresponding spacecrafts. Given the initial 6DOF state of each spacecraft at time $t = t_0$, the orbit-attitude

dynamical flow is propagated to obtain the 6DOF states at the desired time t.

$$\begin{aligned} \boldsymbol{X_T}(t) &= \boldsymbol{f}_{\text{OrbAtt}}(\boldsymbol{X_T}(t_0), t) \\ \boldsymbol{X_C}(t) &= \boldsymbol{f}_{\text{OrbAtt}}(\boldsymbol{X_C}(t_0), t) \end{aligned} \tag{2.87}$$

For example, the 6DOF state of the target spacecraft is $\boldsymbol{X_T} = [\boldsymbol{x_T}; \boldsymbol{v_T}; \boldsymbol{q_T}; \boldsymbol{\omega_T}]$. The orbital states $\boldsymbol{x_{orb}} = [\boldsymbol{x}; \boldsymbol{v}]$ are expressed in the rotating $\{\hat{r}\}$-frame. The attitude states $\boldsymbol{x_{att}} = \left[{}^{\hat{i}}\boldsymbol{q}^{\hat{b}}; \boldsymbol{\omega}^{\hat{b}}\right]$ are composed by the quaternion representing the orientation of the body-fixed $\{\hat{b}\}$-frame respect the inertial $\{\hat{i}\}$-frame, and by the angular velocity of the spacecraft relative to the inertial $\{\hat{i}\}$-frame expressed in its body-fixed $\{\hat{b}\}$-frame.

Once the absolute 6DOF states are available, the relative orbit-attitude states can be directly obtained thanks to the relative 6DOF relations between the chaser and the target spacecrafts.
The relative rotating position $\delta\boldsymbol{x}$ and the relative rotating velocity $\delta\boldsymbol{v}$ are defined as follow.

$$\delta\boldsymbol{x}(t) = \boldsymbol{x_C}(t) - \boldsymbol{x_T}(t) \tag{2.88}$$

$$\delta\boldsymbol{v}(t) = \boldsymbol{v_C}(t) - \boldsymbol{v_T}(t) \tag{2.89}$$

The relative attitude quaternion $\delta\boldsymbol{q}$ can be obtained via applying the rule of successive rotation for the quaternion.

$$\delta\boldsymbol{q}(t) = {}^{\hat{b}_T}\boldsymbol{q}^{\hat{b}_C}(t) = \boldsymbol{q_T}^{-1}(t) \odot \boldsymbol{q_C}(t) \tag{2.90}$$

A rotation matrix $[\delta C] = \left[C_{\hat{b}_T/\hat{b}_C}\right](\delta\boldsymbol{q})$, which transform a vector from the target body-fixed $\{\hat{b}_T\}$-frame to the chaser body-fixed $\{\hat{b}_C\}$-frame, is directly obtained by the relative quaternion through the relation (2.28).
Then, the relative angular velocity $\delta\boldsymbol{\omega}^{\hat{b}_C}$ between the two spacecrafts can be defined as it is seen in the chaser body-fixed $\{\hat{b}_C\}$-frame.

$$\delta\boldsymbol{\omega}^{\hat{b}_C}(t) = \boldsymbol{\omega_C}(t) - [\delta C]\,\boldsymbol{\omega_T}(t) \tag{2.91}$$

Even if the CR3BP represents a powerful toll for preliminary analysis, high-level design stages of a space mission require higher-fidelity models of the dynamics. The implementation of these models is even more important when the mission leverages on non-Keplerian orbits.
The information obtained from preliminary analysis will drive the design and the definition of functional and operational requirements for rendezvous and docking operations in non-Keplerian orbits within the cislunar space.
The higher-fidelity dynamical model will include the gravitational presence of the Earth, the Moon and the Sun in their actual position obtained from ephemeris data. The gravitational pull and the gravity gradient torque will be included in the dynamical model, while the perturbation due to the gravitational attraction of the massive bodies on a finite extended body has been neglected.
Also the SRP effects can be included in the ephemeris model to further increase its accuracy. Its acceleration effect is expected to be negligible, while the differential torque may be of particular concern in the relative rotational dynamics of large space infrastructure (in particular, considering the large solar array surfaces which will supply the power to a lunar space station).

The dynamical model is conveniently expressed in the reference inertial J2000 $\{\hat{I}\}$-frame. The absolute orbital states of the extended rigid bodies of the target T and of the chaser C are described by the position vectors $\boldsymbol{x_T}$ and $\boldsymbol{x_C}$ of the center of mass of the corresponding spacecraft. The four-dimensional quaternion ${}^{\hat{I}}\boldsymbol{q}^{\hat{b}_T}$ and ${}^{\hat{I}}\boldsymbol{q}^{\hat{b}_C}$ describe the orientation of the body-fixed frames $\{\hat{b}_T\}$ and $\{\hat{b}_C\}$, which are aligned to the principal axis of inertia of the spacecrafts, relative to the inertial

J2000 $\{\hat{I}\}$-frame.

It should be highlighted that the relative orbit-attitude dynamics of a chaser in proximity of a target moving on a non-Keplerian orbit in cislunar space strongly depends on the absolute state of the target. Therefore, the absolute 6DOF dynamics of the target spacecraft, defined in section 2.6, has been included together the relative 6DOF dynamics of the chaser spacecraft.

$$\boldsymbol{X_T}(t) = \boldsymbol{f}^{\text{Ephem}}_{\text{OrbAtt}}(\boldsymbol{X_T}(t_0), t) \tag{2.92}$$

The relative orbital dynamics in inertial J2000 $\{\hat{I}\}$-frame is straightforwardly obtained by differentiating in time the relative position vector.

$$\delta\ddot{\boldsymbol{x}} = \ddot{\boldsymbol{x}}_{\boldsymbol{C}} - \ddot{\boldsymbol{x}}_{\boldsymbol{T}} \tag{2.93}$$

The development of the relative rotational dynamics requires more attention. In fact, it describe the attitude motion of the chaser body-fixed $\{\hat{b}_C\}$-frame relative to the target body-fixed $\{\hat{b}_T\}$-frame. Therefore, the relative dynamics is expressed respect to a non-inertial frame. Considering the relative attitude motion relations in equation (2.90) and (2.91), the relative attitude dynamics of the chaser with respect to the target can be expressed in the chaser body-fixed $\{\hat{b}_C\}$-frame.

$$\begin{aligned}
\delta\dot{\boldsymbol{\omega}}^{\hat{b}_C} = \mathbb{I}_C^{-1}\Bigg\{ & -\left[\delta\boldsymbol{\omega}^{\hat{b}_C}\times\right]\mathbb{I}_C\,\delta\omega^{\hat{b}_C} - \left[\delta\boldsymbol{\omega}^{\hat{b}_C}\times\right]\mathbb{I}_C[\delta C]\,\boldsymbol{\omega_T} + \mathbb{I}_C\left[\delta\boldsymbol{\omega}^{\hat{b}_C}\times\right][\delta C]\,\boldsymbol{\omega_T} \\
& - \left[[\delta C]\boldsymbol{\omega_T}\times\right]\mathbb{I}_C\,\delta\boldsymbol{\omega}^{\hat{b}_C} + \boldsymbol{N_C} \\
& - [\delta C]\Big[\Big([\delta C]^T\mathbb{I}_C[\delta C] - \mathbb{I}_T\Big)\mathbb{I}_T^{-1}\Big(\boldsymbol{N_T} - [\boldsymbol{\omega_T}\times]\,\mathbb{I}_T\,\boldsymbol{\omega_T}\Big) \\
& + [\boldsymbol{\omega_T}\times]\Big([\delta C]^T\mathbb{I}_C[\delta C] - \mathbb{I}_T\Big)\boldsymbol{\omega_T}\Big] - [\delta C]\boldsymbol{N_T}\Bigg\}
\end{aligned} \tag{2.94}$$

In this formulation of the dynamics ([37] and [38]), the matrix $\mathbb{I}_C$ and $\mathbb{I}_T$ are the inertia tensors of the chaser and target spacecrafts in principal axes. The relative angular velocity $\delta\boldsymbol{\omega}^{\hat{b}_C}$ is expressed in the chaser body-fixed $\{\hat{b}_C\}$-frame, while $\boldsymbol{\omega_T}$ is the absolute angular velocity of the target expressed in its body-fixed $\{\hat{b}_T\}$-frame. The rotation matrix $[\delta C]$ is the DCM describing the relative attitude of the chaser respect the target, as defined before. Finally, $\boldsymbol{N_C}$ and $\boldsymbol{N_T}$ are the external torques acting on the chaser vehicle and on the target space station and they are expressed in the chaser and target body-fixed frames, respectively.
The relative angular velocity $\delta\boldsymbol{\omega}^{\hat{b}_C}$ is available from the propagation of the relative attitude dynamics. Then, the relative attitude kinematics is directly obtained in the quaternion formalism, as in equation (2.38).

$$\delta\dot{\boldsymbol{q}} = \frac{1}{2}\left[\boldsymbol{\Omega}(\delta\boldsymbol{\omega}^{\hat{b}_C})\right]\,\delta\boldsymbol{q} \tag{2.95}$$

In the assumed rendezvous scenario, the design of the GNC system will consider the chaser as the active vehicle which has to drive its motion to perform the docking. While the target space station will be a passive vehicle, which maintains its nominal motion along a non-Keplerian orbit in cislunar space.
The control action are included in the relative dynamical model as additional external force and torque terms acting on the chaser spacecraft, or equivalently as translational and rotational acceleration additional terms. However, if desired, the simplicity of the developed dynamical model allows to include the control of the target vehicle as well.

In practical proximity operations, the chaser and/or the target spacecraft will have available

relative and absolute measurements. For example, the chaser is expected to be equipped with several imaging cameras for relative 6DOF determination. Also the target space gateway could have a radar system for safety reason. Moreover, both the spacecraft should have an absolute navigation system probably based on a ground-tracking system, such as the Deep Space Network. Once a navigation system has the information about the relative 6DOF states and the absolute orbit-attitude states of one vehicle, the estimation of the absolute 6DOF state of the other spacecraft can be directly obtained thanks to relative relations (2.88) - (2.91). Alternatively, the relative 6DOF state can be obtained through the same relations by knowing the absolute state of both the spacecraft.

The navigation system may employ the relative and absolute orbit-attitude dynamics equations, or a simplified version of them (such as linearized 6DOF relative dynamics), to numerically propagate in-time the motion with its on-board software. These model may be exploited to increase the navigation accuracy in cislunar environment by filtering the relative measurements available from on-board measurements. Finally, the propagation in-time of the relative 6DOF states allows the guidance system to compute the optimal trajectories to perform the rendezvous and docking between the two spacecrafts.

Chapter 3

DIFFERENTIAL CORRECTOR ALGORITHM

In order to determine the path going from an initial to a final point, driven by the dynamics of the system, a Two-Point Boundary Value Problem (TPBVP) has to be solved. For a system described by non-linear second-order differential equation, find the solution is not a trivial answer. Moreover, closed-form analytical solutions does not exist for the differential equations driving the dynamics of a body under the gravity field influence of more than one primary attractor. Consequently, numerical methods are typically used to find approximate solutions satisfying desired mission requirements and boundaries in the restricted three-body problem, as well as in higher-fidelity models. Numerical Shooting Differential Corrector converts any TPBVP into a simpler Initial Value Problem (IVP), and it has been extensively exploited in CR3BP applications.

In this chapter, a multiple-shooting differential corrector has been developed for a general problem in the coupled orbit-attitude CR3BP dynamical system. Then, this numerical corrector has been leveraged to compute periodic orbit-attitude solutions and families of Libration Point Orbits in the simplified-coupled CR3BP. They will constitute the basis reference orbits for the orbit-attitude invariant manifolds analysis.

3.1 Multiple-Shooting Differential Corrector

The idea at the base of differential correctors method comes from the possibility of gather information about the linear variational dynamics in the "vicinity" of a reference solution via the gradients of the dynamical system. The corrector iteratively corrects an initial guess condition to obtain the final desired condition, that is solution of the problem within a numerical tolerance.
The developed shooting differential corrector is based on the multiple-variable Newton-Raphson method.

$$\boldsymbol{\nu}_{k+1} = \boldsymbol{\nu}_k - DF(\boldsymbol{\nu}_k)^{-1}\boldsymbol{F}(\boldsymbol{\nu}_k) \tag{3.1}$$

Where $\boldsymbol{\nu}_k$ is the free variable vector at the k-th iteration which contains the n free variables, $\boldsymbol{F}$ is the constraint function vector representing the m constraints, and DF is the Jacobian matrix of the constraint function with respect to the free variable.
In the case of $n > m$, a minimum norm solution is applied.

$$\boldsymbol{\nu}_{k+1} = \boldsymbol{\nu}_k - DF^T(\boldsymbol{\nu}_k)\left(DF(\boldsymbol{\nu}_k)DF^T(\boldsymbol{\nu}_k)\right)^{-1}\boldsymbol{F}(\boldsymbol{\nu}_k) \tag{3.2}$$

An initial guess for the first iteration has to be given in the "vicinity" of the solution, otherwise the corrector could not lead to convergence.

Multiple-shooting algorithm is an improved extension of the single-shooting concept, which allows more flexibility and robustness. Basically, a single-shooting correspond to a multiple-shooting composed by only two patch point. A graphical interpretation of the numerical corrector algorithm for a general problem is shown in figure 3.1.
The coupling nature of the system suggests the development of an orbit-attitude differential corrector in order to correct contemporaneously the translational and the rotational motion of the body (e.g. the spacecraft) [17].

The trajectory is divided in N patch point, $\boldsymbol{X_j}$, with the corresponding $(N-1)$ arcs. Each patch point has 12 degrees of freedom which uniquely define the states of the rigid body.

$$\boldsymbol{X_j} = [x; y; z; v_x; v_y; v_z; q_1; q_2; q_3; \omega_1; \omega_2; \omega_3]_j = \left[\boldsymbol{x_{orb}}_j;\ {}^i\boldsymbol{q}^b_j;\ {}^i\boldsymbol{\omega}^b_j\right] \tag{3.3}$$

Note that only three quaternion component are needed because the fourth is defined by the quaternion constraint.
The time of flight, T_j, is assumed to be the same for each arc. In this way, the patch points are equally displaced along the trajectory. Moreover, the total time of flight of the solution is $T = (N-1)T_j$, being T_j constant for each arc. Propagating the orbit-attitude dynamics for the j-th patch point $\boldsymbol{X_j} = \left[\boldsymbol{x_{orb}}_j;\ {}^i\boldsymbol{q}^b_j;\ {}^i\boldsymbol{\omega}^b_j\right]$, along the j-th arc for a time T_j, yields to the final condition $(\boldsymbol{X_j})^t = \left[\left(\boldsymbol{x_{orb}}_j\right)^t;\ \left({}^i\boldsymbol{q}^b_j\right)^t;\ \left({}^i\boldsymbol{\omega}^b_j\right)^t\right]$.
The set of all the patch point states is augmented with the time of flight of each arc in order to build the free variable vector.

$$\boldsymbol{\nu} = \left[\boldsymbol{x_{orb}}_1;\ {}^i\boldsymbol{q}^b_1;\ {}^i\boldsymbol{\omega}^b_1; \dots; \boldsymbol{x_{orb}}_j;\ {}^i\boldsymbol{q}^b_j;\ {}^i\boldsymbol{\omega}^b_j; \dots; \boldsymbol{x_{orb}}_N;\ {}^i\boldsymbol{q}^b_N;\ {}^i\boldsymbol{\omega}^b_N \,|\, T_j\right] \tag{3.4}$$

The constraint function can be distinguished in two main parts: the internal states continuity constraint and the specific problem constraint.

$$\boldsymbol{F} = \begin{bmatrix} \left(\boldsymbol{x_{orb}}_1\right)^t - \boldsymbol{x_{orb}}_2 \\ \left({}^i\boldsymbol{q}^b{}_1\right)^t - {}^i\boldsymbol{q}^b{}_2 \\ \left({}^i\boldsymbol{\omega}^b{}_1\right)^t - {}^i\boldsymbol{\omega}^b{}_2 \\ \vdots \\ \left(\boldsymbol{x_{orb}}_j\right)^t - \boldsymbol{x_{orb}}_{j+1} \\ \left({}^i\boldsymbol{q}^b{}_j\right)^t - {}^i\boldsymbol{q}^b{}_{j+1} \\ \left({}^i\boldsymbol{\omega}^b{}_j\right)^t - {}^i\boldsymbol{\omega}^b{}_{j+1} \\ \vdots \\ \left(\boldsymbol{x_{orb}}_{N-1}\right)^t - \boldsymbol{x_{orb}}_N \\ \left({}^i\boldsymbol{q}^b{}_{N-1}\right)^t - {}^i\boldsymbol{q}^b{}_N \\ \left({}^i\boldsymbol{\omega}^b{}_{N-1}\right)^t - {}^i\boldsymbol{\omega}^b{}_N \\ \hline \\ \boldsymbol{F}_{\text{specific}} \\ \\ \end{bmatrix} \tag{3.5}$$

The internal continuity of the solution is independent from the observing frame. Therefore, it can be written directly in the states $\boldsymbol{X_j}$. During the procedure, the algorithm ensures the quaternion sign continuity at each patch point.
Internal continuity gives $12(N-1)$ constraint equations. The other constraint equations form the

specific problem constraint. They describe the actual objective of the correction algorithm, such as find a periodic solution or target a desired final condition. Periodicity and phasing constraints can be exploited to obtain periodic solution. Targeting scheme may be applied in a open-loop long-range approach to target desired check points during the rendezvous mission, or in a simple station-keeping strategy.
Furthermore, the orbital motion along z-axis can be simplified in the case of planar orbit. The free variables z and v_z of each patch point are removed from the free variables and set equal to zero. This simplification avoids possible fluttering behaviour of the orbit, which could represent convergence difficulties for the correction algorithm.

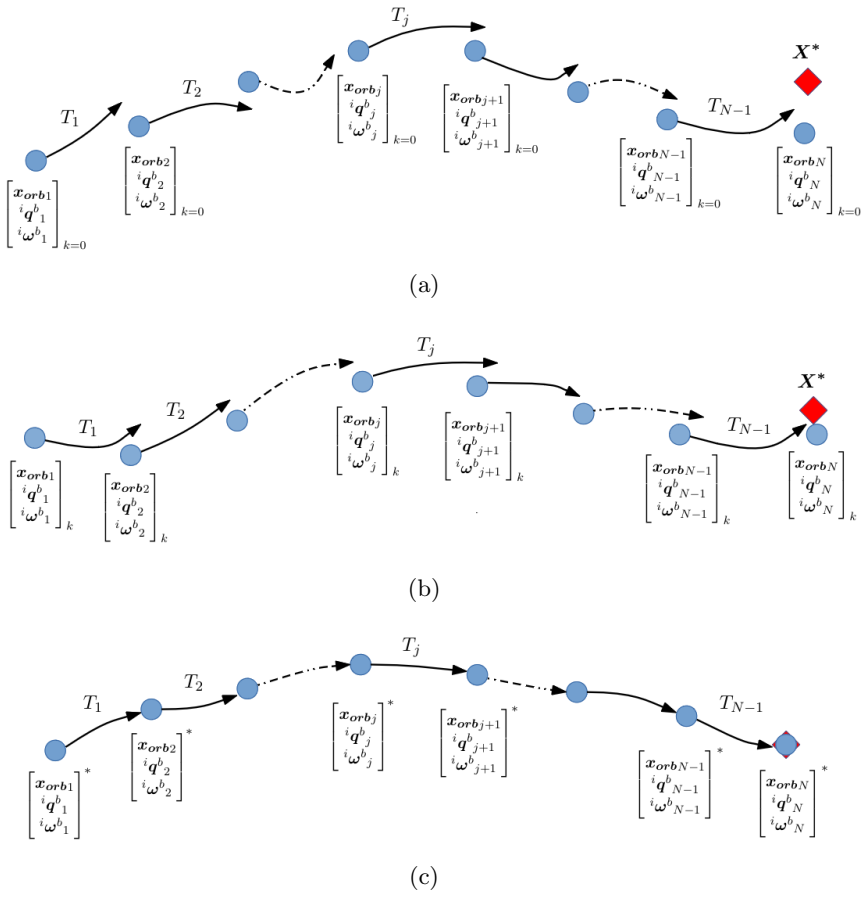

Figure 3.1: Graphical representation of the multiple shooting differential corrector during different phases of the algorithm. Initial guess (a). At the k-th iteration (b). Converged solution (c)

From the definition of the constraint function $\boldsymbol{F}$ in (3.5), a general structure for the Jacobian of the constraint function can be identified.

$$DF = \begin{bmatrix} A_1 & -I & & & & & B_1 \\ & \ddots & \ddots & & & & \vdots \\ & & A_j & -I & & & B_j \\ & & & \ddots & \ddots & & \vdots \\ & & & & A_{N-1} & -I & B_{N-1} \\ C_1 & \cdots & C_j & \cdots & \cdots & C_N & D \end{bmatrix} \tag{3.6}$$

The I blocks are 12-dimensional identity matrix, the A_j blocks are 12-by-12 matrices, while the B_j blocks are 12-by-1 vectors. The dimensions of the matrices C_j and D_j are respectively n_c-by-12

and n_c-by-1, where n_c is the number of specific constraints.
The terms A_j and B_j builds the part corresponding to the internal continuity constraint, while the terms C_j and D forms the part corresponding to the specific constraint of the problem.
The $-I$ terms appear due the presence of the initial condition of the $(j+1)$-th patch point for the j-th internal continuity constraint.
The A_j blocks represents the variations of the final condition of the j-th arc due to the variations in the initial condition of corresponding arc. It corresponds to the definition of the STM of the j-th arc.

$$A_j = \Phi_j = \Phi\left(j\,T_j, (j-1)\,T_j\right) = \begin{bmatrix} \frac{\partial\,(\boldsymbol{x})^t}{\partial \boldsymbol{x}} & \frac{\partial\,(\boldsymbol{x})^t}{\partial \boldsymbol{v}} & \frac{\partial\,(\boldsymbol{x})^t}{\partial \boldsymbol{q}} & \frac{\partial\,(\boldsymbol{x})^t}{\partial \boldsymbol{\omega}} \\ \frac{\partial\,(\boldsymbol{v})^t}{\partial \boldsymbol{x}} & \frac{\partial\,(\boldsymbol{v})^t}{\partial \boldsymbol{v}} & \frac{\partial\,(\boldsymbol{v})^t}{\partial \boldsymbol{q}} & \frac{\partial\,(\boldsymbol{v})^t}{\partial \boldsymbol{\omega}} \\ \frac{\partial\,(\boldsymbol{q})^t}{\partial \boldsymbol{x}} & \frac{\partial\,(\boldsymbol{q})^t}{\partial \boldsymbol{v}} & \frac{\partial\,(\boldsymbol{q})^t}{\partial \boldsymbol{q}} & \frac{\partial\,(\boldsymbol{q})^t}{\partial \boldsymbol{\omega}} \\ \frac{\partial\,(\boldsymbol{\omega})^t}{\partial \boldsymbol{x}} & \frac{\partial\,(\boldsymbol{\omega})^t}{\partial \boldsymbol{v}} & \frac{\partial\,(\boldsymbol{\omega})^t}{\partial \boldsymbol{q}} & \frac{\partial\,(\boldsymbol{\omega})^t}{\partial \boldsymbol{\omega}} \end{bmatrix} \tag{3.7}$$

The B_j terms represent the variations of the final condition of the j-th arc due to the variations in the time of flight T_j along each arc. It can be derived manipulating the expression of the contemporaneous variation in the state, as presented by Greebow in [31].

$$B_j = j\,\dot{\boldsymbol{X}}_{\boldsymbol{j+1}} - (j-1)\,\Phi_j\,\boldsymbol{X}_{\boldsymbol{j}} \tag{3.8}$$

The C_j and D blocks represents the sensibility of the specific constraints of the problem respectively due to a variations in the state variables of the j-th patch point and to a variation of the time of flight T_j along each arc.

3.2 Orbit-Attitude Periodic Solution

A periodic orbit-attitude solution in the coupled CR3BP is defined as the continuity between the initial and the final condition in both orbital and attitude states seen by an observer standing in the synodic $\{\hat{r}\}$-frame. Orbital period T_{orb} and attitude period T_{att} may be different, but an integer ratio between these periods yields to a periodic orbit-attitude solution.
A periodic orbit-attitude Libration Point Orbits can be identified in the coupled CR3BP by the set of twelve independent orbit-attitude states at a generic location along the periodic solution $\boldsymbol{X_0} = [x, y, z, v_x, v_y, v_z, q_1, q_2, q_3, \omega_1, \omega_2, \omega_3]$, plus the orbital period T. Once the initial condition of a periodic solution is selected, the non-dimensional time $t \in [0, T]$ allows to identify any point along that orbit.

In the classical CR3BP an infinite number of planar and non-planar orbits exist in the vicinity of the five libration points. An even larger number of periodic solutions is expected in the orbit-attitude CR3BP, where the orbital trajectories may be associated to spinning or librating periodic attitude behaviours. The first step to explore the orbit-attitude CR3BP coupling aims to find natural periodic solutions in the simplified-coupled motion for the most known symmetric Libration Point Orbit (LPO) families in the vicinity of the collinear libration point: Lyapunov orbit, Distant Retrograde Orbit (DRO), Halo orbit and Nearly Rectilinear Halo Orbit (NRHO).
This is a practical approach to find possible ordered or bounded attitude behaviour for a spacecraft travelling along a periodic orbit in the CR3BP framework. Moreover, the orbits around L_1 and L_2 are solutions of most immediate interest for application scenarios in the Earth-Moon system. They may be an useful preliminary approximation of a more dynamically complex multi-body

environment by assuming orbital station keeping for the reference LPO, needed due its intrinsic instability. Therefore, these solution may represent interesting natural trajectories that might be exploited to relieve the task of the Orbital and Attitude Control System (OACS) via the natural gravity gradient control.
These natural orbit-attitude behaviours could open the door to new concept mission design. Slowly diverging or marginally stable rotational behaviour may be an useful attitude configuration for many space infrastructure, such as manned habitats in the proximity of the Moon, or micro/nano spacecraft with low control capability.

3.2.1 Differential Correction Method

A periodicity condition may be formulated simply as the continuity between the final condition after a full orbital period along the orbit and its initial condition. These two point are represented by the last and the first patch point employed in the differential corrector. In the context of the coupled orbit-attitude CR3BP, the periodicity is defined as the one seen from a rotating observer fixed on the synodic $\{\hat{r}\}$-frame for both orbital and attitude states of the orbit.
The orbital states $\boldsymbol{x_{orb}}$ are already available in rotating point of view, and the periodicity condition can be directly introduced. Instead, the rotational motion of the spacecraft in the orbit-attitude dynamics is expressed relative to the reference inertial $\{\hat{i}\}$-frame. The attitude quaternion ${}^{\hat{i}}\boldsymbol{q}^{\hat{b}}$ of the spacecraft relative to the $\{\hat{i}\}$-frame needs to be transformed to quaternion describing the attitude of the body respect the synodic frame ${}^{\hat{r}}\boldsymbol{q}^{\hat{b}}$. Also the angular velocity of the spacecraft ${}^{i}\boldsymbol{\omega}^{b}$ is expressed respect the inertial frame. However, its transformation is not necessary in this case. By definition, the $\{\hat{r}\}$-frame has been assumed to rotate at constant angular rate relative to the $\{\hat{i}\}$-frame. Because this angular motion offset is constant and it does not depends explicitly from time, the angular velocity observed in the $\{\hat{i}\}$-frame differs only of a constant offset from the angular velocity observed in the $\{\hat{r}\}$-frame. Therefore, if a solution has angular velocity periodic in the $\{\hat{i}\}$-frame, it will be periodic also in the $\{\hat{r}\}$-frame. It follows that the periodic constraint on the angular velocity can be expressed respect both the frames.
It should be noted that the orbital dynamics has one integral of motion within the context of simplified-coupled motion, which corresponds to the well-known Jacobi constant in the classical CR3BP. This implies that only 5 constraints are necessary for the periodicity of the 6 orbital states. The sixth constraint will result redundant, and it can be exploited for other purposes, such as the phasing of the members of the orbit-attitude family.
Now all the ingredients are ready to define the specific constraint for periodic orbit-attitude orbit in the simplified-coupled CR3BP motion.

$$\boldsymbol{F}_{\text{specific}} = \left[\begin{array}{c} x_N - x_1 \\ z_N - z_1 \\ v_{x_N} - v_{x_1} \\ v_{y_N} - v_{y_1} \\ v_{z_N} - v_{z_1} \\ \hline y_1 \\ \hline {}^{r}\boldsymbol{q}^{b}{}_N - {}^{r}\boldsymbol{q}^{b}{}_1 \\ {}^{i}\boldsymbol{\omega}^{b}{}_N - {}^{i}\boldsymbol{\omega}^{b}{}_1 \end{array}\right] \begin{array}{c} \text{Orbital states} \\ \text{periodicity} \\ \\ \\ \\ \\ \hline \text{Phasing} \\ \hline \text{Attitude states} \\ \text{periodicity} \end{array} \tag{3.9}$$

The first part of the specific constraint represent the orbital states periodicity. The phasing constraint is exploited to obtain the initial point of the converged periodic solution on the xz-

plane. This is a typical initial condition exploited to identify symmetric orbits in the classical CR3BP. The last part of the constraint ensures the attitude states periodicity. Again, the solely independent variable of the quaternion are necessary to define the constraint.
The set of these 12 constraints plus the internal patch point continuity constraints constitute the constraint function (3.5) to find periodic orbit-attitude LPO in the simplified-coupled CR3BP using the multiple-shooting differential corrector algorithm.

The matrix C_1, C_N and D are the only blocks which survive in the specific constraint part of the Jacobian matrix DF in (3.6). The matrices C_1 and C_N are the derivatives of the specific constraint function respect the states of the first and last patch points.

$$C_1 = \begin{bmatrix} -1 & & & & \\ & -I_{4\times4} & & & \\ 1 & & & & \\ & & & -\dfrac{\partial\, {}^r\boldsymbol{q}^b{}_1}{\partial\, {}^i\boldsymbol{q}^b{}_1} & \\ & & & & -I_{3\times3} \end{bmatrix} \quad , \quad C_N = \begin{bmatrix} 1 & & & & \\ & I_{4\times4} & & & \\ 0 & & & & \\ & & & \dfrac{\partial\, {}^r\boldsymbol{q}^b{}_N}{\partial\, {}^i\boldsymbol{q}^b{}_N} & \\ & & & & I_{3\times3} \end{bmatrix} \tag{3.10}$$

The derivatives between the reduced quaternions relative to the $\{\hat{r}\}$-frame and the reduced quaternion relative to the $\{\hat{i}\}$-frame can be derived from combining the rule of successive rotation for quaternions in equation (2.36) and the variational form of the quaternion constraint (2.74).

$$\frac{\partial\, {}^r\boldsymbol{q}^b{}_j}{\partial\, {}^i\boldsymbol{q}^b{}_j} = \begin{bmatrix} \cos(t_j/2) & \sin(t_j/2) & 0 \\ -\sin(t_j/2) & \cos(t_j/2) & 0 \\ \dfrac{q_1}{q_4}\sin(t_j/2) & \dfrac{q_2}{q_4}\sin(t_j/2) & \cos(t_j/2)+\dfrac{q_3}{q_4}\sin(t_j/2) \end{bmatrix} = T_R\left(t_j,\, {}^i\boldsymbol{q}^b{}_j\right) \tag{3.11}$$

In this formulation $t_j = (j-1)T_j$ is the time at the j-th patch point. Note that it is assumed that at the first patch point the time is $t_j = 0$, which corresponds to the initial condition with the reference $\{\hat{i}\}$-frame aligned to the $\{\hat{r}\}$-frame. Instead, at the last patch point the time is $t_j = (N-1)T_j$, which corresponds to the orbital period T.

$$\frac{\partial\, {}^r\boldsymbol{q}^b{}_1}{\partial\, {}^i\boldsymbol{q}^b{}_1} = I_{3\times3} \quad , \quad \frac{\partial\, {}^r\boldsymbol{q}^b{}_N}{\partial\, {}^i\boldsymbol{q}^b{}_N} = T_R\left((N-1)T_j,\, {}^i\boldsymbol{q}^b{}_N\right) \tag{3.12}$$

The 12-by-1 block D represents the sensibility of variation of the specific constraint respect a variation in the time of flight T_j of each arc.

$$D = \left[0_{6\times1};\, \frac{\partial\, {}^r\boldsymbol{q}^b_N}{\partial T_j};\, 0_{3\times1}\right] \tag{3.13}$$

Note that only the orientation of the body relative to the $\{\hat{r}\}$-frame at the final patch point has an implicit dependence with the time of flight T_j. This relation is reflected in the derivatives of

the reduced quaternion at the last patch point respect the time length of the arcs T_j.

$$\begin{aligned}\frac{\partial\, {}^r\boldsymbol{q}^b{}_N}{\partial T_j} &= \left.\frac{\partial t_j}{\partial T_j}\right|_{t_j=t_N} \cdot \left.\frac{\partial\, {}^r\boldsymbol{q}^b{}_j}{\partial t_j}\right|_{t_j=t_N} \\ &= (N-1)\frac{1}{2}\begin{bmatrix} -\sin(t_N/2) & \cos(t_N/2) & 0 & 0 \\ -\cos(t_N/2) & -\sin(t_N/2) & 0 & 0 \\ 0 & 0 & -\sin(t_N/2) & -\cos(t_N/2) \end{bmatrix}\begin{bmatrix} q_1 \\ q_2 \\ q_3 \\ q_4 \end{bmatrix}\end{aligned} \tag{3.14}$$

Where q_1, q_2, q_3, q_4 are the components of the quaternion ${}^i\boldsymbol{q}^b{}_N$.

Note that, the so defined specific constraint may be easily augmented to obtain a periodic solution of a desired orbital period T_d.

$$(N-1)T_j - T_d = 0 \tag{3.15}$$

This augmented problem may be exploited to correct a previously converged solution close enough to the desired periodic orbit. For example once a near-resonance orbit is obtained, it can be corrected to obtain the resonance solution.

3.2.2 Continuation Schemes

Multiple-shooting differential corrector algorithms are exploited to obtain a single point solution corresponding to an individual trajectory which satisfy a particular problem defined via the constraint function, such as periodic orbit-attitude Libration Point Orbits. Once a converged solution is found, it is generally useful to expand the subspace of solutions around that particular point and constitute a family of related solutions.
Families of solutions allow to obtain more insights about the dynamical characteristics of the solutions and about the dynamics of the system within some range of its space. They also allow to obtain a wider set of options which may be compared among each other to find a compromise for mission design applications.
Moreover, the development of a continuation scheme for a converged solution is a good benchmark to test the differential corrector algorithm capabilities.
Many techniques are available to generate families of solutions. The single-parameter continuation and pseudo arc-length continuation are the most popular schemes and are largely applied in astrodynamics within the CR3BP framework.

Single Parameter Continuation

Single-parameter continuation schemes are the most intuitive and simple continuation process that can be used. They are based on small adjustment of one parameters which characterize the family of the solutions. Once a first solution has been found thanks to any differential corrector algorithm, an iterative process is applied to generate an entire family of topologically related trajectories. At each iteration, the last converged solution is perturbed in any desired parameter associated with the family to obtain a new initial guess for the differential corrector algorithm. The returned solution is a new member of the family. Commonly selected parameters represent physical quantities of the trajectory, such as the time of flight or the energy level. Note that, during the continuation process, the step size of the featuring parameter and/or the type of parameter itself may be changed.

Single-parameter continuation schemes are general and can be easily implemented in autonomous procedures to find periodic or non-periodic solutions.

In this investigation, the families of periodic orbit-attitude solutions are explored in the simplified-coupled CR3BP within the Earth-Moon system. The parametrization has been applied for the orbital period $T_{orb} = (N-1)T_j$, the Cartesian coordinates of the first patch point x_0 and z_0, and the inertial ratio characterizing a symmetric spacecraft K_a. Moreover, the orbit-attitude Halo orbits are explored by varying the mass parameter μ. Those orbits will be exploited in the following analysis to find dynamical similarities within the same family and will allow comparison among different families.
Note that, using single-parameter continuation schemes, the differential corrector algorithm employed may be slightly modified to obtain a stronger control over the desired parameter continuation. This can be achieved by adding an additional specific constraint that will match the selected parameter, for example on the time of flight, of each new member to a desired value given from the step size adopted in the continuation scheme.

Pseudo Arc-Lenght Continuation

The typical parameter exploited in single-parameter continuation are typically simple and have some physical meaning. Pseudo arc-length continuation schemes may be considered as a special case of simple-parameter continuation. They aims to continue the family along a particular direction, which is built to be tangent to the space of solutions of the family.
The tangential direction is obtained as the null space direction of the Jacobian matrix DF of the last converged solution $\boldsymbol{\nu}^*$.

$$\boldsymbol{k} = \text{null}(DF(\boldsymbol{\nu}^*)) \tag{3.16}$$

The null direction $\boldsymbol{k}$ represents a non-trivial solution of the problem (3.1).
The pseudo arc-length continuation identify a step size Δs along the tangential direction of the family. This direction has the same dimensions of the free variable $\boldsymbol{\nu}$ of the problem, and consequently the arc-length step Δs does not posses any physical meaning. To require the new member of the family $\boldsymbol{\nu}^{(n)}$ to be shifted along the tangential direction of the family $\boldsymbol{k}$ at the last converged solution $\boldsymbol{\nu}^{*(n-1)}$ with an arc-length step Δs, a new constraint equation is added to the constraint function $\boldsymbol{F}$ defined in (3.5).

$$\left(\boldsymbol{\nu}^{(n)} - \boldsymbol{\nu}^{*(n-1)}\right) \cdot \boldsymbol{k} - \Delta s = 0 \tag{3.17}$$

Therefore, an augmented constraint function $\boldsymbol{G}$ can be defined.

$$\boldsymbol{G}\left(\boldsymbol{\nu}^{(n)}\right) = \begin{bmatrix} \boldsymbol{F}\left(\boldsymbol{\nu}^{(n)}\right) \\ \left(\boldsymbol{\nu}^{(n)} - \boldsymbol{\nu}^{*(n-1)}\right) \cdot \boldsymbol{k} - \Delta s \end{bmatrix} = \boldsymbol{0} \tag{3.18}$$

The derivatives of the augmented problem $\boldsymbol{G}\left(\boldsymbol{\nu}^{(n)}\right)$ respect to the free variable $\boldsymbol{\nu}^{(n)}$ yields to the augmented Jacobian matrix DG.

$$DG\left(\boldsymbol{\nu}^{(n)}\right) = \begin{bmatrix} DF\left(\boldsymbol{\nu}^{(n)}\right) \\ \boldsymbol{k}^T \end{bmatrix} \tag{3.19}$$

Finally, the new member of the family is obtained via iterative correction thanks to the multiple-variable Newton-Raphson method applied for the augmented constraint.

$$\boldsymbol{\nu}_{k+1} = \boldsymbol{\nu}_k - DG(\boldsymbol{\nu}_k)^{-1}\boldsymbol{G}(\boldsymbol{\nu}_k) \tag{3.20}$$

As opposed to the single-parameter continuation, the pseudo arc-length continuation does not require a previous knowledge of the user about the family evolution. This strategy exploit a continuation parameter which is neutral (extrinsic) respect the problem definition and typically guarantees the generation of a unique family of solutions, avoiding possible jumps to other families during the continuation process.

3.2.3 Results and Analysis

As said before, the differential corrector algorithm requires an initial guess at its first iteration. This initial guess has to be close enough to a solution, otherwise the correction algorithm could have problem in convergence. Each initial guess exploited to find periodic orbit-attitude Libration Point Orbits are obtained from a software developed internally the Department of Aerospace Science and Technology (DAER) at Politecnico di Milano [19]. This software requires some user defined inputs which are fundamental in order to pilot the algorithm in the desired direction.
The first step consists in selecting the orbital features of the desired periodic solution. The family and the period of the non-Keplerian orbit, such as an Halo orbit, are defined via the initial conditions obtained from the classical periodic orbital dynamics. The inertial properties of the spacecraft are required as second input. A periodic orbit-attitude solutions is associated uniquely to the inertial moments of the spacecraft, and in particular to their ratios. Then, the algorithm asks for the angular rate and the initial orientation of the spacecraft. These states do not have to generate already a periodic motion, but they are fundamental to circumscribe the rotational behaviour subspace to be explored.

The developed multiple-shooting differential corrector has been successfully applied to find periodic solutions in the coupled orbit-attitude CR3BP dynamics exploiting the initial conditions obtained for different families of orbit known from the classical orbital CR3BP. The assumed dynamical model represents the coupled orbit-attitude dynamics within the Earth-Moon system, ignoring any external perturbation but the gravitational effects of the two primaries, such as solar radiation pressure or the gravitational pull of the Sun. The effects due to the second-order term coming from the coupling of the attitude on the orbital dynamics has been considered at the beginning of this investigation. However, the results shows its influence has negligible impact on the periodic solutions obtained from the differential corrector algorithm considering space structures with reasonable mass distribution for nowadays and near future mission in the Earth-Moon system, such as the manned space station around the Moon. This is in line also to what has been seen in other works [18, 17].

A periodic orbit-attitude solution for an example Halo orbit is shown in figure 3.2. The Earth-Moon L_1 Halo orbit shows the same features known from the classical CR3BP. The orbit is symmetric respect the xz-plane. Moreover, it is expected the xy-plane symmetry, leading to the existence of "Northern" and "Southern" solutions also in the orbit-attitude dynamics. The Halo orbit can be characterized via the maximum vertical amplitude A_z and the orbital period T. The obtained Halo orbit has $A_z \simeq 68.8 \cdot 10^3$ km ($\simeq 0.1790$ [ndim]) and orbital period $T \simeq 10.8$ days ($\simeq 2.5010$ [ndim]). The orbit is travelled clockwise respect the libration point. The spacecraft is assumed a 20 tons class spacecraft with transversal moment of inertia $I_1 = I_2 = I_t$ and the axial moment of inertia $I_3 = I_a$. The mass distribution of the spacecraft is the one of a disk-like body with ratio between the maximum moment of inertia ($I_{max} = I_t$) and the minimum moment of inertia ($I_{min} = I_a$) equal to $k = 10/7$. The obtained periodic attitude behaviour corresponds to a simple spinning configuration (relative the inertial frame) about the $\hat{\boldsymbol{b}}_3$ axis. The quaternion evolution of the body relative to the synodic $\{\hat{r}\}$-frame are shown in figure 3.2(b). They describe a librating rotational behaviour of the body frame about the $\{\hat{r}\}$-frame with the symmetric-axis

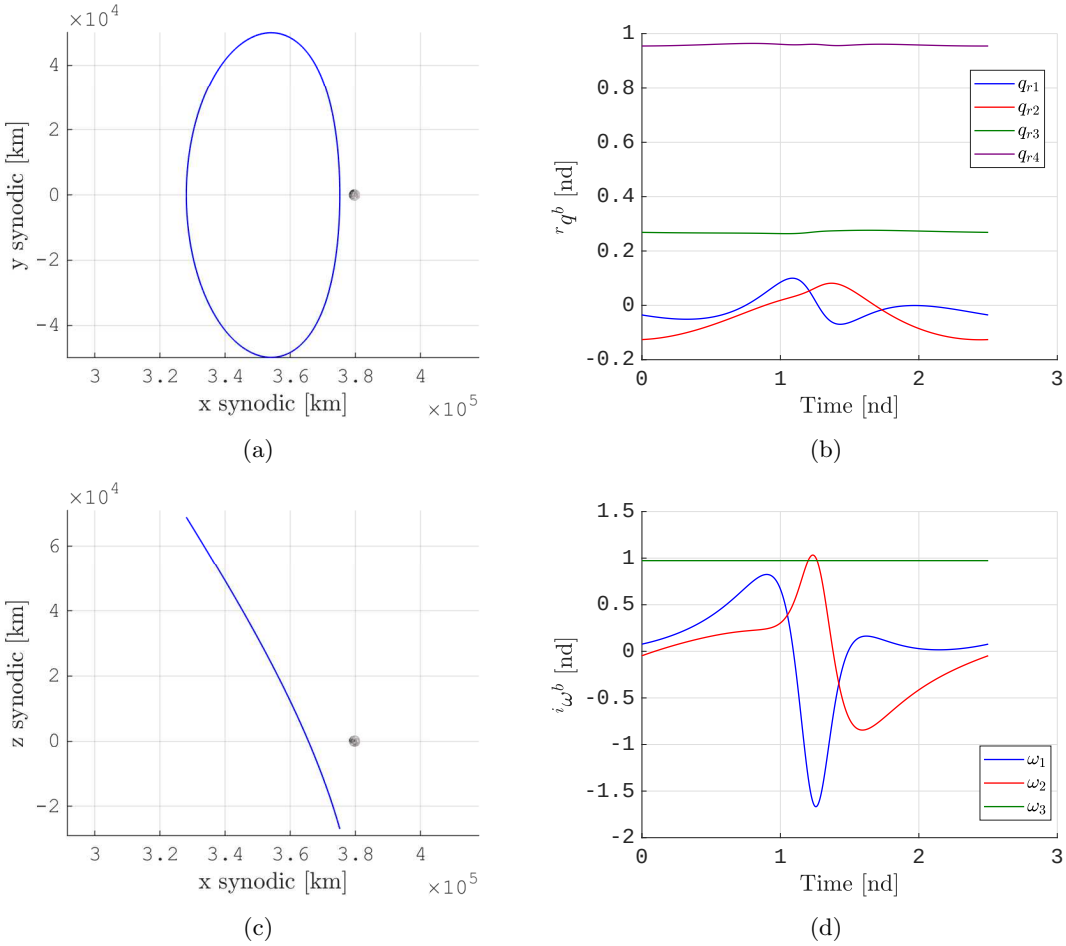

Figure 3.2: Example of periodic orbit-attitude solution. Earth-Moon L_1 Halo orbit: maximum vertical amplitude $A_z = 68.8 \cdot 10^3$ km ($A_z = 0.1790$ [ndim]), orbital period $T = 10.8$ days ($T = 2.5010$ [ndim]) for a disk-like spacecraft

of the spacecraft quasi-aligned to $\hat{\boldsymbol{z}}$ and no overall rotation.
It should be noted the passage of the spacecraft close to the Moon results in a visible angular acceleration due to the stronger gravity gradient effect exerted by the second primary. The Earth-Moon L_1 Halo orbit presented in figure 3.2 is exploited to generate iteratively new members of its family with the same inertial properties of the spacecraft via the pseudo arc-length continuation. The range of solution generated can be associated to the high amplitude L_1 Halo orbits. Their maximum vertical amplitude A_z goes from about $58.8 \cdot 10^3$ km ($\simeq 0.1530$ [ndim]) up to about $71.1 \cdot 10^3$ km ($\simeq 0.1850$ [ndim]) with the corresponding orbital periods T ranging from 11.8 days ($\simeq 2.7270$ [ndim]) to 10.3 days ($\simeq 2.3779$ [ndim]). As can be seen in figure 3.3, the family continuation returned a set of periodic orbit-attitude solution which maintains similar features in both traslationalal and rotational behaviours.
The continuation algorithm developed has encountered high difficulties to further expand the family in both the directions. It seems the coupled periodic orbit-attitude behaviour of the obtained family is bounded to this particular region among the periodic orbital family known from the classical CR3BP.

This kind of distributed fragmentation of families seems to be typical of the periodic orbit-attitude libration point orbits, especially for nutational rotational motion of the body relative the synodic frame. It is like the periodic attitude dynamics are allowed to exist only within certain region of the orbit with specific energy levels. Those results can be explained considering the

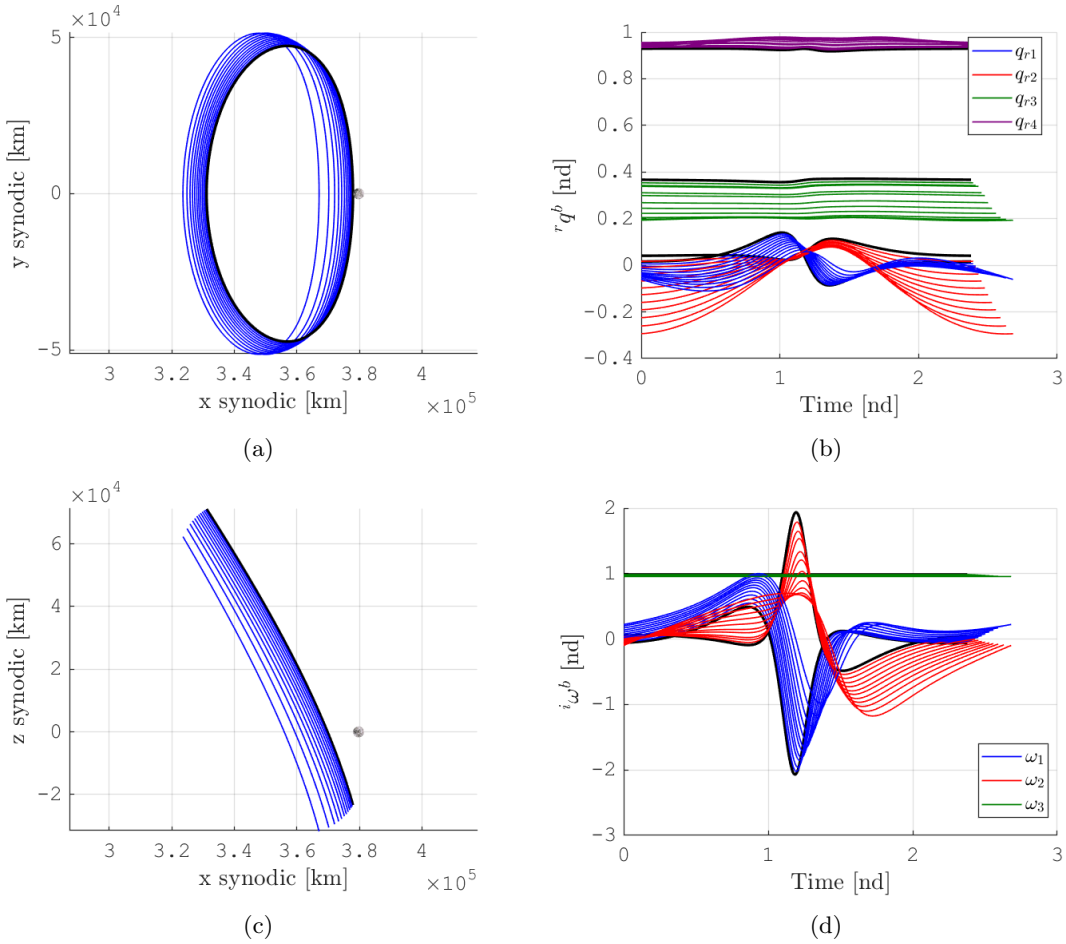

Figure 3.3: Periodic orbit-attitude Earth-Moon L_1 Halo family. Orbit projection on the xy synodic plane (a). Orbit projection on the xz synodic plane (c). Quaternion of the body relative to the synodic frame (b). Angular velocity profile (d)

dynamical bifurcations along the family and the changes in the stability properties associated to rotational motion. However, further analysis will be required for a better understanding of these behaviours.

The same procedure has been applied to find existing periodic orbit-attitude solutions for Near Rectilinear Halo Orbits, Lyapunov orbits and Distant Retrograde Orbits.
For periodic orbit-attitude NRHO, the mass distribution of the spacecraft represents again a disk-like body similar to the one considered for the Halo orbit, but now its axis of symmetry corresponds to the body axis $\hat{\boldsymbol{b}}_1$. The family generated via pseudo arc-length continuation is shown in figure 3.4. The periodic orbit-attitude family of Earth-Moon L_1 Northern NRHO obtained has maximum out-of-plane amplitude Az ranging from $88.9 \cdot 10^3$ km ($\simeq 0.2312$ [ndim]) to $73.3 \cdot 10^3$ km ($\simeq 0.1907$ [ndim]). These orbits present all the characteristics they have in the classical CR3BP. They are featured by a quasi-planar orbital path and by a quite close passage to the secondary attractor, in this case the Moon. This class of orbits are known to exhibit nearly-stable behaviour favourable for orbital station-keeping. They offer nearly-constant communication contact with Earth and high visibility time of lunar South or North pole. In fact, the NRHOs resemble some sort of high polar orbit of the Moon which is synchronously aligned to the synodic frame. Moreover, they avoid lengthy eclipses of the Sun by the Earth, maximizing the capacity of solar energy generation. Finally, the costs to reach a NRHO from the Earth are not prohibitive both in propellant and transfer time, and those orbits may offer an easy transfer link to and from the lunar surface. All

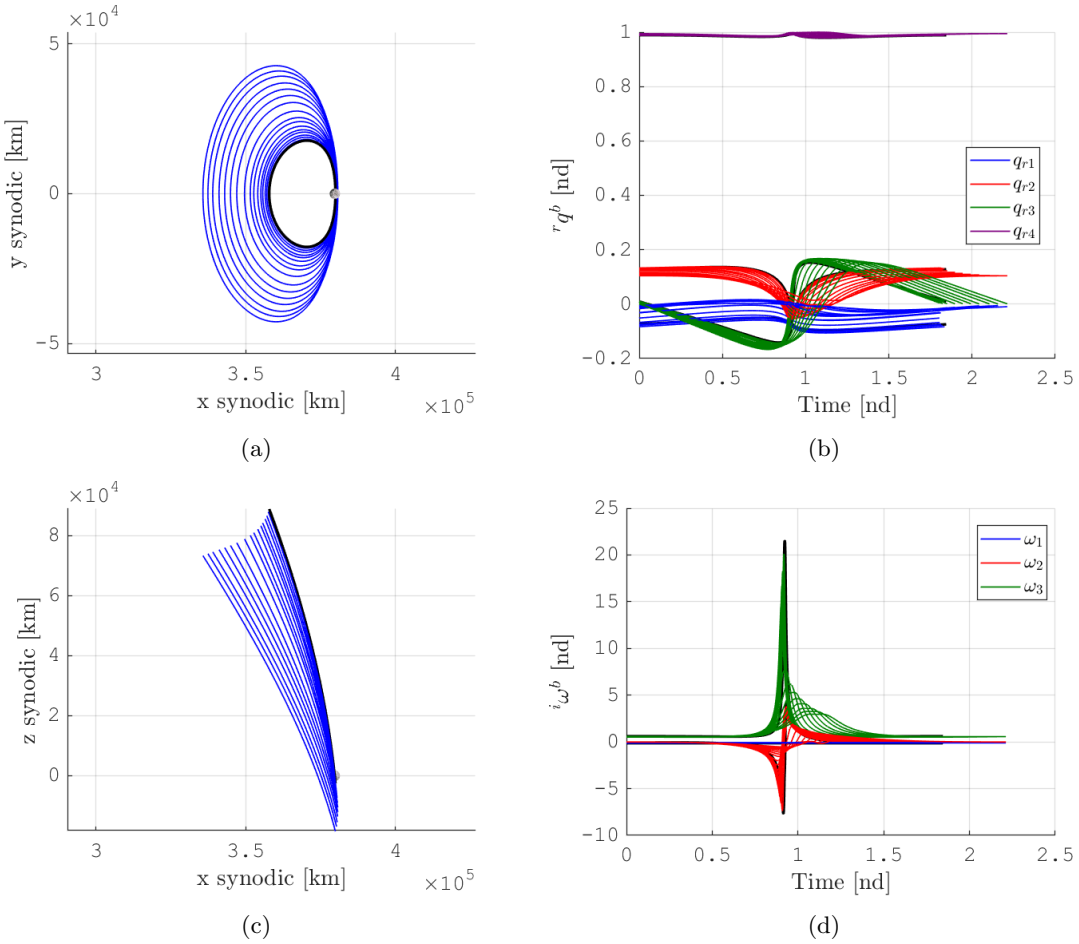

Figure 3.4: Periodic orbit-attitude Earth-Moon L_1 Northern NRHO family. Orbit projection on the xy synodic plane (a). Orbit projection on the xz synodic plane (c). Quaternion of the body relative to the synodic frame (b). Angular velocity profile (d)

these features make NRHOs a very attractive choice as staging orbit for the future cislunar space station.

However, the very close passage to the Moon is reflected on the rotational motion through a huge rise in the angular acceleration, as can be seen in figure 3.4(d). This effect, which has been observed already for the Halo family, is highly emphasized and seems to be a feature typical of the periodic orbit-attitude NRHO. The high angular acceleration could be problematic for large space structure integrity, because they could affect the flexible dynamics of the structure.

The figures in 3.5 report the profiles of the orbital period and of the perilune distance of the investigated L_1 NRHO family. The orbital period presents a minimum in the middle of the family, but all the higher NRHOs are characterized by an orbital period of about 8 days.

It should be noticed that the perilune distance can be considered an alternative identification parameter for NRHO families. The perilune distance decreases while the maximum out-of-plane amplitude increases. It seems to approach asymptotically zero while the orbital period increases. The continuation process has encountered numerical difficulties to continue the family in this direction due to the high sensitivity of the dynamics in the regions closer to the Moon which leads to high gravity gradients in both orbital and attitude states. Selecting the apolune point as initial point of the orbit and an even number of patch points allows to avoid the presence of a patch point in the perilune point. Increasing the number of patch point should lead to a more robust and consistent correction algorithm. However, larger number of patch point means some of them

will be placed near the highly sensible zone of the orbit in both attitude and orbital states, leading to problems in convergence of the differential corrector.

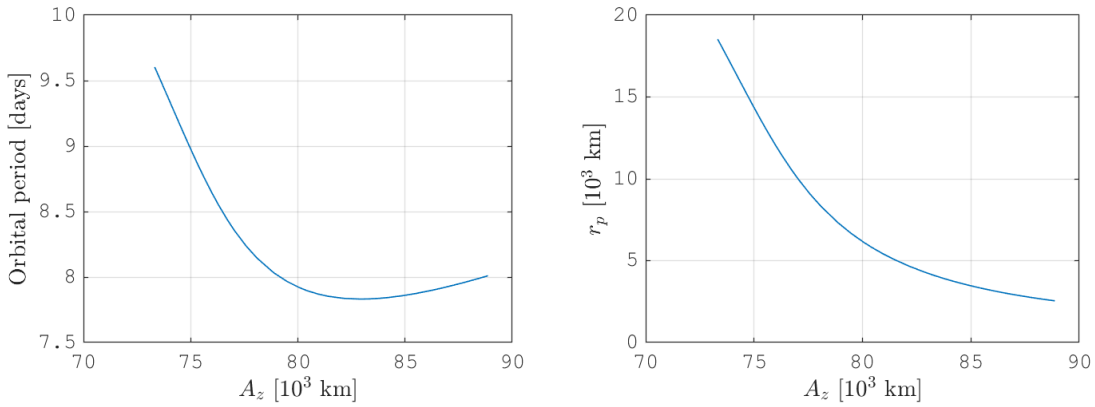

Figure 3.5: Orbital period and perilune distance profile of the orbit-attitude NRHO family

Single-parameter continuation strategies have been successfully employed to find families of periodic solutions varying different parameters associated to the orbit. This parameter may be associated directly to the orbit, such as the orbital period T or the initial Cartesian coordinates x_0 or z_0, but it may also represent parameters characterizing the dynamical system, such as the mass parameter μ or the mass distribution of the spacecraft.
Spacecraft structure are typically designed to be symmetric or quasi-symmetric for many beneficial reasons in attitude dynamics and in manufacturing. Therefore, the selection of rod-like and disk-like bodies is a reasonable approximation for a spacecraft. Its inertial shape can be uniquely associated to the ratio between the transversal moment of inertia and the axial moment of inertia.

$$K_a = I_t/I_a \tag{3.21}$$

Using this formulation, an inertial ratio $K_a = 1$ represents spherical-like or cubic-like bodies. A $K_a > 1$ defines a rod-like spacecraft, while $K_a < 1$ defines a disk-like spacecraft.
Many librating attitude behaviours have been found thanks to the differential corrector and continued varying K_a via single-parameter continuation. Also spinning attitude periodic solutions has been found along planar orbits, e.g. Lyapunov orbits and DROs.
This investigation has been focused on the characterization of the relative dynamics of the coupled CR3BP, however future studies may be conducted to better characterize existing periodic orbit-attitude solution in relation with the mass distribution of the spacecraft.

It is known that the mass parameter μ identify uniquely the two primary attractors constituting the non-dimensional system in the Restricted Three-Body Problem. The mass parameter is bounded within $\mu \in [0, 0.5]$. The lower limit corresponds to the classical Keplerian model. Instead the upper limit describe a perfect binary system composed of two identical attractors.
The Earth-Moon system corresponds to $\mu \simeq 0.01215$. A continuation of the family toward $\mu = 0$ means to find periodic solution in a system with an increasing dimension of the first primary respect the secondary, such as the Sun-Earth system or the Mars-Fobos system. Continuing the family in the direction $\mu = 0.5$ correspond to find periodic solution in a system with an increasing dimension of the secondary attractor towards the primary. These systems may be particularly interesting to approximate the gravitational environment in the vicinity of asteroids, such as binary system with similar attractors or gravity field generated by an asteroid modelled as two lumped masses, such

as asteroids having a duck-like shape similar to the one of comet 67P/Churyumov-Gerasimenko encountered in the Rosetta mission. However, the asteroid scenario may lead to have no more a negligible effect of the attitude on the orbital dynamics due to the gravitational attraction of the primaries on a finite extended space structure.
The orbit-attitude Halo orbit presented in figure 3.2 is continued in the mass parameter up to values in the order of $\mu \sim 10^{-6}$, similar to the one representing the Sun-Earth system. The generated family of periodic solutions is reported in figure 3.6. The color of the orbits in figures 3.6(a) and

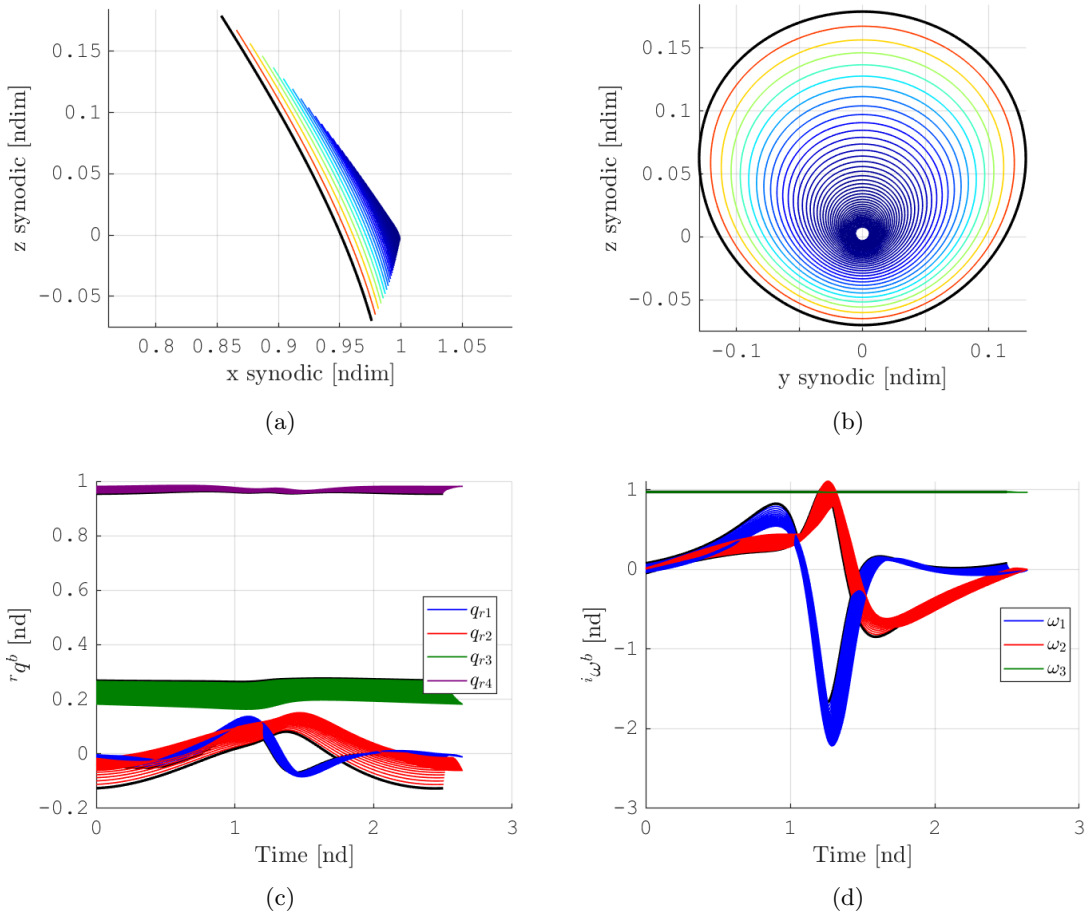

Figure 3.6: Continuation of orbit-attitude Halo family varying mass parameter μ

3.6(b) identify the mass parameter value: from red for $\mu \sim 10^{-2}$ up to dark blue for $\mu \sim 10^{-6}$. Now the characteristic length used before for the Earth-Moon system loses its meaning. Therefore, the solutions are reported in non-dimensional quantities.
The orbits of the family seem to keep their shape, but they become smaller and smaller while the mass parameter decreases.
The rotational motion remains similar through the family, and the nutational behaviour tends to decrease it intensity as μ approaches zero. This is justified by the lower gravitational importance of the secondary primary, thus a lower gravity gradient torque which affect the oscillation in the attitude motion.

3.3 Targetter

Find a trajectory departing from a given initial point and arriving at a desired final point is a typical problem in orbital mechanics. In the differential corrector, a final target condition can be

imposed simply by adding constraint equations at the last patch point of the trajectory. Within the orbit-attitude space, the final point may be constrained for both the orbital and attitude states.

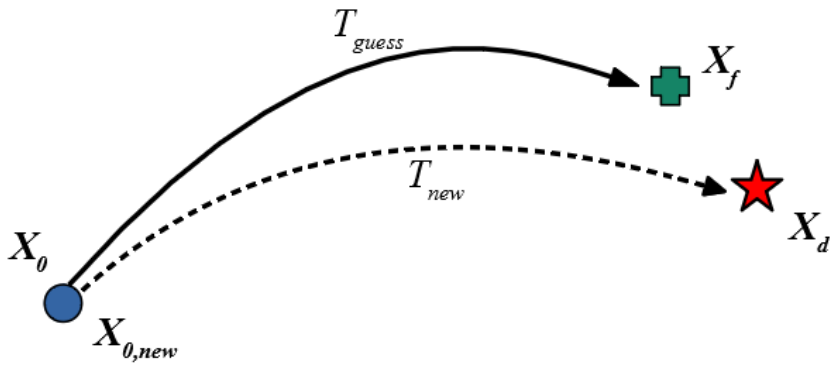

Figure 3.7: Sketch of the targeting scheme

In the simplest case, the specific constraint corresponds to the difference of the actual states at final patch point and a fixed desired point representing the arrival condition. For example, let consider to target a desired final orbital state $\boldsymbol{x_d} = [\boldsymbol{x}; \boldsymbol{v}]$, that may represent the insertion on a nominal periodic orbital LPO in the CR3BP.

$$\boldsymbol{F} = \left[\boldsymbol{x} - \boldsymbol{x_d}\right] \tag{3.22}$$

The same type of constraint may be extended to the orbit-attitude space for the insertion on a nominal periodic orbit-attitude LPO. Any other kind of mission requirements can be accomplished, for example including attitude states, time of flight, a set of Keplerian parameters, altitude or flight path angle in the constraints. Also small correction maneuvers may be optionally included by adding loose constraints at continuity requirement at the internal patch point for the velocity states.
Once the mission requirements are defined as specific constraint equation, they are added to the internal patch point continuity constraint to build the global constraint function of the differential corrector.
In the case of departure from a given orbit-attitude condition, the initial position and quaternion vector components are removed from the free variables $\boldsymbol{\nu}$. Also the initial angular velocity may be removed from the set of the free variable if desired. If so, at the initial point only an orbital impulsive maneuver will be allowed. For same considerations, the constraint on the velocity at the final condition may be avoided, leaving only the position constraint. In this case, the targetter represents a two-impulsive transfer maneuver. The exclusion of some of the original free variables is reflected in the elimination of the corresponding rows and columns from the constraint function vector $\boldsymbol{F}$ and Jacobian DF.

3.4 Final Remarks

The developed correction algorithms has been employed to find periodic orbit-attitude Libration Point Orbits within the simplified-coupled CR3BP and the continuation schemes has been able to generate different families for Halo orbits, NRHOs, Lyapunov orbits and DROs.
The orbital solutions investigated are symmetric orbits, but in principle the same algorithm with

few modification should be capable to find any kind of periodic solution (always if the initial guess would be well posed).
The set of orbit-attitude families computed in this chapter will be exploited in the following of this investigation to explore and analyse the relative dynamics existing in proximity of periodic LPO of the simplified-coupled CR3BP to have some insights on how to characterize the motion of spacecrafts orbiting in the vicinity of periodic orbit-attitude natural solution in cislunar space.
A wider and deeper characterization of the existing natural periodic solutions and families in the coupled orbit-attitude CR3BP may be argument of future investigations. Those orbits may offer interesting insights about periodic or quasi-periodic solutions as approximation of an higher fidelity orbit-attitude model. They could be exploited in future application scenarios of different nature considering not only orbital dynamics as in the classical CR3BP, but also attitude behaviours.
Future work may be addressed to exploit the differential corrector targetter to explore simple station keeping strategies in the coupled orbit-attitude CR3BP as a direct extension of those already developed for the orbital dynamics only.
Other interesting mission scenario could aim to develop an open-loop impulsive controller for far range phases of rendezvous mission or for formation flying applications in the coupled orbit-attitude CR3BP thanks to the development of dedicated targetter differential corrector algorithm.

Chapter 4

ORBIT-ATTITUDE INVARIANT MANIFOLDS

Once orbit-attitude periodic solution are discovered, the exploration of dynamical structures associated to these periodic motions, such as invariant manifold surfaces and quasi-periodic behaviours, constitutes the next fundamental step in the characterization of the solution space of complex dynamical system like the CR3BP.

In this chapter, the Floquet's theory will be discussed and applied to the orbit-attitude CR3BP problem. The orbital and the attitude modes constituting the local approximation of the global invariant manifolds are presented in a novel perspective to characterize the relative 6DOF dynamics in proximity of non-Keplerian orbits existing in the CR3BP environment.

4.1 Floquet Theory

This section presents the fundamental theorems and the main concepts for the analysis of non-linear system, which will be applied in the following to the orbit-attitude motion in the CR3BP. Let be $\boldsymbol{f}$ an autonomous non-linear system of differential equations.

$$\dot{\boldsymbol{x}} = \boldsymbol{f}(\boldsymbol{x}) \tag{4.1}$$

Where $\boldsymbol{f} \in C^1(E)$ and E is an open subset of $\mathbb{R}^n$. Let define the dynamical flow $\phi_t(\boldsymbol{x}) = \phi(\boldsymbol{x}, t)$ as the flow driven by (4.1) and passing through the initial point $\boldsymbol{x}$. Assume that a periodic orbit Γ of period T exists in the system (4.1).

$$\Gamma : \boldsymbol{x} = \gamma(t) = \phi_t(\boldsymbol{x_0}) \quad 0 \leq t \leq T \tag{4.2}$$

This means that any point of the orbit can be characterized by the initial point x_0 and the time t. The latter is the time needed to reach the desired point $\boldsymbol{x}$ on the periodic orbit through the flow ϕ starting from the point $\boldsymbol{x_0}$.
The linearization of (4.1) about Γ is defined by the following non-autonomous linear system.

$$\delta\dot{\boldsymbol{x}} = A(t)\delta\boldsymbol{x} \tag{4.3}$$

For a periodic orbit $A(t) = D\boldsymbol{f}(\gamma(t))$, which means it is a continuous and T-periodic matrix. The fundamental matrix $\Phi(t)$, is a non-singular $n \times n$ matrix, which satisfy the next fundamental matricial differential equation.

$$\dot{\Phi}(t) = A(t)\Phi(t) \tag{4.4}$$

The State Transition Matrix $\Phi(t)$, also denoted as STM, represents the linear mapping of the variational evolution about a reference flow ϕ_t. Therefore, it has to satisfy the initial condition $\Phi(0) = I$.
For a periodic orbit, the Floquet's Theorem says that, for all $t \in \mathbb{R}$, any fundamental solution matrix of the system (4.3) can be written in the following particular form.

$$\Phi(t) = Q(t)\, e^{Bt} \tag{4.5}$$

Where $Q(t)$ is a non-singular, differentiable, T-periodic matrix, and B is a constant matrix. Furthermore, if $\Phi(0) = I$ then also $Q(0) = I$. It follows that after a full period $Q(T) = I$ and, as a consequence, the definition of monodromy matrix is obtained.

$$\Phi(T) = e^{BT} \tag{4.6}$$

Therefore, the eigenvalues λ_j of the monodromy matrix $\Phi(T)$ are directly related to the eigenvalues ϵ_j of the matrix B.

$$\|\lambda_j\| = e^{\epsilon_j T} \tag{4.7}$$

The eigenvalues ϵ_j are called characteristic exponents of the periodic orbit $\gamma(t)$, while the eigenvalues λ_j are called characteristic multipliers of $\gamma(t)$. Let now apply the following transformation of coordinate to the variational state vector.

$$\boldsymbol{y} = Q^{-1}(t)\delta\boldsymbol{x} \tag{4.8}$$

This transformation reduces (4.3) to an autonomous linear system with constant coefficients.

$$\dot{\boldsymbol{y}} = B\boldsymbol{y} \tag{4.9}$$

This system can be exploited to feature the relative state $\delta\boldsymbol{x}$, e.g. the relative orbital and attitude states of the chaser spacecraft in the vicinity of a periodic orbit in the CR3BP.
As consequence of being an autonomous linear system, all the optimal control theory developed for Linear Time-Invariant (LTI) system may be applied to (4.9). Note that, even if it is possible to develop a "modal" controller, the difficulties lie in bringing back the control to its traditional form due to the problems in finding the analytical form of $Q(t)$. This control could be used to estimate an initial condition for the design of the guidance function, being the "modal" controller based on the modal representation of an approximated relative dynamics of a non-liner system.
Moreover, the knowledge of eigenvalues and eigenvectors of the matrix B allows, not only to diagonalize the system (4.9), but also to decompose the fundamental relation (4.5).

$$\Phi(t) = E(t)\, e^{Jt}\, E^{-1}(0) \tag{4.10}$$

Where J is a constant matrix which diagonal components corresponds to the ϵ_j eigenvalues of B. The matrix $E(0)$ is the matrix of the orbit eigenvectors. The columns of $E(0)$ are constituted from the real and the imaginary part of the eigenvectors of the monodromy matrix. The matrix $E(t)$ is called Floquet Modal matrix and is a non-singular, differentiable, and T-periodic matrix. The columns $\boldsymbol{e_j}$ of the matrix $E(t)$ represents a n-dimensional, non-orthogonal basis to describe the system (4.3) and are defined as Floquet modes.
Equation (4.10) shows that the characteristic exponents ϵ_j describe the rate of departure from the neighbourhood of the orbit $\gamma(t)$, qualitatively proportional to an exponential function. Therefore, the monodromy matrix is so important for non-linear system analysis because it gives access to

the stability information of the orbit via its eigenvalues.
Moreover, the eigenvectors of the monodromy matrix allow to decompose the relative motion in the vicinity of the orbit $\gamma(t)$ through the Floquet modes.
Substituting the Floquet decomposition of the fundamental solution (4.10) into (2.70), a new formulation of the variational equation is obtained.

$$\delta \boldsymbol{X}(t) = \Phi(t,0)\,\delta \boldsymbol{X}(0) = E(t)\,e^{Jt}\,E^{-1}(0)\,\delta \boldsymbol{X}(0) \tag{4.11}$$

The component $\boldsymbol{c}(0) = E^{-1}(0)\,\delta \boldsymbol{X}(0)$ constitutes the decomposition of the initial relative state in its components projected along the Floquet modes. Knowing the time evolution of each Floquet mode $E(t)\,e^{Jt}$, the propagation of the motion can be obtained for any generic initial condition in proximity of the reference orbit.

4.1.1 Stable Manifold Theorem for Periodic Orbits

Let consider the periodic orbit Γ in the non-linear system $\boldsymbol{f} \in C^r$. If the set of the characteristic exponents has at least one eigenvalue ϵ_j with negative real part, then there exists a neighbourhood N_δ of the orbit Γ such that

$$S(\Gamma) = \{\boldsymbol{x} \in N_\delta(\Gamma) \;|\; \Delta(\phi_t(\boldsymbol{x}),\Gamma) \to 0 \;\; as \;\; t \to \infty \;\; and \;\; \phi_t(\boldsymbol{x}) \in N_\delta(\Gamma) \;\; for \;\; t \geq 0\} \tag{4.12}$$

The stable manifold $S(\Gamma)$ of the orbit Γ describe an n_S-dimensional space which is positively invariant under the flow ϕ_t, where n_S is equal to the number of stable eigenvalues ϵ_j.
If the set of the characteristic exponents has at least one eigenvalue ϵ_j with positive real part, then there exists a neighbourhood N_δ of the orbit Γ such that

$$U(\Gamma) = \{\boldsymbol{x} \in N_\delta(\Gamma) \;|\; \Delta(\phi_t(\boldsymbol{x}),\Gamma) \to 0 \;\; as \;\; t \to -\infty \;\; and \;\; \phi_t(\boldsymbol{x}) \in N_\delta(\Gamma) \;\; for \;\; t \leq 0\} \tag{4.13}$$

The unstable manifold $U(\Gamma)$ of the orbit Γ describe a n_U-dimensional space which is negatively invariant under the flow ϕ_t, where n_U is equal to the number of unstable eigenvalues ϵ_j.
The motion along trajectories on the flows belonging to stable or unstable manifolds is synchronized with the motion along the corresponding orbit Γ through a given asymptotic phase t_0 (remember that the time $0 \leq t \leq T$ identify a point along the periodic orbit as $\gamma(t)$). This is one of the most important features of the invariant manifolds. Moreover, the stable and the unstable manifolds intersect trasversally in the orbit Γ.
The local stable manifold $S(\Gamma)$ and the local unstable manifold $U(\Gamma)$ can be exploited to generate the corresponding global stable manifold $W^S(\Gamma)$ and the global unstable manifold $W^U(\Gamma)$. The global stable and unstable manifolds are defined respectively as

$$W^S(\Gamma) = \bigcup_{t \leq 0} \phi_t(\boldsymbol{x}) \;\; with \;\; \boldsymbol{x} \in S(\Gamma) \tag{4.14}$$

$$W^U(\Gamma) = \bigcup_{t \geq 0} \phi_t(\boldsymbol{x}) \;\; with \;\; \boldsymbol{x} \in U(\Gamma) \tag{4.15}$$

The local invariant manifolds are directly linked to the subspace of the monodromy matrix $\Phi(T)$. Let define the reference point $\boldsymbol{x_0} \in \Gamma$ as the initial point of the orbit considered for the monodromy matrix computation. Let define the eigenvalues and the corresponding eigenvectors of the monodromy matrix as λ_j and $\boldsymbol{v_j}$. Let be n_S the number of the stable eigenvalues such that $\|\lambda_j^S\| < 1$, n_U the number of the unstable eigenvalues such that $\|\lambda_j^U\| > 1$, and n_C the number of the center eigenvalues such that $\|\lambda_j^C\| = 1$. The corresponding eigenvectors are denoted as $\boldsymbol{v_j^S}$, $\boldsymbol{v_j^U}$ and $\boldsymbol{v_j^C}$.

It follows that the subspace of the monodromy matrix of the periodic orbit Γ at the reference point $\boldsymbol{x_0}$ is defined as

$$E^S(\Gamma) = Span\left\{\boldsymbol{v_j^S}\right\} \quad \text{with} \quad j = \text{from 1 to } n_S \tag{4.16}$$

$$E^U(\Gamma) = Span\left\{\boldsymbol{v_j^U}\right\} \quad \text{with} \quad j = \text{from 1 to } n_U \tag{4.17}$$

$$E^C(\Gamma) = Span\left\{\boldsymbol{v_j^C}\right\} \quad \text{with} \quad j = \text{from 1 to } n_C \tag{4.18}$$

The Stable Manifold Theorem for periodic orbit [39] says that the local stable and unstable manifolds $W^S(\Gamma)$ and $W^U(\Gamma)$ are tangent to the corresponding stable and the unstable subspaces $E^S(\Gamma)$ and $E^U(\Gamma)$ at the reference point $\boldsymbol{x_0}$. Therefore, the eigenvectors of the monodromy matrix allows to numerically approximate the local stable and unstable manifolds. Then, the global stable and unstable manifolds can be numerically propagated as shown in equations (4.14) and (4.15).

4.1.2 Center Manifold Theorem for Periodic Orbits

Let consider again the periodic orbit Γ in the system $\boldsymbol{f} \in C^r(E)$ where E is an open subset of $\mathbb{R}^n$. Let be n_S the number of characteristic exponents with negative real part, and let be n_U the number of the characteristic exponents with positive real part. Therefore, there will be $n_C = n - n_S - n_U$ characteristic exponents with zero real part. Then, a n_C-dimensional center manifold of the periodic orbit $W^C(\Gamma)$ exists. It will be of class C^r and invariant under the flow ϕ_t. The invariant manifolds $W^S(\Gamma)$, $W^U(\Gamma)$ and $W^C(\Gamma)$ intersect trasversally in the orbit Γ. Furthermore, if the origin has been translated to the reference point $\boldsymbol{x_0}$, the center subspace $W^C(\Gamma)$ is tangent to the center subspace $E^C(\Gamma)$ of the monodromy matrix of Γ at the point $\boldsymbol{x_0}$.
Therefore, the eigenvectors of the monodromy matrix allows to numerically approximate the local stable, unstable and center invariant manifolds.

4.2 Orbit-Attitude Monodromy Matrix

Let consider a periodic solution in the orbit-attitude dynamical system $\boldsymbol{f}_{\text{OrbAtt}}$. The monodromy matrix M related to this periodic orbit-attitude Libration Point Orbit is defined as the STM which is propagated after a full period T.

$$M = \Phi(T + t_0, t_0) \tag{4.19}$$

Orbit-attitude Libration Point Orbits have been defined as periodic solution existing in the dynamical system $\boldsymbol{f}_{\text{OrbAtt}}$, where the orbital states and the attitude states are periodic referring to an observer fixed in the synodic $\{\hat{r}\}$-frame. The periodicity of the attitude states is seen in the quaternion of the body-fixed $\{\hat{b}\}$-frame respect to the rotating $\{\hat{r}\}$-frame. The angular velocity of the body respect the inertial $\{\hat{i}\}$-frame and respect the rotating $\{\hat{r}\}$-frame differ only of a constant, equal to the angular motion of the rotating system. Therefore, a solution with periodic angular velocity in the inertial $\{\hat{i}\}$-frame is periodic also in the rotating $\{\hat{r}\}$-frame.
The monodromy matrix has to be written in the correct form in order to catch the actual eigenstructure around the periodic orbit-attitude LPO seen from a rotating observer.
The integration of the dynamical system including the first-order variational equation for the STM

gives the following linear mapping relation.

$$\begin{bmatrix} \delta\boldsymbol{x} \\ \delta^{\boldsymbol{i}}\boldsymbol{q}^{\boldsymbol{b}}_{\boldsymbol{R}} \\ \delta^{\boldsymbol{i}}\boldsymbol{\omega}^{\boldsymbol{b}} \end{bmatrix}_t = \begin{bmatrix} \Phi_{\boldsymbol{xx}} & \Phi_{\boldsymbol{xq}} & \Phi_{\boldsymbol{x\omega}} \\ \Phi_{\boldsymbol{qx}} & \Phi_{\boldsymbol{qq}} & \Phi_{\boldsymbol{q\omega}} \\ \Phi_{\boldsymbol{\omega x}} & \Phi_{\boldsymbol{\omega q}} & \Phi_{\boldsymbol{\omega\omega}} \end{bmatrix} \begin{bmatrix} \delta\boldsymbol{x} \\ \delta^{\boldsymbol{i}}\boldsymbol{q}^{\boldsymbol{b}}_{\boldsymbol{R}} \\ \delta^{\boldsymbol{i}}\boldsymbol{\omega}^{\boldsymbol{b}} \end{bmatrix}_{t_0} \tag{4.20}$$

The elements of the vector $\delta\boldsymbol{x} = [\delta x; \delta y; \delta z; \delta v_x; \delta v_y; \delta v_z]$ are the variational orbital states, those of $\delta^{\boldsymbol{i}}\boldsymbol{q}^{\boldsymbol{b}}_{\boldsymbol{R}} = [\delta q_1; \delta q_2; \delta q_3]$ are the variation on the independent elements of the quaternion of the body-fixed frame respect to the inertial reference frame, while those in $\delta^{\boldsymbol{i}}\boldsymbol{\omega}^{\boldsymbol{b}} = [\delta\omega_1; \delta\omega_2; \delta\omega_3]$ are the variation on the angular velocity of the spacecraft respect the inertial frame expressed in body coordinates. The blocks $\Phi_{\boldsymbol{ij}}$ represent the STM elements corresponding the partials of the final states of $\boldsymbol{i}$ with respect to the initial states of $\boldsymbol{j}$, where $\boldsymbol{i}$ and $\boldsymbol{j}$ represent orbital, quaternion or angular velocity vectors.
Assuming that the synodic frame is aligned with the inertial reference frame at time $t = 0$, therefore the quaternion identifying the orientation of the body-fixed frame respect the inertial frame coincides with the one referring to the rotating frame.

$$\delta^{\boldsymbol{r}}\boldsymbol{q}^{\boldsymbol{b}}_{\boldsymbol{R}}(0) = \delta^{\,\boldsymbol{i}}\boldsymbol{q}^{\boldsymbol{b}}_{\boldsymbol{R}}(0) \tag{4.21}$$

This means that the initial variational state vector is already in the correct form, and only the final variational state vector has to be manipulated.
At time t, given the quaternion representing the body-fixed frame with respect to the inertial and the rotating frame, respectively ${}^{\hat{i}}\boldsymbol{q}^{\hat{b}} = [q_1; q_2; q_3; q_4]$ and ${}^{\hat{r}}\boldsymbol{q}^{\hat{b}} = [\tilde{q}_1; \tilde{q}_2; \tilde{q}_3; \tilde{q}_4]$, the variational form of equation (2.36) gives the following relation.

$$\begin{bmatrix} \delta\tilde{q}_1 \\ \delta\tilde{q}_2 \\ \delta\tilde{q}_3 \\ \delta\tilde{q}_4 \end{bmatrix} = \begin{bmatrix} \cos(t/2) & \sin(t/2) & 0 & 0 \\ -\sin(t/2) & \cos(t/2) & 0 & 0 \\ 0 & 0 & \cos(t/2) & -\sin(t/2) \\ 0 & 0 & \sin(t/2) & \cos(t/2) \end{bmatrix} \begin{bmatrix} \delta q_1 \\ \delta q_2 \\ \delta q_3 \\ \delta q_4 \end{bmatrix} \tag{4.22}$$

Therefore, the variational relation between the reduced quaternion $\delta^{\boldsymbol{r}}\boldsymbol{q}^{\boldsymbol{b}}_{\boldsymbol{R}}(t)$ and the 4-dimensional quaternion $\delta^{\hat{i}}\boldsymbol{q}^{\hat{b}}(t)$ can be directly derived.

$$\delta^{\boldsymbol{r}}\boldsymbol{q}^{\boldsymbol{b}}_{\boldsymbol{R}}(t) = \begin{bmatrix} \cos(t/2) & \sin(t/2) & 0 & 0 \\ -\sin(t/2) & \cos(t/2) & 0 & 0 \\ 0 & 0 & \cos(t/2) & -\sin(t/2) \end{bmatrix} \begin{bmatrix} \delta q_1 \\ \delta q_2 \\ \delta q_3 \\ \delta q_4 \end{bmatrix} = T(t)\,\delta^{\,\hat{i}}\boldsymbol{q}^{\hat{b}} \tag{4.23}$$

Now, the variational form of the quaternion constraint is derived from equation (2.74).

$$\delta q_4 = -\frac{q_1}{q_4}\delta q_1 - \frac{q_2}{q_4}\delta q_2 - \frac{q_3}{q_4}\delta q_3 \tag{4.24}$$

From equation (4.24), the relation between the variation of the 4-dimensional quaternion and its independent reduced form can be defined.

$$\begin{bmatrix} \delta q_1 \\ \delta q_2 \\ \delta q_3 \\ \delta q_4 \end{bmatrix} = \begin{bmatrix} 1 & 0 & 0 \\ 0 & 1 & 0 \\ 0 & 0 & 1 \\ -q_1/q_4 & -q_2/q_4 & -q_3/q_4 \end{bmatrix} \begin{bmatrix} \delta q_1 \\ \delta q_2 \\ \delta q_3 \end{bmatrix} = V(q_1, q_2, q_3, q_4)\,\delta^{\boldsymbol{i}}\boldsymbol{q}^{\boldsymbol{b}}_{\boldsymbol{R}} \tag{4.25}$$

Substituing (4.25) into (4.23), the variational relation between the reduced form of the quaternions can be expressed in a compact vectorial form.

$$\delta^{\boldsymbol{r}}\boldsymbol{q}^{\boldsymbol{b}}_{\boldsymbol{R}}(t) = T(t)\, V(q_1, q_2, q_3, q_4)\, \delta^{\boldsymbol{i}}\boldsymbol{q}^{\boldsymbol{b}}_{\boldsymbol{R}} = T_R(t, q_1, q_2, q_3, q_4)\, \delta^{\boldsymbol{i}}\boldsymbol{q}^{\boldsymbol{b}}_{\boldsymbol{R}} \tag{4.26}$$

Now, the STM $\tilde{\Phi}(t, t_0)$ seen from a rotating observer is obtained substituting (4.21) and (4.26) into (4.20).

$$\begin{bmatrix} \delta\boldsymbol{x} \\ \delta^{\boldsymbol{r}}\boldsymbol{q}^{\boldsymbol{b}}_{\boldsymbol{R}} \\ \delta^{\boldsymbol{i}}\boldsymbol{\omega}^{\boldsymbol{b}} \end{bmatrix}_t = \begin{bmatrix} \Phi_{\boldsymbol{xx}} & \Phi_{\boldsymbol{xq}} & \Phi_{\boldsymbol{x\omega}} \\ T_R\,\Phi_{\boldsymbol{qx}} & T_R\,\Phi_{\boldsymbol{qq}} & T_R\,\Phi_{\boldsymbol{q\omega}} \\ \Phi_{\boldsymbol{\omega x}} & \Phi_{\boldsymbol{\omega q}} & \Phi_{\boldsymbol{\omega\omega}} \end{bmatrix} \begin{bmatrix} \delta\boldsymbol{x} \\ \delta^{\boldsymbol{r}}\boldsymbol{q}^{\boldsymbol{b}}_{\boldsymbol{R}} \\ \delta^{\boldsymbol{i}}\boldsymbol{\omega}^{\boldsymbol{b}} \end{bmatrix}_{t_0} = \tilde{\Phi}(t, t_0) \begin{bmatrix} \delta\boldsymbol{x} \\ \delta^{\boldsymbol{r}}\boldsymbol{q}^{\boldsymbol{b}}_{\boldsymbol{R}} \\ \delta^{\boldsymbol{i}}\boldsymbol{\omega}^{\boldsymbol{b}} \end{bmatrix}_{t_0} \tag{4.27}$$

Finally, the monodromy matrix as seen from a rotating observer for both orbital and attitude states is equal to the modified STM $\tilde{\Phi}$ which is obtained after one orbital period of propagation.

$$M = \tilde{\Phi}(T, 0) \tag{4.28}$$

This monodromy matrix M fully reflects the point of view of a rotating observer sitting in the synodic frame and catch the information describing the linear approximation of the dynamical structure in the neighbourhood of a periodic solution in the rotating perspective for both the orbital and attitude states.

4.3 Floquet Modes of Coupled Dynamics in Earth-Moon System

Once periodic LPO are found, the invariant manifolds represents the next step to order the chaotic and sensible non-linear dynamics of the orbit-attitude CR3BP. As shown in Floquet's theory, the eigenvectors of the monodromy matrix of a periodic LPO represent the numerical tool to access the global invariant manifolds of the orbit. They are investigated in the orbit-attitude coupled system environment, thus they may be considered as a direct extension of the classical manifolds of the CR3BP in the only orbital motion.
The natural dynamics of the manifolds may offer interesting possibilities for many operational and autonomous implementations of nowadays and future missions. The orbital stable and the unstable manifolds represent efficient and robust approaching and departing trajectories for a cislunar space gateway located on a naturally periodic orbit-attitude trajectory. The orbital center invariant manifolds may offer many possibilities for low-cost formation flying (even for a large number of spacecraft which may have thigh requirements, e.g. cubesat) and for safe waiting checkpoints during the rendezvous mission. The concept can be extended to the attitude invariant manifolds, which may be interesting for low-cost slew maneuver application.
Moreover, the eigenstructure of the flows of the invariant manifolds not only drive the motion of the spacecraft approaching or departing a nominal orbit, but also rules the relative motion of spacecrafts in the vicinity of a periodic orbit.

4.3.1 Model Simplification

In the most general case, the fully-coupled motion leads to have the monodromy matrix $M = \tilde{\Phi}(T, 0)$ as a full matrix.

$$M = \begin{bmatrix} [M_{Orb}] & [M_{OrbAtt}] \\ [M_{AttOrb}] & [M_{Att}] \end{bmatrix} \tag{4.29}$$

Each block is a 6-by-6 matrix. The block $[M_{Orb}]$ refers to the orbital dynamics $[\boldsymbol{f_x}; \boldsymbol{f_v}]$ respect the orbital states $\boldsymbol{x_{orb}}$. The block $[M_{OrbAtt}]$ refers to the orbital dynamics $[\boldsymbol{f_x}; \boldsymbol{f_v}]$ respect the attitude states $\boldsymbol{x_{att}}$. The block $[M_{AttOrb}]$ refers to the attitude dynamics $[\boldsymbol{f_q}; \boldsymbol{f_\omega}]$ respect the orbital states $\boldsymbol{x_{orb}}$. The block $[M_{Att}]$ refers to the attitude dynamics $[\boldsymbol{f_q}; \boldsymbol{f_\omega}]$ respect the attitude states $\boldsymbol{x_{att}}$.

Let now consider the orbit-attitude motion in CR3BP without any additional perturbation, such as solar radiation pressure, but the solely gravitational effects of the two primaries. The cross-coupling term $[M_{OrbAtt}]$ reflects the influence of the attitude on the orbital motion via the second-order term of the gravitational attraction due to the finite extension of the spacecraft.
However, if the cross-coupling term between the attitude states and the orbital dynamics is negligible, the simplified-coupled motion approximation is valid for the orbit-attitude motion in the CR3BP model and the monodromy matrix M becomes a lower triangular block matrix.

$$M = \begin{bmatrix} [M_{Orb}] & [0] \\ [M_{AttOrb}] & [M_{Att}] \end{bmatrix} \tag{4.30}$$

Here, the two diagonal blocks identify separately the orbital and the attitude dynamics.
It follows that also the eigenstructure of M can be related separately to the orbital and attitude manifolds. The eigenvalues of M corresponds to the set of eigenvalues of the two matrices on the diagonal, $[M_{Orb}]$ and $[M_{Att}]$. In this investigation they will be denoted respectively as orbital eigenvalues and attitude eigenvalues. Moreover, in the case of simplified-coupled motion, the block $[M_{Orb}]$ corresponds to the monodromy matrix of the classical CR3BP. Thus, the orbital eigenvalues are the same eigenvalues of the corresponding orbits in the classical CR3BP (which consider the solely orbital dynamics).
It should be noted that, if the model includes the cross-coupling term between the attitude states and the orbital dynamics, the eigenvalues will show a displacement respect those derived from the simplified-coupled motion. This eigenvalue displacement is an alternative index of influence representing the impact of the inertial cross-coupling behaviour driving the motion. If this displacement is no more negligible, the coupling will be reflected also in the eigenvectors components.

In a first approximation, the analysis of relative orbit-attitude motion neglects all the perturbations due to sources which are external to the Earth-Moon system, such as the gravitational pull of the Sun and the solar radiation pressure effects. Therefore, the model will consider only the dynamical flows which are generated by the gravity field interaction of the two primaries, namely the Earth and the Moon.
It should be noticed that, considering nowadays or near-future large-class spacecrafts orbiting about a cislunar non-Keplerian orbit such as a Near Rectilinear Halo Orbit, the effect due to the variational term of the gravitational attraction which is exerted on a finite extended spacecraft by the primaries is negligible compared to the inertial cross-coupling in the opposite direction due to the gravity gradient torque. As a consequence, the inertially simplified-coupled motion is assumed valid for all the following developments.
This model is able to catch the orbit-attitude motion with enough accuracy in many celestial systems, such as in the Earth-Moon system, being a powerful tool that will offer useful information in the early stages of novel space mission looking to these particular locations.

However, there are two possible directions which may lead to a no more valid assumption for an accurate employment of the inertially simplified-coupled model.
In fact, if the dimensions of the spacecraft become so large that they will be comparable to the distance the spacecraft has from the primaries, the variational effect due to the higher-order terms of the gravity pull of the primaries is expected to have a significant impact on both the absolute

and relative dynamics. However, considering system such as the Earth-Moon one, the dimensions of the spacecraft to have a perceptible impact are way too large for near-future spacecraft.
The opposite mission scenario will consider nowadays spacecrafts operating in smaller system, such as missions nearby asteroids. In these cases, the analysis of the two-ways inertial coupling could be of interest for future work.

4.3.2 Orbital and Attitude Modes

In the simplified-coupled orbit-attitude CR3BP, the eigenstructure identified by the monodromy matrix can be distinguished in two separated dynamical structures, composed by six modes each. The orbital modes are defined as the modes corresponding to the eigenvalues of the $[M_{Orb}]$ matrix, while the attitude modes are those related to the eigenvalues of the matrix $[M_{Att}]$. The eigenvalues of the monodromy matrix come in reciprocal pairs. It should be noted that, for a periodic orbit-attitude solution, there is always a pair of trivial eigenvalues equal to plus (or minus) unity for both orbital and attitude modes. They represent the periodicity behaviour of the orbit in orbital and attitude states respectively. The remaining two pairs may appear as real or complex eigenvalues/eigenvectors. They feature the stability properties of the periodic LPO and the structure of natural flows in its vicinity. A stable mode corresponds to an eigenvalue of the monodromy matrix, real or complex, so that $\|\lambda_j\| < 1$. An unstable mode is associated to an eigenvalue with $\|\lambda_j\| > 1$. Finally, center modes are related to eigenvalues with $\|\lambda_j\| = 1$, which means they are laying on the unitary circle in the complex plane.
Note that in this investigation, the difference between the periodic and the quasi-periodic (or center) behaviours are deliberately differentiated in a marked way even if they constitute together the center subspace (and manifolds) of the periodic orbit.
A periodic solution is defined marginally stable in linear approximation if and only if all the eigenvalues of its monodromy matrix satisfy the condition $\|\lambda_j\| \leq 1$. If any of the eigenvalues is unstable, also the periodic solution is intrinsically unstable. Note that, if a stable mode exists, also an unstable mode will be present. Therefore, a marginally stable periodic LPO will have all the eigenvalues on the unitary circle in the complex plane.
This classification may be performed separately for orbital and attitude behaviours in the case of the simplified-coupled motion. The one-way coupling approximation implies that the families of periodic orbit are the same of the classical CR3BP. Therefore, the stability properties of the orbital behaviours correspond to those already known from the classical CR3BP. At the same time, as already noticed, many different attitude periodic behaviours (librational and/or spinning) may exist for the same periodic orbital family. Some of them may be marginally stable, others may be unstable.
A stability index ν can be defined to synthesize the stability information deriving by the eigenvalues of the monodromy matrix M.

$$\nu = \frac{1}{2}\left(\|\lambda_{max}\| + \frac{1}{\|\lambda_{max}\|}\right) \tag{4.31}$$

Here, λ_{max} represents the dominant eigenvalue of orbital or attitude dynamics. When the stability index is equal to unity ($\nu = 1$), the corresponding motion is marginally stable in linear approximation and means a family of quasi-periodic solution exists in the vicinity of the reference orbit. Instead, a stability index greater than one ($\nu > 1$) is evidence of instability behaviours in the vicinity of the reference orbit. A larger value ν means that mutation due to variation in proximity of a nominal orbit are likely to results in faster departure behaviours from the reference.
It should be noted that, for the simplified-coupled CR3BP motion, this stability index can be evaluated separately for the orbital and attitude dynamics. An orbit-attitude LPO may result

marginally stable in both orbital and attitude motion, as well as only in one behaviours, or neither of them.
According to the Floquet theory, the eigenvectors of the monodromy matrix give access to other useful information. Each orbital and attitude eigenmode $\boldsymbol{e_j}$ obtained from the monodromy matrix M is a 12-dimensional vector which represents the local direction of the corresponding invariant manifold.

$$\boldsymbol{e_j} = \Big[\delta x;\, \delta y;\, \delta z;\, \delta v_x;\, \delta v_y;\, \delta v_z;\, \delta q_1;\, \delta q_2;\, \delta q_3;\, \delta \omega_1;\, \delta \omega_2;\, \delta \omega_3\Big] \tag{4.32}$$

The first six elements describe the direction of the mode in the orbital space, while the last six elements represent the direction in the attitude space.
It should be highlighted that, the orbital modes does not have the solely orbital part but also an important attitude component. This is due to the strong influence of the orbital path on the attitude dynamics through the gravity gradient torque. By contrary, the attitude modes have a negligible orbital component, because the attitude motion weakly affects the orbital dynamics. This supports the assumption of the 6DOF simplified-coupled CR3BP model as reasonable approximation to carry out preliminary investigation about the relative motion of large space structures moving on staging orbit in cislunar space.

4.3.3 Method and Algorithm

The numerical algorithm developed to find and propagate the invariant manifolds for any periodic solution in the coupled orbit-attitude system is similar to the one typically employed for the classical CR3BP [27].
Once computed the monodromy matrix $M = \tilde{\Phi}(T, 0)$, the orbital and the attitude modes are identified via the eigenvalues. Then, the orbital and the attitude Floquet modal basis, $E_{orb}(0)$ and $E_{att}(0)$, are computed from the corresponding eigenvectors. Each column $\boldsymbol{e_j}$ of those matrices represents one Floquet mode of the periodic orbit-attitude LPO.
For a complex conjugate pair of eigenvalues, the corresponding phase space is a 2-dimensional surface. It is tangent to the space generated by the span of the real and the imaginary part of the eigenvectors. Therefore, the real and imaginary part of the eigenvectors can be separated to obtain two linearly independent eigenmodes.
Numerical errors inherited from floating-point computation make challenging to detect eigenvectors degeneracy. The function "eig()" in MATLAB returns a pair of distinct approximated eigenvalues, slightly displaced from ± 1. If they result in a complex conjugate pair, the procedure to find the two corresponding modes is the same exploited for a complex conjugate pair of eigenvalues. Otherwise, if they are real, a dedicated method is applied. The eigenvalues and the eigenvectors of the periodic modes are approximated as

$$\begin{aligned} \|\lambda\| &= (1+\epsilon) \\ \|\lambda\| &= (1+\epsilon)^{-1} \simeq (1-\epsilon) \\ \boldsymbol{v_a} &= \boldsymbol{v_{P1}} + \gamma \boldsymbol{v_{P2}} \\ \boldsymbol{v_b} &= \boldsymbol{v_{P1}} - \gamma \boldsymbol{v_{P2}} \end{aligned} \tag{4.33}$$

Where $\boldsymbol{v_{P1}}$ and $\boldsymbol{v_{P2}}$ are the eigenvectors corresponding to the periodic modes P_1 and P_2, while $\epsilon, \gamma \ll 1$. The two periodic eigenmodes are obtained manipulating the equations (4.33).

$$\begin{aligned} \boldsymbol{v_{P1}} &= \frac{\boldsymbol{v_a} + \boldsymbol{v_b}}{2} \\ \boldsymbol{v_{P2}} &= \frac{\boldsymbol{v_a} - \boldsymbol{v_b}}{2\gamma} \end{aligned} \tag{4.34}$$

The classical method explores the invariant manifolds via discretization. Therefore, the periodic orbit-attitude LPO is discretized in N points. The n-th point along the LPO is identified by the corresponding time $t_n = T(n-1)/N$.
The Floquet modes are propagated to the n-th point through the STM seen from a fixed observer respect the synodic frame.

$$\boldsymbol{v_j} = \tilde{\Phi}(t_n, 0)\, \boldsymbol{e_j} \tag{4.35}$$

Each propagated mode $\boldsymbol{v_j}$ represents the approximated local direction in the 12-dimensional oribit-attitude space of the corresponding global invariant manifold (stable, unstable or center), because they are tangent with the local subspace at the location t_n along the orbit.
Each mode is normalized to represent a unit versor. Alternatively, the orbital modes may be normalized respect their position component, while the attitude modes may be normalized respect their quaternion component. This allows to have a direct control on the perturbation magnitude to be added at the nominal orbit. In this investigation different perturbation magnitude are explored. Three different classes of distance are selected to represent respectively the far range, the mid range and the close range phases typical of a rendezvous and docking mission scenario. A distance equal to 50 km ($\simeq 1.3007 \times 10^{-4}$ [ndim]) is selected for the far range characterization. A distance of 5 km ($\simeq 1.3007 \times 10^{-5}$ [ndim]) will identify the mid range phase. A distance of 200 m ($\simeq 5.2029 \times 10^{-7}$ [ndim]) is employed to feature the close range scenario. This last distance is chosen to be comparable to the one defined in nowadays docking procedures to begin the final approach of crew/cargo vehicle along the docking port line of the ISS. For the attitude modes analysis a perturbation equal to 1 degree has been selected, corresponding to a perturbation $\varepsilon \simeq 1^\circ/2 \times \pi/180$.
A small perturbation along the direction of the eigenmode $\boldsymbol{v_j}$ moves the spacecraft onto the 12-dimensional surface of the global invariant manifold from the nominal periodic orbit. Important to remark that the lower the perturbation magnitude is, the better the numerical approximation will be. However, if the perturbation is too small, the required period of propagation becomes larger to obtain an impactful visualization of the trajectories belonging to the manifold.
Being the Floquet modes obtained from the monodromy matrix $\tilde{\Phi}(T, 0)$, they describe the "local" direction of the "global" manifolds expressed in the synodic point of view for both orbital and attitude motion. To correctly find the initial point to propagate the orbit-attitude manifolds, the perturbation has to be added coherently to the full orbit-attitude states $\boldsymbol{X}(t_n)$ of the LPO.
The orbital states $\boldsymbol{x_{orb}}(t_n)$ are already expressed in the rotating $\{\hat{r}\}$-frame, therefore the orbital perturbation can be added directly. Instead, the attitude states $\boldsymbol{x_{att}}(t_n)$ are expressed respect the inertial $\{\hat{i}\}$-frame and particular attention must be paid. The attitude quaternion ${}^{\hat{i}}\boldsymbol{q}^{\hat{b}}$ is transformed to the body quaternion respect the synodic frame ${}^{\hat{r}}\boldsymbol{q}^{\hat{b}}$ (as seen in section 2.3.3), so that the attitude quaternion will be expressed in the same perspective of the Floquet modes. Now, the perturbation can be added to the independent variable $[q_1; q_2; q_3]$ of ${}^{\hat{r}}\boldsymbol{q}^{\hat{b}}$, hence q_4 is derived from the quaternion constraint relation. Then, the quaternion is converted back to the inertial $\{\hat{i}\}$-frame to obtain a perturbed state which can be directly propagated through the orbit-attitude dynamics. Finally, the angular velocity ${}^{\hat{i}}\boldsymbol{\omega}^{\hat{b}}$ differs only for a constant respect the angular velocity seen from a rotating observer, so it is not important respect which frame it refers to. Hence, also for the angular velocity states the perturbation is simply added.
Once the perturbed states are obtained at the N points along the LPO, the natural orbit-attitude dynamics is propagated in time to identify the global invariant manifolds surfaces. The stable manifold trajectories are obtained via reverse-time propagation, while the unstable manifold trajectories employ forward-time integration. Propagating forward or backward in time is neutral for the center manifolds trajectories, hence it has been decided to propagate them forward in time.
In the relative motion investigation, it is interesting to explore all the different modes propagated

forward in time, because they represent the evolution in time of each Floquet mode in which any initial offset condition relative the nominal LPO may be decomposed.

4.4 Orbit-Attitude Manifolds of Halo Orbit

The characterization of the modal dynamics is now presented for an orbit-attitude family of Halo orbit in the simplified-coupled CR3BP. A family of orbit-attitude Halo orbit has been chose as first non-Keplerian orbits in cislunar space to be investigated because it describe a simple, periodic, symmetric, non-planar orbit and it is one of the most known families of solutions in the CR3BP. Furthermore, they hallows to highlight several detail about the coupled 6DOF dynamics of non-Keplerian orbits in the Earth-Moon system, and its discovered outcomes may be extended also to other classes of cislunar orbits.
In particular, the investigated family corresponds to the Earth-Moon L_1 Northern Halo family which has been displayed in figure 3.3. The family associates the orbital path of Halo orbits and the librational attitude behaviour about the synodic frame of a disk-like spacecraft with inertial ratio $K_a = 0.7$ and axis of symmetry aligned to $\hat{\boldsymbol{b}}_3$. The eigenvalues location in the complex plane of a representative member of this orbit-attitude Earth-Moon L_1 Halo family are shown in figure 4.1. The orbital eigenvalues are associated to blue circles, while the attitude eigenvalues corresponds to

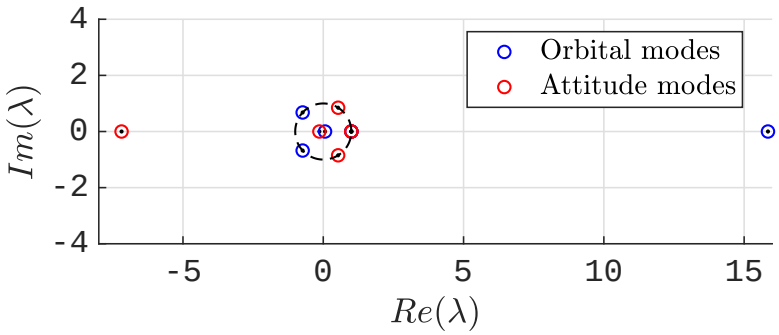

Figure 4.1: Orbit-attitude eigenvalues in the complex plane of an Earth-Moon L_1 Halo orbit

red circles. As expected, the orbital modes maintain the typical configuration of Halo orbits known from the classical CR3BP: one pair of eigenvalues in +1 is associated to the periodic modes, one pair represents the stable/unstable manifolds, and one pair implies the presence of quasi-periodic behaviours around the orbit. The same classification can be carried out for the rotational motion of the orbit. Apart the trivial pair associated to the periodic modes, the librational attitude behaviour of the selected Halo family is characterized by one pair of stable/unstable modes and one pair of center modes. Therefore, the members of the orbit-attitude L_1 Halo family are intrinsically unstable orbits in both orbital and attitude motion.
More information can be obtained analysing the stability index associated to the orbit-attitude Halo family in function of the vertical amplitude A_z. As can be seen in figure 4.2, the stability index associated to the orbital motion ν_{orb} decreases as the orbit increases in amplitude. This implies that larger orbits becomes less unstable. By contrary, the same family increases the attitude stability index ν_{att} as the orbit increases its vertical amplitude. Therefore, the instability behaviour of the rotational motion becomes stronger for larger amplitude orbits, probably due to the higher angular rates resulting from a closer passage to the Moon.
It should be highlighted that the stability index associated to the rotational motion remains quite low for all the Halo investigated: from $\nu_{att} = 2$ for the lower Halo considered, up to $\nu_{att} \simeq 6$ for

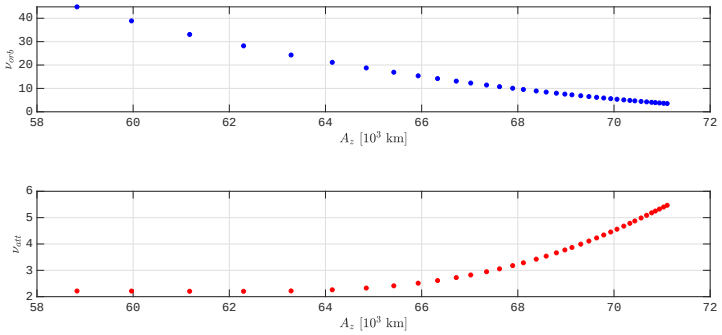

Figure 4.2: Orbital and attitude stability index of the Earth-Moon L_1 Halo family

the highest orbit. Instead, the orbital stability index presents a quite large variation even in a small interval of A_z: starting from a quite high value $\nu_{orb} \simeq 40$, it decreases up to $\nu_{orb} < 5$ for Halo orbits higher than $A_z = 70 \times 10^3$ km.
Moreover, being the orbital stability index of the set of large Halo orbits not too large, the relative dynamics of the orbital modes is expected to allow to distinguish both the periodic and the exponential behaviours of the orbital Floquet modes.

The well-known orbital manifolds discovered in the classical CR3BP dynamics are now extended to the coupled orbit-attitude CR3BP system. The selected representative member belonging to the considered orbit-attitude Earth-Moon L_1 Northern Halo family has vertical amplitude $A_z \simeq 68.8 \times 10^3$ km ($\simeq 0.1790$ [ndim]) and orbital period $T \simeq 10.86$ days ($\simeq 2.5010$ [ndim]). The absolute 6DOF dynamics of the orbital stable and unstable manifolds of the reference Halo orbit are shown in figure 4.3. The stable and unstable manifolds are illustrated respectively as blue dashed lines in figures 4.3(a) and 4.3(c), and as red dashed lines in figures 4.3(b) and 4.3(d). The stable orbital trajectories slowly approach the nominal orbit clockwise. In a specular way, the orbital unstable trajectories depart clockwise from the periodic orbit. They has been generated considering a perturbation equivalent to 50 km in position along the corresponding modes. Then, the unstable manifold has been propagated over two orbital period forward in time, while the stable manifold has been propagated backward in time. The resulting set of trajectories are slightly different respect the classical CR3BP. However, these differences are so small that in practice they can be considered absent.
It should be noted that the dynamical structure of stable and unstable orbital manifolds of the Halo family can be subdivided in inner and outer regions. This classification is typical for many LPO families about the libration point L_1 and L_2, such as Lyapunov and Halo orbits. For periodic orbits librating about L_1, the inner toroid contains the trajectories linking the LPO and the first primary P_1, while the trajectories lying on the outer toroid connect the LPO and the second primary P_2. For periodic orbits librating about L_2, the inner toroid contains the trajectories linking the LPO and the second primary P_2, while the trajectories lying on the outer toroid connect the LPO and the outer region of the system beyond the L_2 gateway.
The evolution of the attitude quaternion profiles along the orbital stable and unstable manifolds are reported respectively in figures 4.3(e) and 4.3(f). It is evident the rotational dynamics slowly approaches and departs the nominal periodic solution accordingly with the orbital dynamics of the manifold. Note that the attitude on stable and unstable manifolds is very similar respect the nominal periodic solution at least for the first orbital period. However, all the perturbation accumulated along the manifold are strongly magnified during the second perilune passage due to the high gravity gradient torque of the Moon. As a consequence, the rotational motion begins its

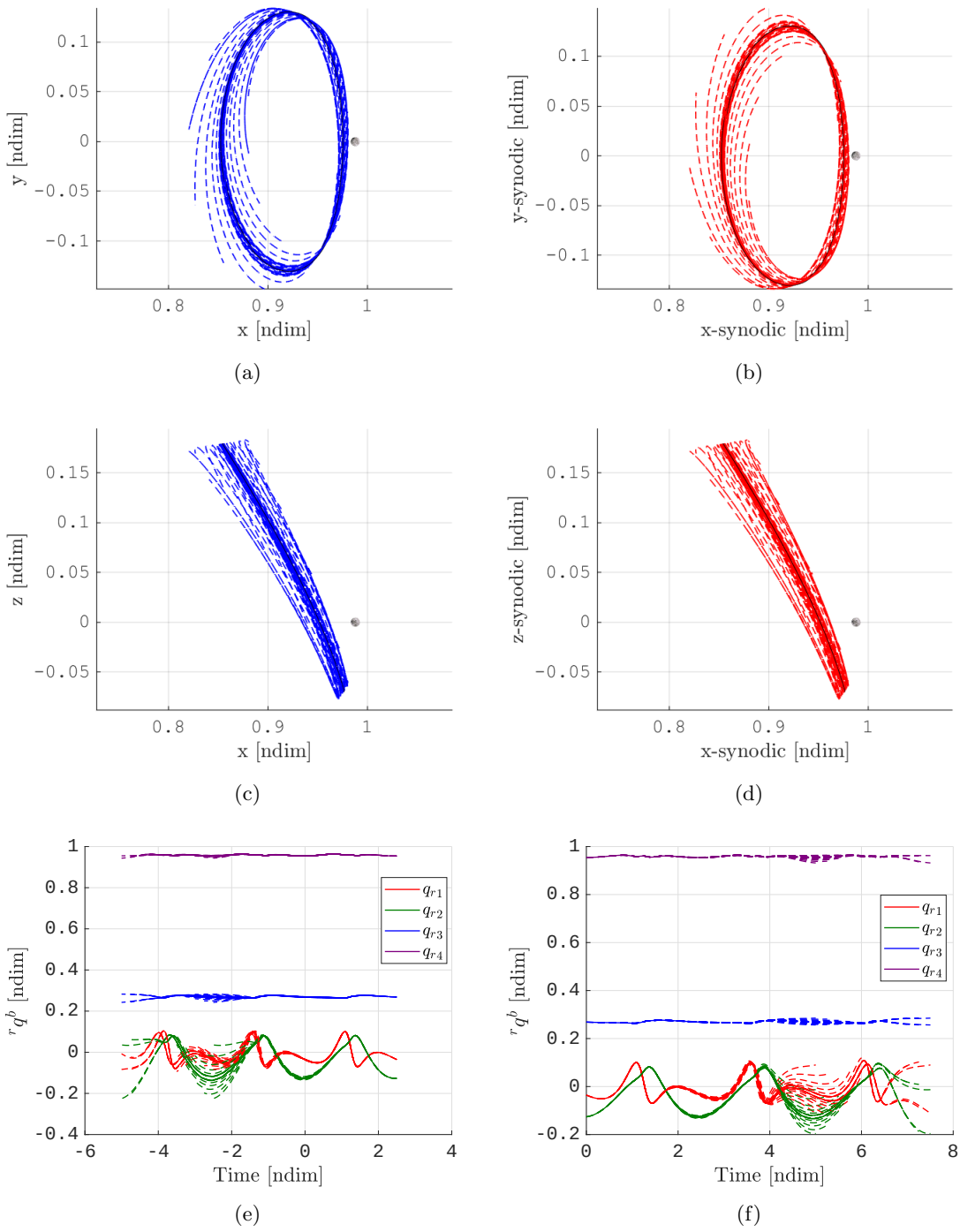

Figure 4.3: Absolute orbital and attitude dynamics of stable (blue) and unstable (red) invariant manifold of the reference Earth-Moon L_1 Halo orbit

drifting apart from the nominal equilibrium constituting the periodic behaviour.
This is again an alerting clue of the highly sensible dynamics of the CR3BP, particularly in the proximity of primary attractors. It suggests a careful planning of the mission in order to minimize proximity operations during the closer passages to the Moon along the periodic LPOs. However, the same sensibility may be exploited to maximize efficiency of the operations demanded to the Orbital and Attitude Control Subsystem (OACS) to obtain the desired departing or approaching trajectories.

4.4.1 Orbital Modes of Orbit-Attitude Halo Orbit

The absolute point of view of the dynamical structure of the invariant manifolds, in particular the stable and unstable trajectories, allows to gather useful information about low energy transfers possibilities through the whole system of the CR3BP. However, the relative point of view of the dynamical structure of the invariant manifolds is of great interest because it characterize the evolution of the dynamical modes that feature the relative dynamics of a spacecraft in the vicinity of a reference nominal periodic orbit.
The configuration of the eigenvalues associated to a periodic motion describes the composition of its dynamical eigenstructure. In the case of simplified-coupled CR3BP, the orbital modes characterize mainly the relative orbital motion in the vicinity of the reference orbit, but they affect contemporaneously the attitude behaviour.
The unstable, stable and center invariant manifolds of the reference Halo has been investigated in their relative motion in the vicinity of the periodic solution. In this investigation the different modes are identified via different colors: red for the unstable modes, blue for the stable modes, violet for the periodic modes, and green for the center modes.
Let start by considering the natural dynamics of orbital Floquet modes considering two identical spacecrafts located at apolune as initial condition: the target spacecraft lies on the reference nominal Halo orbit, while the chaser spacecraft is located on the selected orbital modes. The nominal

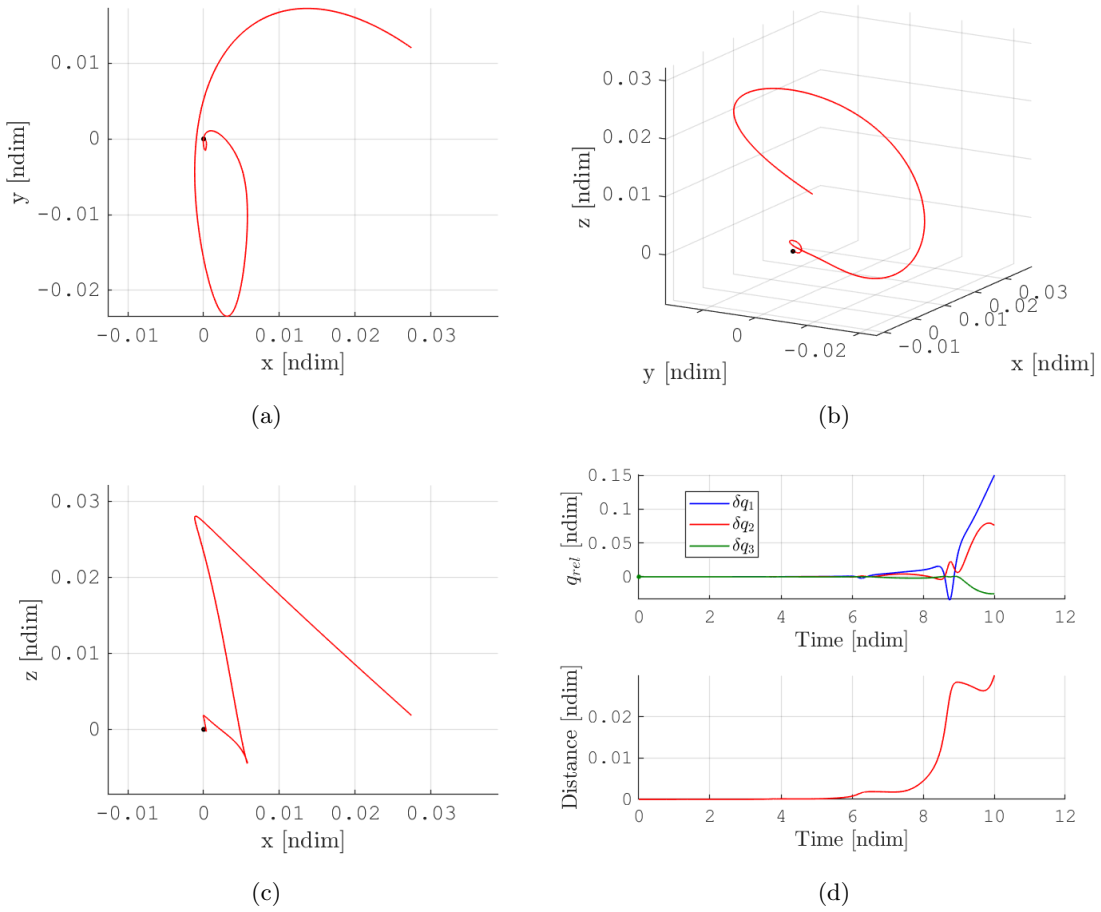

Figure 4.4: Relative orbit-attitude motion over 4-orbital period of the unstable orbital mode of Earth-Moon L_1 Halo orbit with $A_z \simeq 68.8 \times 10^3$ km ($\simeq 0.1790$ [ndim]). Relative orbital dynamics 3D point of view (b), projection on xy-plane (a) and on xz-plane (c) of synodic frame. Time evolution of relative attitude and distance (d).

condition at apolune is perturbed along the unstable mode by a small perturbation magnitude

equivalent to an offset of 200 meters in position (in the order of 5×10^{-7} in non-dimensional unit). This small perturbation allows to obtain a better approximation of the orbital modes in the proximity of the nominal orbit.

Figure 4.4 shows the natural evolution over four orbital period of relative orbital and attitude dynamics of the chaser spacecraft on the orbital unstable mode, respect the target spacecraft on the reference periodic orbit. The relative orbital motion in three-dimensional point of view is reported in figure 4.4(b), while figures 4.4(a) and 4.4(c) shows its projection over the xy-plane and the xz-plane of the synodic frame. The time evolution of relative attitude and of relative distance are reported in figure 4.4(d). Note that this unstable mode corresponds to trajectories in the outer region of the unstable orbital invariant manifold.

As expected from Floquet theory, both orbital and attitude relative motions seem to be governed by the combination of a periodic and an exponential behaviours.

For the orbital component, the presence of a recurrent spiralling behaviour diverging from the nominal motion is evident. Due to the diverging exponential behaviour, only the orbital path occurred in the last two orbital period can be easily distinguished in the figures. However, by observing the motion from a closer point of view it would be noticed that it presents the same spiralling shape at each orbital period.

It should be noted that the attitude on the unstable manifold remains very close to the one of the target on the reference orbit up to about $t = 9$ [ndim], corresponding to the fourth perilune passage on the nominal orbit. At this point, as shown in figure 4.4(d), the chaser spacecraft on the unstable mode has reached a significant distance from the nominal orbit. This distance is in the order of hundreds of kilometers and is comparable to the one reached at the beginning of the drift apart of the attitude motion for the manifolds already observed in figure 4.3.

The same procedure is applied to obtain the orbital and attitude evolution over two orbital periods of the stable orbital mode, which is shown in figure 4.5. The propagated stable mode correspond to a trajectory in the inner region of the stable orbital manifold. This information can be obtained thanks to the position of initial point of the mode, highlighted by a circled point at the beginning of the relative trajectory. It is evident that the stable mode has a spiralling behaviour very similar to the one observed for the unstable mode, but now it tends to converge exponentially to the nominal motion. Also the attitude motion converges to the nominal one in a similar manner. Therefore, a chaser spacecraft on the stable mode will naturally synchronise in both the orbital and attitude motion of the target spacecraft placed on the reference nominal orbit.

The pair of orbital eigenvalues in $+1$ is associated to two different periodic modes. In this investigation, these modes will be denoted as P1 and P2, where P stands for "periodic".

Figure 4.6 reports the orbital and attitude motion of the mode P1 seen from the relative point of view respect the nominal periodic solution. The orbital relative motion of P1 results in a periodic path with a drop-like shape. This kind of relative orbit is characteristic of all the Halo orbits. The mode P1 identifies a motion on the same nominal orbit, but which is immediately shifted backward or forward along the same orbit. This happens because the eigenmode P1 lies on the time derivatives of the initial state of the reference orbit which corresponds to the direction of propagation of the nominal motion.

Let assume the target spacecraft on the reference nominal orbit and an identical chaser spacecraft on the mode P1. The chaser and the target will be on the same nominal orbit, but the chaser is shifted to a position immediately backward or forward respect the target. The relative position is shifted of a constant phase angle. As a consequence, at the apolune the relative distance is at its minimum, while the picks in relative distance corresponds at the perilune passages. This is due to the elastic effect associated to the different velocities along the orbit. If the spacecrafts are moving slower, they will be closer to keep the time gap constant. Vice versa, they will be farther when

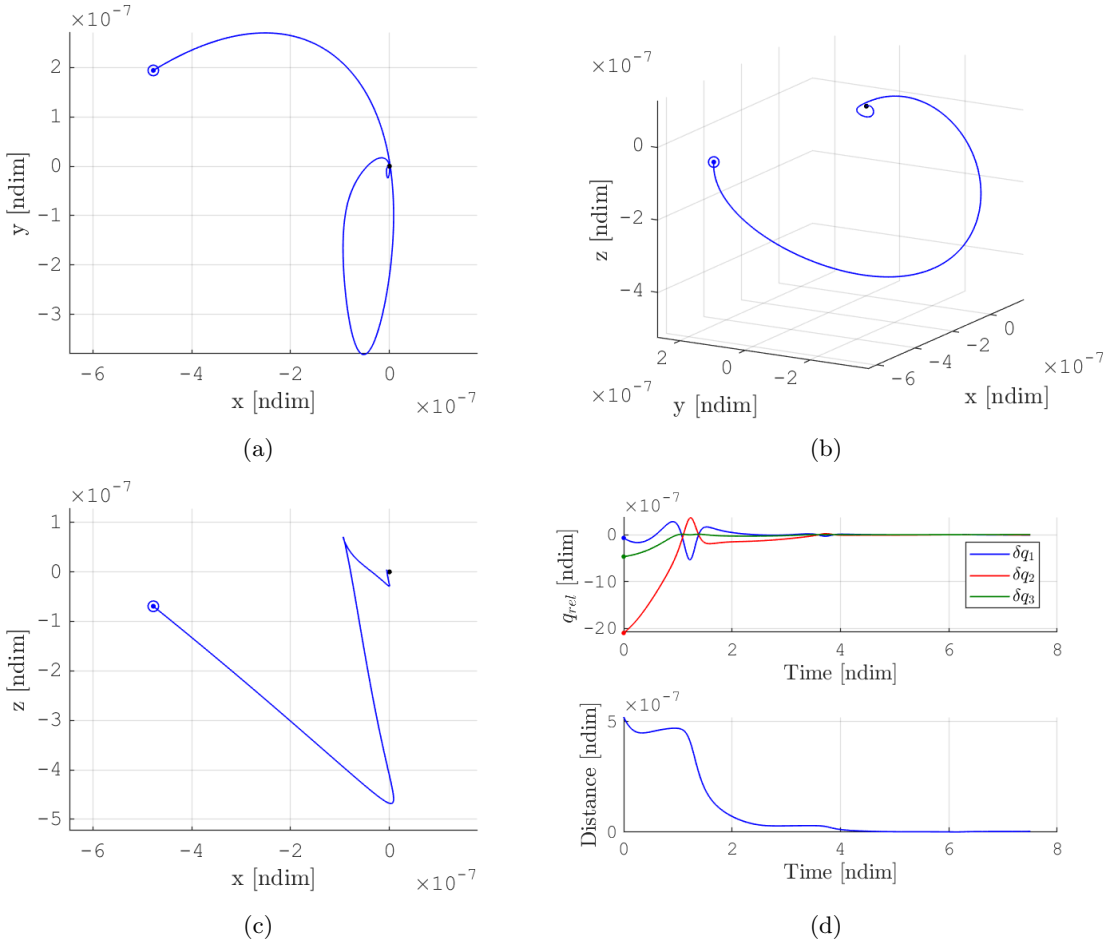

Figure 4.5: Relative orbit-attitude motion over 3-orbital period of the stable orbital mode of Earth-Moon L_1 Halo orbit with $A_z \simeq 68.8 \times 10^3$ km ($\simeq 0.1790$ [ndim]). Relative orbital dynamics 3D point of view (b), projection on xy-plane (a) and on xz-plane (c) of synodic frame. Time evolution of relative attitude and distance (d).

they move faster.

It should be noticed that also the relative attitude has a periodic behaviour. However, its amplitude is negligible due to the small orbital relative distance between target and chaser. Thus, the absolute orientation of the chaser can be considered almost equal to the one of the target on nominal orbit.

During the fourth orbital period of propagation the motion begins to diverge. This behaviour is associated to the numerical sensitivity of the problem. The numerical errors accumulated during the numerical integration excite the unstable modes, which will become dominant if the propagation is extended for other few orbital period. Even if this is a numerical problem, it suggests a very interesting concept for actual application: it does not matter how accurately you can target a desired theoretical periodic solution because there is always something that modify your solution and the unstable mode will surely become dominant sooner or later if there is no counteraction by any active control.

The mode P2 has been propagated for four orbital periods and its orbital and attitude evolution is reported in figure 4.7. This mode is associated to the so called "generalized eigenvector". This direction should be tangent to the family of the periodic solutions. A small perturbation along this direction generates a new periodic solution with a slightly different period. Therefore, a chaser spacecraft on the mode P2 will be on a slightly smaller or larger orbit respect the nominal one of the target, starting the motion side by side at the initial condition. Particularly, the relative

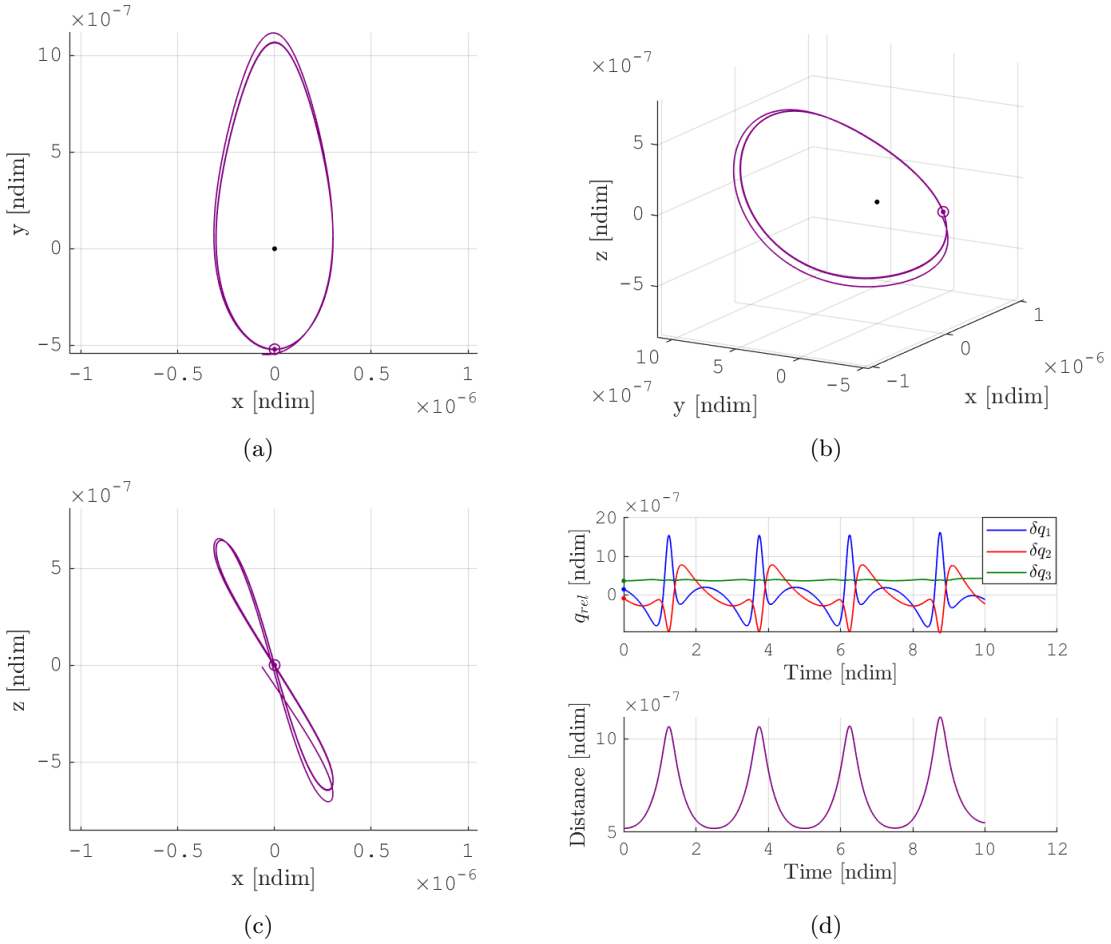

Figure 4.6: Relative orbital and attitude motion over 4-orbital period of the periodic orbital mode P1 of Earth-Moon L_1 Halo orbit with $A_z \simeq 68.8 \times 10^3$ km ($\simeq 0.1790$ [ndim]). Relative orbital dynamics 3D point of view (b), projection on xy-plane (a) and on xz-plane (c) of synodic frame. Time evolution of relative attitude and distance (d).

trajectory in the figure corresponds to the relative motion of a chaser spacecraft on a slightly larger halo orbit of the same family, which remains progressively behind the target. This can be noticed from the position of the initial condition of the relative motion: at apolune, the chaser lies along the $\hat{\boldsymbol{x}}$-axis with a greater vertical component.

The last two orbital modes of the Halo family are associated to a pair of complex conjugate eigenvalues lying on the unit circle of the complex plane and identify the center subspace of the periodic solution. Figure 4.8 reports the orbital evolution of the center orbital modes C1 and C2, obtained via the propagation of natural dynamics over four orbital periods.

The chaser spacecraft has an oscillating behaviour composed by recurrent trajectory curves that form more complex geometries. As expected for a quasi-periodic mode, the relative orbit remains bounded in the vicinity of the nominal motion. This can be observed in the time evolution diagram of the distance between chaser and target, shown in figure 4.9. Also the relative attitude of the center modes presents oscillating behaviours. However, they are visible only with a focus on the three indipendent component of the relative quaternion q_{rel}, because the amplitude of oscillation in relative attitude is negligible since the distance between chaser and target is smaller than hundreds of kilometers considering the dimensional form of the problem.

It is important to notice that the dimensional scale of the orbital motion is much larger respect the one of the attitude. Even if the magnitude of the relative attitude may be comparable to

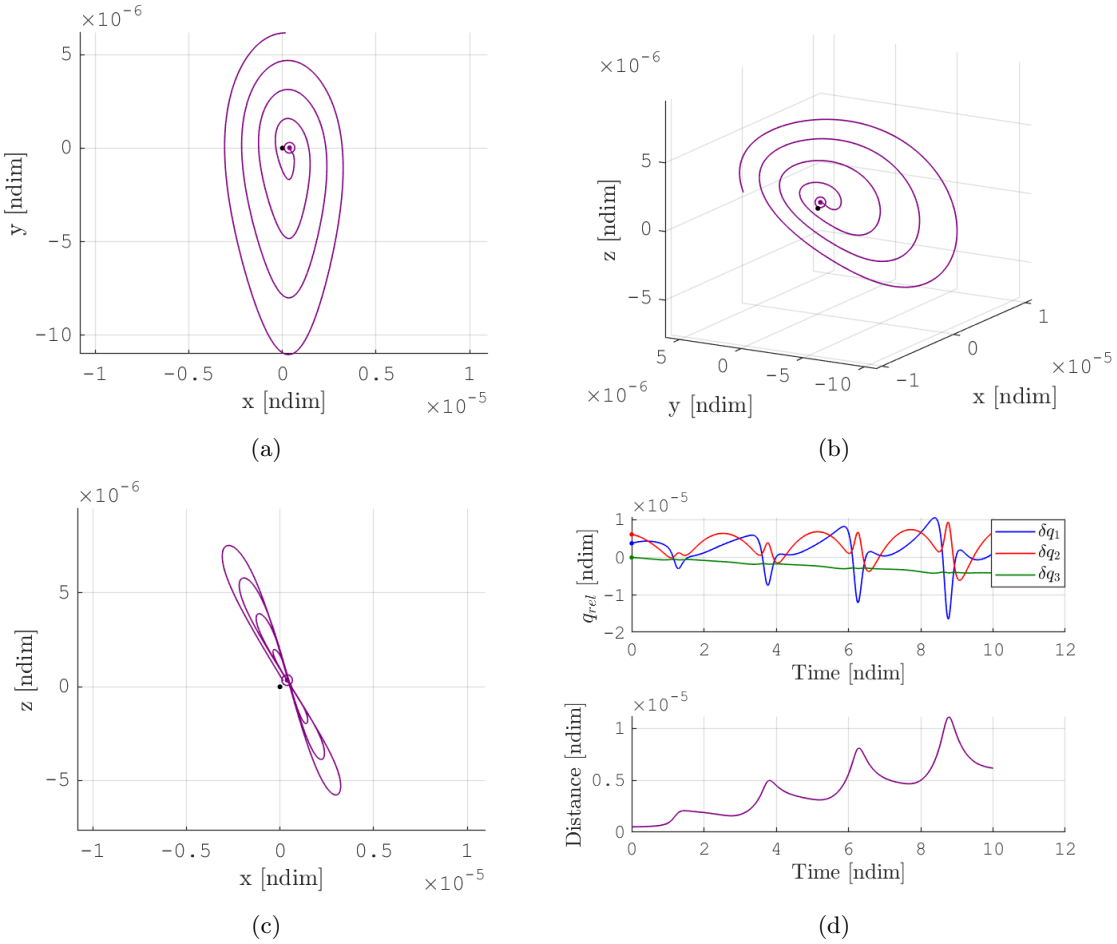

Figure 4.7: Relative orbital and attitude motion over 4-orbital period of the periodic orbital mode P2 of Earth-Moon L_1 Halo orbit with $A_z \simeq 68.8 \times 10^3$ km ($\simeq 0.1790$ [ndim]). Relative orbital dynamics 3D point of view (b), projection on xy-plane (a) and on xz-plane (c) of synodic frame. Time evolution of relative attitude and distance (d).

the relative orbital distance in the non-dimensional form, in practice the relative attitude motion results almost unaffected since the spacecraft on any orbital mode does not reach large distances from the nominal periodic motion. In the case of large amplitude Halo orbit, this limit seems to be reached for distances not lower than thousands of kilometers, as it has been shown for the unstable mode.

The orbital and attitude motions of each mode change with the phase angle t_0 which identify the initial location on the orbit to propagate the natural dynamics of target and chaser spacecrafts. The same procedure can be applied to propagate the orbital modes considering multiple discretized points along the nominal orbit as initial condition. The obtained motions can be superposed to approximate the surfaces of the invariant manifolds seen in relative point of view.

Figure 4.10 shows the relative motion surface associated to the unstable and the stable modes of the reference orbit-attitude Halo orbit which has been propagated considering twenty discretized point equispaced in time along the orbital period.

Two independent conical surfaces are identified by the relative unstable and stable trajectories. It is evident the initial position of the stable mode lies on different location of the conical surface identifying the stable manifold. The corresponding trajectories move on the approaching-cone with a spiralling behaviour, maintaining a certain separation from the adjacent trajectories. The unstable trajectories identify a departing conical surface, presenting the same behaviours of the

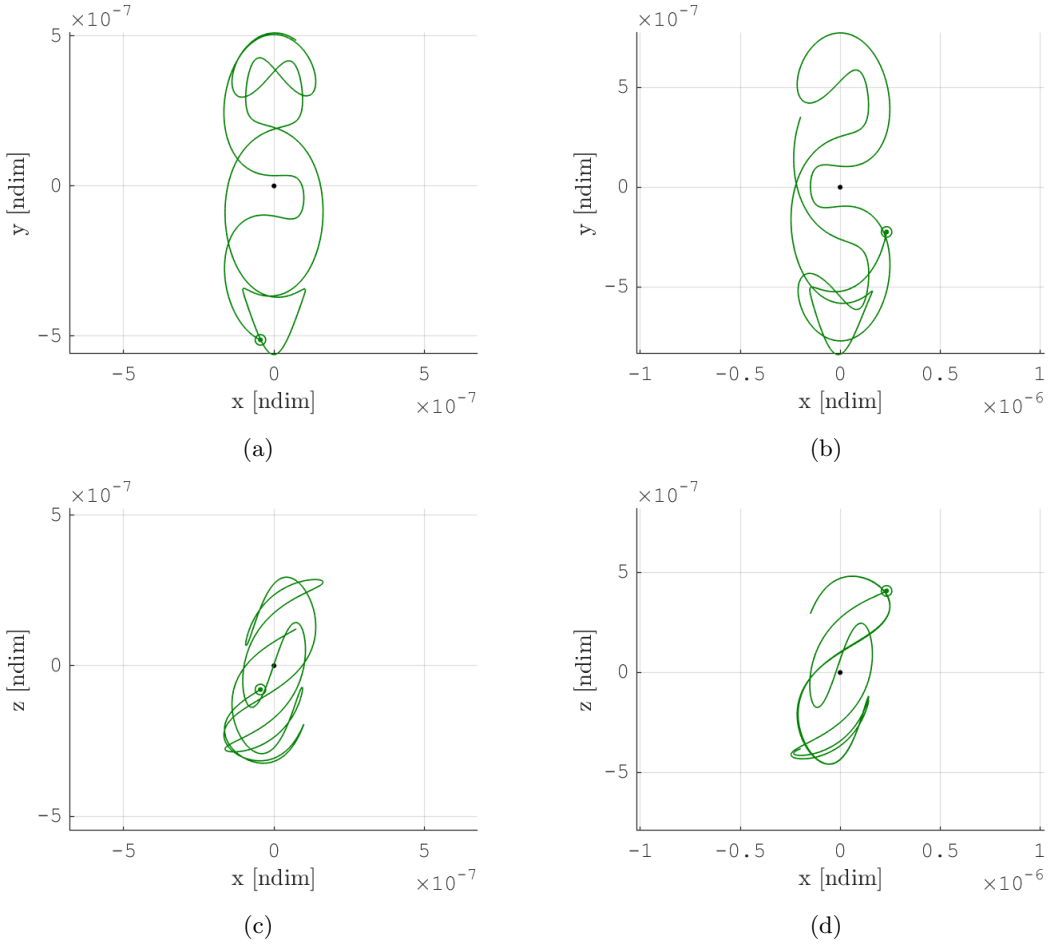

Figure 4.8: Relative orbital motion over 4-orbital period of the center orbital modes C1 (a, c, e) and C2 (b, d, f) of Earth-Moon L_1 Halo orbit with $A_z \simeq 68.8 \times 10^3$ km ($\simeq 0.1790$ [ndim]). Relative orbital dynamics 3D point of view (a, b), projection on xy-plane (c, d) and on xz-plane (e, f) of synodic frame

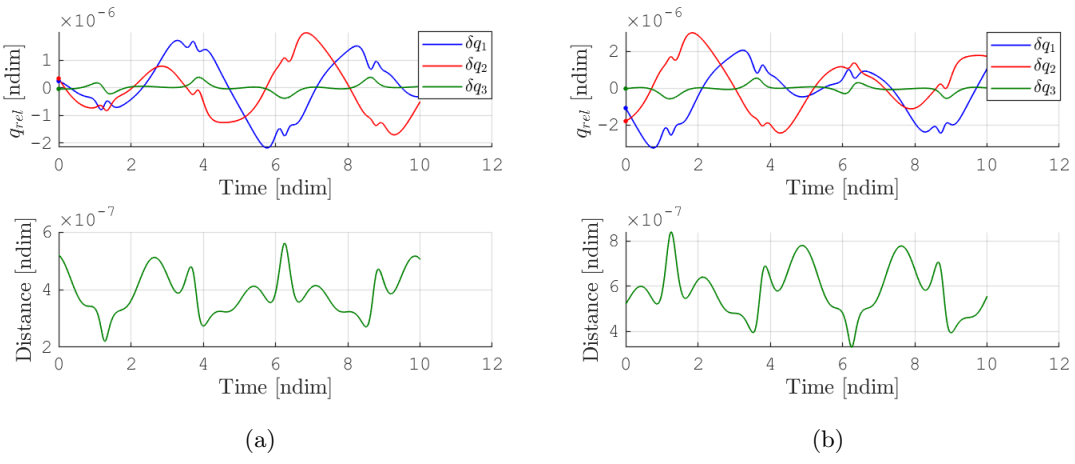

Figure 4.9: Time evolution of relative attitude and relative distance over 4-orbital period of the center orbital modes C1 (a) and C2 (b) of Earth-Moon L_1 Halo orbit with $A_z \simeq 68.8 \times 10^3$ km ($\simeq 0.1790$ [ndim]).

stable motion.

It should be noticed that a specular conical surface exists for both the unstable and stable manifold. The two surfaces constitute two opposite (departing or approaching) cones with coincident tip at the origin. They represent the inner and the outer regions of the corresponding manifold.

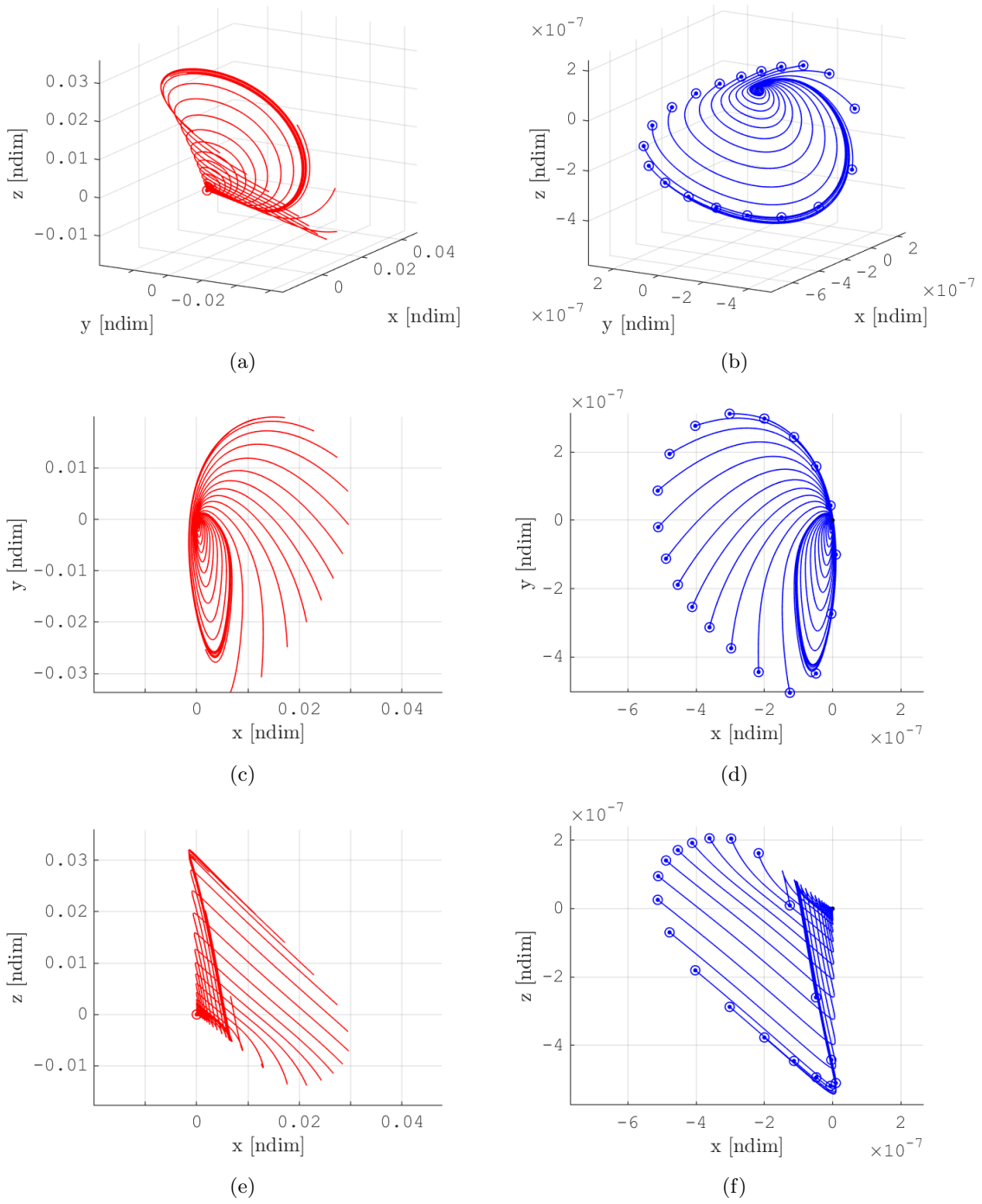

Figure 4.10: Relative orbital motion over 2-orbital period of trajectories belonging to unstable orbital mode (red) and stable orbital mode (blue) of Earth-Moon L_1 Halo orbit with $A_z \simeq 68.8 \times 10^3$ km ($\simeq 0.1790$ [ndim]). Relative orbital dynamics 3D point of view (a, b), projection on xy-plane (c, d) and on xz-plane (e, f) of synodic frame.

Let consider an unstable manifold trajectory, when it is very close to the periodic orbit, to explain this conical-spiralling shape behaviour. The periodic orbit represents the equilibrium condition of the dynamics between the gravity field of the two primaries, in this particular case the Earth and the Moon. A spacecraft released on the unstable manifold will slowly drift apart from the equilibrium condition driven by the natural dynamics. If the spacecraft get closer to the second primary being on the inner region of manifold, it will run along the orbit in a slightly faster way respect the

nominal motion. Therefore, the chaser spacecraft will have a position forward on the orbit respect the target, which periodically increases. Vice versa, if the chaser is on the outer region of the manifold, it will be backward respect the target spacecraft. This increasing phase displacement combined with the natural flow departing from the equilibrium solution and the three-dimensional nature of the Halo orbit will result in the observed conical-spiralling behaviour.
An analogous reasoning can be carried out to explain the trajectories of the stable manifold.

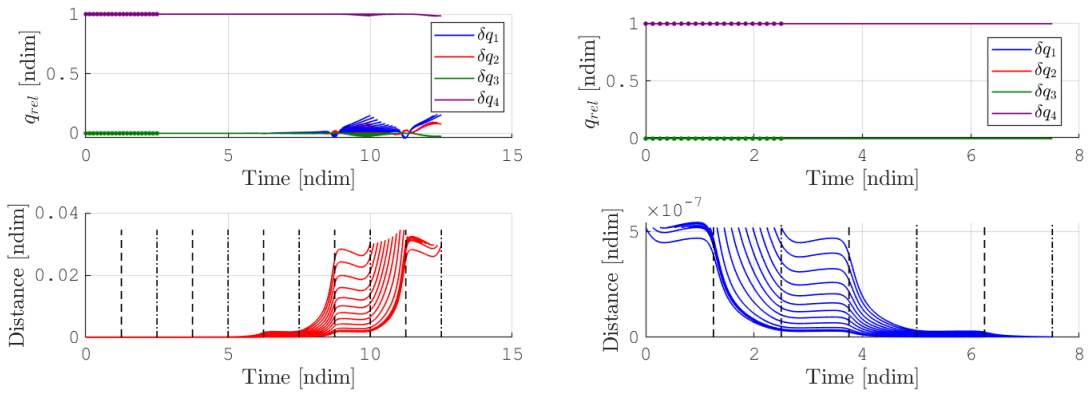

(a) (b)

Figure 4.11: Time evolution of relative attitude and relative distance over 2-orbital period of trajectories belonging to unstable (a) and stable (b) orbital manifold of Earth-Moon L_1 Halo orbit with $A_z \simeq 68.8 \times 10^3$ km ($\simeq 0.1790$ [ndim])

In figure 4.11, the time evolution of the relative attitude of the unstable and stable trajectories of the manifolds are shown in function of the corresponding relative distance. It should be highlighted that a chaser on stable or unstable orbital manifold has an initial relative attitude very small. Then, the attitude motion of a chaser on the unstable orbital manifolds remains very close to the one of the target on the nominal orbit while large distances are not reached. Instead, the attitude of a chaser on the stable orbital manifolds synchronizes naturally to the one of the target spacecraft.
As expected from the Floquet theory, the natural relative dynamics of stable and unstable manifold result as combination of an exponential approaching or departing evolution and a periodic behaviour. The relative distance diagrams highlight an additional behaviour characterizing the relative dynamics of unstable and stable manifolds: a strong diverging or approaching phase of the mode take place near the perilune passage, while the spacecrafts keep their distance almost constant during the remaining part of the orbit.
However, the stagnating region for the unstable manifold corresponds to the second half of the orbit going from perilune (vertical dashed lines) to apolune (vertical dash-dot lines). Instead, the stagnating region of stable manifold is associated to the first half of the orbit. Therefore, the perilune passage acts like a catalyst for the approaching/departing dynamics. This behaviour is reflected also in the spacing between the trajectories of the manifolds in figure 4.10. The relative trajectories starting from the quieter region of the corresponding manifold are close together, while those starting from the faster region are scattered on over the whole manifold surface.

The periodic orbital modes P1 and P2 together the quasi-periodic center orbital modes C1 and C2 constitute the center orbital manifold space of the orbit. These modes maintain similar trajectories to those observed previously in propagated motion with initial condition at apolune alone.
The orbital paths show almost identical trajectory shapes with different amplitude depending on

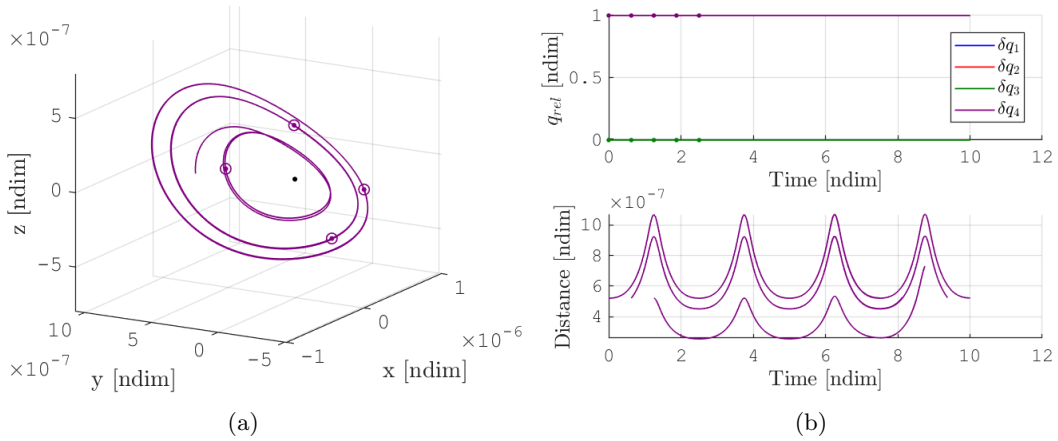

Figure 4.12: Relative orbital and attitude motion over 3-orbital period of trajectories associated to periodic orbital mode P1 of Earth-Moon L_1 Halo orbit with $A_z \simeq 68.5 \times 10^3$ km ($\simeq 0.1790$ [ndim])

the location on nominal orbit selected as initial condition. All the center modes have $\|\lambda_j\| = 1$. Thus, as expected from Floquet theory, they are characterized by a periodic behaviour alone, while the exponential function component is absent. It follows, that the amplitude of the bounded motion is a direct consequence of the initial location along the periodic orbit.
Figure 4.12 shows the 6DOF relative dynamics of a chaser on the periodic mode P1 starting from four different phase angle location equally spaced along the reference Halo orbit and propagated for three orbital period. Figure 4.13 shows the 6DOF relative dynamics of a chaser on the center modes C1 and C2 starting from six different phase angle location equally spaced along the reference Halo orbit and propagated for four orbital periods.
The relative attitude dynamics of the chaser remains very close to the one of nominal orbit for all the mode constituting the center manifold since there is a small distance between chaser and target spacecrafts.

It should be highlighted that the orbital behaviours of the relative orbit-attitude dynamics associated to orbital stable and unstable invariant manifolds remain similar across the whole family of the Halo orbit librating about L_1 and L_2. However, the increasing instability behaviour of smaller amplitude Halo orbit leads to a stronger dominance of the exponential approaching/diverging behaviour of the manifold. Therefore, the characteristic step-wise behaviour is enhanced for high Halo orbits, while a smoother and faster approaching/diverging evolution is observed on lower Halo orbits due to the higher values of their orbital eigenvalues. As a direct consequence of the lower orbital 3-dimensional evolution and of the faster exponential behaviour, the aperture of the conical surface of the manifolds becomes smaller and smaller, up to eventually collapse into a planar motion at the bifurcation with Lyapunov orbits.

Also periodic modes describe similar orbital and attitude relative dynamics across the Halo family.
The relative 6DOF dynamics of quasi-periodic modes is featured by a characteristic low frequency of oscillation which influences the final geometry of the center modes. Eventually, interesting relative orbital path of the chaser may be identified when the oscillation frequency becomes resonant with the orbital period of the target. Figure 4.14 shows a case of close-resonance center modes corresponding to a member belonging to the reference Earth-Moon L_1 Northern Halo family with vertical amplitude $A_z \simeq 71.1 \times 10^3$ km ($\simeq 0.1850$ [ndim]). The motion of the modes have been propagated over four orbital periods. The close-resonance solutions shows a quite-ordered orbital path hovering around the nominal reference orbit.

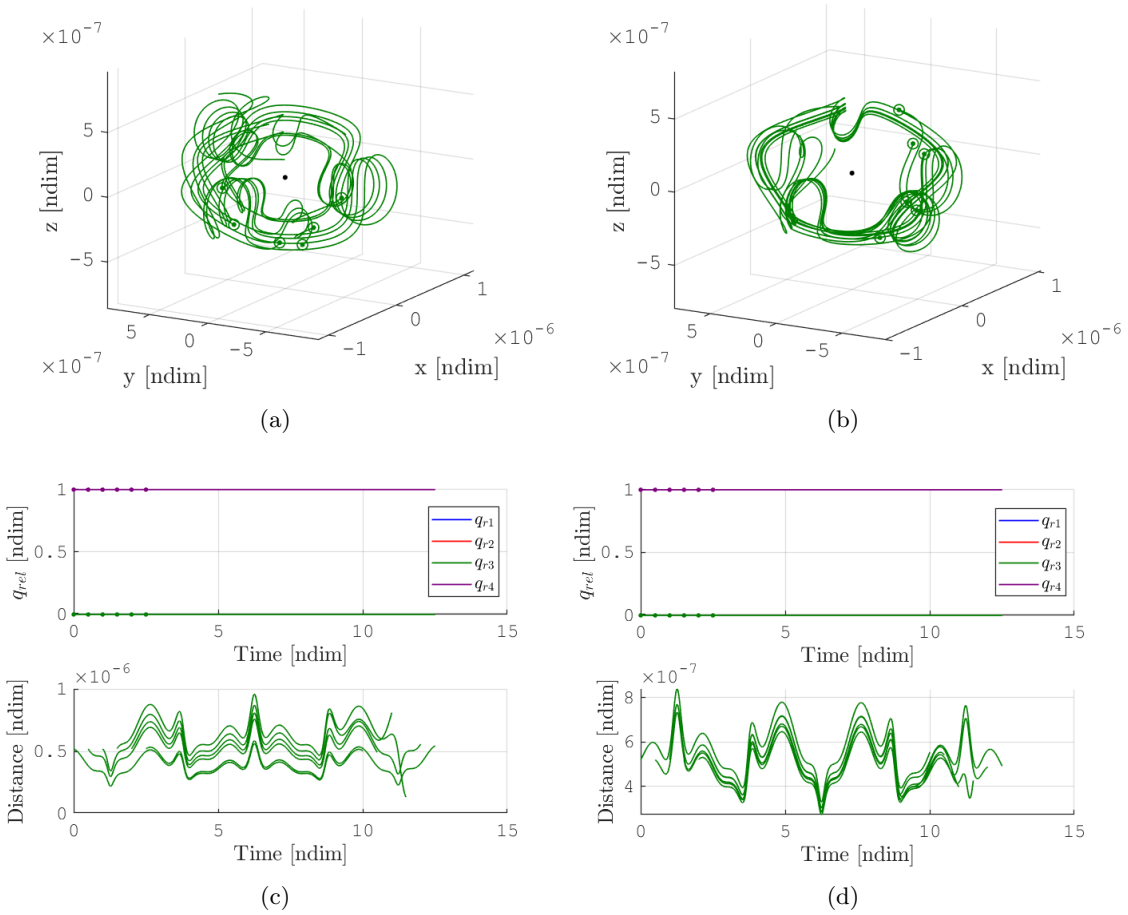

Figure 4.13: Relative orbital and attitude motion over 4-orbital period of trajectories associated to center orbital modes C1 (a, c) and C2 (b, d) of Earth-Moon L_1 Halo orbit with $A_z \simeq 68.5 \times 10^3$ km ($\simeq 0.1790$ [ndim])

The most interesting outcome to be highlighted regards the relative attitude dynamics of each orbital modes belonging to a periodic orbit-attitude natural orbit in the coupled CR3BP, approximating gravitational environment such as the Earth-Moon system: in practice, the attitude motion of a chaser spacecraft on any orbital mode in the vicinity of a target spacecraft on the reference nominal periodic orbit remains synchronized to the attitude dynamics of the target, leading to an almost null relative attitude motion.
This suggest that, small variation in the orbital states will not affect significantly the attitude dynamics because the gravity gradient torque acting on chaser and target is almost the same. Instead the orbital dynamics is dominated by the orbital modes

4.4.2 Attitude Modes of Orbit-Attitude Halo Orbit

The same modal analysis just presented for the orbital modes of the orbit-attitude L_1 Halo family can be applied also to its attitude modes.

If the approximation through the simplified-coupled CR3BP is valid, the attitude modes will have only a significant rotational dynamics and no relative orbital motion.
The stable/unstable attitude modes will results in slowly naturally approaching/diverging behaviours respect to the reference periodic attitude solution. The center attitude mode will characterize a small oscillating behaviour about the reference rotational motion.

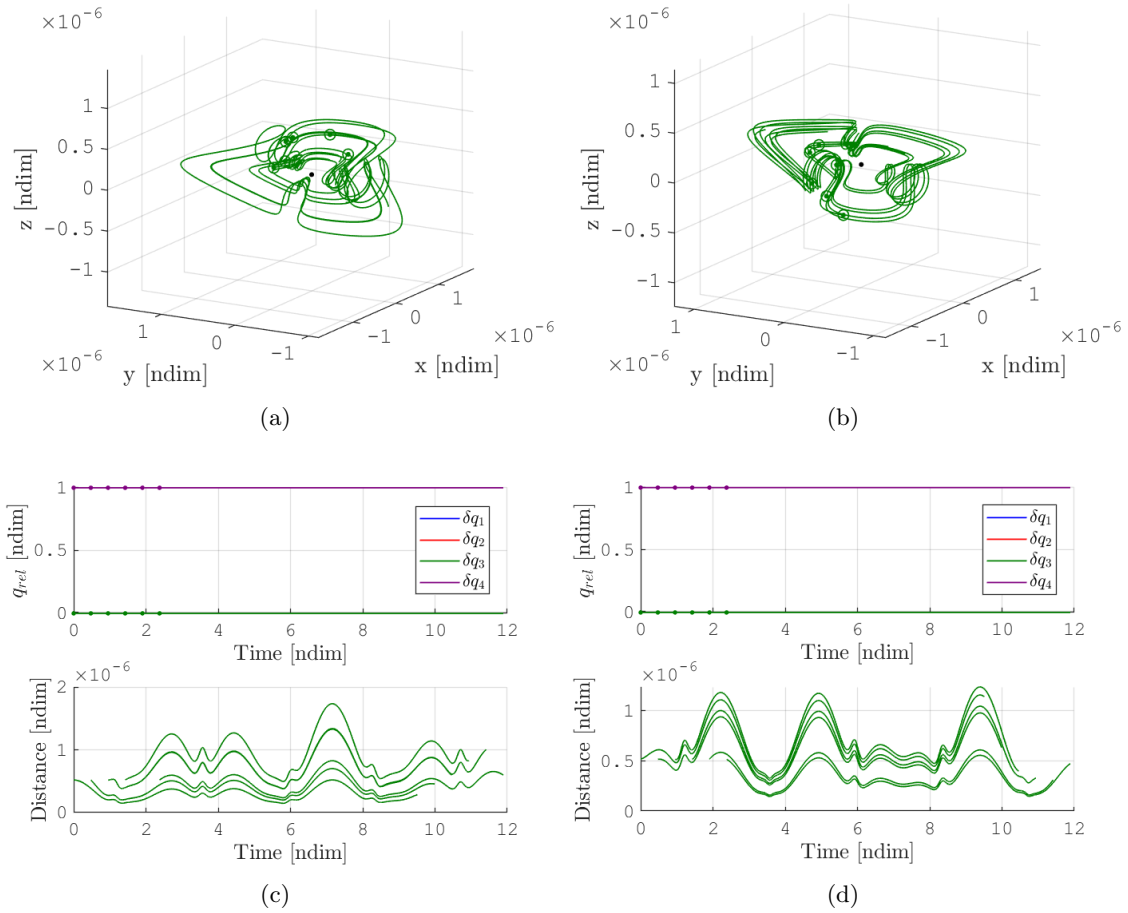

Figure 4.14: Relative orbital and attitude dynamics over 4-orbital period of center orbital modes C1 (a, c) and C2 (b, d) of Earth-Moon L_1 Halo orbit with $A_z \simeq 71.1 \times 10^3$ km ($\simeq 0.1850$ [ndim])

4.5 Orbit-Attitude Manifolds of NRHO

Near Rectilinear Halo Orbits are of great interest for practical application in the Earth-Moon system. They have been often proposed as stagin orbit in cislunar space by international space agencies because many of their properties are suitable to host a manned cislunar space station in future.

The Earth-Moon L_1 Northern NRHO family shown in figure 3.4 is choosen as reference for the investigation of proximity relative dynamics. The attitude dynamics shows a librational behaviour about the synodic frame for a disk-like spacecraft with inertial ratio $K_a = 0.7$ and axis of symmetry aligned to $\hat{\boldsymbol{b}}_1$. However, the observed outcomes can be extended to the other NRHO families in the cislunar system.

Important insights can be obtained by the linear stability analysis of the orbital and attitude eigenvalues characterizing the periodic orbits of this family. The low values of the orbital stability index ν_{orb}, shown in figure 4.15(a), suggest a slowly diverging behaviour of the orbital dynamics, which eventually becomes marginally stable for NRHO orbit with vertical amplitude between $A_z = 73 - 74.5 \times 10^3$ km. The attitude stability index ν_{att} has values way larger than unity, thus the attitude dynamics is expected to be characterized by faster rate of divergence.

The main cause of attitude instability could be attributed to the strong gravity gradient torque of the perilune passage region of the orbit, which has highly sensible dynamics and magnifies any small perturbation. This is reflected in higher values of ν_{att} for larger vertical amplitude A_z, be-

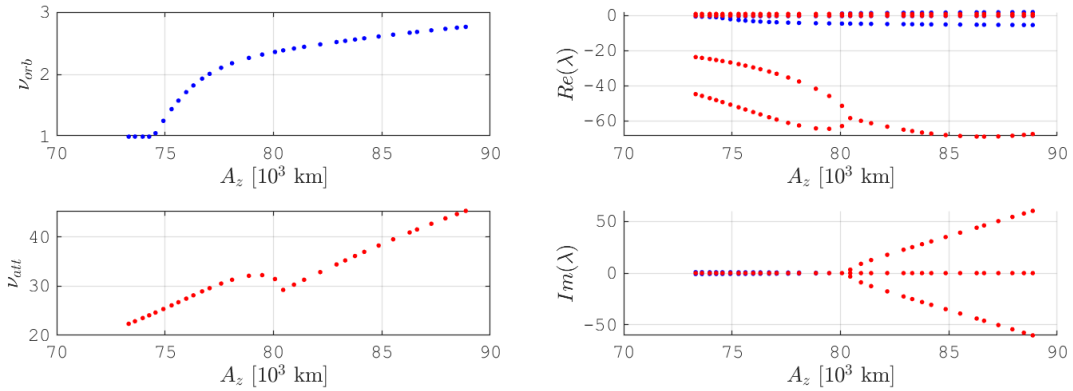

Figure 4.15: Linear stability analysis of the orbit-attitude Earth-Moon L_1 Northern NRHO family. Orbital (blue) and attitude (red) stability index in function of the vertical amplitude A_z (a). Real and complex components of eigenvalues in function of A_z (b)

cause a NRHO with larger A_z corresponds to a closer perilune passage.
This means particular attention shall be given to the natural attitude dynamics of NRHO orbits because some sort of stabilization action, such as dual-spin stabilization, may be required in the perilune region.
Figure 4.15(b) reports the evolution of the real and complex component of the eigenvalues associated to the orbital modes (blue dots) and attitude modes (red dots), in function of the vertical amplitude A_z of the NRHO family. It is evident a bifurcation take place for the unstable attitude modes about $A_z = 80 \times 10^3$ km (about 0.2081 [ndim]). The bifurcation happens also for the corresponding stable attitude eigenmodes, forming a quadruplet of complex eigenvalues and indicator of even stronger instability behaviours.

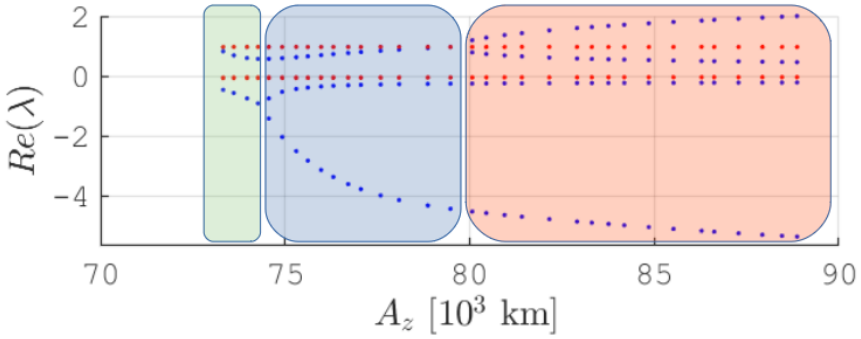

Figure 4.16: Focus on small real components of orbital (blue) and attitude (red) eigenvalues in function of the vertical amplitude A_z of the Earth-Moon NRHO family

Among the members of Earth-Moon L_1 NRHO family, three different configuration of orbital eigenvalues can be identified in figure 4.16. A set of linearly marginally stable in orbital dynamics NRHO orbits have vertical amplitude between $A_z = 73 - 74.5 \times 10^3$ km. A first bifurcation in the orbital eigenvalues, at $A_z \simeq 74.5 \times 10^3$ km, results in a set of NRHO characterized by one pair of stable/unstable orbital mode and one pair of center orbital mode. A second bifurcation in orbital eigenvalues takes place at $A_z \simeq 80 \times 10^3$. The NRHO with larger A_z are characterized by two pairs of stable/unstable orbital modes and with no center modes.
The orbital and the attitude modes of NRHOs share the same features observed in the family of Halo orbits: orbital modes includes also a relevant attitude component, while the attitude modes

has negligible orbital component.
However, an important difference has to be highlighted for the dynamical structure of the unstable and stable manifolds of NRHOs respect the Halo families. The fore mentioned classification of inner and outer toroids is not possible for the stable and unstable orbital manifolds. Respect the Halo families, the orbit of NRHO families are already strongly related to the second primary P_2. The departing and approaching trajectories present a bouncing behaviour back and forth the inner and the outer regions in the vicinity of the reference orbit.
For sake of simplicity, let consider a trajectory on the unstable manifold. Then, the same reasoning can be extended to the stable trajectories which travel the manifold flow in the opposite direction. At each perilune passage, the unstable trajectory will be at a greater distance from the reference orbit respect the previous passage and in the opposite region. Once the manifold reach a largely enough distance from the reference orbit, the next perilune passage will depart ultimately the trajectory from the cislunar space. The described bouncing behaviour of the unstable and stable trajectories can be observed in figure 4.17. To have a clear representation of the bouncing behaviour, only the trajectory associated to orbital modes approximated at the apolune has been propagated over few orbital periods. The reference orbit has been chosen as a cislunar orbit-attitude NRHO with vertical amplitude about $A_z \simeq 78.1 \times 10^3$ km, which corresponds to $\simeq 0.2031$ in non-dimensional form. Its orbital period is about 8.15 days, equal to $\simeq 1.8760$ non-dimensional time. The applied perturbation along the stable and unstable modes corresponds to 50 km in position, equal to $\simeq 1.3 \times 10^{-4}$ non-dimensional unit. Then, the natural dynamics has been propagated over 5 orbital periods.

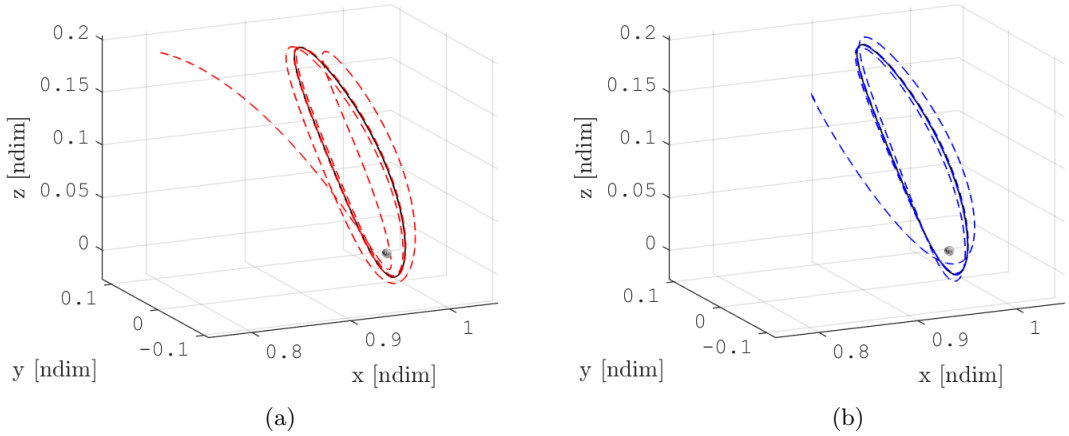

Figure 4.17: Absolute orbital dynamics of unstable and stable trajectories of an Earth-Moon L_1 NRHO

4.5.1 Orbital Modes of Orbit-Attitude NRHO

Let start the modal analysis of the orbit-attitude Earth-Moon L_1 NRHO family from the member with vertical amplitude $A_z \simeq 78.1 \times 10^3$ km ($\simeq 0.2031$ in non-dimensional length) and orbital period $T \simeq 8.15$ days ($\simeq 1.8760$ in non-dimensional time). Its perilune distance is $r_p \simeq 8.3 \times 10^3$ km ($\simeq 0.0216$ non-dimensional length). The orbital dynamics of this orbit is characterized by one pair of stable/unstable plus one pair of quasi-periodic orbital modes, while two pairs of stable/unstable feature its attitude dynamics. Both the periodic orbital and attitude modes are associated to a pair of eigenvalues in $+1$. Therefore, this orbit belongs to the set of orbit-attitude NRHOs highlighted in blue in figure 4.16. The configuration of orbital and attitude eigenvalues associated to this orbit are shown in figure 4.18 as blue and red circles, respectively.

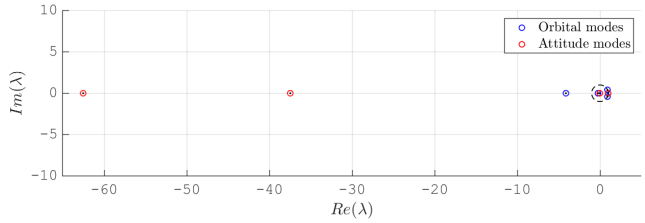

Figure 4.18: Orbital and attitude eigenvalues of the Earth-Moon L_1 NRHO. $A_z \simeq 78.1 \times 10^3$ km ($\simeq 0.2031$ [ndim])

Let assume a target spacecraft moving on the nominal reference orbit. The 6DOF natural relative dynamics of each manifold is propagated considering a chaser spacecraft lying on the corresponding orbital mode considering different locations along the reference orbit as initial condition.
In order to well approximate the initial condition of the chaser spacecraft on the orbital modes, the perturbation magnitude is selected equal to 200 meters in position distance ($\simeq 5 \times 10^{-7}$ non-dimensional unit).
As it has been already observed for the Halo family, the orbital modes of the NRHO present a negligible relative attitude dynamics since the relative distance between target and chaser spacecraft is lower than ~ 1000 km (~ 0.003 in non-dimensional units). Therefore, the modal analysis is focussing the discussion about the only relative orbital dynamics of the orbital modes.

Let begin the modal analysis from the stable and unstable orbital modes. Figure 4.19 shows

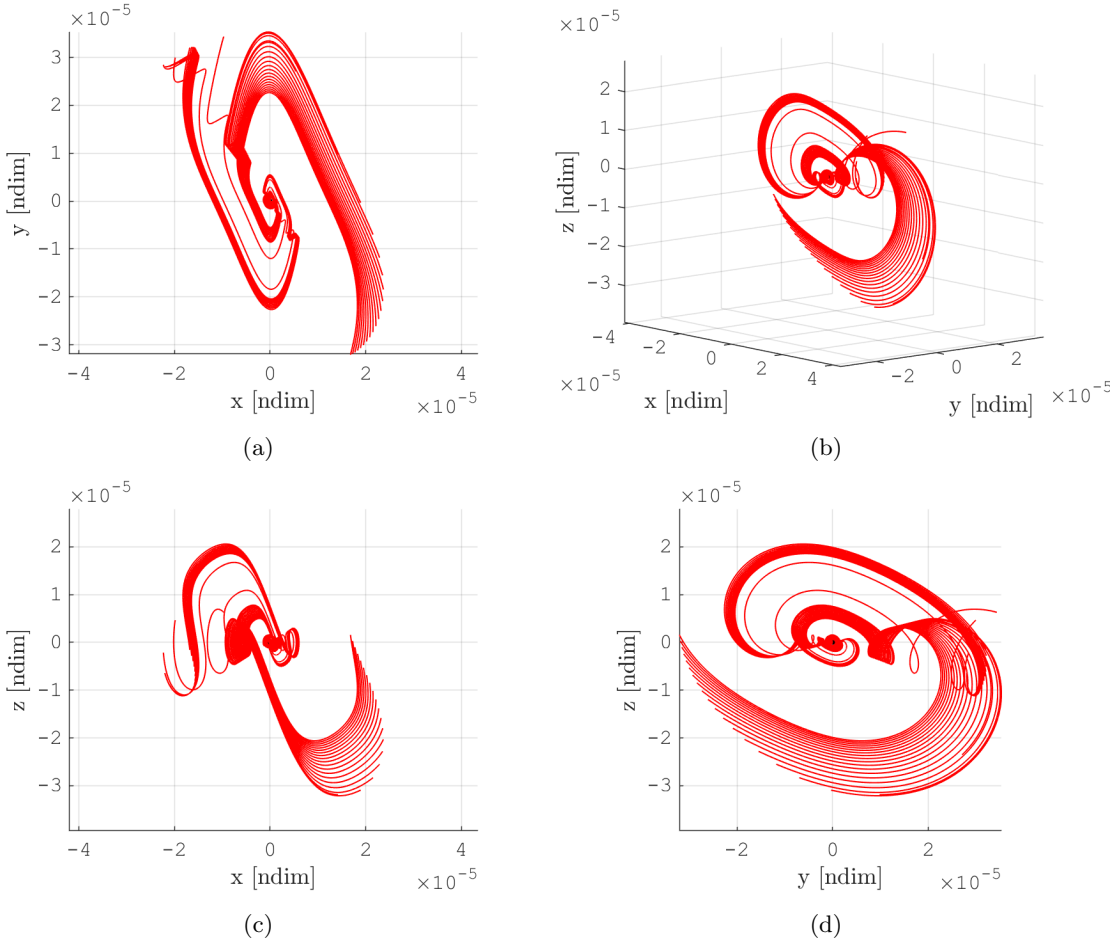

Figure 4.19: Relative orbital dynamics over 3-orbital period of unstable orbital mode trajectories. Earth-Moon L_1 Northern NRHO with $A_z \simeq 78.1 \times 10^3$ km ($\simeq 0.2031$ [ndim])

the relative orbital dynamics of the unstable orbital manifold seen in the synodic $\{\hat{r}\}$-frame point of view. It has been obtained by discretizing the nominal orbit in 40 nodes equispaced in phase angle, and propagating the 6DOF dynamics of target and chaser spacecrafts over 3 orbital period. The same procedure has been applied for the stable orbital manifold, and its relative orbital dynamics seen in the $\{\hat{r}\}$-frame is shown in figure 4.20. The observed orbital structure of the unstable

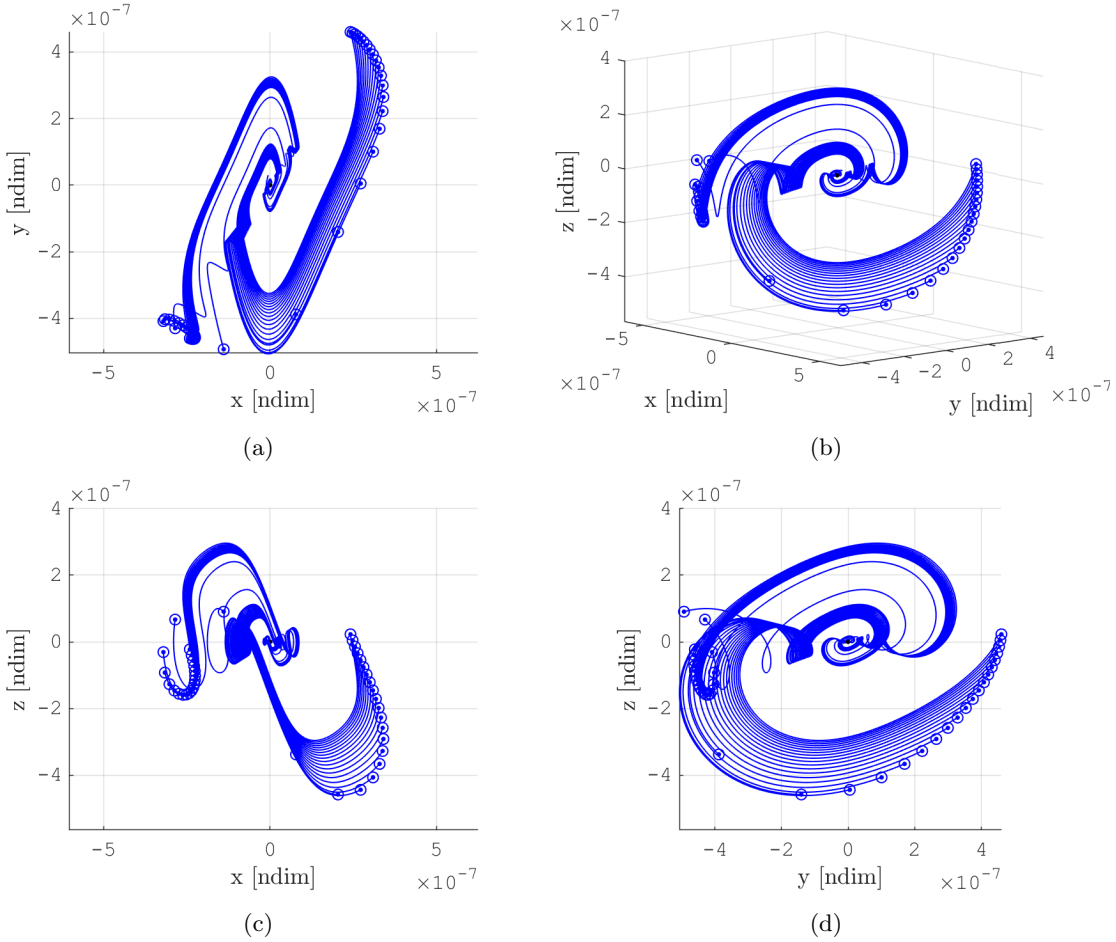

Figure 4.20: Relative orbital dynamics over 3-orbital period of stable orbital mode trajectories. Earth-Moon L_1 Northern NRHO with $A_z \simeq 78.1 \times 10^3$ km ($\simeq 0.2031$ [ndim])

and stable orbital manifolds is characteristic of all the NRHOs existing about the collinear point L_1 and L_2. The spiralling-conical structure observed before for the Halo families is now strongly deformed. Two opposite spiralling-conical regions are still present. The bouncing effect, observed before for the absolute dynamics of the manifolds in figure 4.17, is now seen in relative orbital dynamics as wide curves that connect the two opposite small spiralling-conical regions.
For both the unstable and stable manifolds, every perilune passage of target and chaser spacecrafts on the absolute reference orbit corresponds approximately to the xz-plane crossing of the wide curves of the relative orbital trajectories.
In correspondence of each perilune passage for chaser and target spacecrafts, the relative orbital dynamics of the unstable trajectories quickly evolve on the wide curve departing from the conical-spiralling region. Then, the relative dynamics on the wide curve progressively slows down while target and chaser continue their travel towards the apolune. It eventually finishes to enter a new spiralling motion at a significantly larger distance than before on the opposite cone of the manifold. Then, a new cycle can begin.
The stable trajectories describe the same dynamical structure, but they are travelling in the op-

posite direction and eventually converge towards the target.
It should be noticed that actually only half of the unstable and stable orbital manifold surfaces is shown in figures 4.19 and 4.20. In fact, the empty space of the relative manifold is filled by a symmetric dynamical structure identifying the trajectories belonging to the same orbital mode but having the initial condition perturbed in its opposite direction.

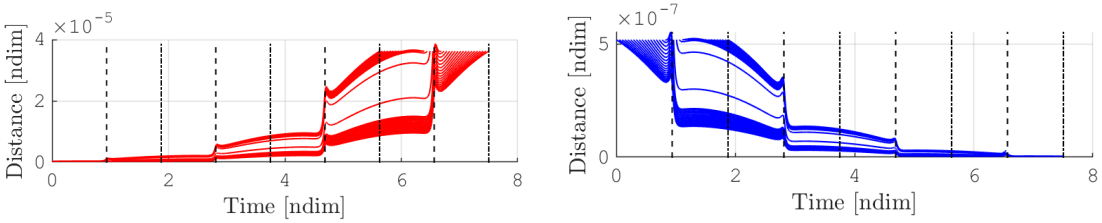

Figure 4.21: Relative distance evolution over 3-orbital period of unstable and stable orbital mode trajectories. Earth-Moon L_1 Northern NRHO with $A_z \simeq 78.1 \times 10^3$ km ($\simeq 0.2031$ [ndim])

Figure 4.21 reports the time evolution profiles of the relative distance of the chaser spacecraft respectively on the unstable (red) and on the stable (blue) orbital trajectories. Every perilune event is reported via vertical dashed lines, while every apolune event is shown as vertical dash-dot lines. It should be highlighted that the distance between target and chaser has a steep variation at each perilune passage. This exponential step-like evolution is quite characteristic of all NRHOs.
The stable trajectories may represent interesting reference natural corridors for rendezvous applications. A chaser spacecraft (for example cargo or crewed vehicle, station module or ascent/descent vehicle) could target a manifold injection point along a stable trajectory, for example exploiting an open-loop controller based on a dedicated targetter differential corrector algorithm. Then, it will follow the natural dynamics approaching the target spacecraft (the LPO-G), requiring only small maintenance correction in order to cancel out possible external perturbations or injection and navigation errors. Finally, only the last relative arc would be performed via a continuous controlled trajectory to complete the docking maneuver.
It should be highlighted that stable trajectories shows the beginning of departing behaviour on the unstable manifold after a perilune passage, if the time of integration is sufficiently long to be affected by numerical errors. In fact, the perilune region manifests high dynamical sensibility due to the high gravity gradients, which makes any perturbation a possible trigger to shift the natural dynamics from the stable to the unstable manifold.
The trajectories of unstable orbital manifold represent natural flows drifting apart from the target. In a rendezvous and docking operation scenario, any contingency or abort procedure at any point during the approaching phase may leverage on the unstable orbital manifold to drift away from the target and reach a safe condition with minimum collision risks. The same unstable flow may be exploited in undocking operations in order to naturally reach a position far enough from the space gateway and contemporaneously avoid any control maneuver that could worsen the condition of the spacecrafts if any anomaly should arise.
In rendezvous and docking operations, a particular reference frame is typically assumed in the analysis of relative orbital dynamics between target and chaser: the Local Vertical-Local Horizontal (LVLH) frame. In this investigation the LVLH-frame has been defined similarly to what is usually done in Low Earth Orbit (LEO). The origin of the LVLH-frame is located at the target position along the nominal orbit. The R-bar $\hat{\boldsymbol{z}}_{LVLH}$ points towards the Moon, which is the main attractor for NRHOs. The H-bar $\hat{\boldsymbol{y}}_{LVLH}$ is opposite to the direction of the instantaneous orbital angular momentum of the target orbit seen in the rotating frame, $\boldsymbol{h} = \boldsymbol{x} \times \boldsymbol{v}$. The V-bar $\hat{\boldsymbol{y}}_{LVLH}$

completes the right-handed triad. Figure 4.22 shows the relative trajectories of unstable (red) and

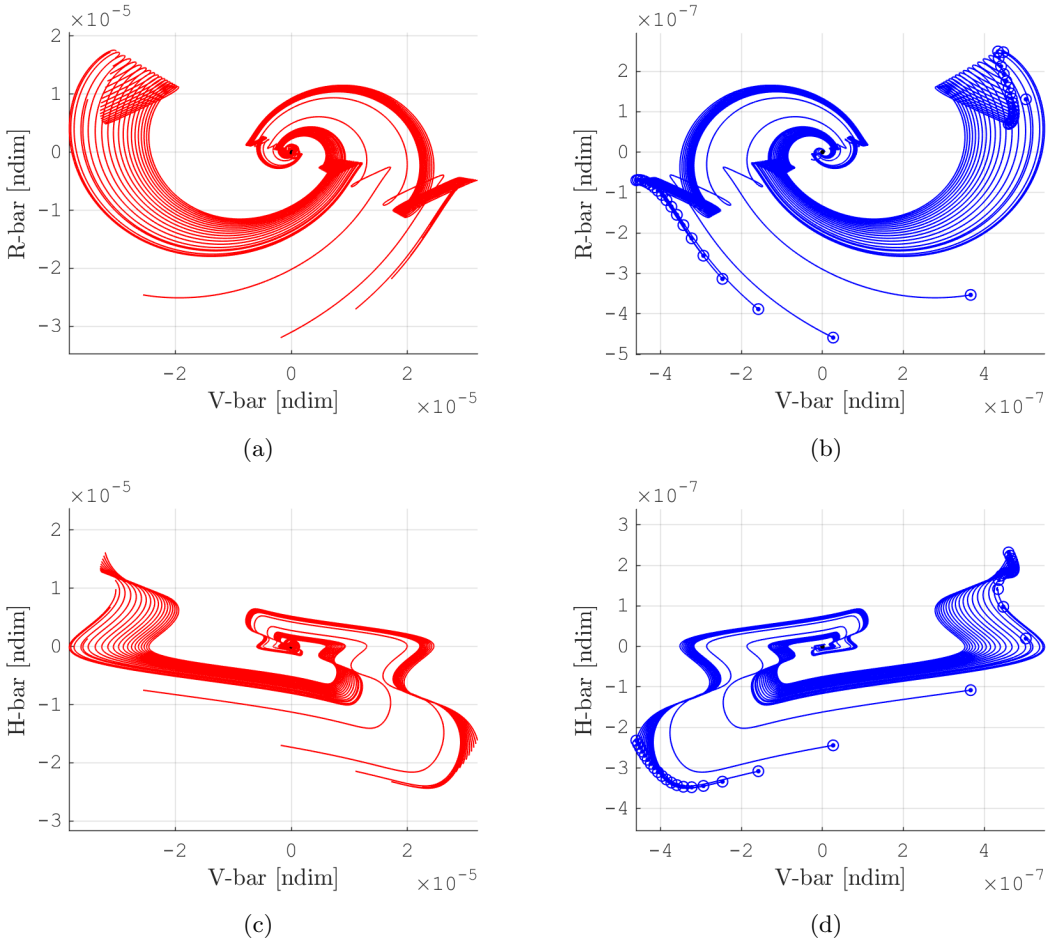

Figure 4.22: Relative orbital dynamics over 3-orbital period of unstable and stable orbital mode trajectories in target centered LVLH-frame. Earth-Moon L_1 Northern NRHO with $A_z \simeq 78.1 \times 10^3$ km ($\simeq 0.2031$ [ndim])

stable (blue) orbital manifolds seen from the LVLH-frame point of view. The regions, observed before in the rotating point of view, can be distinguished easily in a double-spiralling structure. Moreover, the wide curves going back and forth along the V-bar manifest even more clearly the characteristic bouncing behaviour of the NRHOs.

Let continue the modal analysis with the periodic orbital modes P1 and P2. The relative trajectories identified by these modes resemble the drop-like shape geometries already seen for the same mode of the Halo family. The closer passage to the second primary (the Moon) of the NRHOs results in higher orbital velocity, and the enhanced elastic effect is reflected in a greater elongation of P1 and P2 modes. Figures 4.23(a) and 4.23(b) show respectively the orbital dynamics associated to periodic modes P1 and P2 of the reference Earth-Moon L_1 NRHO. The time evolution of the relative distance between target and chaser in the diagrams 4.23(c) and 4.23(d) highlight clearly the elastic effect mentioned before. Figure 4.24 reports the orbital modes P1 and P2 in the LVLH-frame point of view. Both the periodic modes present a relevant evolution in the pseudo-orbital plane identified by the V-bar and the R-bar. Furthermore, the LVLH-frame representation allows an immediate interpretation of the orbital motion associated to the periodic modes. A chaser on the mode P1 in figure 4.24(a) is ahead on the same orbit of the target spacecraft. Instead, a chaser on the mode P2 in figure 4.24(b) is on a periodic orbit with a slightly larger period respect the reference orbit of the target. Moreover, figure 4.24(d) tells this orbit has a slightly lower A_z.
The nature of the mode P1 offers a useful relative periodic orbit that can be leveraged as safe

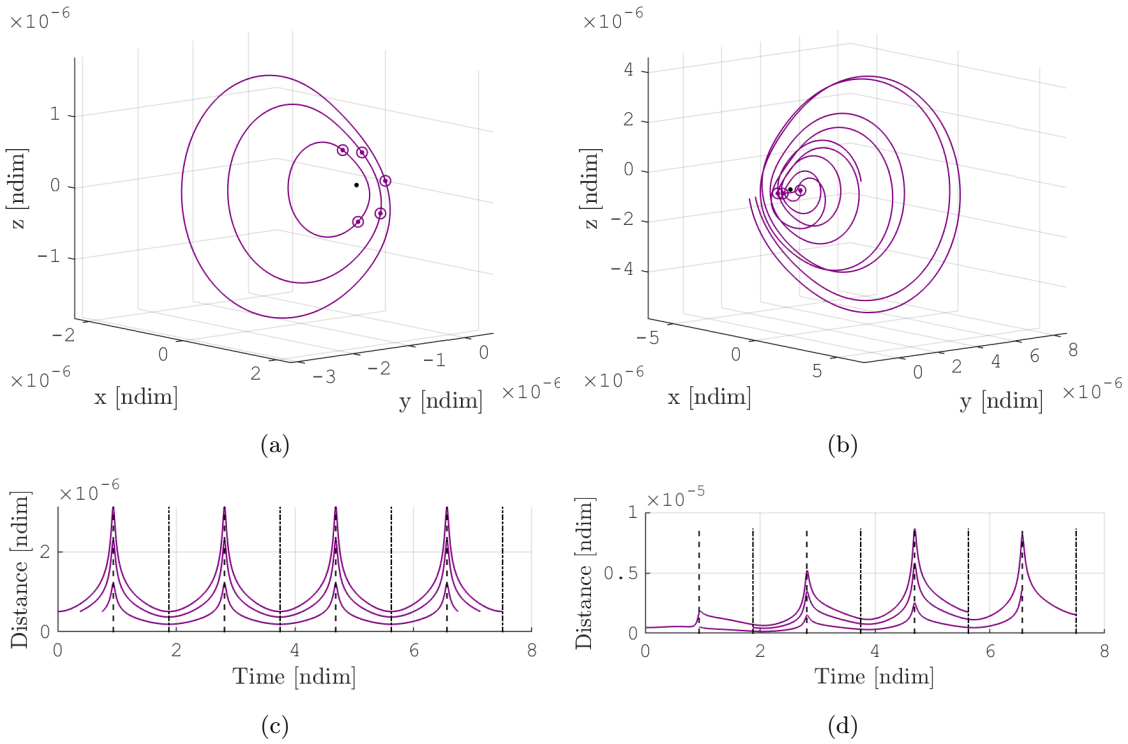

Figure 4.23: Relative orbital dynamics over 3-orbital period of periodic orbital modes P1 and P2 trajectories. Earth-Moon L_1 Northern NRHO with $A_z \simeq 78.1 \times 10^3$ km ($\simeq 0.2031$ [ndim])

checkpoints during the approaching phases of rendezvous and docking operation. For example a chaser spacecraft could wait on this relative orbit the authorization from ground station to proceed its proximity maneuvers.

The last pair of orbital modes is associated to quasi-periodic motion. As representative mode of the center orbital manifolds of the NRHO, figure 4.25 shows the orbital path of the center mode C1 propagated over 6 orbital period, and see in the target centered LVLH-frame. This particular case is considering apolune as initial condition of the target on the reference orbit. The wide arcs composing the center mode behaviour are characteristic of NRHOs, direct consequences of the close passage to the Moon. These arcs constitute complex hovering motions of the chaser spacecraft around the target. An oscillating behaviour having a longer period respect the one of the orbit characterize these particular orbital dynamical structures, which resembles the oscillating behaviour observed in literature for ephemeris NRHO.
The same perturbation in position magnitude generates similar trajectory path structures, but with a smaller amplitude if the spacecraft initial condition along the reference orbit is closer to the perilune region. In fact, the velocity component of the orbital modes increases its importance when the initial condition of the relative motion corresponds to target and chaser closer to the perilune passage.
It should be noticed that in figure 4.25 are reported the propagation of the center orbital mode C1 for target and chaser starting at apolune at reference time $t_0 = 0$ and $t_0 = T$. The numerical errors in the approximation of the mode results in the small mismatch between the two propagated modes. These errors are coming from all the numerical approximation are considered in the analysis: not perfect periodic orbit-attitude orbit, integration errors, numerical approximation of eigenvectors.

The just presented orbital modes are characteristics of all the members belonging to the class of NRHOs having one pair of stable/unstable mode and one pair of center mode. The pair of eigenvalues associated to the center mode of this class eventually bifurcate in a new pair of sta-

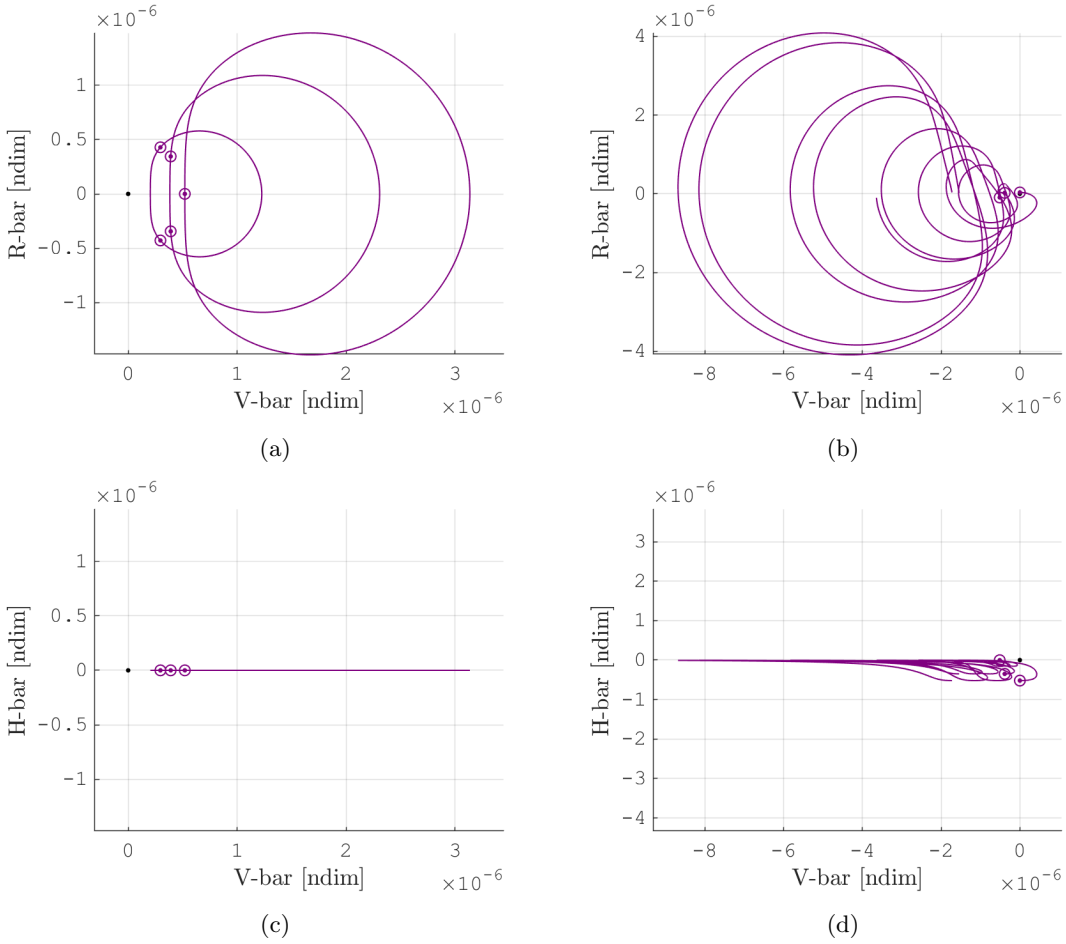

Figure 4.24: Relative orbital dynamics over 3-orbital period of periodic orbital modes P1 and P2 trajectories in LVLH point of view. Earth-Moon L_1 Northern NRHO with $A_z \simeq 78.1 \times 10^3$ km ($\simeq 0.2031$ [ndim])

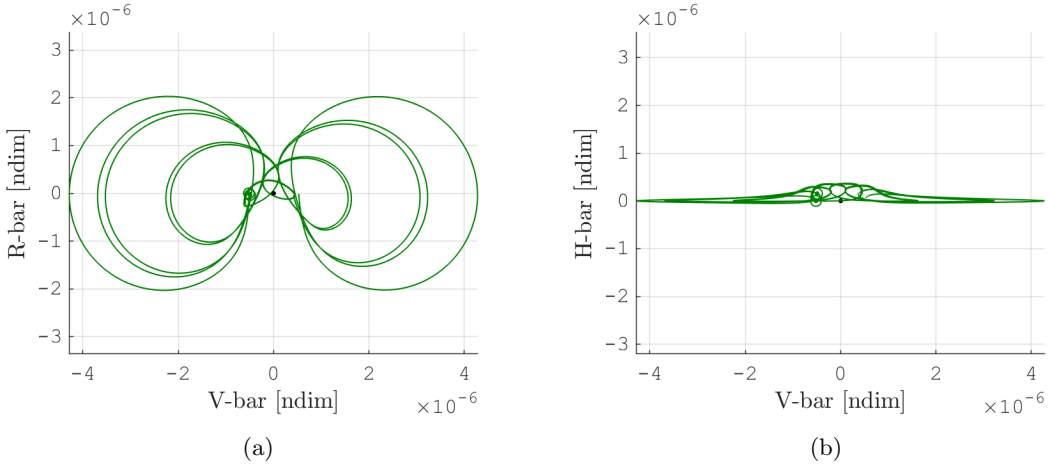

Figure 4.25: Relative orbital dynamics over 6-orbital period of center orbital modes C1 trajectories in LVLH point of view. Earth-Moon L_1 Northern NRHO with $A_z \simeq 78.1 \times 10^3$ km ($\simeq 0.2031$ [ndim])

ble/unstable eigenmode, which remain closer to the unitary circle in the complex plane. They identify a new class of NRHOs, highlighted in red in figure 4.16.

The "dominant" pair of stable/unstable orbital modes and the pair of periodic modes P1 and P2 keep the same features observed in the previous class of NRHO. The main difference corresponds to the substitution of the pair of center modes with a pair of "lightly" stable/unstable modes,

denoted as S2 and U2. Figures 4.26 and 4.27 report the relative orbital dynamics of orbital

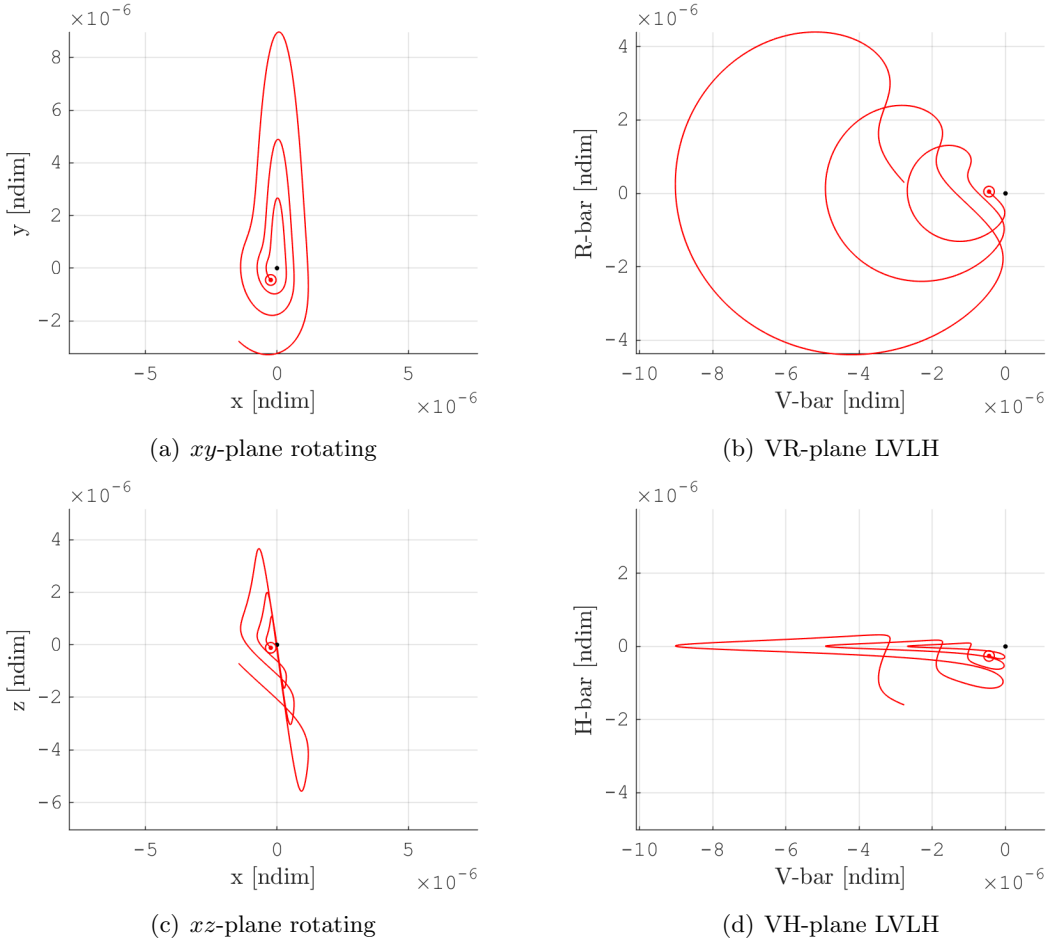

(a) xy-plane rotating (b) VR-plane LVLH

(c) xz-plane rotating (d) VH-plane LVLH

Figure 4.26: Relative orbital dynamics over 3-orbital period of unstable orbital mode U2 in synodic and LVLH point of view. Earth-Moon L_1 Northern NRHO with $A_z \simeq 85.5 \times 10^3$ km ($\simeq 0.2225$ [ndim])

modes U2 and S2 seen from target centered synodic frame point of view and from LVLH frame point of view. The selected representative member of this class of NRHOs has a vertical amplitude $A_z \simeq 85.5 \times 10^3$ km, equal to $\simeq 0.2225$ non-dimensional length.
The orbital structure of these modes remember the one of the periodic orbital modes, in particular P2. In fact, the slightly diverging/approaching behaviour of this mode is way weaker respect the "dominant" unstable/stable modes and, as a consequence, they are strongly influenced by the periodic component of the orbit.

The last observed class of NRHOs is constituted by linearly marginally stable orbits. As for any linearly marginally stable orbit, the orbital dynamical flow in proximity of these NRHOs is constituted only by the center orbital manifold.
The orbital mode P1 identifies a chaser on the same periodic reference orbit of the target, but located in a forwards or backwards position. The P2 mode is associated to a chaser orbiting on a slightly larger or smaller natural periodic orbit respect the target. The remaining modes describe a 4-dimensional space of quasi-periodic motion bounded in vicinity of the reference nominal orbit.

A final consideration has to be highlighted observing the normalized direction of the NRHO's orbital modes in the 6-dimensional space of orbital state. Considering the non-dimensional model, the importance of the velocity components becomes more and more dominant respect to those of the position when the orbital mode is approximated closer to the perilune region of the orbit.
This behaviour seems to reflect the intrinsic natural structure of quasi-periodic NRHO identified in

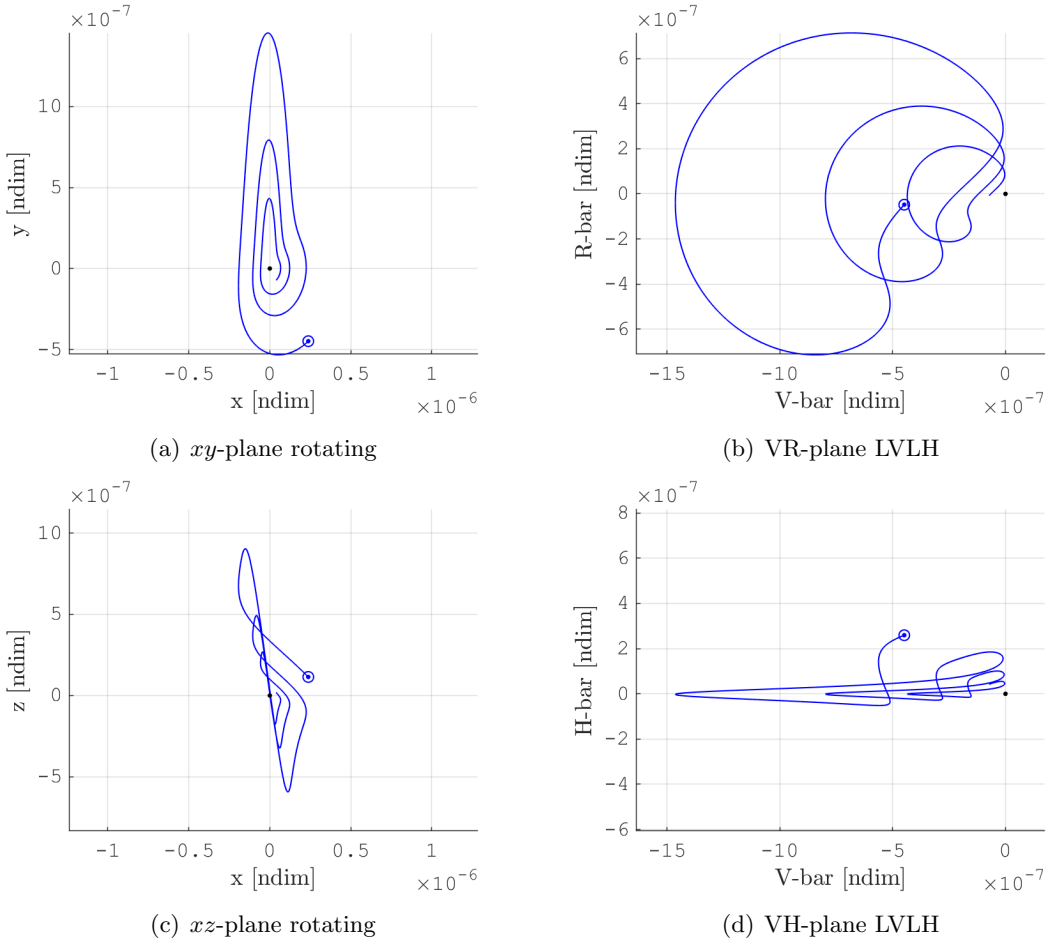

(a) xy-plane rotating

(b) VR-plane LVLH

(c) xz-plane rotating

(d) VH-plane LVLH

Figure 4.27: Relative orbital dynamics over 3-orbital period of stable orbital modes S2 in synodic and LVLH point of view. Earth-Moon L_1 Northern NRHO with $A_z \simeq 85.5 \times 10^3$ km ($\simeq 0.2225$ [ndim])

the higher-fidelity ephemeris model. In fact, the ideal toroids enclosing ephemeris NRHO shrinks quite significantly at the perilune, where any revolution passes very close to each others. By the contrary, at the apolune the toroids shows a relevant enlargement and the revolution path are quite distributed.
The same concept can be exploited also in the design of station-keeping strategies which would employ an admissible "tollerance toroid" around the ideal motion of the spacecraft along the orbit.

4.5.2 Attitude Modes of Orbit-Attitude NRHO

Again, the attitude modes associated to periodic orbits in the 6DOF simplified-coupled CR3BP have negligible orbital component. These modes characterize the relative attitude dynamics, describing the evolution of the relative rotational dynamics due to a small perturbation in the attitude of the target respect its reference natural periodic motion. However, the same concept can be extended also to describe the relative rotational dynamics due to small perturbation in attitude of a chaser spacecraft moving on a reference orbital modes in proximity of the periodic solution.
The attitude mode of the reference NRHO family has two pair of stable/unstable modes, as can be seen in figure 4.15(b). The existence of two unstable modes and an high attitude stability index ν_{att} associated to the reference NRHO family suggest that the attitude dynamics will be very sensible to any minimal perturbation.
The pairs of periodic attitude modes represent the continuation directions to find new kind of natural periodic attitude motion for the same orbit.

Again, the stable modes represent attitude dynamical flows that slowly converge to the reference natural orbit-attitude motion, while the unstable attitude manifolds diverge from the reference periodic behaviour.

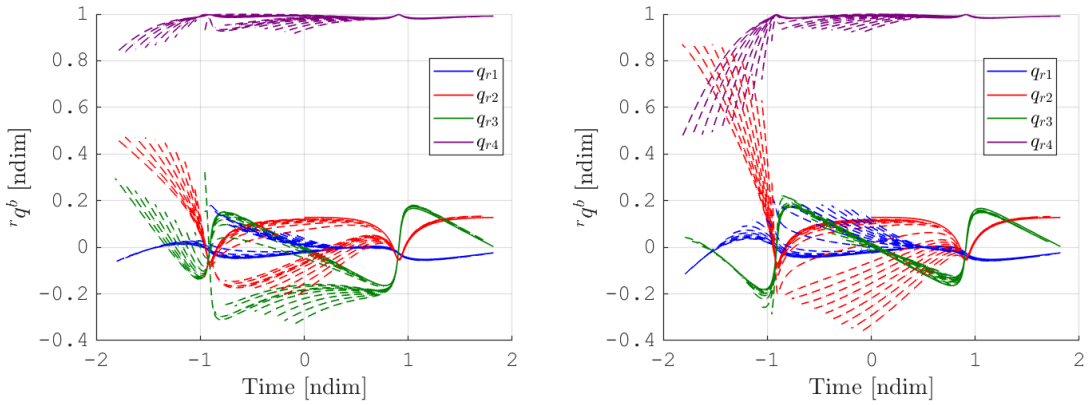

(a) Stable attitude mode S1 (b) Stable attitude mode S2

Figure 4.28: Absolute attitude dynamics of stable attitude manifolds S1 (a) and S2 (b) propagated over one orbital period. Earth-Moon L_1 Northern NRHO with $A_z \simeq 80.5 \times 10^3$ km ($\simeq 0.2093$ [ndim])

This behaviour is evident in figure 4.28, which shows the absolute attitude motion characterizing the stable attitude modes S1 and S2 propagated over one orbital period.
The same procedure can be followed to generate the unstable attitude manifolds U1 and U2, which are shown in figure 4.29.

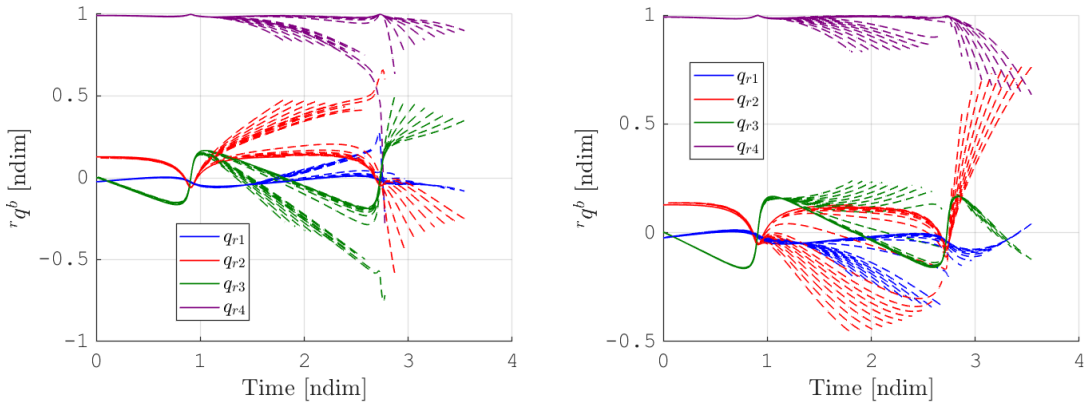

(a) Unstable attitude mode U1 (b) Unstable attitude mode U2

Figure 4.29: Absolute attitude dynamics of unstable attitude manifolds U1 and U2 propagated over one orbital period. Earth-Moon L_1 Northern NRHO with $A_z \simeq 80.5 \times 10^3$ km ($\simeq 0.2093$ [ndim])

It should be highlighted how the unstable attitude motions quickly diverge from the periodic motion even if the attitude perturbations introduced are very small (less than one degree). All the unstable attitude manifolds begin to diverge in an evident way at the perilune passage of the spacecraft, remarking the high dynamical sensibility of this region. This suggest that some sort of stabilization (passive or active) shall be provided, especially in the perilune region of the NRHO otherwise any natural periodic rotational motion will diverge.
By contrary, the perilune region is for the stable attitude manifolds the synchronization point with the reference natural rotational motion.
A combination of active control torque with stable and unstable attitude flows could be exploited

to perform low cost large slew maneuver applications. However, these kind of maneuver can't be performed in short execution time because the natural dynamics of the modes is directly associated to the orbital period of the reference orbit. Moreover, an high attitude accuracy will be required before entering the perilune region to control and exploit at its maximum the natural drift of the attitude.
The same reasoning can be applied to a chaser spacecraft moving along an orbital mode in proximity of the reference orbit. In fact, an high attitude accuracy is required to correctly tuning the 6DOF dynamics of any orbital mode corridor with the natural periodic motion of the reference orbit. If not the case, at the next perilune passage the attitude dynamics will be quickly dominated by the unstable attitude mode and it will drift away.
Considering the rendezvous scenario, this behaviour is an additional reason to avoid proximity and docking operations close to the sensible perilune region, while the apolune region offers a favourable zone for this kind of operations. Moreover, this "quiet" zone cover most of the orbital period of a NRHO, providing a large temporal window each orbit.

4.6 NRHO in Ephemeris Model

It has been already highlighted the Earth-Moon system is significantly influenced by the perturbations due to the gravitational presence of the Sun and by the eccentricity of the orbit of the Moon. Therefore, it is fundamental to extend the modal analysis just performed in the CR3BP idealization to an higher-fidelity model if a space mission aims to exploit natural periodic orbits in cislunar space and its orbital modes.
In this investigation, a preliminary analysis of the relative dynamics of two spacecrafts orbiting about a possible cislunar staging orbit trajectory is considered.
In general, any periodic natural solution obtained in the CR3BP can be associated to a ballistic quasi-periodic motion in the higher-fidelity ephemeris model. Those trajectories are usually similar to the ones described by the quasi-periodic toroids in the CR3BP.
It should be noticed that the transition of the orbit to an higher-fidelity ephemeris model is significantly affected by the reference initial epoch, because it is directly related to the evolution of the relative configuration of the main gravitational attractors of the system.

4.6.1 Reference Staging Orbit of Target Spacecraft

Nearly-periodic motion of ephemeris NRHOs are enclosed within a toroid, which is "tight" near the perilune passage and becomes "loose" in the apolune region, characterized by variable trajectory patterns from one revolution to another. This behaviour can be account mainly to three causes. First of all, the sensible perilune region will empathize any small perturbation and any slightly different passage may results in a diverging trajectory. Secondly, the perturbations associated to the higher-fidelity forces respect the CR3BP idealization have a greater impact on the dynamics in the apolune region of the NRHO. Finally, this toroidal dynamical structure is intrinsically characterizing the NRHO, resembling the orbital center quasi-periodic manifold of the CR3BP model.
The trajectories over different revolutions present an osculating behaviour, which can be larger or smaller depending on the orbit. In literature has been seen that, it is possible to achieve nearly-periodic orbits quite similar to the pattern obtained in the idealized CR3BP for Halo orbits with very large and very small perilune radius. However, it seems to exist a transition zone in the middle of Halo families where it is very difficult obtain motions resembling the characteristics periodicity behaviours [40].

In this investigation, one of the members belonging to the L_1 Northern NRHO family is chosen as reference cislunar staging orbit for the target spacecraft. This orbit has a vertical amplitude in the order of $A_z \simeq 80 \times 10^3$ km, and a perilune distance about $r_p \simeq 3900$ km, while its orbital period is about $T \simeq 7.8$ days long.
The reference initial epoch has been settled in the end of 2023. It represents a realistic temporal window for the beginning of the assembling operations of firsts modules composing the Lunar Orbital Platform.
The non-dimensional initial orbital states obtained from the reference NRHO in the CR3BP model are coherently dimensionalized and transformed to the Moon-centreed inertial J2000 $\{\hat{I}\}$-frame, considering the instantaneous information of the Earth-Moon system gathered from ephemeris data. Also, the attitude states are transformed from being expressed respect the instantaneous synodic $\{\hat{\hat{r}}\}$-frame to the $\{\hat{I}\}$-frame representation. Then, the transitioned initial condition of the target spacecraft are propagated in the orbit-attitude ephemeris dynamical model.
A variation of the initial epoch strongly influences the whole dynamics because it changes the configuration evolution of the three main attractor constituting the Earth-Moon-Sun ephemeris model. Especially considering the simple transition procedure implemented in this investigation, even a variation of few days may result in completely different behaviours.

Due to the more sensible dynamics, the transition to ephemeris model of points belonging to the perilune region of the NRHO results in trajectories departing almost immediately from the nominal path described in the CR3BP. Instead, the propagation of the dynamics in the ephemeris model of transitioned initial condition belonging to the apolune region results in trajectories that remains orbiting in cislunar space for few orbital period before departing on an unstable manifold. For example, in figure 4.30 has been shown the trajectory obtained from the propagation in the ephemeris model over two orbital period, considering as initial condition the apolune of the reference NRHO transitioned by settling the 18th November 2023 as initial epoch. This trajectory (blue line) has been compared respect the nominal reference orbit obtained in the CR3BP model (red line) in both the synodic and the inertial point of view, respectively in figures 4.30(a) and 4.30(b). It should be noticed that the trajectory propagated in ephemeris model remains quite

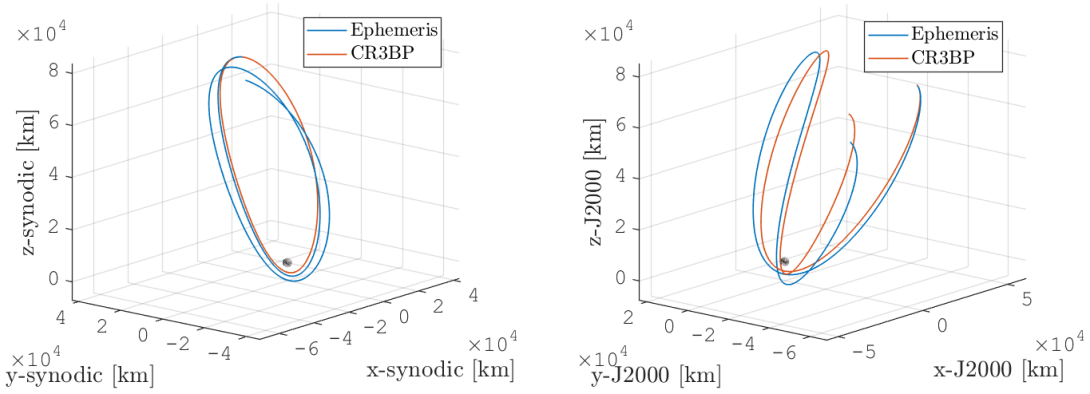

(a) Rotating point of view (b) Inertial point of view

Figure 4.30: Orbital dyamics of 6DOF CR3BP NRHO propagated in ephemeris model over 2-orbital period

close to the nominal behaviour up to the first perilune passage. Here, the accumulated errors initiate the departing behaviour of the spacecraft from cislunar space. However, the trajectory resembles nearly-periodic behaviours during the first three orbital period. Therefore, it may offer interesting preliminary outcomes from the analysis of the relative dynamics.
The apolune has been selected as initial condition because it represents the most favourable dynam-

ical region for proximity, rendezvous and docking operations. Furthermore, the apolune region is less sensible to errors that may be introduced during the transition to the ephemeris model allowing an easier transition of the reference orbit from the CR3BP idealization.

In literature, many methods of transitioning between the CR3BP and higher-fidelity models have been developed and well documented. In future work one of these algorithms could be employed to refine the initial condition of the target spacecraft and deepening the understanding of relative motion in an higher-fidelity model. All these methods are based on the same concept idea. They starts from the reference periodic orbit solved in the CR3BP model. A certain number of patch point are identified, then they are stacked to cover the desired duration of the mission. Each of them is associated to a particular time tag, which represents the instantaneous epoch when the spacecraft will pass through them. Then, the patch point are transitioned to the ephemeris model considering their time tag. A correction algorithm is implemented to minimize the continuity error under a certain tollerance value and return the ballistic nearly-periodic NRHO.

Figure 4.31 reports the attitude dynamics evolution of the target spacecraft, which is moving on the trajectory in figure 4.30. The solid lines shows the attitude dynamics of the target propagated

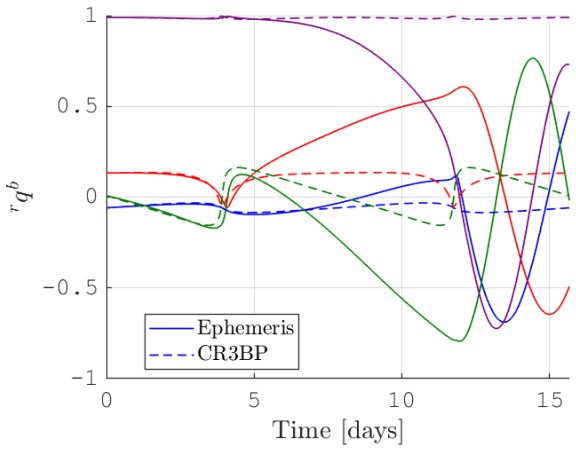

Figure 4.31: Attitude dyamics of 6DOF CR3BP NRHO propagated in ephemeris model over 2-orbital period

in the ephemeris model, while the dashed lines are associated to the quaternions profile of the nominal attitude on the reference NRHO in the CR3BP.
As well as for the orbital trajectory, the attitude remains quite close to the nominal one up to the first perilune passage. After that event, the spacecraft attitude begins to diverge from the periodic behaviour ending up to tumbling without apparent control. Being the periodicity behaviour of the attitude dynamics strictly related to the one of the orbital path, it is expected to have a visible improvement by employing a more refined solution identifying an actual nearly-periodic NRHO in ephemeris dynamics. It should be noticed that the attitude behaviour presents sudden variation every time the spacecraft passes the perilune. This response behaviour is an additional remark of the importance to provide an attitude stabilization action especially during the perilune passage.

4.6.2 Stable and Unstable Orbital Modes

Considering rendezvous and docking applications, the stable and unstable manifolds represent reliable and robust natural reference corridors for a chaser spacecraft (for example cargo and crewed vehicles, station modules, or lunar service modules, etc.), which can be exploited in approaching operations to a target (namely the LOPG) or departing procedures (from the gateway after undocking, or from a formation). Obtain preliminary insights about the natural dynamics

behaviours of these corridors in an higher-fidelity model is crucial to direct future analysis.
The apolune region has been already highlighted as favourable dynamical region for proximity, rendezvous and docking operations, and it has been chosen as initial condition for simulations in the ephemeris model in this investigation.
The procedure to obtain the initial orbit-attitude states representing the target spacecraft on the reference staging orbit has been already explained in its dedicated section. The initial state of the chaser spacecraft has been obtained following the same concept idea. Starting from the idealized orbit-attitude simplified-coupled CR3BP, the nominal initial condition of the chaser is numerically approximated through the mode corresponding to the desired manifold. Then, the absolute state of the chaser is transitioned to the ephemeris model as for the target according to the selected epoch for the simulation, and the relative states of the chaser respect to the target are derived directly in the inertial J2000 reference $\{\hat{I}\}$-frame for both orbit and attitude components.
The absolute target orbit has been chosen as the orbit-attitude trajectory obtained from the simple transition to the ephemeris model of the nominal states belonging to the apolune of the reference NRHO in the CR3BP considering the 18th November 2023 as initial reference epoch. Its absolute orbital and attitude motion are shown in figures 4.30 and 4.31. The chaser spacecraft has been chosen to be placed along the desired orbital mode at an initial distance proportional to 200 meters considering the standard characteristic length of the Earth-Moon system. Once the initial conditions of target and chaser are determined, they are propagated in the natural orbit-attitude dynamics of the ephemeris model in order to obtain the trajectory and attitude evolution of the spacecrafts.
The motion of the spacecrafts has been propagated for two orbital period. Then, the results coming from the higher-fidelity model can be compared to those coming from the idealized orbit-attitude CR3BP. However, only the results regarding the orbital dynamics are taken in consideration for the comparison. In fact, the attitude evolution of the target seen from a rotating observer quickly diverges immediately after the first half orbital period, and the relative attitude dynamics should be no more considered near the periodic equilibrium condition.
The first mode investigated belongs to the unstable manifold. Figure 4.32 shows the evolution

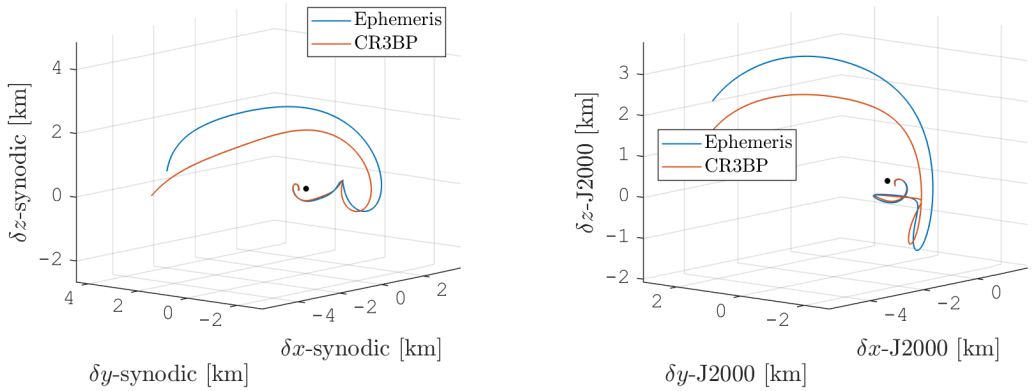

(a) Rotating point of view (b) Inertial point of view

Figure 4.32: Unstable mode of reference staging NRHO propagated in the higher-fidelity ephemeris model over 2-orbital period. Relative orbital motion of the chaser in rotating and inertial J2000 point of view.

of the relative orbital motion of the chaser spacecraft respect to the target propagated in the ephemeris model as a blue line, while the relative motion of the corresponding mode in the ideal CR3BP is drawn as a red line.
Even if the absolute motion in the ephemeris model is considerably affected by the perturbations

due to the variable orbit of the Moon and to the gravitational presence of the Sun, the relative motion of the chaser obtained in the ephemeris dynamical model seems to evolve resembling quite accurately the unstable mode behaviour observed in the ideal CR3BP model.
The same procedure has been applied by placing the chaser spacecraft on the stable manifold. In

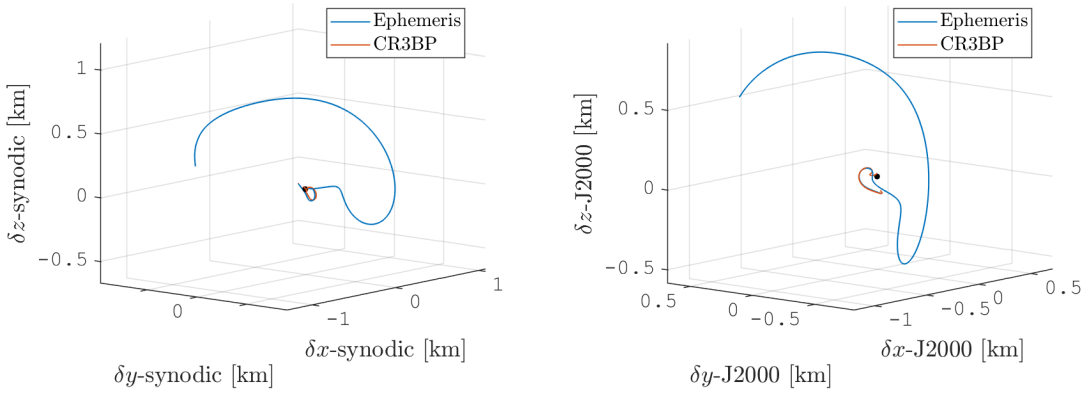

(a) Rotating point of view (b) Inertial point of view

Figure 4.33: Stable mode of reference staging NRHO propagated in the higher-fidelity ephemeris model over 2-orbital period. Relative orbital motion of the chaser in rotating and inertial J2000 point of view.

this case the relative motion of the chaser propagated in the ephemeris model begins its evolution following the stable mode behaviour observed in the ideal CR3BP. However, when the spacecraft reach the perilune region, the relative motion seems to transit towards the unstable manifold. This hints that the motion of the stable mode is highly sensible to any kind of perturbations introduced by the forces of the higher-fidelity ephemeris model. The cumulative effect of these perturbations excite the unstable mode of the relative motion, which eventually becomes more relevant than the stable mode component that asymptotically approaches the target. This result can be easily observed in the final part of the relative motion of the chaser spacecraft shown in figure 4.33, which is resembling quite accurately the relative motion behaviour of the chaser placed on the unstable mode reported in figure 4.32.
A refinement of the initial condition of the target in order to obtain an actual "narrow" nearly-periodic ephemeris NRHO is expected to extend the period of similarity respect the orbital modes resulted in the CR3BP idealization.

4.7 Final Remarks

In this chapter, a modal analysis has been developed in order to characterize the relative orbital and attitude motion of a chaser spacecraft in proximity of a target spacecraft placed on periodic non-Keplerian orbit belonging to different families existing near the saddle points in the coupled orbit-attitude CR3BP. However, the same conceptual analysis can be extended to any kind of non-linear system having periodic solutions. It allows to identify the characteristic modes which govern the relative dynamics in proximity of the periodic equilibrium solution in a non-linear dynamical problem.
In particular, this analysis has been considering nowadays large spacecraft structures orbiting about natural orbit-attitude periodic Halo orbits and NRHOs near the EML1 Libration Point of the Earth-Moon system. It should be highlighted that this modal analysis is valid only in proximity of the periodic orbit, where the modes maintain their dynamical structure. For example, this limit for the orbital modes of Halo orbits is reached at a distance in the order of 10^4 km, while for the

NRHOs the orbital modes degenerates at a distance in the order of 10^3 km.

The numerical results show that the cross-coupling effect due to the attitude motion on the orbital dynamics expressed through the variation of the net gravitational force exerted by the main attractors on the spacecrafts has negligible effects on the dynamical structure of the eigenmodes. As direct consequence, the relative dynamics is characterized by de-coupled orbital and attitude modes. This approximation has been investigated for the particular case of interest considering hypothetical large modules which may be used to assembly the Lunar Orbital Platform-Gateway as spacecrafts. It should be highlighted that the same approximation is expected to be valid for any case where the dimensions of the spacecrafts are infinitesimal respect the dimension of the system. However, this approximation may loose accuracy if this condition is no more satisfied. Two direction can lead to this violation: considering futuristic extremely large space structures or considering smaller binary systems, such as it could happen for space mission scenario towards asteroids. Therefore, the orbit-attitude dynamics is expected to be fully-coupled over a certain transition boundary which could be identified by the ratio between the dimensions of the system and of the spacecraft.

The eigenvalues of the monodromy matrix can be used to evaluate the stability properties of orbital and attitude modes, while its spectral decomposition allows to find the eigenmodes which are employed to approximate the unstable, stable, periodic and center manifolds. Each mode is constituted by the combination of an exponential and a periodic components which are linked to the corresponding eigenvalues and to the orbital period of the reference solution.

The orbital modes correspond to the classical manifolds of the CR3BP already well-known in literature. They have been reinterpreted from the relative motion point of view and explored in the 6DOF domain. Considering the non-dimensional problem, the orbital modes presents a comparable orbital and attitude relative motion. However, once the dimension are reintroduced in the problem, the orbital modes have in practice null relative attitude respect their reference target on the periodic orbit, resulting in a synchronized orbit-attitude motion.

The perilune has been identified as a catalyst of the approaching/departing behaviour of the stable/unstable modes. This is particularly evident for stable and unstable orbital modes of high Halo orbits and NRHOs, where a closer perilune passage correspond to approaching and departing behaviours resembling a step function. Analogously, the stable and unstable attitude modes of these orbits present a steep variation in the attitude motion at each perilune passage. Therefore, the perilune region is characterized by a faster and very sensible orbital and attitude dynamics.

A departing procedure, for example from a space station or from a formation, may exploit the unstable manifold corridor to increase naturally and safely the distance of the spacecraft from its initial condition, employing a small "departure tuning" operation just before the perilune region. The stable orbital modes may represent slowly phased approaching routes to the target, while the chaser keeps the attitude naturally synchronised. The analysis of the higher-fidelity ephemeris model shows that gentle orbital corrections are required to maintain the stable behaviour, otherwise it naturally shift to the unstable behaviour. This could be seen as unfavourable point, but it could be also considered as part of the passive safety requirements in the design of rendezvous procedures. The stable manifold could be exploited from the chaser to reach the proximity operation field (from 100 km to 10 km or lower), allowing a smooth transition from absolute to relative navigation.

The periodic and center modes identify bounded motions about the nominal reference orbit. Particular combination of those modes could result in interesting periodic or quasi-periodic relative motions for formation flying applications (also for multiple spacecraft formations) [41].

These relative orbits may be exploited from the chaser as checkpoints during the approaching phase to the target. They would be safe in case of any anomalies (such as misfiring due to engine failure)

and at the same time it will offer a subsequent opportunity to perform a maneuver to continue the approach or to abort the mission. Once the chaser reaches short distances (for example under 1 km), the holding point could be designed to be placed on the unstable manifold in order to privilege the safety requirements of the mission. In fact, the chaser will naturally drift away if no further actions takes place to end the approach.
The apolune region is characterized by a quieter orbital and attitude dynamics. It may represent a preferable location from the point of view of the Guidance, Navigation and Control (GNC) subsystem to perform complex proximity operations, such as rendezvous and docking.
The perilune region has been already recognized as favourable point to schedule periodic orbital corrections for station-keeping operations of high Halo orbits and NRHO [23]. Moreover, the highly sensible attitude dynamics characterizing the perilune region of these orbits suggests to provide an attitude stabilization action at least during the perilune passage, while it could be not required in the rest of the orbit.

It should be remembered that this analysis has considered the target and the chaser as symmetric spacecraft having equal inertial ratio. Considering the same family of orbit-attitude periodic solutions, a spacecraft with different inertia ratio and orbiting about the same reference orbit will have a similar but still slightly different periodic attitude behaviour. Note that this is true only if the cross-coupling effect of the attitude on the orbital dynamics is negligible.
Therefore, a new target/chaser couple constituted by identical spacecrafts but varying their inertia ratio is expected to have the same orbital modes that will be synchronized respect the new periodic attitude behaviour. The attitude modes are expected to show similar behaviours. However, if the family of orbit-attitude periodic solution has encountered a bifurcation in the attitude modes while changing the inertia ratio parameter, the phase space of the attitude modes will be characterized by a different eigenstructure.
If the chaser will have an inertia ratio different from the target, the orbital modes are expected to remain unchanged in their orbital motion. However, the attitude motion of the spacecrafts is expected to be no more synchronized, but instead it will show some kind of bounded oscillations.

Chapter 5

CHASER NATURAL DRIFT FROM OFFSET POSITION

The rendezvous and docking procedures may be designed as the succession of multiple approaching steps among a desired number of checkpoints. As shown in chapter 4, the center and the unstable orbital manifolds may be exploited in the design of these holding points.
However, simple offset position from the target may be selected as holding point during proximity operations in the design of the docking mission. Their location may be driven from practical purposes, such as the requirement to keep an open communication link with the ground station on Earth during the final steps of the docking phase. Moreover, they have to account for operational constraints, such as power and thermal control requirements on the attitude of the spacecrafts or constraints about the Sun illumination of the target when the docking phase takes place.

Chapter 4 shows that the cross-coupling term due to the attitude motion on the orbital dynamics is in practice negligible for application interesting nowadays spacecrafts in proximity of a non-Keplerian orbit in cislunar space. Moreover, it can be assumed that the attitude control system installed on the spacecrafts will be able to deal with the external torques of this environment (mainly the gravity gradient torque due to the Moon and the SRP torque) to handle the attitude motion according to mission requirements. Therefore, the only relative orbital dynamics will be focus of particular attention.

In this chapter, the relative dynamics of a chaser having an initial offset position is investigated within the CR3BP in order to have further insights about the natural drift behaviours in proximity of its target placed on Halo orbits and NRHOs, due to their applicative relevance. The informations acquired will be used in the design of final rendezvous approach for the translation along the docking port axis. The safety requirements will be considered as the main concern in this phase of the mission. The worst case scenario to avoid would be an impact between the chaser (namely a crewed or a cargo vehicle) and the target (namely the cislunar gateway) after a successful insertion onto the offset position holding point for proximity operation (HP-prox) due to the natural drift of the chaser in non-nominal condition (e.g. misfiring due to an engine failure).

5.1 Method and Algorithm

As before, the target is assumed to be placed on a nominal periodic non-Keplerian orbit in cislunar space. The relative dynamics of the chaser spacecraft will be analysed through the fully non-linear orbit-attitude coupled CR3BP model.
It should be noticed that, even if the main goal of this investigation has its focus on the solely orbital dynamics, the model has been developed considering the coupled 6DOF relative dynamics.

This effort justifies the will of developing an instrument which would allow a more comprehensive understanding of the coupled orbit-attitude relative dynamics. In this way, the analysis will be generalized and it would be relatively easy to cover other operational applications (e.g., considering the CR3BP model idealizing other binary system such as Sun-Earth or Mars-Fobos system, or asteroid environment where the relevance of natural relative attitude drift would be expected to be relevant).

The periodic LPO of the target is discretized in N points, which are identified by the orbital mean anomaly $\theta_N = t_N/T_{orb}$. Next, at each point the initial state of the chaser spacecraft is obtained by adding an offset position to the nominal state of the target. In order to study the behaviours of the chaser while in proximity of the target on LPO in cislunar space, the initial offset distance has been selected to range from few hundreds of meters up to few tens of kilometers. For the close-field holding point a representative value for the initial distance has been chosen equal to 200 m ($\simeq 5.2 \times 10^{-7}$ in non-dimensional length), while for the far-field range the representative distance corresponds to 50 km ($\simeq 1.3 \times 10^{-4}$ non-dimensional length). It should be noticed that this values has been used as representative example. Therefore, they can be modified in order to accommodate other Rendezvous, Proximity Operation and Docking (RPOD) requirements in future analysis.
It should be remembered that, in the CR3BP formulation, the orbital state $\boldsymbol{x}_{\text{orb}} = [\boldsymbol{x}; \boldsymbol{v}]$ of both the chaser and the target have been expressed in the synodic $\{\hat{r}\}$-frame, while the attitude states $\boldsymbol{x}_{\text{att}} = \left[{}^{i}\boldsymbol{q}^{b}; {}^{i}\boldsymbol{\omega}^{b}\right]$ are relative the inertial $\{\hat{i}\}$-frame. In this investigation, the initial offset position of the chaser is obtained adding an initial relative position in the desired direction respect the orbital states of the target. The relative velocity between the chaser and the target has been chosen null from the rotating point of view. It should be noticed that, from an inertial point of view, the initial velocity of the two spacecraft will be different due to the rotation of the $\{\hat{r}\}$-frame.

$$\boldsymbol{v_i} = \left(\frac{d\boldsymbol{x}}{dt}\right)_i = \left(\frac{d\boldsymbol{x}}{dt}\right)_r + \boldsymbol{\Omega} \times \boldsymbol{x} = \boldsymbol{v_r} + \boldsymbol{\Omega} \times \boldsymbol{x} \tag{5.1}$$

The relation between the inertial velocity $\boldsymbol{v_i}$ and the rotating velocity $\boldsymbol{v_r}$ shows that the relative velocity between the chaser and the target will be small in the case of proximity operation near a LPO in the Earth-Moon system.
The initial attitude states of the chaser has been chosen equal to the nominal condition of the target on the periodic orbit-attitude LPO. In the particular case of spacecrafts with similar inertia distribution (equal, or quasi, inertia ratios of the bodies), the attitude motion of the chaser will result synchronized to the nominal one while the relative orbital motion remains in proximity of the target. This behaviour is expected to be true for all the families of periodic orbit-attitude motions when the system present a negligible cross-coupling effect of the attitude motion on the orbital dynamics, such as in the Earth-Moon system.
Future analysis could be directed in the study of the orbit-attitude drift considering spacecraft with different inertia distribution or belonging to different families of periodic attitude motion on the same LPO.

Once the initial condition of chaser and target spacecraft are defined, the natural dynamical flow described by the non-linear orbit-attitude CR3BP model can be propagated for the desired period of time. Then, the relative motion between the chaser and the target is obtained from the absolute motion of the two spacecrafts.

The relative orbital motion of spacecraft in formation flying and proximity operation are typically represented in a particular orbital frame: the Local Vertical Local Horizontal (LVLH) frame. An equivalent definition of the LVLH frame has been defined in the Moon-Centred Rotating (MCR)

frame and it will be exploited to represent the evolution of the natural drift of the chaser from the target on Halo orbits and NRHO. The definition of LVLH frame in MCR version may be representative for families of LPO in the CR3BP which resemble orbits around the Moon, such as high Halo orbits and DROs.

In this investigation, plus and minus directions of the axis constituting the LVLH frame in the MCR version are selected as particular initial offset position directions for the natural drift of the chaser spacecraft. The obtained results may also be considered as the natural relative orbital evolution of a probe after being realised from its mothership at a given distant along particular direction.

5.2 Natural Drift on Halo Orbits

A representative HALO orbit has been selected among the members of the EML1 orbit-attitude family of Halo orbits corrected in the chapter 3. Its orbit is identified by a vertical amplitude $A_z \simeq 68.8 \times 10^3$ km (or $\simeq 0.1790$ non-dimensional length) and an orbital period $T \simeq 10.8$ days ($\simeq 2.5010$ in non-dimensional time). Figure 5.1 shows how the LVLH frame, defined in the MCR

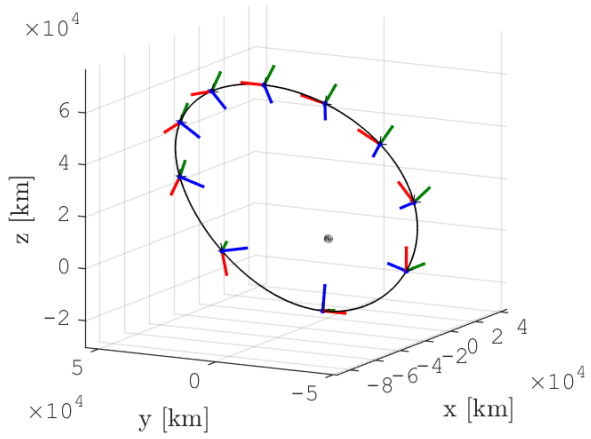

Figure 5.1: Reference EML1 Halo orbit represented in the Moon-Centred Rotating frame

version, is oriented in different locations of the reference Halo orbit. In this representation the radial direction (R-bar) is associated to the blue versor, the in-track direction (V-bar) corresponds to the red versor, while the green versor is the cross-track direction (H-bar).

The chaser spacecraft is placed at 200 m from the target along the different axis direction of the LVLH frame. From the rotating frame point of view, the chaser initially holds a null relative velocity respect to the target. Next, the natural drift has been propagated over two orbital periods, lasting about 21 days. The mean anomaly θ_0 identifies the location of the spacecrafts along the Halo orbit at the beginning of the free drift propagation. Figure 5.2 shows the relative trajectories of the chaser in the LVLH frame of the target. The blue lines are associated to the free drift starting from an initial offset position of the chaser along the plus and minus R-bar. The drift starting from an initial offset along the plus and minus V-bar are reported as red lines. The green lines represent the drift starting from an initial offset along the plus and minus H-bar.
As expected, the relative motion of the chaser always ends up being dominated by the characteristic spiralling-conical behaviour associated to the unstable orbital mode. The maximum departing behaviour is observed near the perilune, due to the higher sensibility of the dynamics in this region. For Halo orbits, the initial offset position along the R-bar axis results as the most unstable initial condition. Instead, an initial offset position of the chaser along the V-bar and the H-bar

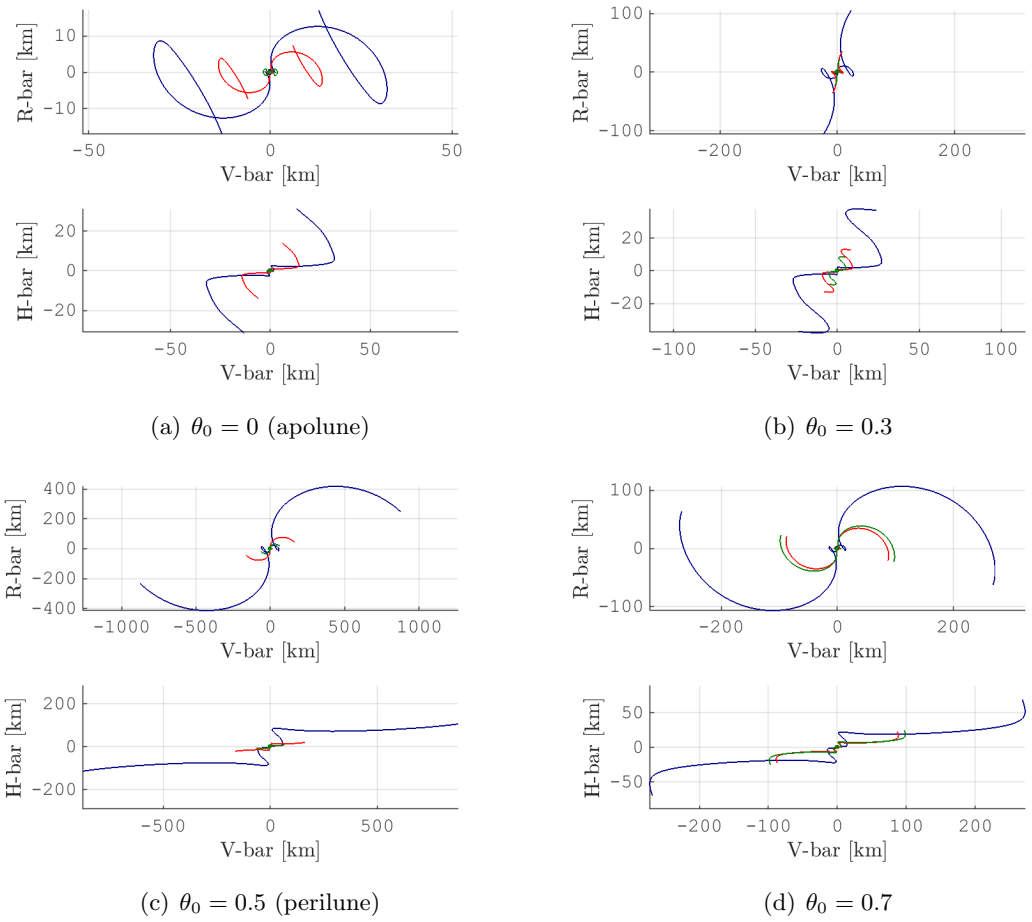

(a) $\theta_0 = 0$ (apolune)

(b) $\theta_0 = 0.3$

(c) $\theta_0 = 0.5$ (perilune)

(d) $\theta_0 = 0.7$

Figure 5.2: Natural drift of the chaser from initial offset position along LVLH frame axis and propagated over 2-orbital period: blue line from R-bar, red line from V-bar, green line from H-bar.

seems to have a weaker departing behaviour. In fact, a small initial offset along the V-bar put the chaser on an orbit almost equal to the nominal and in a position just forward or backward the target. While, the H-bar for Halo orbits is almost the direction of the family continuation. Therefore, the relative motion from these offset directions is expected to remain closer to the target in the initial part of the drift.

Figures 5.3 and 5.4 show a focus of the relative orbital trajectories of the chaser spacecraft in proximity of the target starting the free drift from different initial mean anomalies θ_0 along the reference orbit. In these figures, a Keep-Out Sphere (KOS) with radius 200 m (equal to the initial offset distance) has been highlighted in light blue.
A symmetric behaviour of the natural drift trajectory is evident in all the results considering the chaser starting from equal initial offset position distance along opposite directions.
The free drift of the chaser from an initial offset along the R-bar (blue line) starts almost immediately the spiralling-conical departing behaviour independently from the initial location of the spacecrafts along the orbit.
Also the natural drift starting from an offset along the V-bar (red line) and the H-bar (green line) show analogous departing behaviours when the initial location θ_0 of the spacecrafts is placed in the second half of the reference orbit (from perilune to apolune). Instead, when the initial location of the spacecrafts is in the first half of the orbit (from apolune to perilune), the chaser describe a slow hovering motion before the departing behaviour becomes dominant. It should be noticed that, the relative trajectory described by a chaser starting from the offset along the V-bar remains

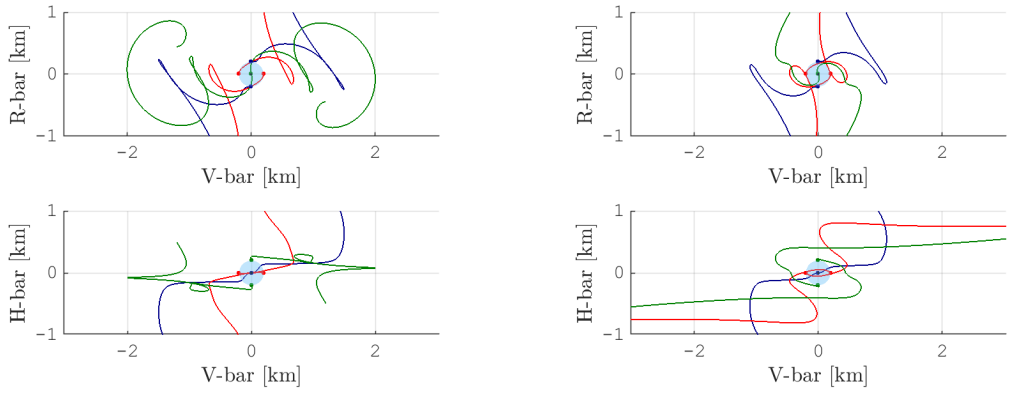

(a) $\theta_0 = 0$ (apolune)

(b) $\theta_0 = 0.1$

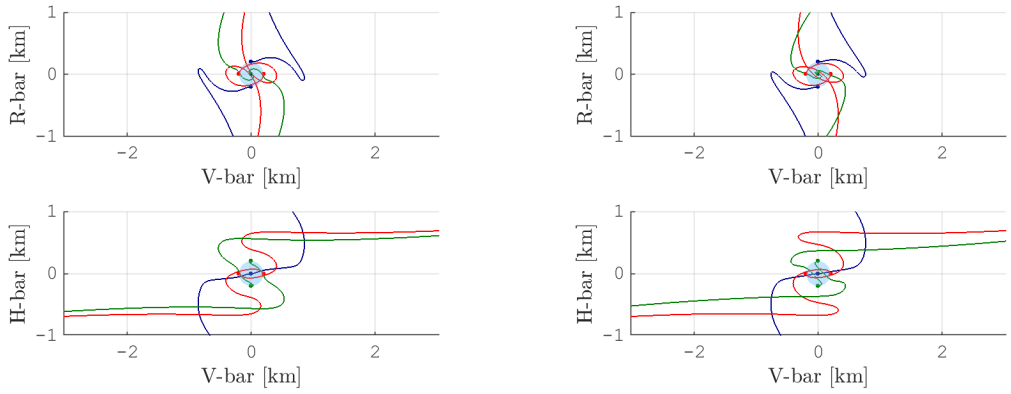

(c) $\theta_0 = 0.2$

(d) $\theta_0 = 0.3$

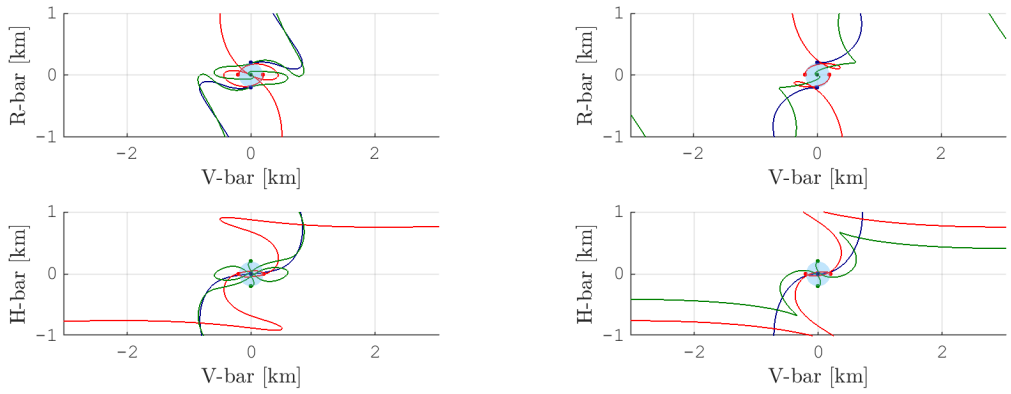

(e) $\theta_0 = 0.4$

(f) $\theta_0 = 0.5$ (perilune)

Figure 5.3: Natural drift of the chaser from initial offset position along LVLH frame axis: blue line from R-bar, red line from V-bar, green line from H-bar. Focus in proximity of the target. Initial location of the target in the first half of the Halo orbit

almost at the same distance during the initial part of its hovering behaviour. By the contrary, for a chaser starting from the H-bar, its free drift enters deeper the KOS as the initial location of the spacecraft θ_0 is approaching the perilune of the orbit.
Analogous natural drift behaviours has been obtained by varying the initial offset distance of the chaser from the target in a range going from 200 m up to 100 km.

From the results of this analysis, the region of the Halo orbit going from the apolune region up to the perilune has been classified as "quieter" region. While, the remaining part of the orbit has

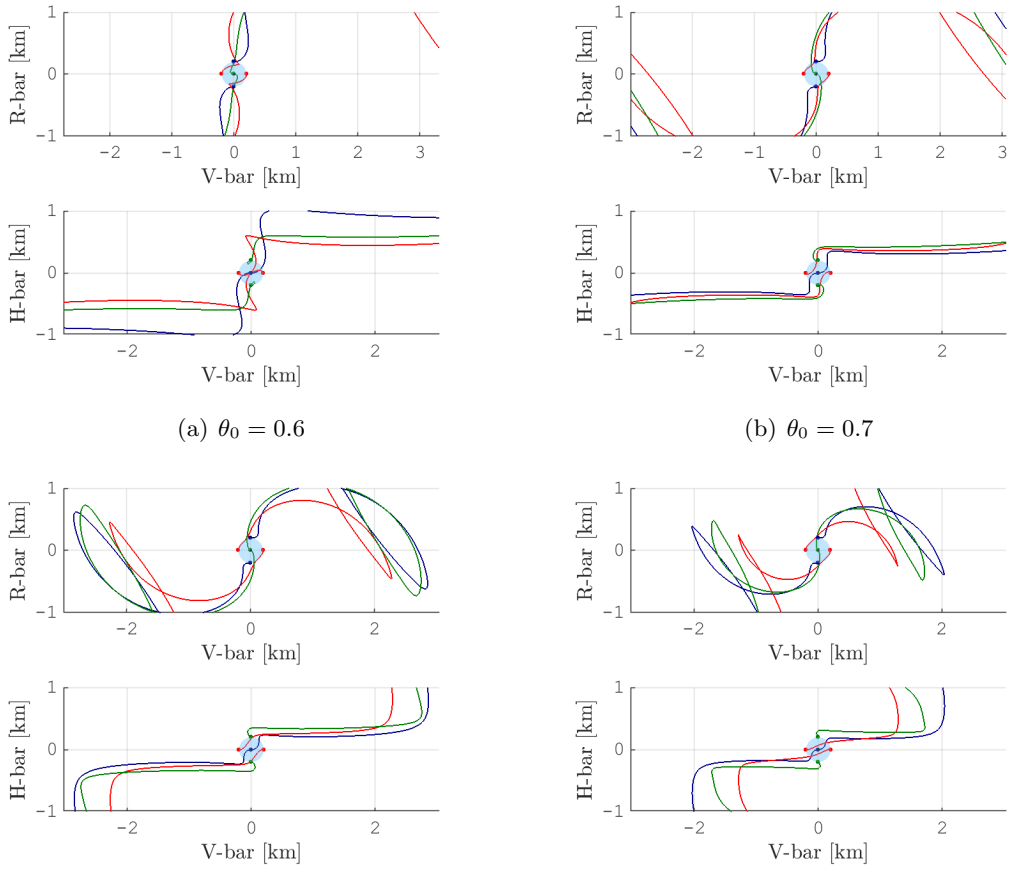

(a) $\theta_0 = 0.6$ (b) $\theta_0 = 0.7$

(c) $\theta_0 = 0.8$ (d) $\theta_0 = 0.9$

Figure 5.4: Natural drift of the chaser from initial offset position along LVLH frame axis: blue line from R-bar, red line from V-bar, green line from H-bar. Focus in proximity of the target. Initial location of the target in the second half of the Halo orbit

been denoted as "restless" region, where the unstable behaviour manifests its dominance from the beginning. This classification based on the behaviours of the natural drift may be justified looking at the features of the orbital modes of Halo orbits described in chapter 4. The unstable mode has a strong departing behaviour during the first half of the orbit and a stagnating behaviour during the second half of the orbit. Vice versa, the stable mode has its stagnating region during the first half of the orbit and an approaching behaviour during the second half of the orbit. The periodic modes have a dominant periodic behaviour which reach its maximum relative distance at perilune and its minimum at apolune, while the center modes are almost constant in amplitude. Therefore, during the first half period of the orbit, the unstable mode departing behaviour is balanced by the other modes. But, during the second half period of the orbit, the unstable mode moves along its stagnating region while the amplitude of the other modes drops. As a consequence, the unstable mode will more easily prevail on the other modes during the second half of the Halo orbit, the "restless" region prone to become unstable.

However, the "quieter" region, observed for this subset of relatively high Halo orbits, is expected to diminish its presence while the reference Halo orbit decreases its vertical amplitude A_z, up to it will eventually disappears. In fact, lower Halo orbits are characterized by a larger value of orbital stability index ν_{orb}, thus the stronger exponential departing behaviour of the unstable mode is expected to easily take over the other modes in a shorter time.

5.3 Natural Drift on NRHO

An analogous analysis has been performed for the family of orbit-attitude NRHO. An EML1 NRHO with a vertical amplitude $A_z \simeq 83.76 \times 10^3$ km ($\simeq 0.2179$ non-dimensional length) and an orbital period $T \simeq 7.84$ days ($\simeq 1.8049$ non-dimensional time) has been selected as reference orbit. This EML1 NRHO is the same orbit which has been exploited as nominal orbit from the CR3BP model for the comparison of the relative dynamics between the ideal CR3BP and the higher-fidelity ephemeris four-body model in section 4.6. Figure 5.5 shows the reference NRHO in the MCR frame. It also shows the orientation of the "rotating" LVLH frame at different equispaced locations θ_0 of the orbit.

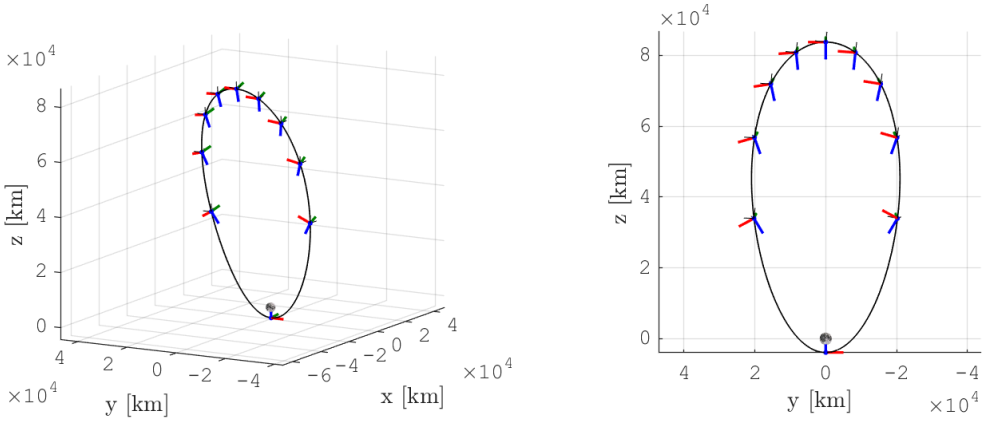

Figure 5.5: Reference staging orbit of the target in the Moon-Centred Rotating frame and LVLH frame at different point of the orbit. EML1 NRHO: $A_z \simeq 83.8 \times 10^3$ km ($\simeq 0.2179$ [ndim]) and $T \simeq 7.84$ days ($\simeq 1.8049$ [ndim])

A chaser is placed at 200 m from the target along each axis direction of the LVLH frame for the different initial position θ_0 along the orbit. At the beginning, the chaser has null relative rotating velocity and null relative attitude states respect to the target. Next, the natural dynamics of the two spacecrafts has been propagated.
Figures 5.6 reports the natural drift of the chaser over two orbital periods, lasting about 16 days, when the apolune is assumed as the initial location of the spacecrafts along the reference NRHO. The relative trajectories has been projected along the LVLH frame and different colours have been associated to different initial offset directions: the blue trajectories identify the free drift of a chaser with initial offset along the R-bar (radial direction to the Moon); the red lines refer to an initial offset position along the V-bar; the green lines are related to an initial offset position along the H-bar (the normal direction to the orbital plane).
As well as in the case of Halo orbits, the natural drift of a chaser starting its relative motion with an offset position along the same axis but from opposite directions presents a symmetric evolution in proximity of a target placed along an NRHO.

Figures 5.6 - 5.9 show the results obtained for the propagation of the natural drift for the spacecrafts starting at different location along the orbit, which are identified by the mean orbital anomaly θ_0 the target spacecraft has at the beginning of the natural drift.
In each figure, the time travel marks of the chaser have been highlighted along the relative trajectories as small diamonds to better understand the time evolution of the natural drift. The time of flight between two of them is equal to one tenth of the orbital period of the NRHO, which corresponds approximately to 19 hours. They allows to easily observe the effects related to the slow dynamics in the apolune region and to the faster dynamics in the perilune region. A denser area of travel marks is formed each orbital period. Only the travel mark corresponding to the

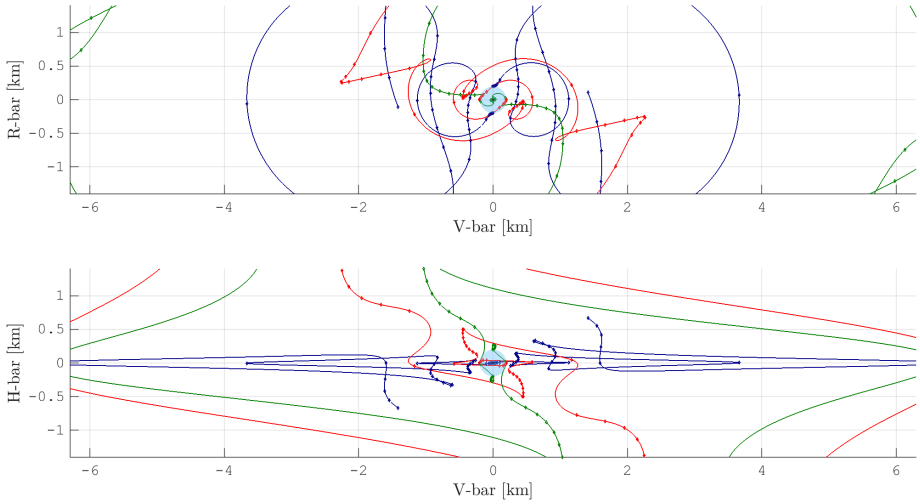

(a) $\theta_0 = 0$ (apolune)

Figure 5.6: Natural drift of the chaser from initial offset position along LVLH frame axis: blue line from R-bar, red line from V-bar, green line from H-bar. Focus in proximity of the target. Initial location of the target at $\theta_0 = 0$, apolune of the NRHO

perilune passage can be seen distinctly separated from the others along the relative trajectories.

When the chaser spacecraft begins the natural drift from an offset position along the R-bar, its relative motion develops almost on the "orbital plane" (RV-plane). It forms recurring arcs that slowly move away from the target increasing their amplitude. This motion resembles a some sort of combination between a slowly departing behaviour and the periodic mode directed along the orbital continuation of the family. However, the motion is expected be dominated from the unstable mode after this initial slowly departing behaviour. The perilune region may act as catalyst for the transition between these two phases.

Figure 5.10 shows the natural drift of a chaser starting from an initial 200 m offset along the R-bar and propagated over four orbital periods. The mean anomaly θ_0 represent the initial position of the target along the NRHO at the beginning of the natural drift. The initial relative motion is similar for any θ_0, and it resembles a combination between the periodic mode and a slowly departing behaviour. However, its amplitude sensibly increases when the initial offset condition is associated to an initial location of the spacecrafts near the perilune. This can be seen comparing the motions reported in figure 5.10. In fact, a perturbation will have an higher effect if it is applied at the closest point of the orbit from the primaries, where the gradient of the gravity force is higher. As a consequence, the transition from the initial motion to the unstable mode happens before, as can be observed in figure 5.10(c). It should be noticed that this effects is expected to be enhanced for NRHO having a closer passage to the secondary attractor (e.g. the Moon), and at the same time their perilune region will shrink.

The natural drift of a chaser starting from an offset along V-bar may present initially bounded relative motion if the initial location of the spacecraft lies on the first part of the orbit, corresponding to the "quieter region" already observed for Halo orbits. Figures 5.7(a), 5.7(b) and 5.8(a) show the strengthening of the influence due to periodic and center modes. However, if the initial perturbation is introduced at location closer to the perilune region, also the unstable mode claims its part. In figure 5.8(b) can be observed a transition behaviour of the relative dynamics towards the unstable mode. Starting condition located on the second half of the NRHO shows an initial hovering drift of the chaser almost along the KOS, before entering on the unstable mode

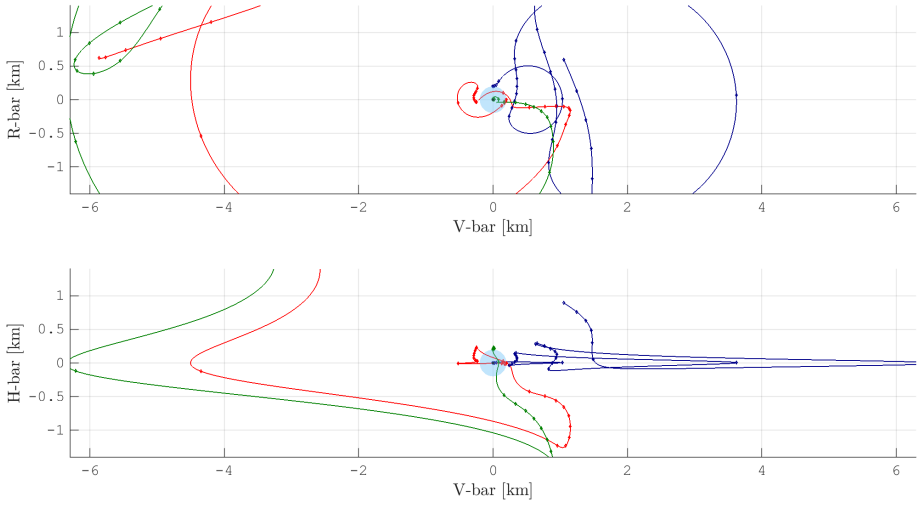

(a) $\theta_0 = 0.1$

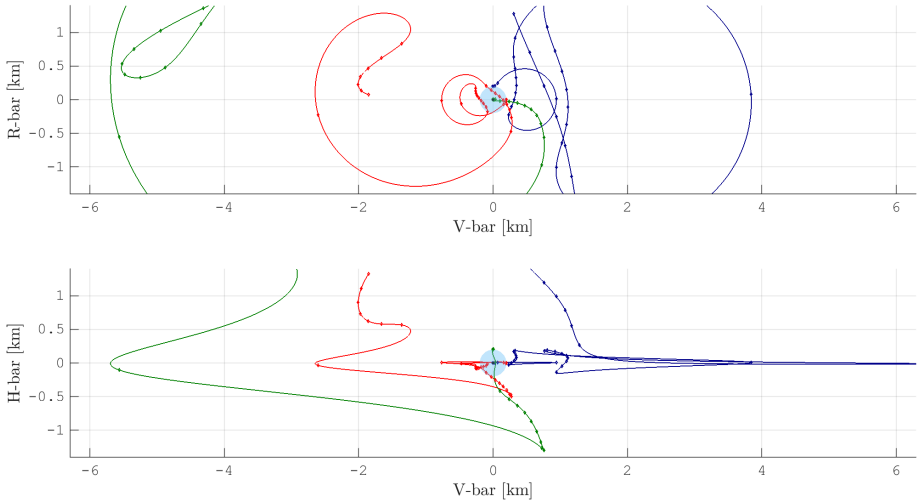

(b) $\theta_0 = 0.2$

Figure 5.7: Natural drift of the chaser from initial offset position along LVLH frame axis: blue line from R-bar, red line from V-bar, green line from H-bar. Focus in proximity of the target. Initial location of the target along the NRHO is identified by the orbital mean anomaly θ_0.

behaviour at the first perilune passage to move away from the target.

The natural drift of a chaser starting from an offset along H-bar seems to be the most unstable among the offset along the LVLH frame axis. In figure 5.8(a) can be noticed that the relative motion starting from an offset along H-bar (green line) tends to cross the KOS resulting in a fast and close passage to the target. This is probably related to the tendency of the system to recover the perturbed equilibrium condition of the chaser towards the target. But due to an oversized recovery action near the perilune, the quasi-equilibrium condition is lost and the free drift departs on the unstable mode.

If the initial offset along H-bar is associated to an initial location of the spacecrafts in the first half of the NRHO ($\theta_0 < 0.5$), the natural drift shows almost the same behaviour. At the beginning it remains almost still near the H-bar axis. Then, it start a fast crossing phase of the KOS during the perilune region in order to depart on the unstable mode afterwards.

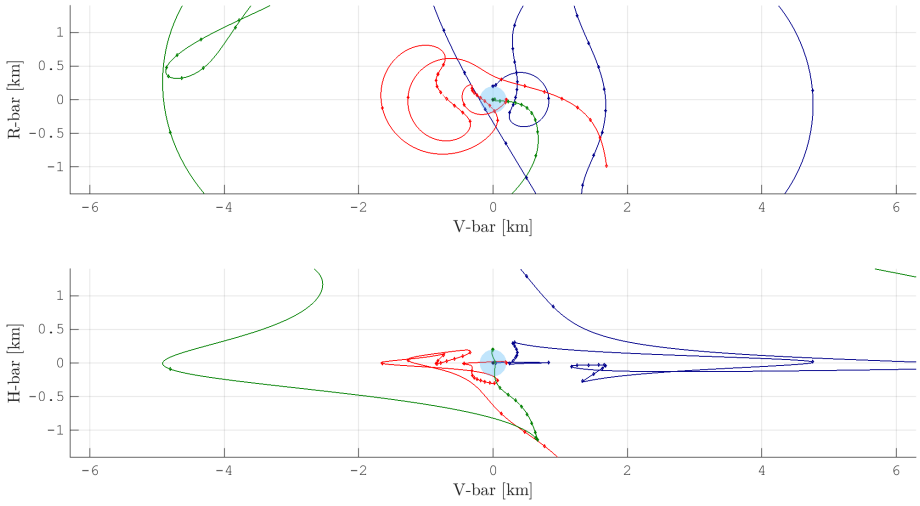

(a) $\theta_0 = 0.3$

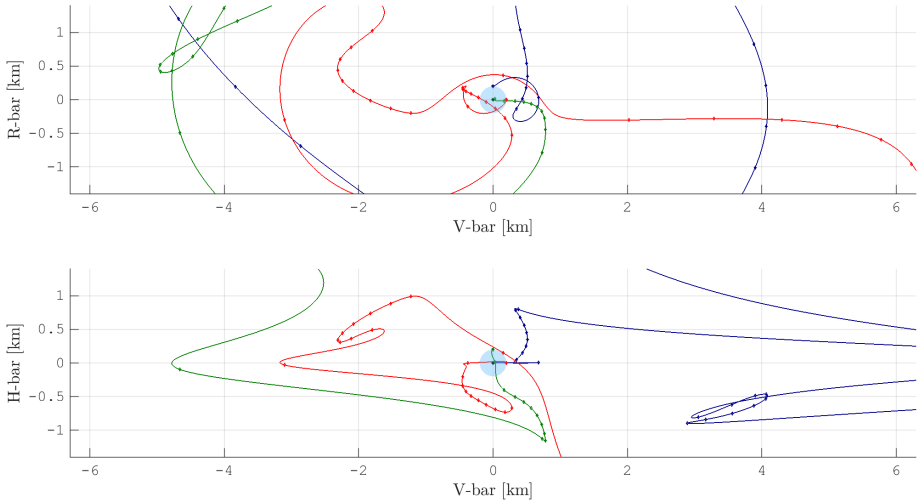

(b) $\theta_0 = 0.4$

Figure 5.8: Natural drift of the chaser from initial offset position along LVLH frame axis: blue line from R-bar, red line from V-bar, green line from H-bar. Focus in proximity of the target. Initial location of the target along the NRHO is identified by the orbital mean anomaly θ_0.

If the natural drift starts when the spacecrafts are located along the second half of the NRHO ($\theta_0 > 0.5$, after the perilune), the chaser initially tends to slowly move away from the target and gradually enter the unstable mode. The more time is available before reaching the perilune region, the more unstable mode has the possibility to avoid the crossing of the KOS.

Finally, it has to be highlighted how the relative trajectories rapidly drift away when the motion is initialized at the perilune condition, as can be seen in figure 5.9(a). In this case the natural motion starting from an H-bar offset crosses the KOS almost along a straight line through the center, which corresponds to the most dangerous condition to be avoided for safety concerns.

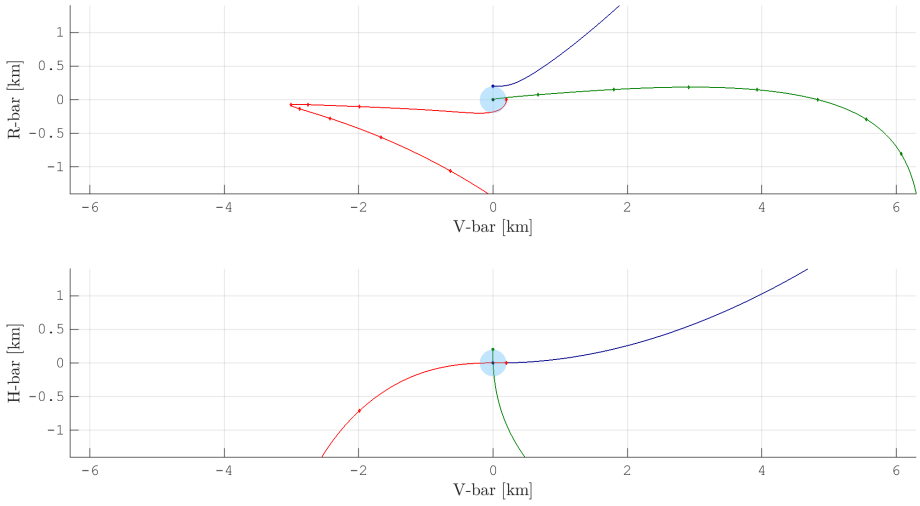

(a) $\theta_0 = 0.5$ (perilune)

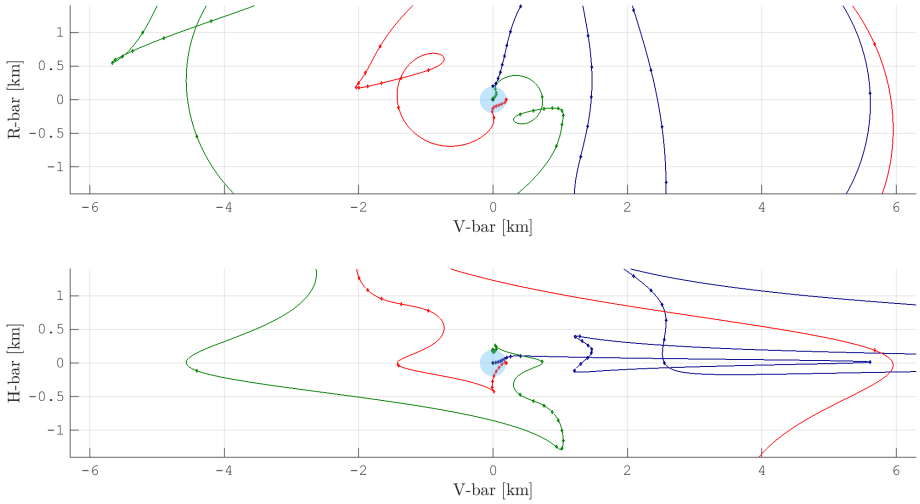

(b) $\theta_0 = 0.6$

Figure 5.9: Natural drift of the chaser from initial offset position along LVLH frame axis: blue line from R-bar, red line from V-bar, green line from H-bar. Focus in proximity of the target. Initial location of the target along the NRHO is identified by the orbital mean anomaly θ_0.

5.4 Final Remarks

In this chapter, a natural drift analysis has been proposed for two representative cases of high Halo orbits and NRHO. The direction of the initial offset position has been selected as the directions of the LVLH frame axis due to their relevance in proximity operation literature. The free drift has been explored also in relation to the different initial location θ_0 of the spacecrafts along the "absolute" orbit. This analysis aims to obtain useful information about possible approaching direction to perform the final phases of rendezvous and docking operations, in particular considering the passive safety concerns of this mission. The same information could be also interpreted from a station-keeping point of view. Safer or hazardous directions may be exploited to enlarge or shrink the ellipsoid of admissible tollerance around the nominal reference position. Furthermore, the free drift analysis gives information on how much time can pass before a corrective maneuver is required to avoid the spacecraft moves too far from its orbit.

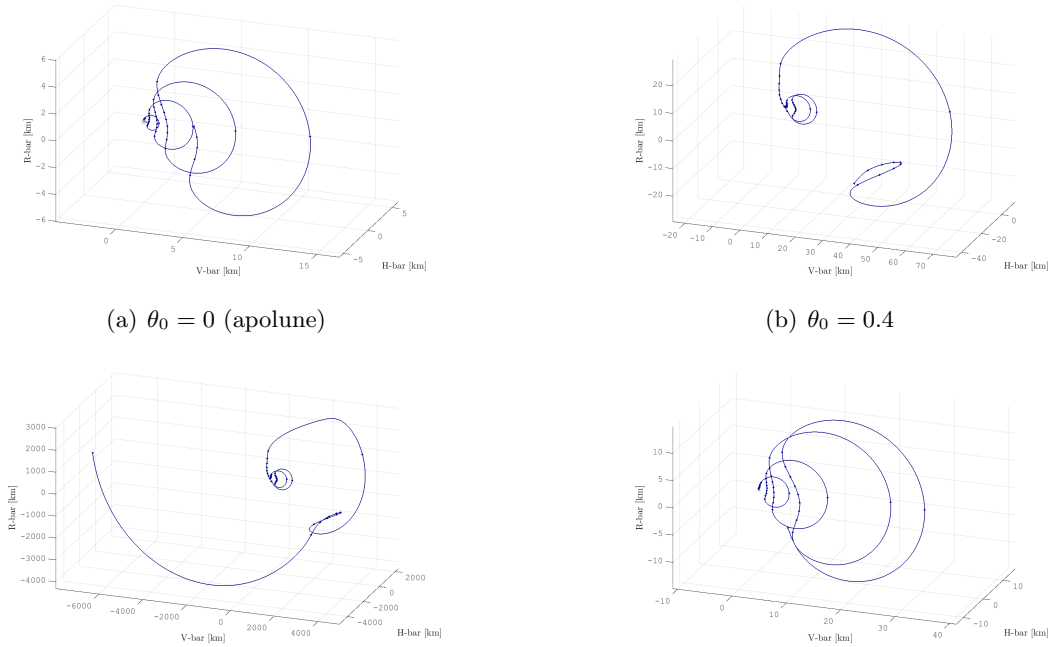

(a) $\theta_0 = 0$ (apolune)

(b) $\theta_0 = 0.4$

(c) $\theta_0 = 0.5$ (perilune)

(d) $\theta_0 = 0.6$

Figure 5.10: Natural drift of the chaser from initial offset position along R-bar and propagated over 4-orbital period. Relative motion propagation over four orbital periods starting from different initial location θ_0 of the spacecrafts along the reference NRHO.

For NRHO, an initial offset position along H-bar involves a higher risk of safety concern in case of non-nominal conditions.
An initial offset along V-bar presents always an initial hovering around the target keeping almost the same distance. Furthermore, if the natural drift is propagated from the initial "absolute" position along the first half of the orbit, the chaser shows a relatively bounded motion in proximity of the target for few orbital periods before departing on the unstable manifold.
Differently from the previous offset directions, an initial offset position along R-bar consistently generates a recurrent slowly departing natural drift behaviour for any initial "absolute" position of the spacecrafts along the whole orbit. Moreover, this relative motion lies almost on the "orbital plane" of the reference NRHO. These two features make this offset direction the most interesting for possible proximity operation applications (e.g. for docking procedures).

It should be noticed that, in any case, the dynamics remains relatively slow since the spacecrafts do not reach the perilune region of the "absolute" reference orbit. This means that if the docking maneuver takes place during the transit of the spacecraft at the apolune of the NRHO, there are about 2/3 days of "slow" relative dynamics available to overcome possible anomalies which may occur. Furthermore, if the anomaly can not be solved before reaching the perilune region of the NRHO, the selection of R-bar as holding point will grant the possibility to return in proximity of the target and recovery the proximity operations (e.g. approaching procedures for docking) after a wide and safe natural arc.

Chapter 6

CISLUNAR RENDEZVOUS AND DOCKING APPLICATION

Cislunar rendezvous and docking operations represents an important milestone for forthcoming space exploration programmes. The deployment of the future in-orbit lunar outpost will lean on several rendezvous and docking/berthing operations to assemble its modules in non-Keplerian cislunar environment, being NRHO the most attractive location for this kind of space infrastructure. This Gateway is central to support a variety of attractive future human and robotic exploration missions on and around the Moon, meanwhile advancing technologies, capabilities and protocols useful for the next journey to Mars and beyond. Several crew and cargo resupply vehicles are expected to visit periodically the space gateway travelling from and to the Earth, as well as a lunar service module would provide affordable transfer options to support lunar surface activities. Any visiting vehicle will have to perform rendezvous and docking/undocking operations in a reliable and autonomous (or quasi-autonomous) manner. Therefore, the 6DOF relative dynamics in non-Keplerian orbits is mandatory to support the cislunar orbital outpost design and implementation, addressing and evaluating practical GNC strategies to manage these complex and dangerous proximity operations.

In this chapter, direct methods will be exploited in order to find feasible 6DOF relative guidance functions to design and perform practical solutions for proximity operations of rendezvous and docking in cislunar non-Keplerian orbits for the lunar orbital gateway.
Although, any space mission is a complex system engineering problem dealing with all the requirements and constraints of each subsystem, the optimal rendezvous guidance problem has been defined within the optimal energy context to asses the feasibility of the rendezvous mission.
Finally, an example of practical rendezvous strategy in cislunar non-Keplerian orbit is presented on the bases of the outcomes of this investigation.

6.1 Rendezvous Guidance Problem Definition

A successful soft docking happens when the contact between chaser and target spacecrafts is characterized by small values of position error and relative velocity, as well as of relative attitude. Therefore, the final phase of rendezvous and docking has to be designed considering the whole 6DOF relative dynamics of the system. The level of accuracy required for practical application of rendezvous and docking in cislunar non-Keplerian orbit is not generally guaranteed by the approximation of the circular restricted three-body model. Therefore, the following design and implementation will be based on the higher-fidelity ephemeris restricted four-body model with perturbations.

According to the analysis in previous chapters, the apolune region of the NRHO has been identified as the most favourable orbit-attitude dynamical environment to perform complex proximity operations such as the approaching phases for docking to the lunar orbital gateway. Therefore, the whole rendezvous and docking phase has been addressed to take place within an arc of about ± 100 degrees in mean anomaly around the apolune of the NRHO.

This phase is expected to occur after a transfer/phasing trajectory, which is not discussed in this investigation. Its task consists into bring the chaser spacecraft in proximity of the target space gateway (~ 100 km) while it is transiting in the apolune region of the NRHO. The final point of the phasing phase will be assumed as the initial condition for the rendezvous and docking phase.

6.1.1 Cislunar Rendezvous Scenario

Space agencies and the International Space Community have evaluated the family of Earth-Moon NRHO as the most attractive location to deploy the LOPG. This analysis assumes the cislunar space station moving on an EML1 Northern NRHO with a vertical amplitude $A_z \simeq 83.8 \times 10^3$ km and a perilune distance $r_p \simeq 3900$ km, corresponding to an orbital period $T \simeq 7.8$ days. The features characterizing the relative orbital dynamical eigenstructure of NRHO remains similar for both L1 and L2 families, as well as for both Northern and Southern orbits. Therefore, the outcomes that will be discussed for the assumed representative orbit can be considered valid for any NRHO orbit.

Many requirements and mission constraints will compete together to drive not only the staging orbit selection but also the attitude configuration of the space station. Few example of these drivers would be the establishment of a communication link with the Earth and the lunar surface, power and thermal management, long-term orbit-attitude maintenance, rendezvous and logistic operations, scientific activities and observations. In this study, the station has been assumed to move with a naturally periodic orbit-attitude motion, which attitude presents a librating behaviour about the Earth-Moon rotating frame. It should be noticed that, if the attitude configuration of the target changes also the approaching procedures will be affected.

The apolune condition of the space station has been assumed as representative initial point for the design of rendezvous and docking (RV&D) sequence. The chaser is assumed to reach the proximity operation distance from the target during a phasing phase prior to the rendezvous. The chaser has to arrive approximately 100 km distance from the target when the lunar gateway is transiting along its second half of the NRHO and sufficiently before the apolune condition. In this way, the navigation system has the time to perform accurate orbital determination, data processing and initialize its sensors for relative navigation. These operations usually last no longer than 24h. Meanwhile, the operation control center and eventually the crew will be busy with list checks and making sure system are performing nominally. Then, the docking mechanism is initialized in advance preparation for the RV&D sequence.
Next, a communication/telemetry link between the chaser spacecraft and the target space station can be established. Communication capabilities between the two vehicles may be required for operational and safety reasons, as well as for navigation functionalities. The proximity communication infrastructure is assumed to be analogous to the one already implemented for ISS proximity operations, e.g. via S-band antenna.
The end of the phasing phase is assumed to happen when the hand-over from absolute to relative navigation is successfully achieved.

As already highlighted in chapter 4, the natural dynamics of non-Keplerian cislunar orbits offers the stable orbital manifolds, which may represent a smart cost effective solution for the design of the phasing and far-approach rendezvous phases. However, the time required to complete the

approach phase will be one of the main concern knowing that natural dynamics of cislunar orbits are quite slow. For example, the characteristic time of the orbital manifolds for NRHOs is in the order of 8 days, which corresponds to their orbital period. An alternative sub-optimal time-saving solution may implement a guidance strategy based on targeting several holding point to reach the close-range rendezvous engagement distance.
The relative attitude of the chaser spacecraft should be not relevant at the stage of phasing phase design, and the requirement to have a controllable absolute attitude should be enough.

The navigation subsystem is assumed to provide the relative and absolute 6DOF states from the beginning of the proximity operations.
The absolute orbital measurements are assumed to be based on ground-tracking support, such as NASA's Deep Space Network (DSN). The absolute attitude will be available from star sensors on-board both the spacecraft and the LOPG. Optical rendezvous sensors (e.g. infra-red and visible cameras) in combination with range and range-rate data obtained from radio-based navigation system will be employed during the far-range rendezvouz phase (such as the radio telemetry system used by the Soyuz and Progress spacecrafts, which is called KURS). The lunar gateway is expected to be equipped with laser reflector, on its body and around the docking port, for a cooperative rendezvous. A modern LIght Detection And Ranging (LIDAR) technology will provide precise relative orbital and attitude information once the chaser spacecraft is within few kilometers from the station.
The establishment of a communication link between chaser and target vehicles will allow the exchange of navigation data. In fact, dedicated relative navigation equipment aboard the space gateway would be assumed for safety reason.

Finally, the actuation problem is not considered in this investigation. The output of the rendezvous optimization will be the ideal guidance control to perform the maneuver. However, the results will be discussed in the optics of actual on-board resource limitations and mission reliability to address also the selection of the actuation equipment.

6.1.2 Direct Transcription of the Cislunar Rendezvous Problem

In the assumed rendezvous scenario, the cislunar space station maintains its nominal orbit-attitude motion, while the chaser has to drive its absolute orbit-attitude dynamics through a control action $\boldsymbol{u}(t)$ in order to perform a soft docking. The control variable $\boldsymbol{u}$ represents the 6DOF control accelerations of the chaser spacecraft which enter directly in the relative dynamics of the chaser respect the target spacecraft in the 6DOF ephemeris four-body dynamical model.

$$\boldsymbol{u}(t) = \left[a_{Cx}; a_{Cy}; a_{Cz}; \alpha_{C1}; \alpha_{C2}; \alpha_{C3}\right] \tag{6.1}$$

The linear acceleration terms a_{Ci} are defined in the inertial J2000 frame, while the rotational accelerations α_{Ci} are defined in the chaser body-fixed frame.

The aim of the guidance system is to find some sort of optimal control profile $\boldsymbol{u}(t)$ to perform the docking to the space station: given the 6DOF relative dynamical system, the optimal guidance is obtained through a constrained optimization of the performance index J.

$$J = \varphi(\boldsymbol{x}_f, t_f) + \int_{t_0}^{t_f} \mathcal{L}\left(\boldsymbol{x}(t), \boldsymbol{u}(t), t\right) dt \tag{6.2}$$

Where $\varphi(\boldsymbol{x}_f, t_f)$ is denoted as Mayer term, while $\mathcal{L}(\boldsymbol{x}(t), \boldsymbol{u}(t), t)$ represents the Lagrange term.
This analysis starts investigating the optimal rendezvous problem under the optimal energy control point of view. Of course, alternative optimality criterions (such as sub-optimal robust solutions)

can be addressed for future rendezvous analysis.
Furthermore, additional operational and functional requirements or constraints for a space mission can force the guidance design out of the classical concepts of Optimal Control Problem (OCP).

In this analysis, direct methods will be used to solve the OCP. They are based on reducing the OCP to a Non-Linear Programming (NLP) problem, by parametrizing the control variable and by transcribing the dynamical system into a finite set of equality constraints. Direct methods often requires a large computational effort, but they are solved using well-established optimization methods, which ensure good robustness, and can easily accommodate path constraints.

It has been decided the 6DOF rendezvous trajectory would be not discretized in multiple arches connected by patch points. Therefore, the control parametrization will have to offer a greater flexibility than a simple linear function, while maintaining a reduced complexity to limit the dimension of the NLP.
The optimization has been decided to be performed over fixed-time rendezvous TOF t_f. As a consequence, only the control parameters are constituting the vector of unknown variable $\boldsymbol{p}$, which will be the solution of the NLP.
The rendezvous TOF t_f was considered within the free variables of the NLP at the beginning of the analysis but, in general, the optimization algorithm results in solutions which keeps t_f almost unchanged from the initial guess for the TOF. The reason of this behaviour may be due to the fact that changing the TOF creates a large variation of the performance function J and the optimization algorithm avoid to follow that direction to continue the minimization.
Future works can be addressed to analyse the rendezvous problem employing the opposite conceptual idea, namely discretizing the rendezvous path in multiple arches and using constant or linear functions to parametrize the control action on each arc.

Different parametrization options have been inspected, but the best convergence behaviour has been obtained by using polynomials and Fourier series.
In particular, a second degree polynomial parametrization seems to be enough robust for the translational control $\boldsymbol{a_C}$. A more complex parametrization (i.e. Fourier series) results in much longer computational time and contemporaneously a worsening for convergence properties.

$$\boldsymbol{a_C} = \boldsymbol{a_0} + \boldsymbol{a_1}\left(\frac{t}{t_{ref}}\right) + \boldsymbol{a_2}\left(\frac{t}{t_{ref}}\right)^2 \tag{6.3}$$

The rotational dynamics is expected to be more sensitive. Thus more flexible parametrizations have been adopted for the rotational control $\boldsymbol{\alpha_C}$, such as a third degrees polynomial or a fourth order Fourier series.

$$\boldsymbol{\alpha_C} = \boldsymbol{\alpha_0} + \boldsymbol{\alpha_1}\left(\frac{t}{t_{ref}}\right) + \boldsymbol{\alpha_2}\left(\frac{t}{t_{ref}}\right)^2 + \boldsymbol{\alpha_3}\left(\frac{t}{t_{ref}}\right)^3 \tag{6.4}$$

$$\boldsymbol{\alpha_C} = \boldsymbol{\alpha_0} + \sum_{k=1}^{4}\left[\boldsymbol{\alpha_k}\cos\left(k\boldsymbol{\tau}\frac{t}{t_{ref}}\right) + \boldsymbol{\beta_k}\sin\left(k\boldsymbol{\tau}\frac{t}{t_{ref}}\right)\right] \tag{6.5}$$

The parameters $\boldsymbol{a_i}$, $\boldsymbol{\alpha_i}$, $\boldsymbol{\beta_i}$, $\boldsymbol{\tau}$ are 3×1, which physical dimensions are determined by the physical quantity they are parametrizing, while the reference time t_{ref} is required to non-dimensionalize the time t.
The parametrization employed in the rendezvous NLP will be referred in this work as "a c b d". The letters "a" and "b" code the type of parametrization of the translational and rotational control action, while the numbers "c" and "d" correspond to the order of each control. For example, a

guidance parametrization "p2f4" is coding a second order polynomial function for the translational control and a fourth order Fourier series for the rotational control.

The constraints of the rendezvous NLP are obtained after the numerical integration of the controlled rendezvous dynamics. In fact, knowing the initial condition of the rendezvous and the control vector $\boldsymbol{p}$, the evolution of relative dynamics of the chaser is defined.

$$\boldsymbol{X}(t) = \boldsymbol{f}(\boldsymbol{X_0}, \boldsymbol{p}, t) \tag{6.6}$$

The initial condition of the cislunar rendezvous problem are defined by the absolute orbit-attitude states of the target orbital gateway $\boldsymbol{X_T}(t_0)$ and by the relative orbit-attitude states of the chaser spacecraft $\boldsymbol{X_0} = \boldsymbol{X}(t_0)$.
The final relative orbit-attitude state $\boldsymbol{X}(t_f)$ at the end of the controlled rendezvous simulation has to satisfy a set of desired boundary condition. Null relative position and velocities as well as attitude states correspond to the most simplistic docking condition which ca be analysed.

$$\begin{cases} \boldsymbol{x}(t_f) &= [0;0;0] \\ \dot{\boldsymbol{x}}(t_f) &= [0;0;0] \\ \boldsymbol{q}(t_f) &= [0;0;0;\pm 1] \\ \boldsymbol{\omega}(t_f) &= [0;0;0] \end{cases} \tag{6.7}$$

It should be noticed that the so developed method can be applied, not only to rendezvous application scenarios, but also for several other proximity and formation flying applications (formation deployment/reconfiguration) only by changing the initial and final relative conditions of the chaser.

However, in practical rendezvous application scenarios, the position vector of the docking hatch will be likely displaced from the center of mass of the space station. It follows the docking boundary condition at time $t = t_f$ will be related to the 6DOF configuration of the space station driven by its absolute orbit-attitude dynamics. Considering an alternative rendezvous operational scenario, the final mating procedure to the space station may be accomplished via berthing, using a commanded robotic arm to grab the chaser vehicle once it arrives in a predetermined location and with a desired attitude in proximity of the orbital gateway.
The definition of an error state vector $[\delta\boldsymbol{x}; \delta\boldsymbol{v}; \delta\boldsymbol{q}; \delta\boldsymbol{\omega}]$ between the relative orbit-attitude state of the chaser from the target orbital gateway and a desired final relative condition $[\boldsymbol{x_d}; \boldsymbol{v_d}; \boldsymbol{q_d}; \boldsymbol{\omega_d}]$ allows to generalize the boundary conditions expressed in (6.7) to any rendezvous problem.

$$\delta\boldsymbol{x} = \boldsymbol{x}(t_f) - \boldsymbol{x_d} \tag{6.8}$$

$$\delta\boldsymbol{v} = \dot{\boldsymbol{x}}(t_f) - \boldsymbol{v_d} \tag{6.9}$$

$$\delta\boldsymbol{q} = \boldsymbol{q_d}^{-1} \odot \boldsymbol{q}(t_f) \tag{6.10}$$

$$\delta\boldsymbol{\omega} = \boldsymbol{\omega}(t_f) - \boldsymbol{\omega_d} \tag{6.11}$$

It should be noticed the attitude control design can be based on different definitions of the attitude quaternion error function, which are widely studied in attitude control literature [42]. During the analysis, faster convergence properties have been observed when the constraint on the final relative quaternion is not enforced in vectorial form as $\delta\boldsymbol{q}_{1:3} = \boldsymbol{0}$, but in a scalar form as $H(\delta q_4) = 0$.

$$1 - \delta q_4^2(t_f) = 0 \tag{6.12}$$

Once the quaternion error function is defined, a desired relative attitude precision can be obtained by tuning the corresponding constraint tollerance option of the NLP.

The boundaries of the rendezvous NLP are selected in order to limit the maximum magnitude of the control effort so that $\|\boldsymbol{u}(\boldsymbol{p},t)\| < u_{max}$ during the whole duration of the rendezvous phase. These boundaries represents the hardware limitation of the actuation equipments installed on the chaser spacecraft.

Finally, the performance index of the NLP for the optimal energy rendezvous (i.e. minimum quadratic control) is defined according to the Lagrange's OCP formulation.

$$J(\boldsymbol{p}) = \frac{1}{2}\int_{t_0}^{t_f} \boldsymbol{u}^T(\boldsymbol{p},t)\,\boldsymbol{u}(\boldsymbol{p},t)\,dt \tag{6.13}$$

The direct transcription of the 6DOF rendezvous guidance problem has been numerically implemented on MATLAB thanks to its embedded optimization tolls. The NLP is solved through a constrained minimization algorithm which exploits the Sequential Quadratic Programming (SQP) method.

6.2 Generic Analysis of Optimal Energy Rendezvous

A generic analysis has been carried out in order to assess the potential capabilities of the developed method. The target space gateway is assumed to be located in vicinity of the apolune of its NRHO following a natural orbit-attitude quais-periodic motion. Random initial relative orbit-attitude states of the chaser vehicle have been explored to cover several realistic operational rendezvous engagement initial condition. Null relative position and velocity, as well as null relative attitude and angular rates has been selected as final desired relative 6DOF state for the rendezvous mission, to obtain qualitative information and performance about the optimal energy 6DOF guidance.

An example of the results obtained by the direct transcription control of the 6DOF RV&D guidance NLP is shown in figure 6.1. The initial relative 6DOF states are random, but representative of a far-range rendezvous initiation. The control has been approximated according to the "p2p3" parametrization, which shows quite fast time of convergence. The relative translational dynamics is expressed in the inertial J2000 reference frame, while the rotational dynamics is expressed in the chaser body-fixed frame. The 6DOF guidance is reported in terms of control force and torque, assuming a chaser spacecraft with a mass $m_C \sim 10^3$ kg and with an inertia moment $\mathbb{I}_C \sim 10^4$ kgm^2. The optimal energy guidance results in large control action at the initial and final point. It progressively evolves from the departure acceleration to the final braking, exploiting at the most the inertial dynamics in the middle of the maneuver. In the presented case, the chaser closes an initial distance of about 70 km through a rendezvous lasting 6 hours long. The chaser starts with an injection velocity error of few centimeters per second and it reaches a maximum relative velocity about 5 meters per second at mid-way of the controlled trajectory. The chaser performs also a large-slew maneuver which smoothly synchronizes the attitude to the target, starting with quite high initial relative angular velocity.

It should be noticed that the guidance control force is almost linear, although it has been parametrized through a quadratic function. This is due to the fact that typical rendezvous TOF are quite shorter respect the characteristic period of the natural dynamics of the NRHO (and more in general of quasi-periodic non-Keplerian cislunar orbits) where target and chaser spacecraft are orbiting. The whole RV&D sequence should be completed within few hours or at maximum two days (in order to satisfy functional and operational requirements according to the protocols designed thanks to the ISS experience of last decades and also considering the time the chaser has already spent during the transfer and phasing phase). Instead, the orbital period of the NRHO

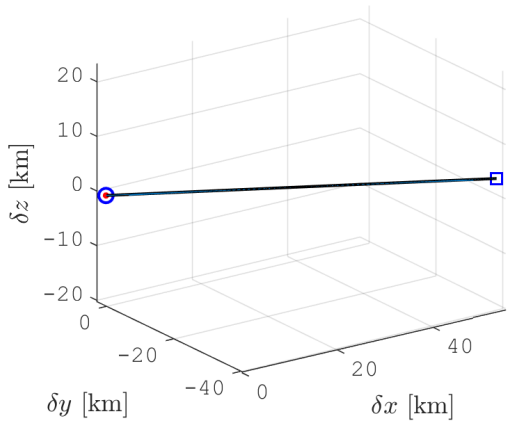

(a) Relative motion (t_0 blue square, t_f blue circle)

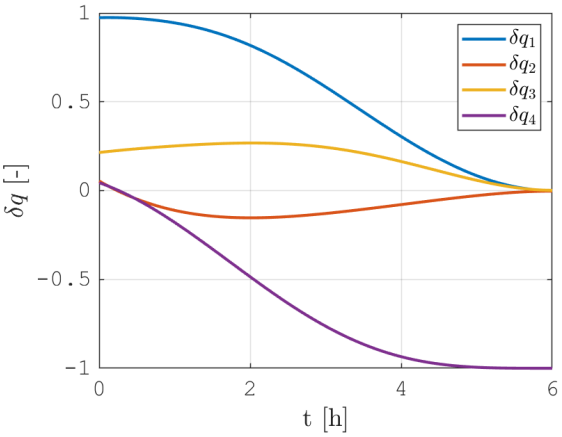

(b) Relative attitude quaternion

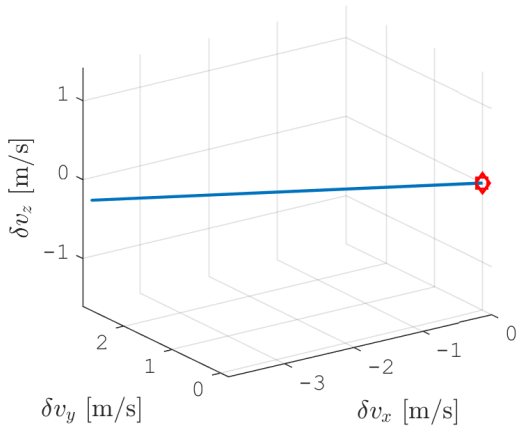

(c) Relative velocity (t_0 red square, t_f red diamond)

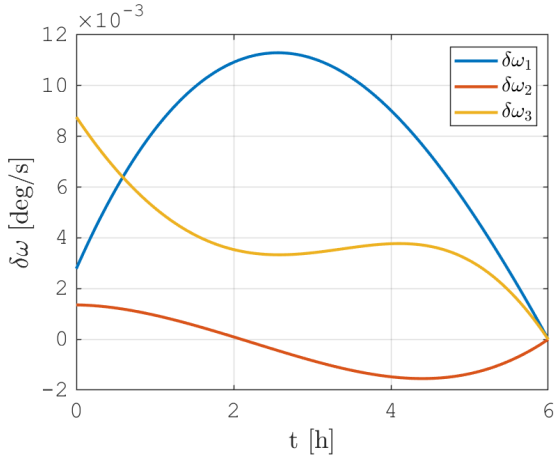

(d) Relative angular velocity

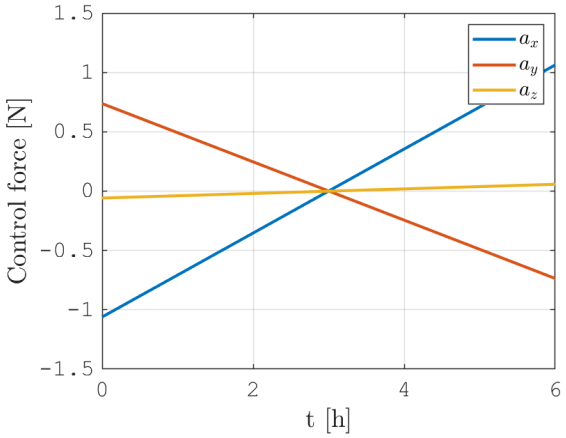

(e) GNC force. Chaser mass $m_C \sim 10^3$ kg

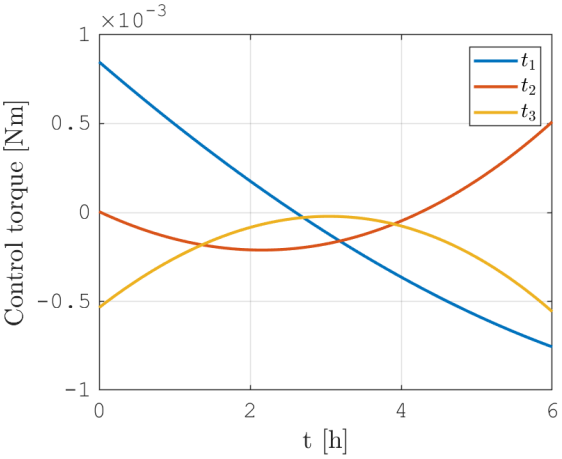

(f) GNC torque. Chaser inertia $\mathbb{I}_C \sim 10^4$ kgm^2

Figure 6.1: Direct transcription control of the 6DOF rendezvous guidance NLP. Rendezvous TOF $t_f = 6$ hours. Spacecraft inertia properties: $m_C \sim 10^3$ kg; $\mathbb{I}_C \sim 10^4$ kgm^2. Random initial relative states for far-range RV&D.

lasts about 7-8 days long. Therefore, the natural dynamics has not the time to affect significantly the optimal energy guidance control and, as a consequence, the controlled relative trajectory results in quasi-straight lines.

The guidance control torque is evidently using also the higher order terms of the control parametrization. This is probably related to the higher sensitivity introduced by the non-linearities describing

the relative rotational dynamics. In particular, when initial conditions request large slew-maneuver and/or they present high initial angular velocity in relation to the rendezvous TOF, the optimization algorithm has problems in solving the rendezvous due to the high gradients generated by the dynamics and it typically results in non-linear guidance functions.
Note that if the time to complete the rendezvous is longer, the optimal energy guidance will tend to use slower angular velocity profile to synchronize the initial attitude offset. When the initial relative angular velocity is smaller enough respect that rate, thus the control torque behaviour will be almost linear. Vice versa, if the initial angular velocity is comparable (such as in figure 6.1) or higher to that rate, the control torque will present relevant non-linear behaviours.

The same maneuver scenario has been solved for different reasonable time of rendezvous. The output control effort are reported in figure 6.2 in terms of ΔV and angular momentum effort ΔL. Typically, the optimal energy guidance results in lower control costs for longer rendezvous TOF.

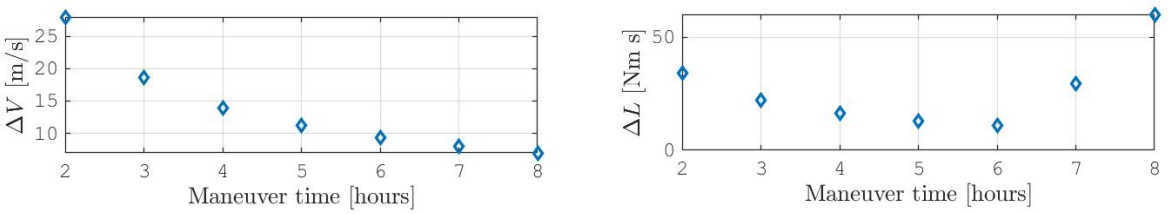

(a) Translational control effort

(b) Rotational control effort

Figure 6.2: Rendezvous control effort in relation to the maneuver TOF, t_f.

Having a lengthy time to complete the maneuver, the guidance is able to spread its control action more effectively. This allows to accelerate and to brake the motion more gently, exploiting at the best the relative inertial motion to minimize the cost (e.g. the fuel consumption).

The developed method shows high robustness and fast convergence time even for complex and quite long rendezvous scenario, especially in the case the guidance has to drive the only orbital dynamics. In particular, the guidance of the rotational dynamics struggles on convergence when the time to perform the rendezvous maneuver are too short or too long. Probably, the optimization algorithm has difficulties to find the guidance function to control the relative angular velocity. This could be related to high demand of control torque out of the guidance capabilities and/or to the high sensitivity of the gradients of the relative rotational dynamics.
For these limiting cases, the optimal energy guidance is more prone to reach the final relative attitude configuration through overshooting or additional rotations, which result in an increase of control costs. This behaviour can be seen in figure 6.2(b), where the angular momentum effort for the rendezvous increases for TOF longer than 6 hours. In these cases, the attitude starts to present an overshooting behaviour due to the high initial angular velocity which is slowly driven by a gentle control action. For example, the rotational motion and guidance of the rendezvous lasting 7 hours long is reported in figure 6.3.

An important outcome concerns the magnitude of the control action requested by the optimal energy rendezvous 6DOF guidance of a quite large chaser spacecraft ($m_C \sim 10^3$ kg), which is shown in figure 6.1. It suggests the equipment of a 6DOF control system independent from the main engines, requiring a sensible throttling capability. The selection of a fully decoupled 6DOF control actuation system will offer the possibility to follow desired relative trajectories and, contemporaneously, it will allow to keep the correct attitude pointing configuration, such as maintaining the target in Line-Of-Sight (LOS).

After the analysis of random initial conditions, also several particular cases has been investigated. The target initial absolute orbit-attitude states have been maintained at the apolune of the

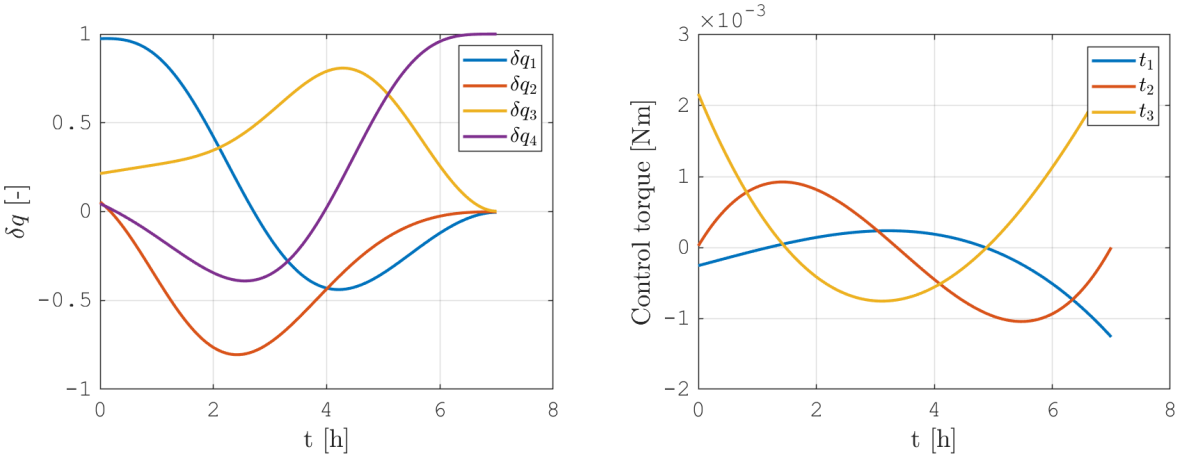

(a) Relative attitude quaternion

(b) GNC torque. Chaser inertia $\mathbb{I}_C \sim 10^4$ kgm^2

Figure 6.3: Direct transcription control of the 6DOF rendezvous guidance NLP: rotational dynamics. Rendezvous TOF $t_f = 7$ hours. Spacecraft inertia properties: $m_C \sim 10^3$ kg; $\mathbb{I}_C \sim 10^4$ kgm^2. Random initial relative states for far-range RV&D.

reference EML1 NRHO. The chaser spacecraft has been placed with an initial offset position along the axis of the "rotating" LVLH-frame (R-bar, V-bar, and H-bar), or along the stable and unstable orbital manifolds. The relative initial condition are obtained from the kinematics relations.

It should observed that, when an "express" rendezvous maneuver is accomplished, the guidance of the orbital dynamics tends to drive the relative motion of the chaser almost along straight lines. This behaviour seems to be independent from the initial offset position direction and from the attitude dynamics. The translational guidance cost depends on the initial distance of the chaser from the target (e.g. the LOPG), the initial relative velocity magnitude and direction of the chaser, and from the TOF requested to perform the rendezvous operations. This is due to the slow dynamics characterizing the apolune region of the cislunar non-Keplerian orbit, which does not enter significantly in the relative controlled dynamics.

6.3 Application Example

The general analysis has demonstrated that the developed 6DOF guidance method is capable to perform rendezvous operations with reasonable cost and time.
The controlled relative orbital motion results along almost-straight trajectories. The attitude guidance is able to perform even large slew-maneuver in order to synchronize the attitude of the chaser with the target one, while performing orbital guidance operations. These capabilities are fundamental for rendezvous and docking procedures.

For what concerning the magnitude of the control action required for the simulated rendezvous conditions, the actuation system of the chaser should be constituted by sensible maneuvering thrusters which will be disposed to allow a complete 6DOF guidance and they will be independent from the main thruster engines. A set of Reaction Wheels (RWs) will work in parallel to the maneuvering thrusters to control the attitude in nominal conditions. In addition to the RW cluster, the set of Control Momentum Gyros (CMGs) on-board the chaser could be included in the relative GNC operations if larger torques would be requested.

Before the rendezvous phase begins, a transfer and phasing phase has to be performed. Its task is to bring the chaser on the non-Keplerian orbit (e.g. the reference EML1 NRHO in this study) from the initial parking orbit. For example, the parking obit could be a Low Earth Orbit (LEO), a

Low Lunar Orbit (LLO), or a different non-Keplerian orbit. Moreover, the phasing phase has also the objective to synchronize the arrival chaser orbital motion with the target spacecraft reaching the proximity operation distance for rendezvous initiation.
A wide literature exists to cover this topic and different strategies have been proposed. Optimal energy solution include stable manifolds dynamics, allowing very low control cost to perform the transfer. However, they follow the slow dynamics of the non-Keplerian cislunar orbits and they will result in extremely long time of flight. This is particularly evident for the nearly-stable NRHOs. Severe operational requirements, namely on the execution time or on the robustness and sensitivity of the maneuvers, may lead the design of faster transfer/phasing solutions at the expense of a larger control cost.

6.3.1 Rendezvous and Docking Strategy

The phasing phase and the far-range rendezvous design has been not addressed in this investigation. However, the design of these phases can be based on a series of impulse maneuvers or on a continuous guidance control (e.g. employing an optimal energy 6DOF rendezvous guidance) in order to progressively approach the LOPG on the reference NRHO along several checkpoints.

The continuous relative 6DOF guidance presented in this chapter is employed to control the relative motion of the chaser spacecraft along the checkpoints of the close-range rendezvous. Note that, an analogous design can be carried on to develop the far-range rendezvous phase.

The proposed close-range RV&D sequence has been subdivided in two steps: the closing approach and the final approach stages. The former phase has the objective to align the chaser with the docking port of the orbital gateway, while the latter one will drive the chaser along an almost-straight line to complete the RV&D sequence via the final translation.

6.3.2 Closing Approach Stage

After the reception of a "go ahead" command from the Mission Control Center (MCC), the 6DOF guidance has the objective to move the chaser spacecraft to a new waiting point along the docking port axis of the orbital gateway and to align the attitude of the chaser spacecraft to point in the correct direction its docking mechanism and the close-range relative sensor, such as the LIDAR.

In this practical example of proximity rendezvous operation, the safety concern has been privileged during the selection of the checkpoint constituting the RV&D sequence.
The first waiting point (WP1) of the close-range phase is place on the unstable orbital manifold at 1 km distance from the target. The second checkpoint (WP2) has been placed 200 meters away the target and along its R-bar direction, the radial direction towards the Moon.
In this way, if any anomaly occurs, the chaser spacecraft will safely drift away from the target space station. At the same time, the slow departing behaviour shown from the natural dynamics of the unstable orbital manifold and of an offset initial position along the R-bar in the previous chapter will allow the retrieval of the RV&D sequence at the following apolune passage if the anomaly can't be recovered in time.

Figure 6.4 shows the translational and the rotational controlled dynamics of the Closing Approach Stage (CAS) obtained by the optimal energy 6DOF rendezvous guidance and for a maneuver TOF lasting 1 hour long. In figure 6.4(a), the waiting points WP1 and WP2 are respectively reported as a blue square and a blu circle. The target location corresponds to the red dot which is surrounded by a KOS sphere with a radius equal to 100 meters.

As expected, the controlled orbital dynamics moves the chaser along an almost-straight line and the translational control guidance is almost linear. In figure 6.4(a), the orbital guidance is

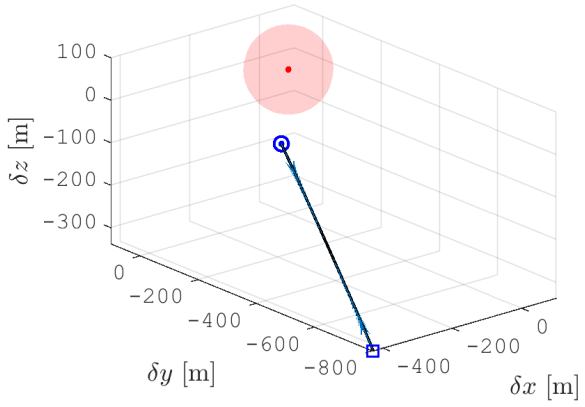

(a) Relative motion(t_0 = WP1 blue square, t_f = WP2 blue circle)

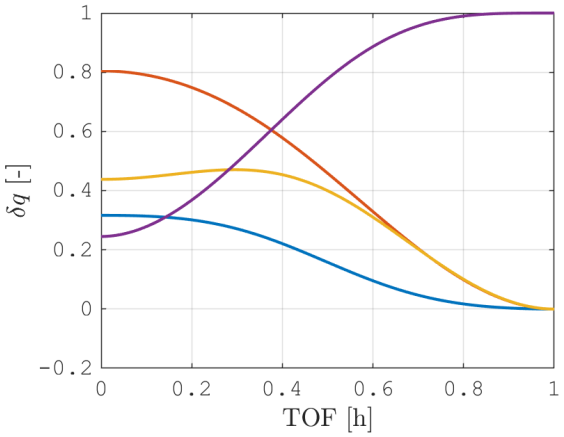

(b) Relative attitude quaternion

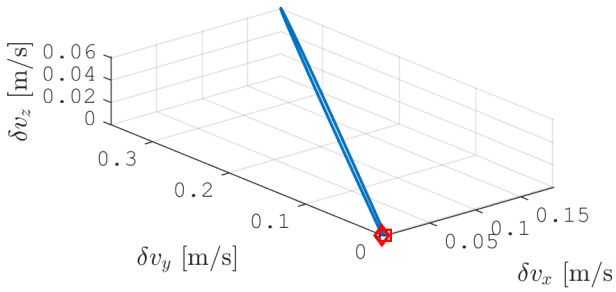

(c) Relative velocity (t_0 = WP1 red square, t_f = WP2 red diamond)

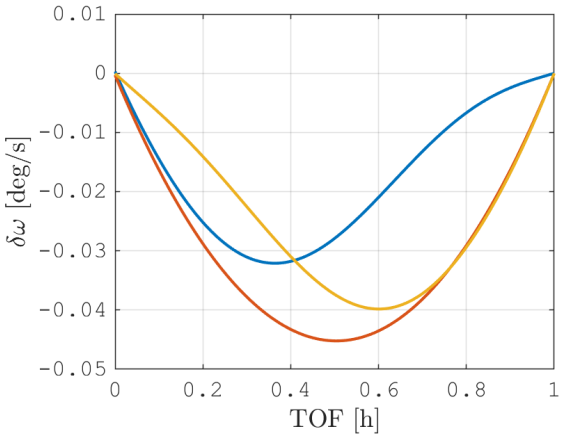

(d) Relative angular velocity

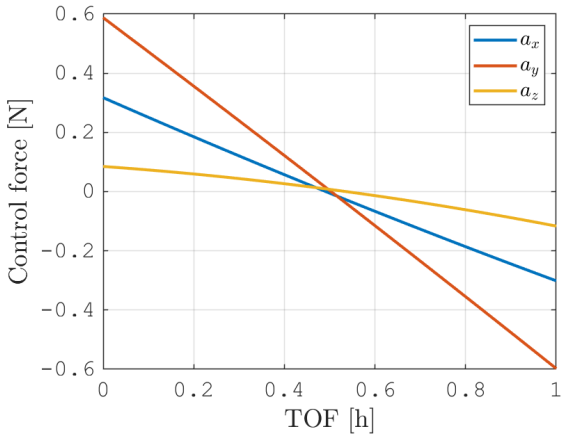

(e) GNC force. Chaser mass $m_C \sim 10^3$ kg

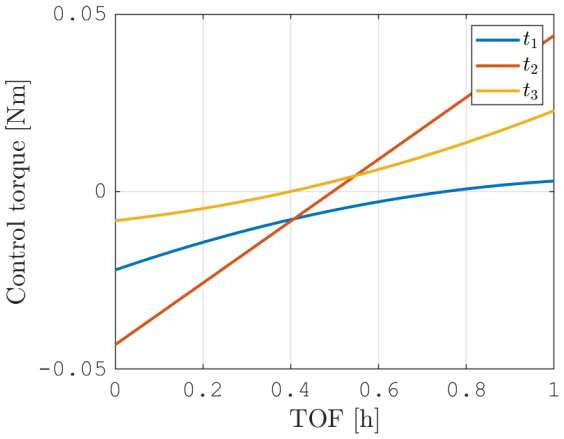

(f) GNC torque. Chaser inertia $\mathbb{I}_C \sim 10^4$ kgm^2

Figure 6.4: Closing approach phase: orbital and attitude dynamics of the optimal energy 6DOF guidance. Maneuver TOF $t_f = 1$ hour. Chaser spacecraft inertia properties: $m_C \sim 10^3$ kg; $\mathbb{I}_C \sim 10^4$ kgm^2. Random initial relative attitude states

represented via thin blue arrows representing the intensity and the direction of the control force profile during the maneuver. It is evident that the control action is constituted by a first accelerating stage which is followed by a braking stage.

A random initial attitude configuration has been assumed in this investigation. The successful synchronization demonstrates the capability of the 6DOF guidance to perform the desired maneuver. It should be noticed that in this case the optimal control results in an almost linear control torque which drive the attitude of the chaser smoothly to be synchronous to the one of the target. Therefore, the 6DOF guidance is capable to reach the docking port alignment and, contemporaneously, to point the docking port mechanism and the relative sensors in the correct direction to continue the proximity RV&D sequence.

6.3.3 Final Approach Stage

Once the chaser vehicle reaches the WP2, another "go ahead" command from the MCC is requested to continue the docking sequence with the Final Approach Stage (FAS).
After the docking alignment point WP2, the final translation is performed almost along the R-bar. At the same time, the attitude of the chaser has to be maintained synchronized with the one of the target space station to not break the correct pointing of the chaser docking mechanism to the target docking port. Note that the possibility of tracking continuously the target during docking procedures is allowed by the de-coupled 6DOF actuation control system of the chaser spacecraft.

The FAS is solved through the direct transcription of the optimal energy 6DOF guidance and a maneuver TOF equal to 1 hour. The results of the translational and rotational controlled motion are reported in figure 6.5.
Figure 6.5(a) shows the relative orbital motion driven by the nominal GNC. It is expressed in the "inertial" LVLH frame of the target spacecraft. The departure point at WP2 is represented by a blue square. the desired arrival condition corresponds to null relative position and velocity, as well as null relative attitude states.
Again, the arrival condition has been selected only as a representative case of a practical docking operation. In actual mission scenario, the docking port will be located in a particular position of the space station. It is likely to be not coincident to the center of mass of the target, and the actual final orbit-attitude condition for the docking will be related to the coupled 6DOF configuration of the target at the time of the docking.
Therefore, the results in figure 6.5 demonstrate the capability of the optimal energy 6DOF guidance to perform the final translation while keeping the pointing of the docking mechanism of the chaser in order to perform the soft docking at the apolune of the cislunar non-Keplerian orbit.

Note that additional checkpoints may be included in the final approach stage for safety reasons. For example, after the first waiting point of the proximity docking sequence for the alignment along the docking port axis at 200 meters, the chaser could have to move through a second alignment waiting point 20 meters away from the target.

6.3.4 Summary of Close-Range Rendezvous and Docking Sequence

The simple close-range RV&D sequence proposed in this analysis allows a safe soft docking of a controlled chaser spacecraft to an orbital gateway orbiting on a NRHO in cislunar space. The proximity operation has been executed at the apolune of the reference orbit.

The RV&D sequence is constituted by the Closing Approach and the Final Approach. Both the stages are lasting 1 hour long. The optimal energy 6DOF rendezvous guidance is employed to solve the RV&D problem.
Figure 6.6, shows the evolution of the relative distance and of the relative velocity of the chaser spacecraft respect the target space station during the two stages of the RV&D sequence. The closing maneuver and the final translation present very similar behaviours to obtain an optimal energy solution even if they start from quite different initial conditions.

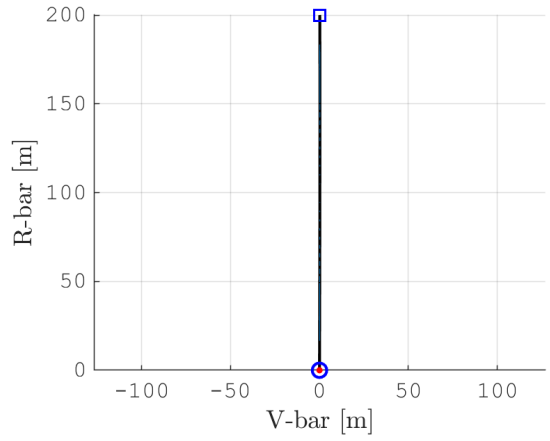

(a) Relative motion (t_0 = WP2 blue square, t_f = DOCK blue circle)

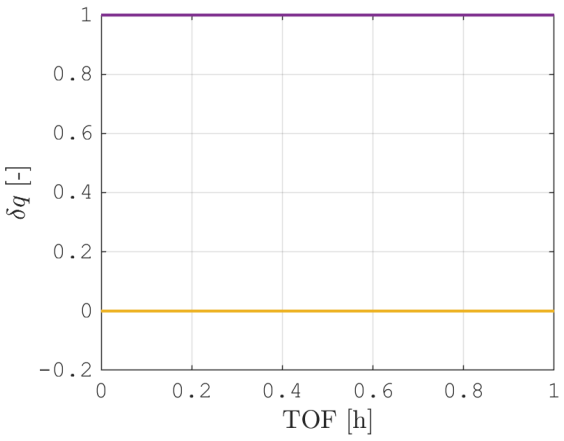

(b) Relative attitude quaternion

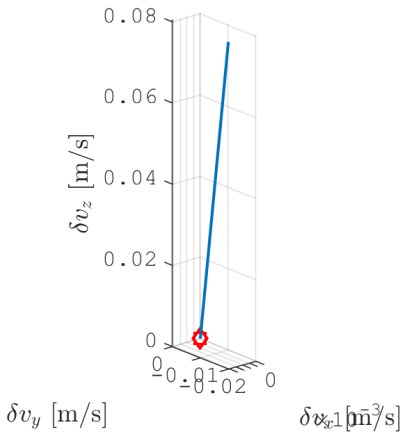

(c) Relative velocity (t_0 = WP2 red square, t_f = DOCK red diamond)

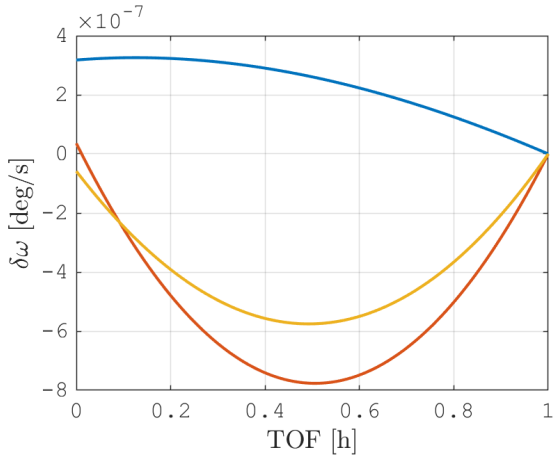

(d) Relative angular velocity

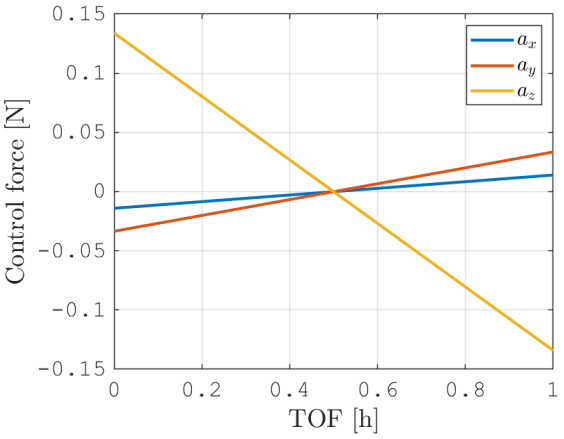

(e) GNC force. Chaser mass $m_C \sim 10^3$ kg

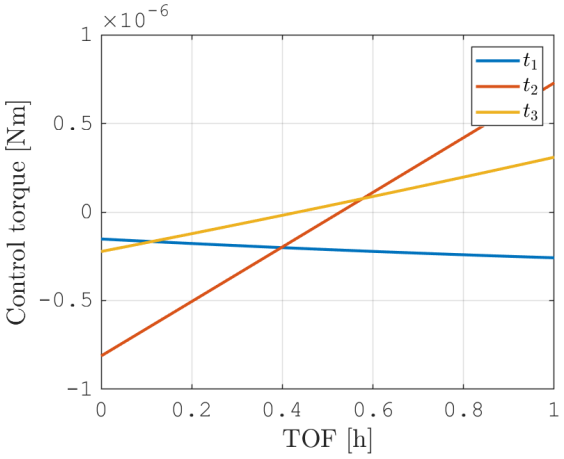

(f) GNC torque. Chaser inertia $\mathbb{I}_C \sim 10^4$ kgm^2

Figure 6.5: Final approach phase: orbital and attitude dynamics of the optimal energy 6DOF guidance. Maneuver TOF $t_f = 1$ hour. Chaser spacecraft inertia properties: $m_C \sim 10^3$ kg; $\mathbb{I}_C \sim 10^4$ kgm^2

The resulting cost to complete the closing maneuver and move the chaser from the WP1 to the WP2 has been estimated equal to $\Delta V = 0.81$ m/s. The final translation along the docking axis has an approximative cost of $\Delta V = 0.17$ m/s.

It should be highlighted that the TOF to complete the sub-phases of the RV&D sequence have

been selected in order to ensure the safety of proximity operation. In particular, the the maximum relative velocity allowed during the closing approach has been fixed at 0.5 m/s, while the maximum relative velocity during the final translation has to be lower than 0.1 m/s.

As final remark, the location of the checkpoint constituting the RV&D sequence in the proposed example have been arbitrary selected for the design of a reasonable application scenario. They may undergo any desired modification if requested from future mission design. However, the developed optimal energy 6DOF guidance could be used to solve the new RV&D sequence and similar solution behaviours are expected to be obtained.

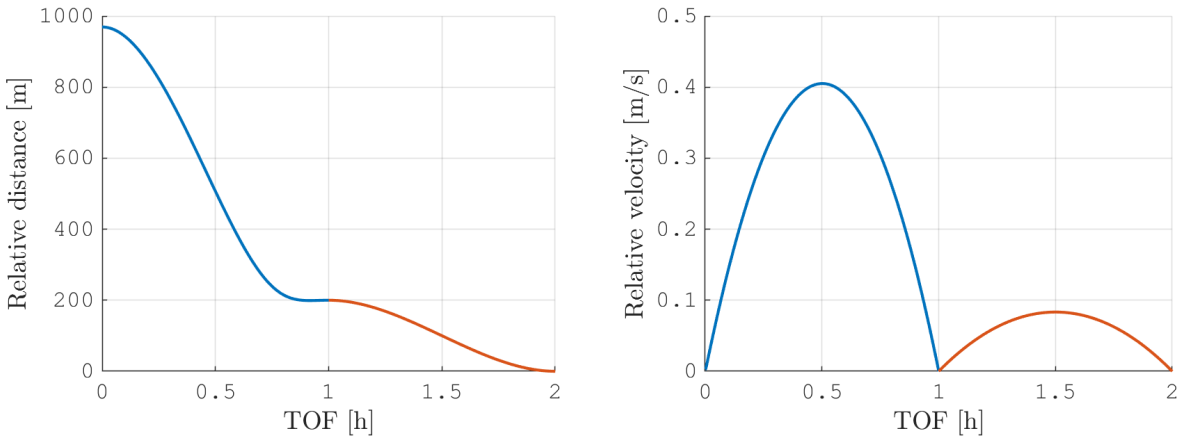

(a) Relative distance profile

(b) Relative velocity profile

Figure 6.6: Close-range rendezvous and docking sequence: relative distance and relative velocity time evolution. Closing Approach Stage in blue, Final Approach Stage in red.

Chapter 7

FINAL SUMMARY AND RECOMMENDATIONS

In the first part of this investigation, a novel perspective of the dynamical phase space structure constituting the orbit-attitude manifolds has been presented to describe the natural relative translational and rotational motion of a spacecraft in proximity of a non-Keplerian orbit, existing in the dynamical environment described by the Circular-Restricted Three-Body Problem (CR3BP). Particular attention has been dedicated to Halo orbits and Near-Rectilinear Halo Orbits (NRHO) of the Earth-Moon system in order to address favourable dynamics and challenging criticalities which would affect the design of the future cislunar space gateway.
Then, the optimal energy 6DOF guidance problem to perform cislunar rendezvous has been transcripted into a Non-Linear Programming (NLP) problem and it has been applied to a simple application scenario to demonstrate its potentiality.

In order to explore the translational and rotational motion of a rigid spacecraft moving in proximity of non-Keplerian orbits existing in the cislunar environment, orbit-attitude dynamical model have been developed. The orbital dynamics is based on the CR3BP formulation, while the rotational motion is represented through attitude quaternion and Euler equations of motion.
The simplest orbit-attitude model includes the solely gravity interactions between the spacecraft and the two primaries of the CR3BP system. This model portrays the one-way inertial coupling due to the orbital motion on the attitude dynamics through the gravity gradient torque. Then, the gravitational pull of the primaries is refined considering the variational force due to the spacecraft finite extension which introduces the two-way inertial coupling.
The gravitational presence of the Sun and the Solar Radiation Pressure (SRP) has been modelled in order to develop a higher-fidelity ephemeris four-body dynamical model to support high-level stages of the cislunar rendezvous design.

7.1 Motion in Proximity of Orbit-Attitude Periodic Solutions

The 6DOF dynamical structures of the orbit-attitude manifolds are explored in proximity of periodic orbit-attitude solution discovered in the Simplified Coupled Model thanks to the application of the Floquet's theory.

Particular attention has been dedicated to the natural dynamics in order to assess the impact of the two-way inertial coupling between the orbital and attitude motion for both the absolute and the relative dynamics. The limit of the assumptions in the Simplified Coupled Model are discussed and the validity of the one-way inertial coupling has been demonstrated to describe the motion of nowadays and near future space infrastructure in cislunar space and environment of similar

systems.

The apolune of NRHO has been identified as favourable region in both orbital and attitude dynamics to perform complex proximity operation, such as rendezvous and docking (RV&D), being characterized by a quiet and slow natural dynamics. Moreover, the apolune region lasts for a large portion of the orbital period of NRHO (at least half orbital period can be considered apolune region). This offers a wide operational window to perform all the proximity operation and, contemporaneously, contingency time is reserved in a favourable dynamical environment to deal with any anomaly could occurs.
By contrary, the perilune region is characterized by a fast and sensible orbit-attitude dynamics due to the high gradients in the gravity field of the Moon. This generates the high instabilities characterizing the natural librating attitude motion discovered for the periodic orbit-attitude NRHO family in the Earth-Moon system. Any diverging behaviour begins its departure at the perilune passage due to the gravitational assist of the Moon fly-by when the cumulative perturbation becomes large enough. This suggest the implementation of a control action during or just before the perilune passage in order to preserve the reference periodic orbit-attitude behaviour.

7.2 Optimal Energy Solutions for Rendezvous NLP in Cislunar Environment

From the analysis of the natural relative dynamics, the phasing transfer has to be designed to reach the NRHO before, or at the beginning, of the apolune region in order to privilege the execution of the RV&D sequence.

An ephemeris cislunar model for the absolute 6DOF motion of the target space gateway and the relative 6DOF motion of a chaser spacecraft is exploited to address cislunar RV&D operations. The orbital and rotational control capability is included in the dynamics of the chaser vehicle, which is employed to solve the 6DOF rendezvous NLP problem.

Operational and functional constraints will limit the time which can be allocated to perform the RV&D operations. In practical scenarios the time of proximity maneuvers will be quite smaller respect the orbital period of non-Keplerian cislunar NRHO (in the order of 7-8 days), which determines the characteristic period of the natural dynamics. As a consequence, the natural dynamics will not enter significantly in the controlled dynamics, as it happens in LEO operations (e.g. the orbital period of the ISS is about 90 minutes).
The optimal energy solutions for “express” rendezvous result in relative trajectories following almost straight lines and they are characterized by a departure acceleration stage which progressively shifts into a braking stage. This behaviours seems to be independent from the initial offset position direction and from the initial attitude of the chaser spacecraft. While the orbital control cost are function of the initial relative distance to be covered, of the initial relative velocity and of the time allocated to perform the maneuver.
The orbital guidance has demonstrated quite robust convergence properties, while the attitude guidance has shown particular difficulties to find the solution for very short and long rendezvous time of maneuvers.

Finally, the rendezvous simulations suggest the implementation of a dedicated cluster of maneuvering thrusters and angular momentum control devices. It has to be highlighted that a decoupled translational and rotational control system on-board the chaser vehicle will offer the benefit to move the spacecraft along the desired relative trajectory and contemporaneously maintaining a suitable attitude configuration to point the relative sensors of the chaser in the correct direction.

7.3 Recommendations for Future Work

The next decade will be one of the most exciting space exploration era from the time of Apollo programmes. The work presented in this investigation represents only a preliminary analysis aiming to put a base for the design of RVD&D operations standards for the cislunar Gateway. There are many interesting aspect of this investigation to be further analysed, and many others to be explored to ultimately supply the cislunar Gateway design. Some of them are suggested in the following.

7.3.1 Exploration of Periodic Orbit-Attitude Solutions

In this research only few particular orbit-attitude periodic solutions has been analysed in the CR3BP dynamical framework. The generation of a wide catalogue of orbit-attitude periodic solutions for each orbital family discovered in the classical CR3BP and their stability analysis could be very useful for future mission design. In this analysis, the systematic classification of the natural periodic attitude behaviours along the orbit has to be inspected at the varying of the shape (namely specified through the inertial ratio) and the initial attitude configuration of the spacecraft respect to the rotating frame. The most common periodic attitude behaviour discovered corresponds to oscillating behaviours of the body-fixed frame about the rotating frame. However, also spinning solutions have been observed.

7.3.2 Transition to Higher-Fidelity Model

In the cislunar dynamical environment, the gravitational presence of the Sun and the eccentricity of the Moon's orbit are the most relevant perturbations affecting the dynamics of the Earth-Moon system.
In this investigation a simple method has been presented to transit the solution obtained in the CR3BP model to an higher-fidelity ephemeris model. However, advanced correction techniques are fundamentals to support the high-level stages of the design of actual space mission directed towards complex dynamical environments such as cilunar non-Keplerian orbits. They will improve the nearly-periodic behaviours of the orbital motion, and as a consequence also in the attitude, for a transitioned solution in the higher-fidelity model.

7.3.3 Attitude Stabilization and Orbit Maintenance

The attitude configuration of the cilunar Gateway is still one of the open point of its design. However, strong instabilities have been observed in the natural attitude dynamics of periodic orbit-attitude NRHO. They suggest the development of an attitude stabilization strategy would be necessary to avoid the diverging behaviours occurring at the perilune passage.
For example, an attitude control method (such as dual-spin stabilization) might be firstly investigated to stabilize the solely attitude dynamics during the perilune passage along the nominal orbit. Then, its performance would be assessed while it is working in pairs with the orbital station-keeping strategy.

7.3.4 Far-Range Rendezvous

The development of a differential corrector targetting scheme, considering both the orbital and the attitude dynamics, can be addressed to the design of an open-loop impulsive control to perform the far-range rendezvous phases of the chaser spacecraft to the target cislunar gateway.

7.3.5 Alternative RV&D Guidance Strategies

Advancing in the design of the cislunar gateway and of the service modules, more information about the vehicles will allow a better modelling of their inertia properties and geometries. The availability of these information and other operational requirements, such as Sun illumination and power/thermal constraints, will leads to the final design of the RV&D strategy.

The presented 6DOF guidance solution has shown its capability to drive the orbit-attitude dynamics of the chaser to design RV&D operations in cislunar space.
However, a different formulation of the rendezvous NLP problem, discretizing the trajectory in multiple arches which are driven by simpler control parametrizations, might improve the efficiency and the flexibility of the 6DOF guidance design for the chaser spacecraft.

Finally, alternative RV&D strategies may be explored in order to control the chaser spacecraft along desired relative path with a desired velocity and attitude evolution.

Bibliography

[1] *The Global Exploration Roadmap*. International Space Exploration Coordination Group, 2018.

[2] R. Whitley and R. Martinez, *Options for Staging Orbits in Cislunar Space*. NASA Johnson Space Center, 2015.

[3] D. L. Richardson, "Halo orbit formulation for the ISEE-3 mission," *Journal of Guidance Control Dynamics*, vol. 3, pp. 543–548, Nov. 1980.

[4] D. C. Folta, M. Woodard, K. Howell, C. Patterson, and W. Schlei, "Applications of multi-body dynamical environments: The ARTEMIS transfer trajectory design," *Acta Astronautica*, vol. 73, pp. 237–249, Apr. 2012.

[5] D. W. Dunham and R. W. Farquhar, "Libration point missions, 1978-2002," in *Libration point orbits and applications*, pp. 45–73, World Scientific, 2003.

[6] J. P. Gardner, J. C. Mather, M. Clampin, R. Doyon, M. A. Greenhouse, H. B. Hammel, J. B. Hutchings, P. Jakobsen, S. J. Lilly, K. S. Long, J. I. Lunine, M. J. Mccaughrean, M. Mountain, J. Nella, G. H. Rieke, M. J. Rieke, H.-W. Rix, E. P. Smith, G. Sonneborn, M. Stiavelli, H. S. Stockman, R. A. Windhorst, and G. S. Wright, "The James Webb Space Telescope," *Space Science Reviews*, vol. 123, pp. 485–606, Apr. 2006.

[7] W. Traub, S. Shaklan, and P. Lawson, "Prospects for Terrestrial Planet Finder (TPF-C, TPF-I, & TPF-O)," p. 36, June 2007.

[8] M. Hechler and J. Cobos, "HERSCHEL, PLANCK AND GAIA ORBIT DESIGN," in *Libration Point Orbits and Applications*, World Scientific, May 2003.

[9] T. R. Kane and E. L. Marsh, "Attitude stability of a symmetric satellite at the equilibrium points in the restricted three-body problem," *Celestial mechanics*, vol. 4, pp. 78–90, Sept. 1971.

[10] W. J. Robinson, "Attitude stability of a rigid body placed at an equilibrium point in the restricted problem of three bodies," *Celestial mechanics*, vol. 10, pp. 17–33, Aug. 1974.

[11] A. Abad, M. Arribas, and A. Elipe, "On the attitude of a spacecraft near a lagrangian point," *Astronomical Institutes of Czechoslovakia*, vol. 40, pp. 302–307, Sept. 1989.

[12] E. Brucker and P. Gurfil, "Analysis of gravity-gradient-perturbed rotational dynamics at the collinear lagrange points," *The Journal of the Astronautical Sciences*, vol. 55, pp. 271–291, Sept. 2007.

[13] B. Wong, R. Patil, and A. Misra, "Attitude Dynamics of Rigid Bodies in the Vicinity of the Lagrangian Points," *Journal of Guidance, Control, and Dynamics*, vol. 31, no. 1, pp. 252–256, 2008.

[14] D. Guzzetti, "Large space structure dynamics in a multi-body gravitational environment," Master's thesis, Politecnico di Milano, 2012.

[15] A. J. Knutson, *Application of Kane's Method to incorporate Attitude Dynamics into the Circular Restricted Three-Body Problem.* PhD thesis, Purdue University, 2012.

[16] A. J. Knutson and K. C. Howell, "Coupled orbit and attitude dynamics for spacecraft comprised of multiple bodies in Earth-Moon Halo orbits," *63rd International Astronautical Congress, Naples, Italy*, 2012.

[17] D. Guzzetti and K. C. Howell, "Natural periodic orbit-attitude behaviors for rigid bodies in the three-body periodic orbits," *ACTA Astronautica*, 2016.

[18] L. Bucci, "Coupled orbital-attitude dynamics of large structures in non-keplerian orbits," Master's thesis, Politecnico di Milano, 2015.

[19] A. Colagrossi and M. Lavagna, "Preliminary results on the dynamics of large and flexible space structures in halo orbits," *ACTA Astronautica*, vol. 134, pp. 355–367, 2016.

[20] W. Fehse, *Automated Rendezvous and Docking of Spacecraft.* Cambridge University Press, Nov. 2003. Google-Books-ID: sX7TacxPrP4C.

[21] *Soyuz rendezvous and docking explained.* European Space Agency (ESA), 2014.

[22] D. Guzzetti, N. Bosanac, A. Haapala, K. C. Howell, and D. C. Folta, "Rapid trajectory design in the earth–moon ephemeris system via an interactive catalog of periodic and quasi-periodic orbits," *Acta Astronautica*, vol. 126, pp. 439–455, sep 2016.

[23] K. Tajdaran, "Incorporation of mission design constraints in floquet mode and hamiltonian structure preserving orbital maintenance strategies for libration point orbits," Master's thesis, Purdue University, 2015.

[24] S. Lizy-Destrez, "Rendezvous optimization with an inhabited space station at EML2," in *25th International Symposium on Space Flight Dynamics (ISSFD), Munich, Germany*, 2015.

[25] N. Murakami, S. Ueda, T. Ikenaga, M. Maeda, T. Yamamoto, and H. Ikeda, "Practical rendezvous scenario for transportation missions to cis-lunar station in earth-moon l2 halo orbit," in *25th International Symposium on Space Flight Dynamics (ISSFD), Munich, Germany*, 10 2015.

[26] A. Colagrossi and M. Lavagna, "Dynamical analysis of rendezvous and docking with very large space infrastructures in non-Keplerian orbits," *CEAS Space Journal*, vol. 10, pp. 87–99, Mar. 2018.

[27] A. Colagrossi and M. Lavagna, "Assembly and operations for a cisluna orbit space station," *68th International Astronautical Congress, Adelaide*, 2017.

[28] L. Bucci, M. Lavagna, and F. Renk, "Phasing and rendezvous operations on non-keplerian orbits in the earth-moon system," *69th International Astronautical Congress, Bremen, Germany*, 2018.

[29] L. Bucci, A. Colagrossi, and M. Lavagna, "Rendezvous in lunar near rectilinear halo orbits," *Advances in Astronautics Science and Technology*, vol. 1, pp. 39–43, aug 2018.

[30] V. Szebehely, *Theory of Orbits: The Restricted Problem of Three Bodies*. Academic Press, New York, 1967.

[31] D. J. Greebow, "Generating periodic orbits in the circular restricted three-body problem with application to lunar south pole coverage," Master's thesis, School of Aeronautics and Astronautics, Purdue University, 2006.

[32] D. C. Folta, N. Bosanac, D. Guzzetti, and K. C. Howell, "An Earth-Moon system trajectory design reference catalog," *Acta Astronautica*, vol. 110, pp. 341–353, May 2015.

[33] F. L. Markley and J. L. Crassidis, *Fundamentals of Spacecraft Attitude Determination and Control*. Springer New York, 2014.

[34] T. R. Kane, P. W. Likins, and D. A. Levinson, *Spacecraft Dynamics*. McGraw-Hill, 2005.

[35] T. A. Pavlak, "Mission design application in the earth-moon system: Transfer trajectories and stationkeeping," Master's thesis, Purdue University, 2010.

[36] T. A. Pavlak, *Trajectory Design and Orbit Maintenance Strategies in Multi-Body Dynamical Regimes*. PhD thesis, Purdue University, 2013.

[37] G. Q. Xing and S. A. Parvez, "Relative attitude kinematics and dynamics equations and its applications to spacecraft attitude state capture and tracking in large angle slewing maneuvers," tech. rep., MIT Lincoln Laboratory, Lexington, Massachusetts, 1999.

[38] G. Q. Xing and S. A. Parvez, "Alternate forms of relative attitude kinematics and dynamics equations," in *2001 Flight Mechanics Symposium*, 2001.

[39] L. Perko, *Differential Equations and Dynamical Systems*. Springer, 2001.

[40] D. C. Davis, S. M. Phillips, K. C. Howell, S. Vutukuri, and B. P. McCarthy, "Stationkeeping and transfer trajectory design for spacecraft in cislunar space," in *AAS/AIAA Astrodynamics Specialist Conference, Columbia River Gorge, Stevenson, Washington*, 2017.

[41] B. G. Marchand, *Spacecraft Formation Keeping near the Libration Points of the Sun-Earth/Moon System*. PhD thesis, Purdue University, 2004.

[42] J. D. Biggs, "A quaternion-based attitude tracking controller for robotic systems," tech. rep., Department of Mechanical & Aerospace Engineering, University of Strathclyde, 2015.

Appendix A

Reference Frames Definition

This appendix resumes all the main reference frames that have been employed through this investigation.

A.1 Inertial and Rotationg Frames

The inertial $\{\hat{i}\}$-frame is defined by the triad $\hat{\boldsymbol{X}}, \hat{\boldsymbol{Y}}, \hat{\boldsymbol{Z}}$. The $\hat{\boldsymbol{Z}}$-axis is aligned with the direction of the angular velocity of the primaries. The synodic $\{\hat{r}\}$-frame is rotating fixed to the primaries, and is composed by the basis $\hat{\boldsymbol{x}}, \hat{\boldsymbol{y}}, \hat{\boldsymbol{z}}$. Both frames are located at the barycenter of the system, O. At time $t = 0$ the rotating frame is assumed to be aligned with the inertial frame. The rotating frame $\hat{\boldsymbol{x}}$-axis is always aligned with the position vector from P_1 to P_2. The $\hat{\boldsymbol{z}}$-axis is aligned with the direction of the angular velocity of the synodic frame, $\boldsymbol{\omega} = \Omega\hat{\boldsymbol{z}}$. The $\hat{\boldsymbol{y}}$-axis completes the right-handed triad. In figure A.1 the inertial $\{\hat{i}\}$-frame is drawn in blue, while the rotating $\{\hat{r}\}$-frame is represented in black.

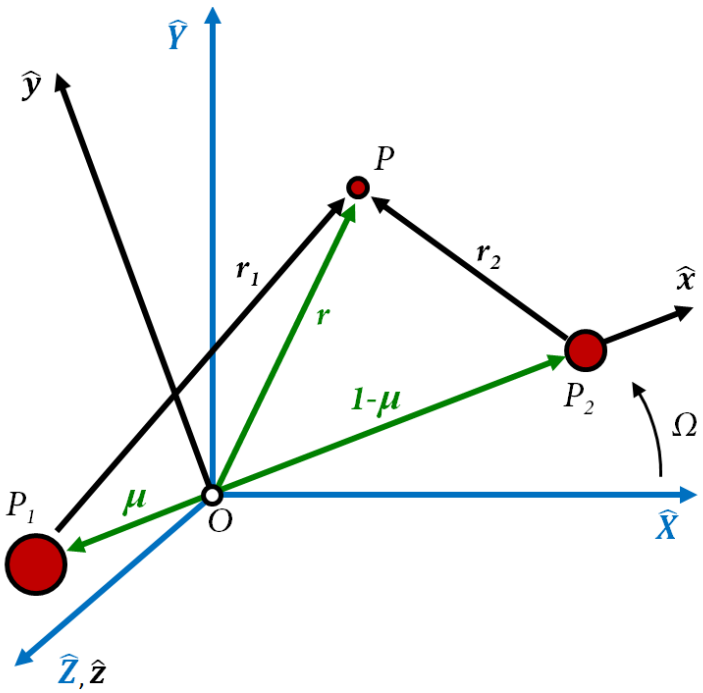

Figure A.1: Graphical representation of the CR3BP

A.2 J2000 and ECLIPTIC-J2000 Reference Frames

The J2000 frame definition is based on the Earth's equator and equinox, determined from observations of planetary motions, plus other data such as the location of extragalactic radio sources. The Ecliptic plane is defined as the mean orbital plane described by the motion of the Earth around the Sun. The $\hat{\boldsymbol{z}}_{J2000}$-axis corresponds to the normal to the mean equator of date at epoch J2000 TDB (Barycentric Dynamic Time), which is approximately Earth's spin axis orientation at that epoch. The $\hat{\boldsymbol{x}}_{J2000}$-axis identifies the intersection of the equatorial and ecliptic planes, which is called vernal equinox. Therefore, by definition it corresponds also to the $\hat{\boldsymbol{x}}$-axis of the Ecliptic J2000 frame. The $\hat{\boldsymbol{z}}$-axis of the Ecliptic J2000 frame correspond to the mean direction of the angular momentum of the Earth motion around the Sun.

A.3 Local Vertical Local Horizontal Frame

The Local Vertical-Local Horizontal (LVLH) frame is commonly used in proximity operations to understand the relative orbital state respect to the target. The LVLH frame is centered at the target spacecraft location. In this investigation the LVLH frame is built referring to the orbital states of the target spacecraft expressed in the Rotating Moon-Centered (RMC) frame. The Moon has been selected as central reference body because Earth-Moon NRHO are the main focus of this work. However analogous definition of the LVLH-frame may consider the orbital states relative to a libration point. These alternative formulation could be useful for the definition of LVLH-frame considering, for example, Lyapunov orbits and Low vertical amplitude Halo orbits.

The $\hat{\boldsymbol{z}}$-axis is in the radial direction going from the spacecraft to the Moon. The $\hat{\boldsymbol{z}}$-axis is in the opposite direction of the angular momentum of the spacecraft orbit seen in the rotating point of view. The angular momentum defined in the inertial point of view can be used if the "inertial" formulation is desired. Then, the $\hat{\boldsymbol{x}}$-axis, which represents the along-track direction, is obtained as vectorial product of the other two axis.